



Faculty Details proforma for DU College Web-site



Title	Dr.	First Name	Pragati	Last Name	Malik	Photograph
Designation	Assistant Professor					
Address	Acharya Narendra Dev College, University of Delhi, Govindpuri, Kalkaji, New Delhi-110019					
Phone No Office	011-26294541					
Residence						
Mobile	9910517371					
Email/	pragatimalik13786@gmail.com pragatimalik@andc.du.ac.in					
Web-Page						
Educational Qualifications						
Degree	Institution				Year	
Ph.D. Chemistry	Department of Chemistry, University of Delhi				2014	
M.Sc. Chemistry	Sri Venkateswara College, Department of Chemistry, University of Delhi				2009	
B.Sc.(H) Chemistry	Sri Venkateswara College, Department of Chemistry, University of Delhi				2007	
Career Profile						
Teaching Experience ~ 10 Years Working as an Assistant Professor in Acharya Narendra Dev College, University of Delhi since July 2014 till Present. Worked as an Assistant Professor in Hansraj College, University of Delhi (Jan 2014 - May 2014). Worked as an Assistant Professor (Guest) in Aurobindo College, University of Delhi (July 13 - Nov. 13), Maitreyi College, University of Delhi (Jan 13 - April 13) and Rajdhani College (September 2009- April 2010)						
Administrative Assignments						
(i) Convenor of Cultural Events Management Committee (2022-Present) (ii) Paper Setting and Evaluation in University of Delhi (iii) Paper Setting in National Testing Agency. (iv) Member of the Cultural Committee (2014 - Present) (v) Member of the Academic Event committee (2018 - Present) (vi) Member of the Sashakt "Women Empowerment" Committee (2016 - 2018)						

(vii) Member of the Proctorial Committee (2014 - 2016)

Areas of Interest / Specialization

Research Area : A DFT Study of II-VI Quantum Dots and Core-Shell Quantum Dots

Research Interest : Computational Chemistry

Specialization : Physical Chemistry

Subjects Taught

Physical Chemistry, Inorganic Chemistry, Organic Chemistry

Publications Profile

1. II-VI core/shell quantum dots and doping with transition metal ions as a means of tuning the magnetoelectronic properties of CdS/ZnS core/shell QDs: A DFT study, Journal Name: Journal of Molecular Graphics and Modelling, Year: March 2022, Volume 111, Page No: 108099, Authors Name: Pragati Malik, Rakhi Thareja, Jyoti Singh, Rita Kakkar.
2. Size Dependent Structural and Electronic Properties of Stoichiometric II-VI Quantum Dots and Gas Sensing Ability of CdSe Quantum Dots: A DFT Study, Journal of Nanoparticle Research, Year: 2022, Authors Name: Jyoti Singh, Rakhi Thareja, Pragati Malik, Rita Kakkar.
3. A DFT Study of Interaction of (CdSe)₃ Quantum Dots with Nucleobases, Journal Name: Advanced Materials Letters, Year: 2021, Volume 12(8), Page No: 1-11, Authors Name: Pragati Malik, Rita Kakkar.
4. Effects of increasing number of rings on the ion sensing ability of CdSe quantum dots: a theoretical study, Journal Name: Journal of Nanoparticle Research, Year: 2018, Volume: 20, Page No. 114, Online ISSN No.: 1572-896X, Print ISSN No.: 1388-0764, Authors Name: Pragati Malik, Rita Kakkar.
5. A Review on CdSe Quantum Dots in Ion Sensing, Journal Name: Advanced Materials Letters, Year: 2014, Volume: 5 (11), Page No.: 612-628, Authors Name: Pragati Malik, Jyoti Singh, Rita Kakkar, ISSN No.: 0976-3961.
6. Quantum Dots for Diagnosis of Cancers: Review Article, Journal Name: Advanced Materials Letters, Year: 2013, Volume: 4 (11), Page No.: 811-822, Authors Name: Pragati Malik, Sunita Gulia, Rita Kakkar, ISSN No.: 0976-3961.
7. Chapter in Book (January 2023) : Book Name : Fibre and Textile Engineering in Drug Delivery System, ISBN: **9780323961172**; Chapter 8 : Multifaceted approach for nanofiber fabrication: Authors Name - Thareja Rakhi, Malik Pragati, Bansal Prerna and Singh Jyoti.

Conference / Presentations /Workshops

Successfully completed a 50-hr International Workshop on Computational Chemistry held from February-April, 2021 organised by Hindu College, University of Delhi in collaboration with Department of Physics, Stockholm University, Sweden and Department of Chemistry, J.V. College, Baraut, U.P.

Successfully completed a 4-Week Induction/Orientation Programme for "Faculty in Universities/Colleges/Institutes of Higher Education" from June 26 - July 24, 2020 and obtained grade A+ Organized By Teaching Learning Centre, Ramanujan College University Of Delhi Under The Aegis Of Ministry Of Human Resource Development Pandit Madan Mohan Malaviya National Mission On Teachers And Teaching.

Successfully completed One Week Faculty Development Programme on "Open-Source Tools for Research" from June 08 - June 14, 2020 organized by Teaching Learning Centre, Ramanujan College University of Delhi under the aegis of Ministry Of Human Resource Development Pandit Madan Mohan Malaviya National Mission On Teachers And Teaching.

Successfully completed **Faculty Development Programme** on "From Chemistry of life to Chemistry of diseases: Understanding Clinical Biochemistry" organized by Daulat Ram College, University of Delhi under DBT Star Scheme (June 2017)

Oral Presentation

Entitled "**Effects of increasing number of rings on ion sensing ability of CdSe quantum dots: A DFT study**" in the National Seminar on "Emerging Economics and Challenges to Sustainability" at Sri Aurobindo College, University of Delhi (2016)

Conference / Presentations /Workshops

1. Successfully completed a 50-Hour International Workshop on in "**Computational Chemistry**" organized by Department of Chemistry, Hindu College, University of Delhi, in collaboration with Department of Physics, Stockholm University, Sweden, Physics Group, BARC, Mumbai and Department of Chemistry, J.V. College, Baraut, U.P held from February – April 2021.
2. Attended a lecture on "**Rational Approaches in Drug Design and Development**" under International Lecture Series entitled "Multifaceted Chemistry: An ever-evolving domain of science" organized by Deshbandhu College, Kalkaji, University of Delhi held on 20/03/2021.
3. Worked as a Team Member in organizing an International Lecture on "**Role of Chemistry in Eradication of Pandemic Covid-19**" by Dr. Vikas Malhotra, held on 17/04/2021, organized by Chemistry Department of Acharya Narendra Dev College, University of Delhi.
4. Participated in one day online national conference on New Frontiers in Biosensing organized by Department of Chemistry, Hansraj College, University of Delhi on 03/04/2021.
5. Part of an Organizing Committee of One-Day Inter-Disciplinary exhibit presentation on "**New Frontiers in Science**" organized by Acharya Narendra Dev College, University of Delhi (October, 2019).
6. Successfully completed a workshop on "**Empowering Teachers: Current Technology Based Educational Contents Creation and Delivery (Using Open Source, Free Software)**" organized by Internal Quality Assurance Cell, ANDC from December 2-6 2019 in the College.

7. Participated in the Faculty Development Programme "**Teachers as Mentors**" organized by Acharya Narendra Dev College, University of Delhi (October, 2018).
8. Worked as a Resource Person in the "**two-day workshop 'Science Pedagogy : Laboratory Learning to Classroom Teaching'**" organized by Acharya Narendra Dev College, University of Delhi (January 20-21, 2016).
9. Participated in Workshop on **Electronic Structure, Atomistic and Statistical Modeling in Chemistry, Materials and Life Sciences** organized by University of Delhi in October' 14.
10. **International Workshop on Gaussian** held in Dec' 12.
11. Workshop on "**Information Literacy and Competency**" organised by Delhi university library system, University of Delhi in the year 2010 & 2011.
12. National Workshop on "**Renewable Energy and Environment**" organized by Ramjas College, University of Delhi in the year 2011.
13. Workshop on "**Bioinformatics and Molecular Modeling In Drug Design**" organised by Dr. B. R. Ambedkar Center for Biomedical Research, University of Delhi in the year 2011.
14. National Seminar on "**Alternative Energy Sources for Sustainable Environment**" organized by Lingaya's University, Faridabad in the year 2011.
15. National Workshop on "**Role of Analytical Techniques in Industry**" organised by Kirori Mal College, University of Delhi in the year 2010.

Awards and Distinctions

Gold Medal for 1st Rank in M.Sc. (Final) from Sri Venkateswara College in University of Delhi South Campus (2008-09).

Silver Medal for 1st Rank in M.Sc. (Previous) from Sri Venkateswara College in University of Delhi South Campus (2007-08).

Qualified **GATE** (March'09) with **Percentile 96.49 & All India rank 229**

Received **Science Meritorious Scholarships from Delhi University** for 2 consecutive years for performance in the academic sessions 2007-08 & 2008-09

Qualified **CSIR-JRF/NET** (Dec'08)

1st Rank in Rashtriya Academy for Computer Education.

Awarded Senior General Knowledge Test Certificate from United Schools Organisation of India.

Awarded certificates for 5 consecutive years for participation in Akhil Bhartiya Sanskriti Gyan Pariksha.

Participated in many skits and Nukkad Natak.

Association With Professional Bodies

Lifetime Membership of “Role of Analytical Techniques in Industry”.

Other Activities

Awarded Certificate for Participation & Pledge in Cancer Aid Society.

Awarded Certificate for Effort in Cancer Aid Society.

SCORECARD

Name : PRAGATI MALIK

Registration No. : CY 3340573

Category : General



Signature of the Candidate

Pragati

PERFORMANCE IN GATE 2009 held on February 08, 2009

Examination Paper: CY - Chemistry		
Number of candidates appeared in this paper		All India Rank
6916		229
Marks out of 100	GATE Score	Percentile Score
48.33	486	96.49
Result : Qualified		

Score Valid Upto : March 15, 2010

The authenticity of this score may be checked with the Organising Chairman, GATE 2009, Indian Institute of Technology Roorkee, Roorkee - 247 667.

The scorecard cannot be used as a proof of category and/or disability status.

Date: March 15, 2009

(Signature)

(Prof. Manoj K. Arofa)
Organising Chairman, GATE 2009

On behalf of the Department of Secondary and Higher Education
Ministry of Human Resource Development, Government of India

PRAGATI MALIK



NAME:	PRAGATI MALIK
ADDRESS:	26/398 NEW MOTI NAGAR, KARAM PURA, NEW DELHI
PIN CODE:	110015

SCORECARD NO. : 301287

- Note :**
1. GATE Admit Card need not be produced together with scorecard at the time of admission.
 2. Qualification in GATE does not guarantee either admission to postgraduate programme or scholarship/assistantship.
- See reverse side for an explanation of GATE score, Percentile score and Sectional paper codes.**

GATE SCORE

The GATE score, awarded in the range of 0 to 1000 reflects the candidate's academic ability and is based on his/her performance in GATE 2009 and the performances of all candidates who appeared in GATE in the last four years 2006-2009. Candidates with the same GATE score from different GATE papers and/or years can be considered to have the same performance level.

$$\text{GATE SCORE} = \frac{1000}{100} \left[a_g + s_g \left(\frac{m - a}{s} \right) \right],$$

where,

- m = marks obtained by the candidate.
- a = average of marks of all candidates who appeared in the paper mentioned on this scorecard in GATE 2009
- s = standard deviation of marks of all candidates who appeared in the paper mentioned on this scorecard in GATE 2009
- a_g = average (global) of marks of all candidates who appeared across all papers and years 2006-2009
- s_g = standard deviation (global) of marks of all candidates who appeared across all papers and years 2006- 2009

The maximum score can be 1000.

PERCENTILE SCORE

The percentile score of a candidate indicates the percentage of candidates who appeared in the same paper and scored less marks than him/her. It is calculated as follows: If N is the total number of candidates appearing in a paper, then the percentile score P is given as,

$$P = (\text{number of candidates who have scored less marks than the candidate} / N) \times 100$$

Sectional Paper Codes

Sectional Paper Codes	
XE - Engineering Sciences	XL - Life Sciences
A - Engineering Mathematics (Compulsory)	H - Chemistry (Compulsory)
B - Fluid Mechanics	I - Biochemistry
C - Materials Science	J - Biotechnology
D - Solid Mechanics	K - Botany
E - Thermodynamics	L - Microbiology
F - Polymer Science and Engineering	M - Zoology
G - Food Technology	



Sri Venkateswara College

(UNIVERSITY OF DELHI)

NEW DELHI

Certificate of Merit

Year: 2008-2009

This is to certify that Pragati Malik

of MSc Chemistry II year has been awarded Balaji Gold medal 05gm.

prize for I position in UOSC

Signature of the Convener
(Association/Dept.)

PRINCIPAL



ACHARYA NARENDRA DEV COLLEGE

University of Delhi

NAAC Accreditation Grade 'A' | NIRF 2021 All India Ranking- 20

CERTIFICATE

Computational Chemistry: A New Approach to Understanding & Solving Chemical Problems

October 6 - 7, 2021

This is to certify that

DR PRAGATI MALIK , ACHARYA NARENDRA DE COLLEGE, UNIVERSITY OF DELHI

has organized the **Two Day National Hands-on workshop (online mode)** organized by Abhikriya, The Chemical Society of Acharya Narendra Dev College, University of Delhi under the aegis of DBT STAR College Scheme and IQAC.

Prof. Sunita Hooda
DBT Star Convenor

Dr Geetu Gambhir
Convenor

Prof. Ravi Toteja
Officiating Principal



ACHARYA NARENDRA DEV COLLEGE

University of Delhi

NAAC Accreditation Grade 'A' | NIRF 2021 All India Ranking- 20

CERTIFICATE

Exploring and Understanding Computational Chemistry Using Gaussian: Molecular Builder and Visualization Tool

March 7 - 10, 2022

This is to certify that

DR PRAGATI MALIK , ACHARYA NARENDRA DE COLLEGE, UNIVERSITY OF DELHI

has organized the **Four Day National Hands-on workshop (online mode)** organized by Abhikriya, The Chemical Society of Acharya Narendra Dev College, University of Delhi under the aegis of DBT STAR College Scheme and IQAC.

Prof. Sunita Hooda
DBT Star Convenor

Dr Geetu Gambhir
Convenor

Prof. Ravi Toteja
Officiating Principal

Letter of Appreciation

We would like to take this opportunity to express our most sincere gratitude to **Dr Pragati Malik of Acharya Narendra Dev College, University of Delhi** for flawless and efficient conduct of session as **Session Chair** during the International e-conference on 'Mitigating environmental issues by sustainable approaches (ICMCESA-2022)' organized by Acharya Narendra Dev College, University of Delhi from February 22-28, 2022 under the aegis of IQAC and DBT Star College Scheme.



Prof. Ravi Toteja
Principal, ANDC
Chairperson ICMCESA





ACHARYA NARENDRA DEV COLLEGE



UNIVERSITY OF DELHI

NAAC ACCREDITATION GRADE - 'A' | NIRF RANK - 20



Under the Aegis of DBT Star Scheme and IQAC

DEPARTMENT OF CHEMISTRY

Organizes

Hands on Workshop
For Undergraduate Students

Introduction to New Experiments

📍 Venue: Chemistry Laboratory - III, IV

📅 Date: 21st April, 2022

🕒 Time: From 9:30 AM to 4:00 PM

Prof. Ravi Toteja
PATRON

Prof. Sunita Hooda
CONVENOR

Dr. Dinesh Kumar Arya
TEACHER-IN-CHARGE

Dr. Pooja Bhagat

Dr. Neeti Misra

Dr. Pragati Malik

Dr. Kavita Mittal

Student Coordinator - Meghana Bisht (8006791945)



ACHARYA NARENDRA DEV COLLEGE

आचार्य नरेंद्र देव कॉलेज

University of Delhi | दिल्ली विश्वविद्यालय
NAAC accredited: 'A' Grade | एन.ए.ए.सी. मान्यता प्राप्त: 'ए' ग्रेड

One-day inter-disciplinary exhibit presentation

NEW FRONTIERS IN SCIENCE

(Under the aegis of DBT - STAR College Scheme)

Certificate of Appreciation

*An appreciation is extended to Dr./ Mr./ Ms. Pragati Malik.....
Dept. of Chemistry.... for being a part of the organizing committee
of One-day inter-disciplinary exhibit presentation on "NEW
FRONTIERS IN SCIENCE" held on October 22, 2019.*

Dr. Ravneet Kaur
Convenor

Dr. Harita Ahuja
Convenor

Dr. Ravi Toteja
Patron

October 22, 2019

Govindpuri, Kalkaji, New Delhi 110019 | गोविंदपुरी, कालकाजी, नई दिल्ली 110019

<http://andcollege.du.ac.in/> | +91-11- 26293224

ACHARYA NARENDRA DEV COLLEGE

University of Delhi, NAAC Accreditation Grade 'A' | NIRF-Rank 20

THIS POSTER HAS BEEN CREATED ON PHOTOSHOP

DO YOU WANT TO LEARN HOW TO DO THIS?



Join us for 2-day Webinar Workshop on

BASICS OF PHOTOSHOP

and its application for Poster Making,
Reports, Photo Editing & Social Media



Resource Person

Sonalika Arora

Digital Marketing Designer

30 Sept - 1 Oct | 4-7 pm

Google Meet Link: <https://meet.google.com/cuy-mirh-fvf>

Organised by

Abhikriya - Chemical Society, Dept. of Chemistry
under the Aegis of DBT star College scheme and IQAC

Prof. Ravi Toteja

Patron

Prof. Sunita Hooda

DBT Coordinator

Dr. Geetu Gambhir

Convener

Dr. Pragati Malik

Co-convener

Certificate provided on successful completion.

Please log-in from desktop/ laptop for hands-on session.



ACHARYA NARENDRA DEV COLLEGE

आचार्य नरेंद्र देव कॉलेज

University of Delhi | दिल्ली विश्वविद्यालय

NAAC accredited: 'A' Grade | एन.ए.ए.सी. मान्यता प्राप्त: 'ए' ग्रेड

*This is to certify that Dr. Pragati Malik
has organized a two day symposium on "Safety
Measures and Laboratory Ethics" organized by
Acharya Narendra Dev College (University of Delhi)
on February 21-22, 2018.*

Dr. Seema Gupta

Dr. Seema Makhija
Coordinators

Dr. Savithri Singh
Principal

February 22, 2018



Acharya Narendra Dev College

(University of Delhi)

राजतोषण

Silver Jubilee Celebrations

This is to certify that.. *Dr. Pragati Malik*.....of Acharya Narendra Dev College, University of Delhi was Resource Person in the two-day workshop "Science Pedagogy: Laboratory learning to Classroom Teaching" organized by Acharya Narendra Dev College (University of Delhi) from January 20-21, 2016.

Dr. Neeti Misra
Coordinator

Dr. Savithri Singh
Principal

January 21, 2016



4TH CCW COMPUTATIONAL CHEMISTRY WORKSHOP - 2021

AIMs (Anubhav Inspiring Masterminds) Institute, New Delhi, India, <https://aimsdelhi.com>
DATE: 26 – 30 APRIL 2021, TIME: 11:30 A.M. – 1:00 P.M. (IST)

Certificate of Participation

This is to certify that [Dr. Pragati Malik, Assistant Professor, Delhi University, India](#) has actively participated in the 4th Computational Chemistry Workshop - 2021 (**CCW-2021**) organized by the Dr. Nikhil Aggarwal, AIMs Institute, Delhi under a Professional Training Program category, held from 26th April 2021 – 30th April 2021 (Five Days) via Online Mode.

Dr. Nikhil Aggarwal
Convener
Director (AIMs Institute), Delhi



DEPARTMENT OF CHEMISTRY
HINDU COLLEGE, UNIVERSITY OF DELHI

In collaboration with
DEPARTMENT OF PHYSICS
STOCKHOLM UNIVERSITY, SWEDEN

PHYSICS GROUP

BHABHA ATOMIC RESEARCH CENTER, MUMBAI

DEPARTMENT OF CHEMISTRY
J.V. COLLEGE, BARAUT, U.P.

INTERNATIONAL WORKSHOP CERTIFICATE

This is to certify that

Dr. Pragati Malik

of Acharya Narendra Dev College has successfully completed a 50-hour
International Workshop on

COMPUTATIONAL CHEMISTRY

held from February-April, 2021.

(Prof. Anju Srivastava)

Principal
Hindu College
Chairperson,
Short term course

(Dr. Reena Jain)

Vice-Principal
Hindu College
Chairperson,
Short Term Course

(Prof. Michael Odelius)

Professor
Department of Physics
Stockholm University
Sweden

(Dr. Shyam Kishore)

Associate Professor
and Head,
Dept. of Chemistry
JV College, UP





Teaching Learning Centre, Ramanujan College
University of Delhi

under the aegis of
MINISTRY OF HUMAN RESOURCE DEVELOPMENT
PANDIT MADAN MOHAN MALAVIYA NATIONAL MISSION ON TEACHERS AND TEACHING



This is to certify that

Dr. Pragati Malik

of

Acharya Narendra Dev College, University of Delhi

successfully completed a 4-Week Induction/Orientation Programme for
"Faculty in Universities/Colleges/Institutes of Higher Education"
from June 26 - July 24, 2020 and obtained
grade **A+**



[Blockchain Hash: 0xf4b69443ff24eb52638610a61065687e73edcdbaa4e572d7aeec5b6af1c9883](https://www.mhrd.gov.in/portal/Blockchain/verify/0xf4b69443ff24eb52638610a61065687e73edcdbaa4e572d7aeec5b6af1c9883)

Dr. S.P. AGGARWAL
Director, TLC
Principal, Ramanujan College

Dr. Alok Ranjan Pandey
Programme Director
Ramanujan College



Department of Chemistry
Deshbandhu College
(University of Delhi)
Kalkaji, New Delhi- 110019



Awards this

Certificate of Participation

to

*Dr. Pragati Malik, Acharya Narendra Dev College,
University of Delhi*

for active participation in the lecture "**Rational Approaches in Drug Design and Development**" under International Lecture Series entitled "**Multifaceted Chemistry: An ever-evolving domain of science**" held on 20/03/2021 through online mode.

Dr. Pratibha Kumari
Program Convenor
International Lecture Series

Dr. Deo Nandan Kumar
Teacher In-Charge
Department of Chemistry

Dr. Rajiv Aggarwal
Principal
Deshbandhu College



Department of Chemistry
RAJDHANI COLLEGE
(University of Delhi)



Certificate of Participation

This is to certify that **Dr. Pragati Malik**

from

Acharya Narendra Dev College, University of Delhi

has participated in two days online workshop from July, 12 – 13 2021

on

“Tools for Exploring Chemistry”

Prof. (Dr.) Rajesh Giri
(Principal)

Dr. Sharmila Yadav
(Convenor)

Dr. Rajni
(Coordinator)

Quantum dots for diagnosis of cancers

Pragati Malik, Sunita Gulia, Rita Kakkar*

Department of Chemistry, University of Delhi, Delhi 110007, India

*Corresponding author. Tel: (+91) 11-27666313; E-mail: rkakkar@chemistry.du.ac.in

Received: 14 March 2013, Revised: 19 May 2013 and Accepted: 08 June 2013

ABSTRACT

The most widely researched and investigated disease, both medically and scientifically, in the current era is the formidable disease cancer. The chances of successful treatment and hence the curability increases if it is diagnosed at an early stage. This can be done only by increasing awareness amongst people about its early diagnosis and screening tests. Cancer screening exams refers to the medical tests to identify people who have disease, often before symptoms of the illness occur. These tests help detecting cancer at its earliest stage when the chances for curing the disease are greatest. Advancements in nanotechnology have made the early screening of cancer possible. In this review, we have discussed the developments in nanotechnology that have encouraged the more recent innovative solutions for early diagnosis and treatment of cancer. Quantum dots, nanometer-sized semiconductors, are the new class of novel biosensors, now being exclusively employed as alternative fluorescent probes due to their unique properties, such as intense and stable fluorescence for a longer time, resistance to photobleaching, large molar extinction coefficients, and highly sensitive detection, due to their ability to absorb and emit light very efficiently. Their size approximates that of individual biomolecules, which offers unique possibilities for the ultrasensitive detection of cancer in persons' serum, tissues, and other body fluids, when tagged with specific antibodies against specific tumor markers. In this review, we have account briefly the applications of semiconductor QDs employed for the early screening and diagnosis of cancer biomarkers between the years 2009-2012. We believe that this review will enable workers in the field to devise new applications of these materials for the early detection of cancer, and ultimate reduction in incidence of the disease. Copyright © 2013 VBRI press.

Keywords: Biomarkers; cancer; core/shell; detection; diagnosis; imaging; quantum dots; targeting; therapy.



Pragati Malik has done her B.Sc. (2007) and M.Sc. (2009) in Physical Chemistry (specialization) from Delhi University (India). She is working in the area of nanoscience and has completed her Ph.D. under Prof. Rita Kakkar in 2013 (University of Delhi, India).



Sunita Gulia did her B.Sc. (2008) and M.Sc. (2010) in Physical Chemistry from Delhi University. She is currently pursuing Ph.D. under the guidance of Prof. Rita Kakkar at the Department of Chemistry, University of Delhi, India. Her research interests include nanoscience, quantum dots and their applications in the biomedical area.



Rita Kakkar, after obtaining a PhD degree in Physical Chemistry from the University of Delhi, undertook research on various topics. She has been teaching physical chemistry at the University of Delhi for the past over three decades. Her main research interests are in Computational Chemistry and related fields. She heads a large research group, which is carrying out computational and experimental studies on catalysis by nanomaterials and by enzymes. Her research on nanoscale materials also includes theoretical and experimental studies on quantum dots and their size-dependent properties for use as semiconductor devices and sensors. Professor Kakkar has over 80 research publications in international journals. She has successfully supervised the work of 33 PhD and 7 MPhil students. She has delivered invited several talks at scientific conferences. She has acted as an International Advisory Member for several conferences on computational chemistry. She regularly reviews manuscripts for many international journals, including those published by the American Chemical Society, Royal Society of Chemistry and Elsevier.

1. Introduction

Cancer continues to be a major problem in the world for the past many years. Early diagnosis and complete treatment of cancer is the corner-stone of the cancer prevention and control strategy, while inappropriate diagnosis and irregular/incomplete treatment with anti-cancer therapy may lead to complications, disease spread and emergence of drug-resistant cancer. In order to ensure proper cancer diagnosis and address the problems of emergence and spread of drug-resistant cancer, it is essential to have complete information of cancer cases.

Cancer is defined as an abnormal and uncontrolled cell growth due to the accumulation of specific genetic and epigenetic defects, both environmental and hereditary in origin, where the cells forget how to die, unlike normal cells which multiply only when the body needs them and die when they are of no use. When cells divide in an unregulated fashion, there is formation of a tumor mass which later gets out of control. The formed tumor cells become resistant to apoptosis and other antigrowth defenses within the body, which ultimately spread to other body organs, and become difficult to be treated [1]. Cancer may develop in any part of the body, including any tissue or organ. Various common types of cancers have been reported, including lung, prostate, breast, ovarian, hematologic, skin, and colon cancer, etc. Environmental factors, such as tobacco smoke, certain chemicals, ionizing radiation, sunlight, alcohol, and genetic factors, such as inherited mutations in oncogenes, tumor suppressor genes and autoimmune dysfunction, are responsible for the development of cancer. Bacterial and viral infections also account strongly for stomach and cervical cancers, respectively. As per recent data, a total of 1,638,910 new cancer cases and 577,190 deaths from cancer are estimated to have occurred in the United States in the year 2012. There has been an overall decline of 0.6% per year in cancer incidence rates in men, with no change in women, whereas cancer death rates decreased by 1.8% per year in men, and by 1.6% per year in women, in the five years from 2004 to 2008 [2]. Due to the various new and advanced techniques developed for the early diagnosis of cancer, the American Cancer Society (ACS) assessed an increase in the average 5-year survival rate for all cancers for the years 1996–2004 to 66%, compared to 50% for the years 1975–1977, whereas the 5-year survival for certain cancers, such as liver, pancreatic, and lung still remains very low (6%–16%). Mainly the amendment in proto-oncogenes, tumor suppressor genes and DNA repair genes contributes to the alteration in normal cell functioning, along with the mismanagement of cell proliferation events, resulting in the development of cancer genotype and phenotype, which is resistant to the natural and inherent death mechanisms. Oncogene causes those cells to survive which are supposed to die, and activation of oncogenes occurs due to the mutation of normal genes, which further affects cell growth and their differentiation. This is responsible for the activation or excess levels of a normal gene product, causing gene rearrangements, point mutations, leading to disturbances in molecular pathways regulating cell growth, increase in the cell division, disturbances in cell growth mechanisms and their survival, metastasis, and, ultimately, tumor formation. This tumor mass turns into a more

aggressive disease: cancer. Certain carcinogenic agents cause mutations in proto-oncogenes to become oncogenes. Although there is a significant role of genetic and genome based technologies in the diagnosis and prognosis of cancer, the emanating biosensor technologies hold promise, and have now been widely employed for early cancer diagnosis and therapy [1, 3].

Tumor suppressor genes (TSGs) or anti-oncogenes are mainly the transcription factors which suppress process mitosis (a cell division process) and, hence, tumor formation, by blocking unscheduled cell growth. The commonly involved TSGs in cancer are retinoblastoma protein (Rb), BRCA1/2, and p53. Rb regulates cell division. Inactivation of the Rb gene leads to point mutations and deletions, and the major cause of many cancers is mutation of the Rb gene [4–6]. The functioning of normal cells is controlled by the apoptosis complex, triggered by the p53 tumor suppressor protein, which mainly regulates programmed cell death. Nearly half of all cancers involve altered p53 genes. Brain, breast, colon, lung, hepatocellular carcinomas and leukemia are found to be associated with the mutations in p53. A DNA repair enzyme, BRCA1 carries out the proofreading of newly replicated DNA for the presence of mutations and removes replication errors, if any, before the cell divides. About 50% of hereditary breast cancers and 80%–90% of hereditary breast and ovarian cancers are due to BRCA1 gene mutations [7, 8]. Thus, cancer results from cumulative mutations of proto-oncogenes and suppressor genes, which together cause the unregulated growth of cells. Therefore, we conclude that the mechanism of cancer involves simultaneous occurrence of two processes leading to cellular malfunctioning occurring at the same time: (i) permanent enabling of cellular replication due to genetic mutation or chromosomal translocation, and (ii) permanent disabling of the apoptosis complex, the suicide complex. The malfunctioning of these two cellular processes leads to uncontrolled cell division, resulting in a cluster of unspecialized cells committing to divide, which ultimately becomes larger and larger, and releases chemicals to promote the formation of malignant tumor, which starts damaging the surrounding tissue by withdrawing essential nutrients and displacing healthy cells [9]. For example, the human epidermal growth factor receptor HER-2 gene is responsible for making HER-2 proteins (receptors on breast cells) which control the development of the breast. However, in case of any abnormality in the HER-2 gene, too many copies of this gene are formed, called as amplification of the gene, which results in an overexpression of the HER-2 protein, causing the breast cells to grow aggressively, with the formation of tumor, leading to the development of breast cancer. A recombinant humanized monoclonal antibody, named trastuzumab, developed against HER-2, is nowadays being used as a standard treatment for breast cancer [10].

2. Cancer biomarkers

The National Cancer Institute defines a tumor marker as “A biological molecule found in blood, other body fluids or tissues that is a sign of a normal or abnormal process or of a condition or disease” [11]. Tumor markers could be a broad range of biochemical entities, basically the endogenous

proteins, lipids, sugars, nucleic acids or other cytogenetic parameters present in blood or other body fluids, tumor tissues whose changes in amount, any abnormality or modifications symbolizes the tumor state, its progress with time and response to various therapies. These tumor associated antigens are very helpful in cancer diagnosis and markers of how well the body responds to a treatment for a disease or condition [3, 12]. The most challenging task in cancer prognosis is to develop a connecting link between cancer biomarkers and the clinically developed therapies for non-invasive detection of tumors at an early stage. Effective tumor markers are in great demand since they have the potential to reduce cancer mortality rates by facilitating diagnosis of cancers at early stages. During the last decade, an improved understanding of carcinogenesis, tumor progression, and advancement in nanotechnology have revealed a large number of potential tumor markers. A partial list of tumor biomarkers is presented in **Table 1**.

Table 1. Common biomarkers utilized for cancer detection [13-15].

Cancer Type	Biomarker
Breast	BRCA1, BRCA2, CA15-3, CA 125, CA 27.29, MUC1, NY-BR-I, ING-I, HER2/NEU, ER/PR
Colon	CEA, EGF, p53
Esophageal	SCC
Liver	AFP, CEA
Lung	CEA, CA19-9, SCC, NSE, NY-ESO-I, CYFRA21-1
Melanoma	Tyrosinase, NY-ESO-I
Ovarian	CA125, HCG, p53, CEA, CA 549, CASA, CA 19-9, CA 15-3, MCA, MOV-I, TAG72
Prostate	PSA, PAP

3. Quantum dots in early diagnosis of cancer

It becomes difficult to treat cancer when the cancer cells have metastasized into a certain sized tumor, which essentially proves the desirability of the early prognosis of cancer. The commonly employed methods for diagnosis of cancer include chemotherapy, immunotherapy, surgery medical imaging, enzyme linked immunosorbent assay (ELISA) and tissue biopsy, etc., but these are less sensitive, and are reliable only for early-stage cancer detection [16]. Colloidal quantum dots (QDs) are bright, photostable fluorophores, a few nanometers in diameter. Also, the nanometer scale is the scale of biological function, i.e. it is the same size range as that of enzymes, DNA and other cellular components [17], which makes possible to employ water-soluble QD complexes to target and image tumor cells. QDs are now being used as alternative fluorescent probes in the biological world. Application of traditional fluorophores, e.g. organic dyes and fluorescent proteins, is limited due to their narrow absorption range, broad emission spectra and short fluorescent lifetimes, whereas QDs, which exhibit broad absorption and narrow emission spectra, are less susceptible to photobleaching than organic dye molecules, due to their inorganic composition. Their absorption and emission wavelengths are tunable by particle size. Their unique optical properties makes them

strongly attractive as *in vivo* and *in vitro* fluorophores in various biological and medical applications, including multiplexed imaging of live tissues, detection and therapy of various diseases, including cancer [18-24]. The best materials for quantum dots are considered to be cadmium sulfide, and cadmium selenide, but these can be highly toxic due to the leaching of cadmium atoms in the biological system. Hence, various encapsulation techniques need to be employed in order to enhance biocompatibility and hence the bio-applicability of these nanoparticles (NPs) [25].

Semiconductor QDs have proven their potential in biomedical fields due to their excellent optical properties. They exhibit size-dependent discrete energy levels. The energy gap increases with decrease in the size of the nanocrystal, thus yielding a size-dependent rainbow of colors (**Fig. 1**). Light wavelengths from ultraviolet to infrared region can be achieved with variation of the size and composition of QDs, making them highly suited for the simultaneous examination of multiple events and molecules [26].

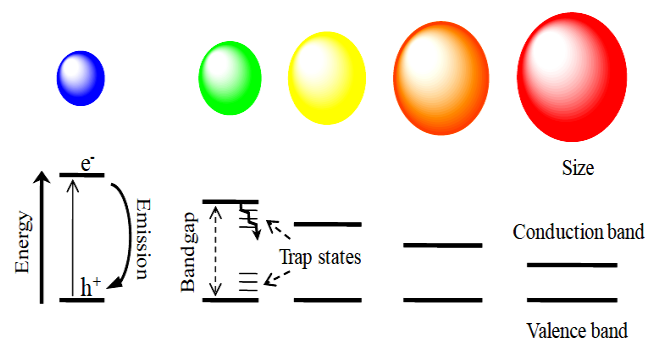


Fig. 1. Illustration of size-tunable QDs and creation of electron-hole pair on photoexcitation [27].

Nowadays QDs are widely employed for targeted anticancer therapies due to an easy manipulation of their surface chemistry by either conjugating them with antibodies, ligands or other biomolecules, directly or indirectly linking them by strategies such as streptavidin-biotin interaction, and by altering their optical and magnetic properties [28]. A single QD can be conjugated to various molecules due to its large surface area to volume ratio, and hence QDs can be designed into more complex multifunctional nanostructures. The antibodies conjugated QDs allow specific recognition and tracking of surface antigens. QDs have been linked covalently to various biomolecules, such as nucleic acids, antibodies, peptides and other ligands for *in vivo* imaging, where the encoding of genes, proteins and various other biomolecules is done by multiple colors and changes in intensities of the QDs [29, 30]. Several reports by researchers prove QDs to be ideal candidates for identifying various types of biomarkers, such as proteins, specific DNA or mRNA sequences, tumor cells, and hence a more effective diagnosis of cancer can be achieved.

QDs possess an important property of easily transferring energy. Thus, the energy of the light falling on a quantum dot passes along to a nearby molecule, which uses this energy to show fluorescence. Self-illuminating QD

conjugates luminesce by bioluminescence resonance energy transfer (BRET) in the absence of external excitation. In this process, the energy from a light-emitting donor molecule is transferred to a nearby acceptor fluorescent molecule nonradiatively, leading to an enhanced sensitivity in bioimaging. As discussed above, one of the greatest advantage of QDs which makes them ideal for *in vivo* imaging is that their emission wavelengths can be tuned throughout the near-infrared (NIR) spectrum with the manipulation in their size, resulting in photostable fluorophores which are highly stable at biological pH values. A deep tissue optical imaging is best in the near-infrared spectrum. Also, hemoglobin and water have local minima in absorption in this spectrum [31, 32].

The applicability of potential QDs to identify live breast cancer cells by employing QDs linked to immunoglobulin G (IgG) and streptavidin to label the HER-2 cancer marker present on the surface of live breast cancer cells was proved [33]. Simultaneous labeling of HER-2 on the cell surface as well as in the nucleus was achieved. Two cellular targets were simultaneously detected with a single excitation wavelength, which proves that different sized and, hence differently colored, QDs could be used together to distinguish different parts of a single cell, leading to multiplex target detection [33]. Antibody-conjugated QDs have made possible the real-time imaging and tracking of single receptor molecules on the surface of living cells with improved sensitivity and resolution [34].

Therefore, compared to other assays, which are time consuming, expensive, labor intensive and have no multiplexing capability, QDs based technology is rapid, easy and economical, and allows quick detection of cancer markers. However, the clinical outcome of any assay developed for cancer strongly depends on the stage at which the malignancy is detected, especially for breast cancer in women and prostate cancer in men [35]. This makes early screening and prognosis of cancer highly important.

4. Surface-modification of quantum dots

Quantum dots are used as bare core only or as core/shell structures. In core/shell structures, the core of a semiconductor is surrounded by a shell (generally a wider bandgap semiconductor material), which allows better passivation of surface defects and enhances the photostability and improves its optical properties. For example, in the absence of a protective shell, CdSe exhibits low quantum yield, but when it is passivated with a higher band gap semiconductor material, ZnS, the CdSe QD's luminescence is improved. Therefore, core/shell structures are better for biological applications than the core-only structures. Alloyed quantum dots, which offer continuous tuning of quantum confinement by variation in the size of the quantum dots or modulation of their chemical composition, have also been synthesized. QDs (whether single or core/shell structures) do not exhibit aqueous solubility as they are generally synthesized in organic solution and are surface-stabilized with hydrophobic organic ligands. Thus, they are necessarily made water soluble by surface modifying them with various bifunctional surface ligands or caps to promote aqueous solubility and enhancing bio-compatibility [36-41].

Quantum dots interact with biomolecules through different types of interactions mechanisms; importantly, peptide linkages or S-S disulfide bonds, electrostatic interactions, hydrophobic and van der Waals interactions. There are various methods for surface modifications of QDs such as (i) silanization, which is done by introducing silica shell covering onto the QDs, (ii) by exchanging the hydrophobic surfactant molecules with bifunctional molecules, i.e. molecules having a hydrophilic end on one side and a hydrophobic end on the other, the most commonly used bifunctional molecules being cysteine, mercaptosuccinic acid, glutathione and mercaptoacetic acid, or (iii) by coating the hydrophobic surface of the QD with a cross-linked amphiphilic polymer, the hydrophilic component of which provides water solubility and the hydrophobic part interacts with the hydrophobic surface of the QD [40]. Other coating techniques include electrostatic interaction, micelle encapsulation, and hydroxylation, as shown in Fig. 2.

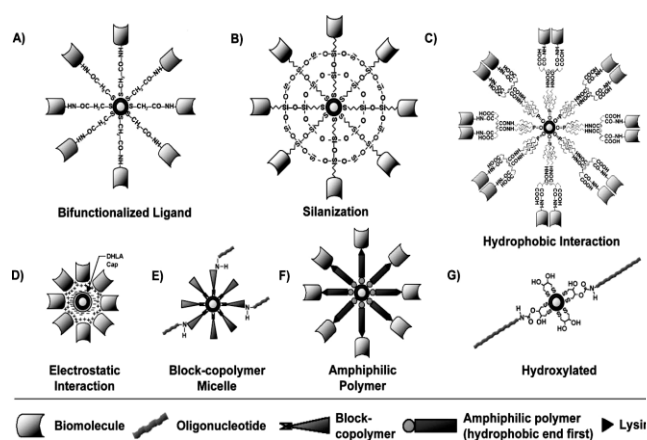


Fig. 2. Surface coatings that permit QDs to interface with biological systems and biorecognition molecules [42].

5. Techniques employed for cancer detection

Various techniques are employed in the biomedical field for the detection of various cancers, out of which the two most widely employed are sentinel lymph node biopsy and photodynamic therapy. These techniques initially used to employ fluorescent dyes, but due to certain advantages of QDs over conventional dyes, QDs have replaced conventional dyes in these techniques. Here, we are giving a brief description of these two techniques.

5.1. Sentinel lymph node biopsy (SLNB)

A sentinel lymph node is the first lymph node to which cancer cells are most prone to metastasize from a primary tumor, and sentinel lymph node biopsy is a surgery that takes out the lymph node tissue to look for cancer in order to determine if a known cancer has spread from the original cancer site. This technique is a means of ultra-staging cancer metastasis and is now the standard in breast cancer surgery (Fig. 3).

It is based on targeting the first draining lymph node at the cancer site to determine the extent of disease spread. A negative SLNB result suggests that cancer has not

developed the ability to spread to nearby lymph nodes or any other organ, and a positive SLNB is an indication of the presence of cancer in other nearby lymph nodes and possibly to other organs as well. Current tracers for SLNB are blue dye and radioisotopes, but they have certain limitations, which can be overcome by the use of QDs that emit in the NIR range (700 nm - 900 nm), as light within this range has maximum depth of tissue penetration and least tissue autofluorescence interference (emission between 400 nm and 600 nm). Thus, the use of QDs overcomes the problem of background tissue autofluorescence, the main problem associated with live animal imaging [43].

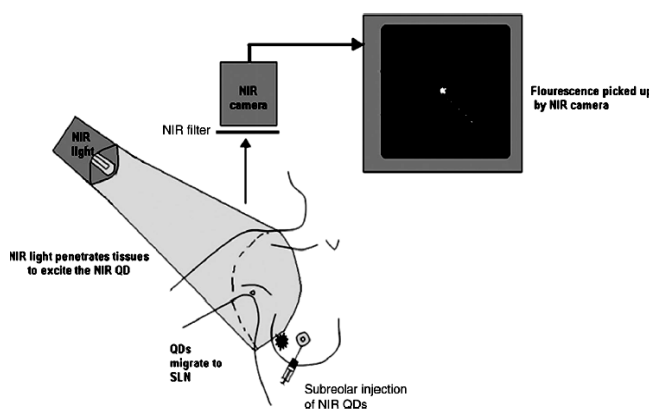


Fig. 3. Near infrared imaging system for SLNB in breast cancer surgery [44].

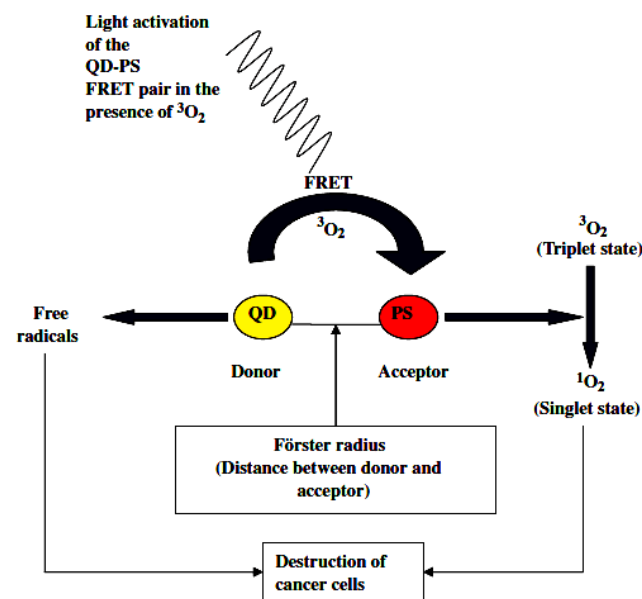


Fig. 4. Mechanism of PDT using quantum dots. Activation of a QD-PS FRET pair by light of a particular wavelength and generation of singlet oxygen which is toxic to cancerous cells and destroys tumor mass [44].

5.2. Photodynamic therapy (PDT)

PDT is considered to be one of the major advances in least invasive therapies for cancer treatment and is now being widely employed instead of surgery in treating various superficial malignancies, including basal cell skin carcinoma, oral, esophageal and lung cancers [44, 45]. This

is based on the destruction of diseased tissues via oxidation and degradation of cellular components using the cytotoxic singlet oxygen ($^1\text{O}_2$) generated from a non-toxic photosensitizer (PS) activated by light of a specific wavelength in the presence of molecular oxygen ($^3\text{O}_2$). Singlet oxygen leads to cellular necrosis and apoptosis of target cells (Fig. 4).

Higher quantum efficiency, greater photostability, high molar extinction coefficients and tunable emission spectra in the near infra red region make QDs ideal donors for the fluorescence resonance energy transfer (FRET) process in order to know the exact cancer site for specific targeted action [46].

6. Cancer detection using quantum dots

Earlier studies open new avenues for application of QDs as bioimaging tools and their applicability in multiplexed imaging by various researchers. Their photostability makes them ideal candidates for multicolor imaging and for studying various events in living cells. Fig. 5 shows the biological applications of quantum dots in imaging and in cellular tracking.

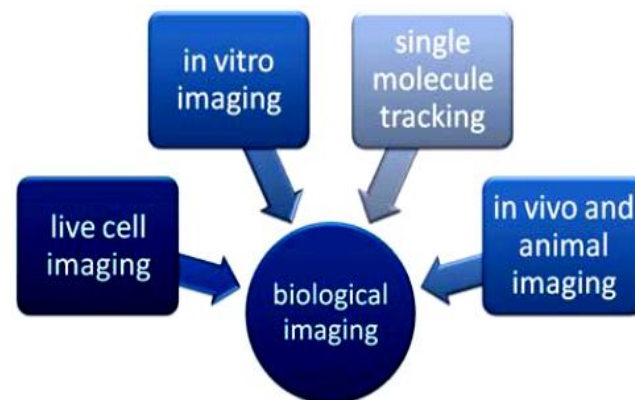


Fig. 5. Biomedical applications of quantum dots [47].

For the early and accurate cancer cells detection, use was made of dendrimer/QD nanocrystals (NCs) as an ECL signal probe for cancer cells [48]. This study is advantageous, since large numbers of CdSe/ZnS QDs were assembled onto the dendrimer NCs due to the many functional amine groups of NCs, which greatly amplifies QDs ECL signals. Targeting of blood vessels and cancer cells was done using QDs, wherein the surfaces were conjugated with specific peptides [49]. Earlier in 2004, QDs encapsulated with an ABC triblock copolymer proved the multiplexed fluorescence imaging of human prostate cancer biomarkers developing in mice due to the successful binding of the QD-antibody to tumor specific antigens [50]. QDs spontaneously endocytosed by HeLa cancer cells retained their bright fluorescence when mercaptoacetic acid-coated CdSe/ZnS QDs were covalently conjugated to the transferrin protein, indicating that QDs could be used as intracellular labels [51].

Folic acid (FA), an oxidized form of folate, shows a high binding affinity for folate receptors ($K_d \sim 10^{-10}$ M) [52]. An over-expression of the membrane associated folic acid receptor (FR) makes FA as a potential marker for a variety

of tumors, such as ovarian, prostate and breast cancers, since FR generally does not expressed in normal tissues but is over-expressed in these tumor cells [53]. The diagnosis of cancers in which FR is over-expressed was carried out [54] and the role of bovine serum albumin (BSA) as a bridge molecule to form FA-BSA-CdTe/ZnS QD conjugates for cancer diagnosis was elucidated. The greater selectivity of FA-BSA-QDs compared to only BSA coated QDs was concluded from this study.

Mucin 1 (MUC1), a glycoprotein, expressed on most epithelial cell surfaces, is considered to be a useful biomarker for the diagnosis of early cancers. Cheng *et al* designed A three-component DNA system (quencher, QD-labeled reporter and the MUC1 aptamer stem) was designed [55], where the role of the fluorescent QDs is to selectively detect the MUC1 peptide. A strong fluorescence was observed in the absence of the MUC1 peptide, but the fluorescence intensity decreased in its presence. This allowed the detection of MUC1 in the nanomolar range. Burkitt's lymphoma, an acute blood cell cancer, is the most common cancer in children in equatorial Africa [56], and the Ramos cell is a human Burkitt's lymphoma cell. An assay utilizing CdTe QDs for the sensitive qualitative and quantitative analysis of Ramos cells out of a mixture of various cancerous cells has been developed [57]. High fluorescence intensity was observed due to loading of large numbers of CdTe QDs tags on the surface of the Ramos cells and the formation of a DNA-CdTe QDs sheath.

6.1. Detection of lung cancer

Lung cancer has been ranked the No. 1 killer of all cancers. Only 15% of lung cancers are detected when they are localized, and the majority is diagnosed in the advanced stages of the disease, since there are few or no symptoms in the early stages of the disease. Hence, the early detection of lung cancer is highly desirable for improving survival from this disease. A new concept of detecting multiple cancer markers in a single sample was proposed by combining QD labels with enzyme labels for the simultaneous detection of three cancer markers in human serum with equal detection limits up to ng mL^{-1} level for the three markers. A multiplexed detection of the three lung cancer markers neuron-specific enolase (NSE), carcinoembryonic antigen (CEA) and cytokeratin fragment (Cyfra21-1) was achieved by coupling one QD label with two enzyme labels. This is considered to be a sensitive and selective method of detection of multiple targets, since no cross-reaction between the three cancer markers occurs when they are simultaneously detected [58].

A comparative study of the ability of quantum dots immunofluorescence histochemistry (QDs-IHC) and conventional immunohistochemistry (IHC) for the detection of caveolin-1 and PCNA in the lung cancer tissue microarray [59] concluded that both methods could precisely detect the expression of caveolin-1 and PCNA markers, but a higher sensitivity is obtained with QDs-IHC than with conventional IHC. In another work [60], the simultaneous detection of two lung cancer biomarkers (CEA and NSE) based on the use of dual-color QDs was carried out by employing two antibodies, two antigens and two detection antibodies, which on mixing formed sandwiched complexes in homogeneous solution. This was

followed by the addition of streptavidin coated polystyrene beads into the resultant system. Dual-color QDs with emission maxima at 525 and 655 nm were added which reacted with the detection antibodies. The results showed that CEA and NSE could be sensitively determined with equal detection limits upto the 1.0 ng mL^{-1} level. This method is advantageous, as the multiplex fluorescence could be achieved simultaneously for CEA and NSE, and the homogeneous antibody-antigen reaction made the whole detection simpler and efficient. Also, no cross-reaction is observed during the simultaneous detection using the above-mentioned QDs [60].

International standards divide lung cancer into two types: small cell lung cancer and non-small cell lung cancer (NSCLC). NSCLC accounts for approximately 85% of all cases of lung cancer and is a type of epithelial cancer [61]. Cytokeratins are intermediate filaments of the cytoskeleton that are specifically expressed in epithelial cells, considered to be protein markers for the detection of epithelial tumor cells [62]. Human lung-specific gene Lunx and surfactant protein-A (SP-A) have been employed as diagnostic markers for the detection of micrometastases in NSCLC patients [63,64]. A method for detecting lung cancer micrometastases in peripheral blood has been proposed [61] by synthesizing magnetic NPs over-coated with pan-cytokeratin (pan-ck) antibody and QDs over-coated with Lunx and SP-A antibodies. These doubly-labeled QDs were then utilized for the detection of lung cancer micrometastases in NSCLC patients.

6.2. Detection of breast cancer

Breast cancer (BC) is the second most common type of cancer and the fifth most common cause of cancer deaths in the US and the world. About 20%-30% breast cancer patients show over-expression of HER-2 (human epidermal growth factor receptor 2) in tumor cells [65,66]. Hereditary breast cancer is commonly due to an inherited mutation in the BRCA1 and BRCA2 genes. In normal cells, these genes help preventing cancer by making proteins that keep the cells away from growing abnormally. An inherited mutated copy of either gene from a parent raises the risk of developing breast cancer during the lifetime of a child. Hence, development of therapeutic techniques for breast cancer biomarkers is highly important for the treatment of breast cancer. Since anti-HER-2 antibodies inhibit the growth of HER-2-overexpressing breast cancer cells, it is considered to be the most effective therapy in HER-2-positive breast cancer patients, and nowadays it is being widely employed by generating various recombinant monoclonal antibodies like trastuzumab [10,67-69]. Immunohistochemistry (IHC) and fluorescence *in situ* hybridization (FISH) used to be considered the most widely employed techniques for detecting HER-2 in breast cancer patients [70], but, due to certain limitations of these two techniques, HER-2 detection using QDs based fluorescent probes has attracted much attention [71-81] in recent times. The applicability of QDs for detecting breast cancer biomarker HER-2 on the surface of breast cancer SK-BR-3 cells utilizing QD-535 and QD-630 has been proved [71]. The clinical application of QD-based technology for the quantitative determination of HER-2 expression in breast cancer tissues has been subsequently developed [82]. Later,

various research groups have worked upon and are still working on staining HER-2 overexpressing breast cancer cells using anti-HER-2 antibody conjugated QDs. A method for the early stage cancer diagnosis and imaging based on folate-decorated NPs of biodegradable polymers for QDs modification has been developed [52]. The *in vitro* cellular uptakes of these surface-modified QDs, as investigated by confocal laser scanning microscopy, proved that MCF-7 breast cancer cells are due to overexpression of folate receptors than to the cellular uptake by NIH 3T3 fibroblast cells which are of low expression of folate receptors [52]. Another QDs based breast cancer sensing [83] involved three kinds of antibodies: the first one, the capture antibody anti-Her2/neu, was used to capture the SK-BR3 breast cancer cells; the second antibody, the labeling antibody, anti-EpCAM, was used for labeling the captured SK-BR3 cells; and the third antibody, against anti-EpCAM, which was conjugated to QDs, was used for imaging the captured cells. These antibodies conjugated QDs proved to be promising candidates for the sensitive and specific imaging of cancer cells. The potentiality of QD-based immunofluorescent nanotechnology for the simultaneous imaging of HER-2 and estrogen receptor (ER) was explored by making use of CdSe/ZnS QDs conjugated with streptavidin (QD-SA) probes with an emission wavelength of 605 nm (605-QD-SA) and 545 nm (545-QD-SA), hence providing new insights into BC heterogeneity [84]. It was found that QD-IHC displays BC heterogeneity more sensitively than conventional IHC.

Virus-based NPs are also becoming popular nowadays in diagnostic techniques for the detection of tumors in the early stage. Work in this direction was initiated [85] by attaching QDs to HER-2 specific M13 bacteriophage antibodies for the detection of cancer lesions and cellular imaging, and by conjugating these HER-2 specific antibodies with end coat proteins of the phage to create HER-2 specific monoclonal antibodies. CdTe QDs attached to the phage displayed specific HER-2 antibodies to form a stable complex QD-Ab. The studies illustrated the value of HER-2 phage-QD complex as a useful cancer detection tool. An algorithm to assess the HER-2 status using QDs-based nanotechnology and spectral analysis by introducing a new parameter "total HER-2 load" [86] could be helpful in formulating a better targeted therapy for BC therapy.

6.3. Detection of prostate cancer

The most commonly diagnosed cancer and the second leading cause of cancer related deaths in American men is prostate cancer [87], which is now becoming an increasingly common cancer in some Asian and Eastern European countries as well, because of the adoption of the western lifestyle. In India, the prevalence is relatively low, but is increasing by 1% every year. The goal of early screening of prostate cancer is the hope that it can be treated more effectively.

Prostate stem cell antigen (PSCA), a cell surface antigen, predominantly expresses prostate specificity. Prostate-specific antigen (PSA) is made by both normal and cancerous cells in the prostate gland. It is mostly found in semen, but a small amount is also found in blood. The chances of developing prostate cancer increases as the PSA level raises. An extensive research has been carried out and

still continues in order to develop therapies for curing prostate cancer. Use of cys-diabodies, which are small, bivalent tumor targeting antibody fragments, has made possible the simultaneous detection of two tumor antigens on LNCaP/PSCA prostate cancer cells (which express PSCA and HER2) in culture using two immunoQdots (iQdots), anti-HER2 iQdot 655 and anti-PSCA iQdot 800, and by conjugating cys-diabodies specific for HER-2 as well as prostate stem cell antigen with amino polyethylene glycol (PEG) Qdot 800 [88]. Correlation and comparison of the results for the detection of PSCA obtained via QDs based immunolabeling and those obtained via conventional IHC concluded that QDs exhibit superior sensitivity for higher PSCA expression in prostate tissue than conventional IHC, along with greater long-term photostability, proving QDs to be better candidates for *in-vivo* imaging [89]. However, in an earlier study [90], the results of QD based immunolabeling were compared with those from the conventional immunohistochemical staining for detecting PSCA in bladder tumor tissues, and it was concluded that both methods show similar sensitivity in the PSCA expression correlated with tumor stage [90]. Biosensing technology called surface plasmon-coupled emission (SPCE) is based on surface plasmon resonance (an optical detection process based on the absorption of light by a thin metal film when a polarized light hits a prism covered by the thin metal layer). The ZnS-capped CdSe QDs enhanced SPCE technique was used for the detection of prostate specific antigen (PSA) by conjugating QDs with PSA antibodies and by using a 405 nm wavelength laser in order to excite emission of QDs-labeled PSA antibodies. The limit of detection of PSA achieved by this technique was reported as 10 fg mL^{-1} [91].

E-cadherin, considered to be a principal mediator of cell-cell adhesion in epithelial tissues, has been extensively studied to determine its role in cancer metastasis. The loss of E-cadherin expression or function is linked to increased invasive potential [92], metastatic potential [93] and poorer disease diagnosis [94, 95]. A comparative study of the adhesion mechanisms in both healthy and cancerous epithelial cells was carried out [96] by utilizing the scanning near-field optical microscopy technique in conjunction with quantum dot labeling and the differences were studied both morphologically and phenotypically in healthy and cancerous cells. It was found that E-cadherin is predominantly located around the cell periphery and within filopodial extensions in healthy prostate epithelial cells (PNT2), whereas no E-cadherin labeling was found around the periphery of the cells in metastatic prostate adenocarcinoma cells (PC-3).

6.4. Detection of colorectal cancer

Colorectal cancer (CRC) is a term used to represent cancer that develops in the colon or the rectum, but, depending on where it starts, it is referred to separately as colon cancer or rectal cancer. CRC is the second most common cause of cancer related deaths worldwide [97] and the metastases derived from CRC are responsible for such cancer-related deaths [98]. In order to detect circulating colorectal cancer cells, an immunoassay developed [99] by making use of magnetic beads coupled with epithelial cell adhesion molecule (EpCAM) antibody and monoclonal cytokeratin

19 (CK19) antibody could separate the circulating tumor cells from body fluids. The formed complexes were then tagged with streptavidin-conjugated QDs and the fluorescent signal of QDs confirmed the detection of circulating tumor cells surface antigens.

6.5. Targeting and imaging melanoma

Melanoma, a type of skin cancer is the third and most deadly skin cancer which begins in melanocytes, but can also begin in other pigmented tissues like in the eye or in the intestines [100] and accounts for about 75% of skin cancer deaths worldwide [101, 102]. Although, compared to other skin cancers, melanoma is less common; it is much more dangerous and causes the majority of deaths related to skin cancer. Therefore, a method of melanoma targeting and imaging is very important for its early prognosis and effective therapy. Melanoma can often be detected early when it is most likely to be cured. In the direction of early detection of melanoma, extensive research has been done on the applicability of QDs, and this has been worked upon [103] with the utilization of dendrimers functionalized nonmaterial. Dendrimers are repetitively branched polymers and highly ordered structures which, when coated over the NP surfaces, result in an alteration in the charge, functionality, stability and reactivity of NPs. Biocompatibility and cellular uptake of NPs are exclusively enhanced when modified with dendrimers [104-106]. CdSe QDs surface modified with polyamidoamine dendrimers [107] were conjugated with arginine-glycine-aspartic acid peptides. These modified QDs were water-soluble with high quantum yield and good biocompatibility specifically used to target human umbilical vein endothelial cells (HUVEC) and A375 melanoma cells and exhibited great potential in tumor prognosis and therapy. Human melanoma cell adhesion molecule CD146 is overexpressed on the surface of melanoma cells. Highly fluorescent PEG-capped CdSe/ZnS QDs [108] were synthesized, and melanoma detection was demonstrated by conjugating these QDs with streptavidin (QD-SA) and linking QD-SA with biotinylated goat anti-mouse IgG and mouse anti-human CD146 to label CD146 overexpressed on live and fixed cells. Labeled cells were highly bright and with high photostability, which made possible their easy detection. In order to mimic the *in vivo* tumor environment for evaluating the target specificity of polymer coated QDs, a coculture system consisting of cancer cells mixed with normal cells was developed [109], and the specificity of melanoma antibody-conjugated QDs for melanoma cells rather than melanocytes in the coculture model was proved. A surface antigen ganglioside (GLS) is known in melanoma cells [110] which is not expressed in normal cells but can be expressed in melanoma cells and the extent of GLS expression in melanoma cells depends on the extent of metastasis [111]. Thus, in order to develop an early diagnostic probe of melanoma, the human malignant melanoma ganglioside single-chain antibody (ScFv) was chosen and an anti-human melanoma ganglioside single chain antibody-CdTe QD nanoprobe was developed [112], and the specificity of the nanoprobe for only the melanoma cells was proved by comparing its affinity for human stomach cancer cells and melanoma cells.

Cancer stem cells (CSCs) possess a high potential of differentiation and are more resistant to chemotherapy than non-stem cells. The effect of QDs on the expression of two plasma membrane associated glycoproteins CD44 and CD133, which are considered to be common markers of CSCs [113] in the expression of four different cancerous cells glioblastoma, melanoma, pancreatic and prostate adenocarcinoma, were studied [114] and a positive response for both the markers was found in case of melanoma cells only, while all others were positive only for CD44.

6.6. Imaging pancreatic cancer

The fourth leading cause of cancer related deaths in the United States is considered to be pancreatic cancer with the mean survival rate estimated to be 6 months and less than 5% of all patients diagnosed with pancreatic cancer survive beyond five years [115, 116], mainly due to lack of specific symptoms, as a result of which the disease is diagnosed after reaching an advanced stage [117]. Thus, the only way to increase the survival rate of this disease is by developing novel bioimaging probes which would specifically diagnose pancreatic cancer *in vivo* at the earliest stage without producing any systemic toxicity. For expressing pancreatic cancer cells such as Mia-PaCa, cadmium free InP QDs which possess greater optical stability and no leakage of the toxic ions in biological systems were chosen [118] and mercaptosuccinic-coated InP/ZnS QDs conjugated with antibodies such as anticlaudin 4 and anti-PSCA whose corresponding antigen receptors are known to be overexpressed in both primary and metastatic pancreatic cancer [119-121] were constructed. A method of synthesizing lysine-coated Mn doped CdTeSe/CdS QDs conjugated with monoclonal and polyclonal antibodies with excellent quantum yield has been reported [122]. The Mn species induces magnetism in these QDs. The successful labeling of QD bioconjugates in pancreatic cancer cells such as Panc-1 and MiaPaCa has been shown, which is further helpful in the development of nanoprobe for *in vivo* imaging and therapeutic applications [122].

The applicability of tetraiodothyroacetic acid (tetrac), a thyroid hormone antagonist and anti-proliferative agent, in the treatment of human pancreatic cancer by conjugating PEG-QDs to tetrac has been discussed [123]. A higher level of cellular entry of PEG-QDs (tetrac-PEG-QDs) into pancreatic cancer (PANC-1) cells than the unconjugated PEG-QDs was found.

6.7. Detection of cancer marker type IV collagenase

Type IV collagenase, an extracellular neutral metalloprotease, is involved in tumor invasion and metastasis [124-126]. Alongwith the degradation of type IV collagen (major component of cell membranes), it can degrade type 3, 5 collagen and gelatin. This compelled researchers to develop a rapid, selective and sensitive method for the determination of type IV collagenase for early diagnosis of type IV collagenase-relevant diseases. Conventionally applied methods like gelatin zymography and enzyme linked immunosorbent assay (ELISA) are not often employed for monitoring the activity of type IV collagenase due to their limitations as a multiplexed and a

high-throughput process [127]. A QDs-based FRET biosensor was successfully applied for the detection of the cancer marker type IV collagenase [128] in order to resolve the abovesaid limitations, and it was found to be a much more sensitive and selective method too. This was done by linking peptide between the donors luminescent QDs and small sized acceptor-gold nanoparticles (SAuNPs). After the addition of type IV collagenase to the system, the SAuNPs could detach from QDs because the enzyme cleaves the peptide leading to the disappearance of FRET which allowed the fluorescence of the QDs to return. The enzymatic activity of type IV collagenase was related to the PL change of QDs-based FRET probes and the concentration of type IV collagenase was determined with a detection limit of 18 ng mL^{-1} [128].

6.8. Detection of thyroid carcinoma antigen

The specificity of the JT-95 antibody, which belongs to the class of immunoglobulin M (IgM) group, for detecting thyroid carcinomas antigen has been reported [129,130], and a new detection system has been built by the combination QDs and JT-95 antibody in microscopic analysis, western blotting analysis and ELISA-like system. The possibility of even IgM antibodies to be applicable to the detection system with QDs, which are usually neglected as detection tools due to their lower affinity (dissociation constant $> 10^{-5} \text{ M}$), has also been proved. An effective application of luminescent surface modified CdSe QDs conjugated with the IgM antibody to recognize the associated thyroid carcinoma antigen has been reported [131], and it was possible to quantify the antigen in the range of $1.56\text{-}100 \mu\text{g mL}^{-1}$. Thus, the feasibility of labeling of JT95 and other IgM class antibodies with QDs further proves the applicability of IgM antibodies in the diagnosis of cancers [131].

7. Conclusion

Various researches carried out using quantum dots prove the applicability of QDs as promising diagnostic tools for the early and accurate detection of tumor cells, multiplexed tissue, intracellular imaging, and immunohistochemistry. Due to their advantages, such as single source excitation, narrow emission, high quantum yield, long fluorescence time and high photostability, bioconjugated-QDs have now replaced the conventionally used organic fluorescent dyes in various tumor targeting and imaging applications. The major problem associated with QDs is their toxicity and hydrophobicity, which hinders their applicability in biological systems and the biomedical field. These problems are overcome by using non-cadmium based QDs such as InP QDs and carrying out surface passivation. Recent developments in the field of QDs therefore generate a hope for the early detection of cancer cells. This is due to their encapsulation using polymers, conjugation with various biomolecules and antibodies, thereby making them suitable for targeting specific cancerous cells. Therefore, the high fluorescence of QDs in comparison to other detection methods and their unique size-dependent optical properties can be explored in the design and development of highly sensitive molecular imaging tools for *in vivo* imaging and therapeutic applications.

8. Future perspectives

Our ultimate goal is to convert QD technology back into clinical diagnostic purposes. QDs have proved to be excellent fluorescent bio-probes in biological and biomedical research. Their properties render them to be used for *in vivo* and *in vitro* molecular and cellular imaging and lead to major advances in cancer detection and diagnosis, and image-guided drug delivery of chemotherapeutic agents. QDs have replaced the current tracers in SLNB, and are employed as photosensitizers in PDT. Although QD technology is still not in much use due to their hydrophobicity, toxicity and many issues need to be solved in order to apply them safely in clinical medicine and assays for targeting, imaging and drug delivery. However, there is still a hope for further improvements in enabling their applications as more sensitive, qualitative and quantitative tools for measurements of population of cancerous cells, in targeting and localizing metastasis, improving signal intensity, and tracking drug delivery in live tissues. QD technology can prove to be a simple, rapid and successful platform for the early and sensitive prognosis of cancer biomarkers with great precision and accuracy, and hence anti-cancer therapies in future in order to completely eradicate cancer.

Abbreviations

BC Breast cancer, **BRET** Bioluminescence resonance energy transfer, **BSA** Bovine serum albumin, **CRC** Colorectal cancer, **CSCs** Cancer stem cells, **ELISA** Enzyme linked immunosorbent assay, **ER** Estrogen receptor, **FA** Folic acid, **FISH** Fluorescence *in situ* hybridization, **FR** Folic acid receptor, **FRET** Fluorescence resonance energy transfer, **GLS** Ganglioside, **IgG** Immunoglobulin G, **IgM** Immunoglobulin M, **IHC** Immunohistochemistry, **iQdots** ImmunoQdots, **MUC1** Mucin 1, **NPs** Nanoparticles, **NSCLC** Non-small cell lung cancer, **PDT** Photodynamic therapy, **PEG** Polyethylene glycol, **PS** Photosensitizer, **QDs** Quantum dots, **QDs-IHC** Quantum dots Immunofluorescence histochemistry, **SLNB** Sentinel lymph node biopsy, **SPCE** Surface plasmon-coupled emission, **SAuNPs** Small sized acceptor-gold nanoparticles, **TSGs** Tumor suppressor genes.

Acknowledgements

PM thanks the Council for Scientific and Industrial Research (CSIR), New Delhi, for a Senior Research Fellowship (Grant No. 09/045(0873)/2009 EMR-I). SG thanks the University Grants Commission (UGC), New Delhi, for a Junior Research Fellowship (Grant No. 20-06/2010(i)EU-IV).

Reference

1. Bohunicky, B.; Mousa, S. A.; *Nanotechnol. Sci. Appl.* **2011**, *4*, 1.
DOI: [10.2147/NSA.S13465](https://doi.org/10.2147/NSA.S13465)
2. Sieger, R.; Naishadham, D.; Jemal, A.; *CA: Cancer. J. Clin.* **2012**, *62*, 10.
DOI: [10.3322/caac.20138](https://doi.org/10.3322/caac.20138)
3. Bhatt, A. N.; Mathur, R.; Farooque, A.; Verma, A.; Dwarakanath, B. S.; *Indian. J. Med. Res.* **2010**, *132*, 129.
4. Farrell, W. E.; Clayton, R. N.; *Endocr. Relat. Cancer.* **2003**, *10*, 323.
DOI: [10.1677/erc.0.0100323](https://doi.org/10.1677/erc.0.0100323)
5. Stirzaker, C.; Millar, D. S.; Paul, C. L.; Warnecke, P. M.; Harrison, J.; Vincent, P. C.; Frommer, M.; Clark, S. J.; *Cancer Res.* **1997**, *57*, 2229.
6. Greger, V.; Debus, N.; Lohmann, D.; Höpping, W.; Passarge, E.; Horsthemke, B.; *Hum. Genet.* **1994**, *94*, 491.
7. Ford, D.; Easton, D. F.; Stratton, M.; Narod, S.; Goldgar, D.; Devilee, P.; Bishop, D. T.; Weber, B.; Lenoir, G.; Chang-Claude, J.; Sobol, H.; Teare, M. D.; Struwing, J.; Arason, A.; Scherneck, S.; Peto, J.; Rebbeck, T. R.; Tonin, P.; Neuhausen, S.; Barkardottir, R.; Eyfjord, J.; Lynch, H.; Ponder, B. A. J.; Gayther, S. A.; Birch, J. M.;

- Lindblom, A.; Stoppa-Lyonnet, D.; Bignon, Y.; Borg, A.; Hamann, U.; Haites, N.; Scott, R. J.; Maugard, C. M.; Vasen, H.; Seitz, S.; Cannon-Albright, L. A.; Schofield, A.; Zelada-Hedman, M.; *Am. J. Hum. Genet.* **1998**, *62*, 676.
8. Miki, Y.; Swensen, J.; Shattuck-Eidens, D.; Futreal, P. A.; Harshman, K.; Tavtigian, S.; Liu, Q.; Cochran, C.; Bennett, L. M.; Ding, W.; Bell, R.; Rosenthal, J.; Hussey, C.; Tran, T.; McClure, M.; Frye, C.; Hattier, T.; Phelps, R.; Haugen-Strano, A.; Katcher, H.; Yakumo, K.; Gholami, Z.; Shaffer, D.; Stones, S.; Bayer, S.; Wray, C.; Bogden, R.; Dayananth, P.; Ward, J.; Tonin, P.; Narod, S.; Bristow, P. M.; Norris, F. H.; Helvering, L.; Morrison, P.; Rosteck, P.; Lai, M.; Barrett, J. C.; Lewis, C.; Neuhausen, S.; Cannon-Albright, L.; Goldgar, D.; Wiseman, R.; Kamb, A.; Skolnick, M. H.; *Science.* **1994**, *266*, 66.
DOI: [10.1126/science.7545954](https://doi.org/10.1126/science.7545954)
9. Mansoori, G. A.; Mohazzabi, P.; McCormack, P.; Jabbari, S.; *World. Rev. Sci. Tech. Sustain. Dev.* **2007**, *4*, 226.
DOI: [10.1504/WRSTSD.2007.013584](https://doi.org/10.1504/WRSTSD.2007.013584)
10. Liberato, N. L.; Marchetti, M.; Barosi, G.; *J. Clin. Oncol.* **2007**, *25*, 625.
DOI: [10.1200/JCO.2006.06.4220](https://doi.org/10.1200/JCO.2006.06.4220)
11. National Cancer Institute at the National Institutes of Health: National Dictionary of Cancer Terms.
<http://www.cancer.gov/dictionary?cdrid=45618>
12. National Comprehensive Cancer Network, NCCN Guidelines for Patients: Biomarkers and Targeted Therapy
http://www.nccn.com/index.php?option=com_content&view=article&id=927:biomarkers-and-targeted-therapy&catid=56
13. Tothill, I. E.; *Semin. Cell. Dev. Bio.* **2009**, *29*, 55.
DOI: [10.1016/j.semcdb.2009.01.015](https://doi.org/10.1016/j.semcdb.2009.01.015)
14. Smith, D. S.; Humphrey, P. A.; Catalona, W. J.; *Cancer.* **1997**, *80*, 1852.
DOI: [10.1002/\(SICI\)1097-0142\(199711\)80:9<1852](https://doi.org/10.1002/(SICI)1097-0142(199711)80:9<1852)
15. Meyer, T.; Rustin, G. J. S.; *Brit. J. Cancer.* **2000**, *82*, 1535.
DOI: [10.1054/bjoc.2000.1174](https://doi.org/10.1054/bjoc.2000.1174)
16. Vashist, S. A.; Tewari, R.; Bajpai, R. P.; Bharadwaj, L. M.; Raiteri, R.; *Journal of Nanotechnology* online. **2006**.
DOI: [10.2240/azojono0113](https://doi.org/10.2240/azojono0113)
17. Smith, A. M.; Dave, S.; Nie, S.; True, L.; Gao, X.; *Expert Rev. Mol. Diagn.* **2006**, *6*, 231.
DOI: [10.1586/14737159.6.2.231](https://doi.org/10.1586/14737159.6.2.231)
18. Ghasemi, Y.; Peymani, P.; Afifi, S.; *Acta Biomed.* **2009**, *80*, 156.
19. Niemeyer, C. M.; *Angew. Chem. Int. Ed. Engl.* **2001**, *40*, 4128.
DOI: [10.1002/1521-3773\(200111\)40:22<4128](https://doi.org/10.1002/1521-3773(200111)40:22<4128)
20. Alivisatos, A. P.; *Science.* **1996**, *271*, 933.
DOI: [10.1126/science.271.5251.933](https://doi.org/10.1126/science.271.5251.933)
21. Han, M.; Gao, X.; Su, J. Z.; Nie, S.; *Nat. Biotechnol.* **2001**, *19*, 631.
DOI: [10.1038/90228](https://doi.org/10.1038/90228)
22. Gao, X.; Nie, S.; *J. Phys. Chem. B.* **2003**, *107*, 11575.
DOI: [10.1021/jp0308110](https://doi.org/10.1021/jp0308110)
23. Gao, X.; Nie, S.; *Anal. Chem.* **2004**, *76*, 2406.
DOI: [10.1021/ac0354600](https://doi.org/10.1021/ac0354600)
24. Resch-Genger, U.; Grabolle, M.; Cavaliere-Jaricot, S.; Nitschke, R.; Nann, T.; *Nature Methods*, **2008**, *5*, 763.
DOI: [10.1038/NMETH.1248](https://doi.org/10.1038/NMETH.1248)
25. Veerananarayanan, S.; Poulouse, A. C.; Mohamed, M. S.; Nagaoka, Y.; Iwai, S.; Nakagame, Y.; Kashiwada, S.; Yoshida, Y.; Maekawa, T.; Kumar, D. S.; *Int. J. Nanomedicine.* **2012**, *7*, 3769.
DOI: [10.2147/IJN.S31310](https://doi.org/10.2147/IJN.S31310)
26. Chan, W. C. W.; Maxwell, D. J.; Gao, X.; Bailey, R. E.; Han, M.; Nie, S.; *Curr. Opin. Biotechnol.* **2002**, *13*, 40.
DOI: [10.1016/S0958-1669\(02\)00282-3](https://doi.org/10.1016/S0958-1669(02)00282-3)
27. Frasco, M. F.; Chaniotakis, N.; *Sensors* **2009**, *9*, 7266.
DOI: [10.3390/s90907266](https://doi.org/10.3390/s90907266)
28. Fountaine, T. J.; Wincovitch, S. M.; Geho, D. H.; Garfield, S. H.; Pittaluga, S.; *Mod. Pathol.* **2006**, *19*, 1181.
DOI: [10.1038/modpathol.3800628](https://doi.org/10.1038/modpathol.3800628)
29. Gao, X.; Chan, W. C.; Nie, S.; *J. Biomed. Opt.* **2002**, *7*, 532.
DOI: [10.1117/1.1506706](https://doi.org/10.1117/1.1506706)
30. Bentolila, L. A.; Ebenstein, Y.; Weiss, S.; *J. Nucl. Med.* **2009**, *50*, 493.
DOI: [10.2967/jnumed.108.053561](https://doi.org/10.2967/jnumed.108.053561)
31. Xing, Y.; Rao, J.; *Cancer Biomarkers.* **2008**, *4*, 307.
32. Chan, W. C. W.; Maxwell, D. J.; Gao, X.; Bailey, R. E.; Han, M.; Nie, S.; *Curr. Opin. Biotechnol.* **2002**, *13*, 40.
33. Wu, X.; Liu, H.; Liu, J.; Haley, K. N.; Treadway, J. A.; Larson, J. P.; Ge, N.; Peale, F.; Bruchez, M. P.; *Nat. Biotechnol.* **2003**, *21*, 41.
DOI: [10.1038/nbt764](https://doi.org/10.1038/nbt764)
34. Alivisatos, A. P.; Gu, W.; Larabell, C.; *Annu. Rev. Biomed. Eng.* **2005**, *7*, 55.
DOI: [10.1146/annurev.bioeng.7.060804.100432](https://doi.org/10.1146/annurev.bioeng.7.060804.100432)
35. Ross, J. S.; Hatzis, C.; Symmans, W. F.; Pusztai, L.; Hortobágyi, G. N.; *Oncologist.* **2008**, *13*, 477.
DOI: [10.1634/theoncologist.2007-0248](https://doi.org/10.1634/theoncologist.2007-0248)
36. Medintz, I. L.; Uyeda, H. T.; Goldman, E. R.; Mattoussi, H.; *Nat. Mater.* **2005**, *4*, 435.
DOI: [10.1038/nmat1390](https://doi.org/10.1038/nmat1390)
37. Dubois, F.; Mahler, B.; Dubertret, B.; Doris, E.; Mioskowski, C.; *J. Am. Chem. Soc.* **2007**, *129*, 482.
DOI: [10.1021/ja067742y](https://doi.org/10.1021/ja067742y)
38. Alivisatos, P.; *Nat. Biotechnol.* **2004**, *22*, 47.
DOI: [10.1038/nbt927](https://doi.org/10.1038/nbt927)
39. Schlamp, M. C.; Peng, X.; Alivisatos, A. P.; *J. Appl. Phys.* **1997**, *82*, 5837.
DOI: [org/10.1063/1.366452](https://doi.org/10.1063/1.366452)
40. Wang, J.; Han, S.; Ke, D.; Wang, R.; *J. Nanomater.* **2012**, *2012*, 129041.
DOI: [10.1155/2012/129041](https://doi.org/10.1155/2012/129041)
41. Tiwari, A.; Mishra, A. K.; Kobayashi, H.; A.P.F. Turner (Ed.), *Intelligent Nanomaterials.* WILEY-Scrivener Publishing LLC, USA. **2012**, pp 16-17.
ISBN: [978-04-709387-99](https://doi.org/978-04-709387-99).
42. Klostranec, J. M.; Chan, W. C. W.; *Adv. Mater.* **2006**, *18*, 1953.
DOI: [10.1002/adma.200500786](https://doi.org/10.1002/adma.200500786)
43. Kim, S.; Lim, Y. T.; Soltesz, E. G.; De Grand, A. M.; Lee, J.; Nakayama, A.; Parker, J. A.; Mihaljevic, T.; Laurence, R. G.; Dor, D. M.; Cohn, L. H.; Bawendi, M. G.; Frangioni, J. V.; *Nat. Biotechnol.* **2004**, *22*, 93.
DOI: [10.1038/nbt920](https://doi.org/10.1038/nbt920)
44. Rizvi, S. B.; Ghaderi, S.; Keshtgar, M.; Seifalian, A. M.; *Nano. Rev.* **2010**, *1*, 1.
DOI: [10.3402/nano.v1i0.5161](https://doi.org/10.3402/nano.v1i0.5161)
45. Hopper, C.; *Lancet Oncol.* **2000**, *1*, 212.
DOI: [10.1016/S1470-2045\(00\)00166-2](https://doi.org/10.1016/S1470-2045(00)00166-2)
46. Yaghini, E.; Seifalian, A. M.; MacRobert, A. J.; *Nanomedicine.* **2009**, *4*, 353.
DOI: [10.2217/nmm.09.9](https://doi.org/10.2217/nmm.09.9)
47. Drbholavova, J.; Adam, V.; Kizek, R.; Hubalek, J.; *Int. J. Mol. Sci.* **2009**, *10*, 656.
DOI: [10.3390/ijms10020656](https://doi.org/10.3390/ijms10020656)
48. Jie, G.; Wang, L.; Yuan, J.; Zhang, S.; *Anal. Chem.* **2011**, *83*, 3873.
DOI: [10.1021/ac200383z](https://doi.org/10.1021/ac200383z)
49. Åkerman, M. E.; Chan, W. C. W.; Laakkonen, P.; Bhatia, S. N.; Ruoslahti, E.; *P. Natl. Acad. Sci. USA.* **2002**, *99*, 12617.
DOI: [10.1073/pnas.152463399](https://doi.org/10.1073/pnas.152463399)
50. Gao, X.; Cui, Y.; Levenson, R. M.; Chung, L. W. K.; Nie, S.; *Nat. Biotechnol.* **2004**, *22*, 969.
DOI: [10.1038/nbt994](https://doi.org/10.1038/nbt994)
51. Chan, W. C. W.; Nie, S.; *Science.* **1998**, *281*, 2016.
DOI: [10.1126/science.281.5385.2016](https://doi.org/10.1126/science.281.5385.2016)
52. Pan, J.; Feng, S. -S.; *Biomaterials.* **2009**, *30*, 1176.
DOI: [10.1016/j.biomaterials.2008.10.039](https://doi.org/10.1016/j.biomaterials.2008.10.039)
53. Weitman, S. D.; Weinberg, A. G.; Coney, L. R.; Zurawski, V. R.; Jennings, D. S.; Kamen, B. A.; *Cancer Res.* **1992**, *52*, 6708.
54. Meng, H.; Chen, J. -Y.; Mi, L.; Wang, P. -N.; Ge, M. -Y.; Yue, Y.; Dai, N.; *J. Biol. Inorg. Chem.* **2011**, *16*, 117.
DOI: [10.1007/s00775-010-0709-z](https://doi.org/10.1007/s00775-010-0709-z)
55. Cheng, A. K. H.; Su, H.; Wang, Y. A.; Yu, H. -Z.; *Anal. Chem.* **2009**, *81*, 6130.
DOI: [10.1021/ac901223q](https://doi.org/10.1021/ac901223q)
56. Rochford, R.; Cannon, M. J.; Moormann, A. M.; *Nat. Rev. Microbiol.* **2005**, *3*, 182.
DOI: [10.1038/nrmicro1089](https://doi.org/10.1038/nrmicro1089)
57. Zhong, H.; Zhang, Q.; Zhang, S.; *Chem. Eur. J.* **2011**, *17*, 8388.
DOI: [10.1002/chem.201003585](https://doi.org/10.1002/chem.201003585)
58. Li, H.; Cao, Z.; Zhang, Y.; Lau, C.; Lu, J.; *Anal. Methods.* **2010**, *2*, 1236.
DOI: [10.1039/C0AY00284D](https://doi.org/10.1039/C0AY00284D)
59. Chen, H.; Xue, J.; Zhang, Y.; Zhu, X.; Gao, J.; Yu, B.; *J. Mol. Histol.* **2009**, *40*, 261.
DOI: [10.1007/s10735-009-9237-y](https://doi.org/10.1007/s10735-009-9237-y)
60. Li, H.; Cao, Z.; Zhang, Y.; Lau, C.; Lu, J.; *Analyst.* **2011**, *136*, 1399.
DOI: [10.1039/C0AN00704H](https://doi.org/10.1039/C0AN00704H)

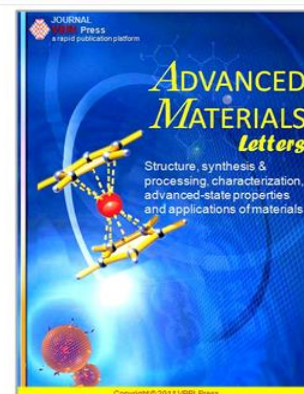
61. Wang, Y.; Zhang, Y.; Du, Z.; Wu, M.; Zhang, G.; *Int. J. Nanomed.* **2012**, *7*, 2315.
DOI: [10.2147/IJN.S30593](https://doi.org/10.2147/IJN.S30593)
62. Pantel, K.; Brakenhoff, R. H.; *Nat. Rev. Cancer.* **2004**, *4*, 448.
DOI: [10.1038/nrc1370](https://doi.org/10.1038/nrc1370)
63. Mitas, M.; Hoover, L.; Silvestri, G.; Reed, C.; Green, M.; Turrisi, A. T.; Sherman, C.; Mikhitarian, K.; Cole, D. J.; Block, M. I.; Gillanders, W. E.; *J. Mol. Diagn.* **2003**, *5*, 237.
64. Betz, C.; Papadopoulos, T.; Buchwald, J.; Buchwald, J.; Dämmrich, J.; Müller-Hermelink, H. K.; *Cancer Res.* **1995**, *55*, 4283.
65. Slamon, D. J.; Clark, G. M.; Wong, S. G.; Levin, W. J.; Ullrich, A.; McGuire, W. L.; *Science.* **1987**, *235*, 177.
DOI: [10.1126/science.3798106](https://doi.org/10.1126/science.3798106)
66. Slamon, D. J.; Godolphin, W.; Jones, L. A.; Holt, J. A.; Wong, S. G.; Keith, D. E.; Levin, W. J.; Stuart, S. G.; Udove, J.; Ullrich, A.; *Science.* **1989**, *244*, 707.
DOI: [10.1126/science.2470152](https://doi.org/10.1126/science.2470152)
67. Cobleigh, M. A.; Vogel, C. L.; Tripathy, D.; Robert, N. J.; Scholl, S.; Fehrenbacher, L.; Wolter, J. M.; Paton, V.; Shak, S.; Lieberman, G.; Slamon, D. J.; *J. Clin. Oncol.* **1999**, *17*, 2639.
68. Hudis, C. A.; *N. Engl. J. Med.* **2007**, *357*, 39.
DOI: [10.1056/NEJMra043186](https://doi.org/10.1056/NEJMra043186)
69. Gayther, S. A.; Mangion, J.; Russell, P.; Seal, S.; Barfoot, R.; Ponder, B. A. J.; Stratton, M. R.; Easton, D.; *Nat. Genet.* **1997**, *15*, 103.
DOI: [10.1038/ng0197-103](https://doi.org/10.1038/ng0197-103)
70. Jimenez, R. E.; Wallis, T.; Tabasczka, P.; Visscher, D. W.; *Modern Pathol.* **2000**, *13*, 37.
DOI: [10.1038/modpathol.3880007](https://doi.org/10.1038/modpathol.3880007)
71. Wu, X.; Liu, H.; Liu, J.; Haley, K. N.; Treadway, J. A.; Larson, J. P.; Ge, N.; Peale, F.; Bruchez, M. P.; *Nat. Biotechnol.* **2003**, *21*, 41.
DOI: [10.1038/nbt764](https://doi.org/10.1038/nbt764)
72. Li-Shishido, S.; Watanabe, T. M.; Tada, H.; Higuchi, H.; Ohuchi, N.; *Biochem. Biophys. Res. Commun.* **2006**, *351*, 7.
DOI: [10.1016/j.bbrc.2006.09.159](https://doi.org/10.1016/j.bbrc.2006.09.159)
73. Tada, H.; Higuchi, H.; Watanabe, T. M.; Ohuchi, N.; *Cancer Res.* **2007**, *67*, 1138.
DOI: [10.1158/0008-5472.CAN-06-1185](https://doi.org/10.1158/0008-5472.CAN-06-1185)
74. Watanabe, T. M.; Higuchi, H.; *Biophys. J.* **2007**, *92*, 4109.
DOI: [10.1529/biophysj.106.094649](https://doi.org/10.1529/biophysj.106.094649)
75. Yu, W. W.; Chang, E.; Falkner, J. C.; Zhang, J.; Al-Somali, A. M.; Sayes, C. M.; Johns, J.; Drezek, R.; Colvin, V. L.; *J. Am. Chem. Soc.* **2007**, *129*, 2871.
DOI: [10.1021/ja067184n](https://doi.org/10.1021/ja067184n)
76. Xing, Y.; Chaudry, Q.; Shen, C.; Kong, K. Y.; Zhau, H. E.; Chung, L. W.; Petros, J. A.; O'Regan, R. M.; Yezhelyev, M. V.; Simons, J. W.; Wang, M. D.; Nie, S.; *Nat. Protoc.* **2007**, *2*, 1152.
DOI: [10.1038/nprot.2007.107](https://doi.org/10.1038/nprot.2007.107)
77. Takeda, M.; Tada, H.; Higuchi, H.; Kobayash, Y.; Kobayash, M.; Sakurai, Y.; Ishida, T.; Ohuchi, N.; *Breast Cancer.* **2008**, *15*, 145.
DOI: [10.1007/s12282-008-0037-0](https://doi.org/10.1007/s12282-008-0037-0)
78. Xiao, Y.; Gao, X.; Gannot, G.; Emmert-Buck, M. R.; Srivastava, S.; Wagner, P. D.; Amos, M. D.; Barker, P. E.; *Int. J. Cancer.* **2008**, *122*, 2178.
DOI: [10.1002/ijc.23320](https://doi.org/10.1002/ijc.23320)
79. Yang, L.; Mao, H.; Wang, Y. A.; Cao, Z.; Peng, X.; Wang, X.; Duan, H.; Ni, C.; Yuan, Q.; Adams, G.; Smith, M. Q.; Wood, W. C.; Gao, X.; Nie, S.; *Small.* **2009**, *5*, 235.
DOI: [10.1002/smll.200800714](https://doi.org/10.1002/smll.200800714)
80. Zdobnova, T. A.; Dorofeev, S. G.; Tananaev, P. N.; Vasiliev, R. B.; Balandin, T. G.; Edelweiss, E. F.; Stremovskiy, O. A.; Balalaeva, I. V.; Turchin, I. V.; Lebedenko, E. N.; Zlomanov, V. P.; Deyev, S. M.; *J. Biomed. Opt.* **2009**, *14*, 021004.
DOI: [10.1117/1.3122775](https://doi.org/10.1117/1.3122775)
81. Xiao, Y.; Gao, X.; Maragh, S.; Telford, W. G.; Tona, A.; *Clin. Chem.* **2009**, *55*, 1307.
DOI: [10.1373/clinchem.2008.120576](https://doi.org/10.1373/clinchem.2008.120576)
82. Chen, C.; Peng, J.; Xia, H. -S.; Yang, G. -F.; Wu, Q. -S.; Chen, L. -D.; Zeng, L. -B.; Zhang, Z. -L.; Pang, D. -W.; Li, Y.; *Biomaterials.* **2009**, *30*, 2912.
DOI: [10.1016/j.biomaterials.2009.02.010](https://doi.org/10.1016/j.biomaterials.2009.02.010)
83. Xu, H.; Wei, H.; Aguilar, Z. P.; Waldron, J. L.; Wang, Y. A.; BMEI '09. 2nd International Conference, Tianjin, **2009**.
84. Chen, C.; Peng, J.; Xia, H.; Wu, Q.; Zeng, L.; Xu, H.; Tang, H.; Zhang, Z.; Zhu, X.; Pang, D.; Li, Y.; *Nanotechnology.* **2010**, *21*, 095101.
DOI: [10.1088/0957-4484/21/9/095101](https://doi.org/10.1088/0957-4484/21/9/095101)
85. Chu, V. H.; Nghiem, T. H. L.; La, T. H.; Ung, T. D. T.; Le, Q. H.; Tong, K. H.; Nguyen, Q. L.; Tran, H. N.; *Adv. Nat. Sci.: Nanosci. Nanotechnol.* **2010**, *1*, 025005.
DOI: [10.1088/2043-6254/1/2/025005](https://doi.org/10.1088/2043-6254/1/2/025005)
86. Chen, C.; Xia, H. -S.; Gong, Y. -P.; Peng, J.; Peng, C. -W.; Hu, M. -B.; Zhu, X. -B.; Pang, D. -W.; Sun, S. -R.; Li, Y.; *Biomaterials.* **2010**, *31*, 8818.
DOI: [10.1016/j.biomaterials.2010.07.091](https://doi.org/10.1016/j.biomaterials.2010.07.091)
87. Lalani, E. N.; Laniado, M. E.; Abel, P. D.; *Cancer Metastas. Rev.* **1997**, *16*, 29.
88. Barat, B.; Sirk, S. J.; McCabe, K. E.; Li, J.; Lepin, E. J.; Remenyi, R.; Koh, A. L.; Olafsen, T.; Gambhir, S. S.; Weiss, S.; Wu, A. M.; *Bioconjugate Chem.* **2009**, *20*, 1474.
DOI: [10.1021/bc800421f](https://doi.org/10.1021/bc800421f)
89. Ruan, Y.; Yu, W.; Cheng, F.; Zhang, X.; Larré, S.; *Sensors.* **2012**, *12*, 5461.
DOI: [10.3390/s120505461](https://doi.org/10.3390/s120505461)
90. Cheng, F.; Yu, W.; Zhang, X.; Ruan, Y.; *Int. J. Biol. Makers.* **2009**, *24*, 271.
91. Jin, L. -H.; Li, S. -M.; Cho, Y. -H.; *Biosens. Bioelectron.* **2012**, *33*, 284.
DOI: [10.1016/j.bios.2011.12.043](https://doi.org/10.1016/j.bios.2011.12.043)
92. Chunthapong, J.; Seftor, E. A.; Khalkhali-Ellis, Z.; Seftor, R. E. B.; Amir, S.; Lubaroff, D. M.; Jr. Heidger, P. M.; Hendrix, M. J. C.; *J. Cell. Biochem.* **2004**, *91*, 649.
DOI: [10.1002/jcb.20032](https://doi.org/10.1002/jcb.20032)
93. Onder, T. T.; Gupta, P. B.; Mani, S. A.; Yang, J.; Lander, E. S.; Weinberg, R. A.; *Cancer Res.* **2008**, *68*, 3645.
DOI: [10.1158/0008-5472.CAN-07-2938](https://doi.org/10.1158/0008-5472.CAN-07-2938)
94. Richmond, P. J.; Karayiannakis, A. J.; Nagafuchi, A.; Kaisary, A. V.; Pignatelli, M.; *Cancer Res.* **1997**, *57*, 3189.
95. Umbas, R.; Isaacs, W. B.; Bringuier, P. P.; Schaafsma, H. E.; Karthaus, H. F. M.; Oosterhof, G. O. N.; Debruyne, F. M. J.; Schalken, J. A.; *Cancer Res.* **1994**, *54*, 3929.
96. Walker, K. -A. D.; Morgan, C.; Doak, S. H.; Dunstan, P. R.; **2012**, *7*, e31592.
DOI: [10.1371/journal.pone.0031592](https://doi.org/10.1371/journal.pone.0031592)
97. Ferlay, J.; Parkin, D. M.; Steliarova-Foucher, E.; *Eur. J. Cancer.* **2010**, *46*, 765.
DOI: [10.1016/j.ejca.2009.12.014](https://doi.org/10.1016/j.ejca.2009.12.014)
98. Thorsteinsson, M.; Jess, P.; *Eur. J. Surg. Oncol.* **2011**, *37*, 459.
DOI: [10.1016/j.ejso.2011.01.025](https://doi.org/10.1016/j.ejso.2011.01.025)
99. Gazouli, M.; Lyberopoulou, A.; Pericleous, P.; Rizos, S.; Aravantinos, G.; Nikiteas, N.; Anagnou, N. P.; Efsthathopoulos, E. P.; *World. J. Gastroenterol.* **2012**, *18*, 4419.
DOI: [10.3748/wjg.v18.i32.4419](https://doi.org/10.3748/wjg.v18.i32.4419)
100. Gray-Schopfer, V.; Wellbrock, C.; Marais, R.; *Nature.* **2007**, *445*, 851.
101. Goldstein, A. M.; Tucker, M. A.; *Curr. Opin. Oncol.* **1993**, *5*, 358.
102. Rigel, D. S.; Carucci, J. A.; *CA Cancer J. Clin.* **2000**, *50*, 215.
DOI: [10.3322/canjclin.50.4.215](https://doi.org/10.3322/canjclin.50.4.215)
103. Shan, J.; Tenhu, H.; *Chem. Commun.* **2007**, *44*, 4580.
DOI: [10.1039/B707740H](https://doi.org/10.1039/B707740H)
104. Pan, B.; Cui, D.; Gao, F.; He, R.; *Nanotechnology.* **2006**, *17*, 2483.
DOI: [10.1088/0957-4484/17/10/008](https://doi.org/10.1088/0957-4484/17/10/008)
105. Pan, B.; Cui, D.; Sheng, Y.; Ozkan, C.; Gao, F.; He, R.; Li, Q.; Xu, P.; Huang, T.; *Cancer Res.* **2007**, *67*, 8156.
DOI: [10.1158/0008-5472.CAN-06-4762](https://doi.org/10.1158/0008-5472.CAN-06-4762)
106. Pan, B.; Gao, F.; He, R.; Cui, D.; Zhang, Y.; *J. Colloid. Interface. Sci.* **2006**, *297*, 151.
DOI: [10.1016/j.jcis.2005.09.068](https://doi.org/10.1016/j.jcis.2005.09.068)
107. Li, Z.; Huang, P.; Lin, J.; He, R.; Liu, B.; Zhang, X.; Yang, S.; Xi, P.; Zhang, X.; Ren, Q.; Cui, D.; *J. Nanosci. Nanotechnol.* **2010**, *10*, 4859.
DOI: [10.1166/jnn.2010.2217](https://doi.org/10.1166/jnn.2010.2217)
108. Zheng, H.; Chen, G.; DeLouise, L. A.; Lou, Z.; *J. Biomed. Nanotechnol.* **2010**, *6*, 303.
DOI: [10.1166/jbn.2010.1136](https://doi.org/10.1166/jbn.2010.1136)
109. Kim, M. J.; Lee, J. Y.; Nehrbass, U.; Song, R.; Choi, Y.; *Analyst.* **2012**, *137*, 1440.
DOI: [10.1039/c2an16013g](https://doi.org/10.1039/c2an16013g)
110. Tsao, H.; Sober, A. J.; *Dermatol. Clin.* **2005**, *23*, 323.
111. Jr. Ferrari, N. M.; Muller, H.; Ribeiro, M.; Mía, M.; Jr. Sanches, J. A.; *Sao. Paulo. Med. J.* **2008**, *126*, 41.
112. Zhang, X.; Zhang, T.; Wang, B.; Tang, N.; Sun, L.; Luo, Q.; *Afr. J. Pharm. Pharmacol.* **2011**, *5*, 2689.
DOI: [10.5897/AJPP11.733](https://doi.org/10.5897/AJPP11.733)

113. Mizrak, D.; Brittan, M.; Alison, M. R.; *J. Pathol.* **2008**, *214*, 3.
DOI: [10.1002/path.2283](https://doi.org/10.1002/path.2283)
114. Steponkiene, S.; Kavaliauskiene, S.; Purviniene, R.; Rotomskis, R.; Juzenas, P.; *Int. J. Nanomed.* **2011**, *6*, 2437.
DOI: [10.2147/IJN.S24477](https://doi.org/10.2147/IJN.S24477)
115. Hruban, R. H.; Maitra, A.; Kern, S. E.; Goggins, M.; *Gastroenterol. Clin. N.* **2007**, *36*, 831.
DOI: [10.1016/j.gtc.2007.08.012](https://doi.org/10.1016/j.gtc.2007.08.012)
116. Swierczynski, S. L.; Maitra, A.; Abraham, S. C.; Lacobuzio-Donahue, C. A.; Ashfaq, R.; Cameron, J. L.; Schulick, R. D.; Yeo, C. J.; Rahman, A.; Hinkle, D. A.; Hruban, R. H.; Argani, P.; *Hum. Pathol.* **2004**, *35*, 357.
DOI: [10.1016/j.humpath.2003.10.012](https://doi.org/10.1016/j.humpath.2003.10.012)
117. Montet, X.; Weissleder, R.; Josephson, L.; *Bioconjugate Chem.* **2006**, *17*, 905.
DOI: [10.1021/bc060035+](https://doi.org/10.1021/bc060035+)
118. Yong, K. -T.; Ding, H.; Roy, I.; Law, W.-C.; Bergey, E. L.; Maitra, A.; Prasad, P. N.; *ACS Nano.* **2009**, *3*, 502.
DOI: [10.1021/nn8008933](https://doi.org/10.1021/nn8008933)
119. Nichols, L. S.; Ashfaq, R.; Lacobuzio-Donahue, C. A.; *Am. J. Clin. Pathol.* **2004**, *121*, 226.
DOI: [10.1309/K144PHVDDUPDD401](https://doi.org/10.1309/K144PHVDDUPDD401)
120. Argani, P.; Rosty, C.; Reiter, R. E.; Wilentz, R. E.; Murugesan, S. R.; Leach, S. D.; Ryu, B.; Skinner, S. G.; Goggins, M.; Jaffee, E. M.; Yeo, C. J.; Cameron, J. L.; Kern, S. E.; Hruban, R. H.; *Cancer Res.* **2001**, *61*, 4320.
121. Argani, P.; Lacobuzio-Donahue, C.; Ryu, B.; Rosty, C.; Goggins, M.; Wilentz, R. E.; Murugesan, S. R.; Leach, S. D.; Jaffee, E.; Yeo, C. J.; Cameron, J. L.; Kern, S. E.; Hruban, R. H.; *Clin. Cancer Res.* **2001**, *7*, 3862.
122. Yong, K. -T.; *Nanotechnology.* **2009**, *20*, 015102.
DOI: [10.1088/0957-4484/20/1/015102](https://doi.org/10.1088/0957-4484/20/1/015102)
123. Bharali, D. J.; Dier, U.; Davis, P. J.; Mousa, S. A.; *Immunol. Endocr. Metabol. Agents. Med. Chem.* **2009**, *9*, 219.
DOI: [10.2174/187152209790773048](https://doi.org/10.2174/187152209790773048)
124. Seltzer, J. L.; Akers, K. T.; Weingarten, H.; Grant, G. A.; McCourt, D. W.; Eisen, A. Z.; *J. Biol. Chem.* **1990**, *265*, 20409.
125. Seltzer, J. L.; Weingarten, H.; Akers, K. T.; Eschbach, M. L.; Grant, G. A.; Eisen, A. Z.; *J. Biol. Chem.* **1989**, *264*, 19583.
126. Liotta, L. A.; Rao, C. N.; Wewer, U. M.; *Annu. Rev. Biochem.* **1986**, *55*, 1037.
DOI: [10.1146/annurev.bi.55.070186.005133](https://doi.org/10.1146/annurev.bi.55.070186.005133)
127. Patel, B. P.; Shah, P. M.; Rawal, U. M.; Desai, A. A.; Shah, S. V.; Rawal, R. M.; Patel, P. S.; *J. Surg. Oncol.* **2005**, *90*, 81.
DOI: [10.1002/jso.20240](https://doi.org/10.1002/jso.20240)
128. Liu, H.; Liang, G.; T.; Abdel-Halim, E. S.; Zhu, J. -J.; *Anal. Methods.* **2011**, *3*, 1797.
DOI: [10.1039/c1ay05178d](https://doi.org/10.1039/c1ay05178d)
129. Strandh, M.; Ohlin, M.; Borrebaeck, C. A. K.; Ohlson, S.; *J. Immunol. Methods.* **1998**, *214*, 73.
DOI: [10.1016/S0022-1759\(98\)00039-8](https://doi.org/10.1016/S0022-1759(98)00039-8)
130. Fujioka, K.; Manabe, N.; Nomura, M.; Watanabe, M.; Takeyama, H.; Hoshino, A.; Hanada, S.; Yamamoto, K.; Manome, Y.; *J. Nanomater.* **2010**, *2010*, 1.
DOI: [10.1155/2010/937684](https://doi.org/10.1155/2010/937684)
131. Watanabe, M.; Fujioka, K.; Akiyama, N.; Takeyama, H.; Manabe, N.; Yamamoto, K.; Manome, Y.; *IEEE Trans. Nanobiosci.* **2011**, *10*, 30.
DOI: [10.1109/TNB.2011.2125800](https://doi.org/10.1109/TNB.2011.2125800)

Advanced Materials Letters

Publish your article in this journal

ADVANCED MATERIALS Letters is an international journal published quarterly. The journal is intended to provide top-quality peer-reviewed research papers in the fascinating field of materials science particularly in the area of structure, synthesis and processing, characterization, advanced-state properties, and applications of materials. All articles are indexed on various databases including [DOAJ](http://www.doaj.org) and are available for download for free. The manuscript management system is completely electronic and has fast and fair peer-review process. The journal includes review articles, research articles, notes, letter to editor and short communications.



A review on CdSe quantum dots in sensing

Pragati Malik, Jyoti Singh, Rita Kakkar*

Computational Chemistry Laboratory, University of Delhi, Delhi 110 007, India

*Corresponding author. Tel: (+91) 11 27666313; E-mail: rkakkar@chemistry.du.ac.in

Received: 01 April 2014, Revised: 30 June 2014 and Accepted: 30 June 2014

ABSTRACT

The primary aim of this review is to survey the literature on the ion sensing ability of quantum dots. Sensing of both cations and anions is important, since both play significant roles in various ecological and biological processes, which makes it important to ensure their concentration at balanced level. Contamination by heavy metal ions and various anions poses a serious threat to humans, aquatic organisms, and to the environment; therefore detection of these ions (in presence of other cations and anions), which are the major cause of environmental pollution is of immense significance at the present time. Owing to their enhanced fluorescence properties and photostability, QDs offer tremendous scope to be used for ion sensing. They offer several advantages over traditional chemical fluorophores. This review throws light on the mechanism adopted by CdSe QDs to act as fluorophores. Owing to their enhanced photoluminescence properties, QDs offer selective and sensitive determination of various ions, which is a function of the capping on the surface of the QD nanosensor, i.e. it is possible to tune their sensing ability by changing the capping layer, which influences the QD's interaction with various analytes. Hence, these quantum dots may prove promising candidates in future for sensing approximately all types of analytes. Copyright © 2014 VBRI press.

Keywords: Core/shell quantum dots; analyte detection; luminescence; fluorescence; fluorophore; metal ions sensing; photoluminescence; quantum dots quenching; nanonanosensors.



Pragati Malik has done her B.Sc. (2007) and M.Sc. (2009) in Physical Chemistry (specialization) from Delhi University, India and has completed her Ph.D. under supervision of Prof. Rita Kakkar from University of Delhi in 2013. Her research interests include theoretical studies of nanomaterials, particularly CdSe quantum dots and their interaction with various chemical and bio-analytes in order to develop novel chemical and biosensors.



Jyoti Singh is currently working as an Assistant Professor in Department of Chemistry at Hans Raj College, University of Delhi (India). She has been teaching Physical Chemistry for the past three years. She has completed her Ph.D. under Prof. Rita Kakkar from University of Delhi, India in 2010. Her research interest includes computational studies of quantum dots, their properties especially their magnetism and their applications.



Rita Kakkar, after obtaining a PhD degree in Physical Chemistry from the University of Delhi, undertook research on various topics. She has been teaching Physical Chemistry at the University of Delhi for the past three decades. Prior to that, she taught at Miranda House, University of Delhi. In the field of chemistry education, she is actively involved in designing syllabi of various universities and conducting teacher-training workshops, and for popularizing the use of Molecular

Modelling in teaching chemistry. Her main research interests are in Computational Chemistry and related fields. She heads a large research group, which is carrying out computational and experimental studies on catalysis by nanomaterials and by enzymes. The focus of the research on nanomaterials is to understand the growth, morphologies and stabilities of nanocrystalline forms of metals and metal oxides, their reactivities, and their catalytic role in various reactions, particularly those involving degradation of organic pollutants. Her research on nanoscale materials also includes theoretical and experimental studies on quantum dots and their size-dependent properties for use as semiconductor devices and sensors. Professor Rita Kakkar has over 95 research publications in international journals. She has successfully supervised the work of 35 PhD and 7 MPhil students. She has delivered invited several talks at scientific conferences. She also regularly reviews manuscripts for many international journals, including those published by the American Chemical Society, Royal Society of Chemistry, Wiley and Elsevier.

Contents

1. Introduction
2. Quantum dots
3. Properties of quantum dots
4. Surface modification of quantum dots
5. Quantum dots as sensors
6. Mechanism involved in sensor design
7. Detection of cations using surface modified CdSe QDs
8. Detection of cations using surface modified CdSe based core/shell QDs
9. Detection of anions using surface modified CdSe QDs
10. Detection of anions using surface modified CdSe based core/shell QDs
11. Conclusions
12. Future perspectives
13. Abbreviations
14. References

1. Introduction

In recent years, there has been considerable thrust into the development of sensors in the nanoscale [1-5]. In this review, we discuss the recent advancements in ion sensing using CdSe based quantum dots (QDs). Since metal ions are important, both biologically and ecologically, their detection is essential. Living organisms need varying amounts of heavy metal ions. Humans mainly require metal ions such as iron (Fe), cobalt (Co), manganese (Mn), zinc (Zn), and molybdenum (Mo), but various other heavy metal ions such as lead (Pb) [6] and mercury (Hg) [7] are toxic even at very low concentration and produce serious ill-effects. These are known as toxic metal ions. The ability of toxic metal ions to cause toxicity even at moderately low concentration and their tendency to accumulate in the ecosystem, agriculture and the human body has led to special and widespread attention to them in recent years. As we know, pollution is the result of release of undesirable materials, which leads to the contamination of the environment, as a result of which we are always under the threat of living in a biosphere with some imbalance. Although there are various causes of environmental pollution, the major cause is the industrial effluents, since they ultimately end up in aquatic systems. For example, a high concentration of gaseous oxygen in the atmosphere is highly favorable for causing corrosion of metals and the metal ions from the corroded metal structures eventually enter into the aquatic media by dissolution in rain water. Also, combustion of fuels releases heavy metals and causes pollution of the environment, which further enters into the aquatic environment by the rain water. Due to the above factors, metal ion concentration in aquatic media is much higher than the tolerance limit, which further enters the biological system when the living beings intake the polluted water, and affects their physical condition. The concentration of these metal ions mainly increases in the vicinity of the dumping area and nonstop practice of waste dumping may result in further increments of metal ion aggregation and pollution of groundwater sources. Thus, heavy metal release poses severe trouble for the environment, since they cannot be biodegraded and remain in the soil/water for longer periods, thereby affecting humans and domestic animals. Hence, determination of

heavy metals in the biological system and in aquatic environment has become a necessity for the well-being of society, due to their toxicity and retention by the ecological system [8, 9].

Besides metal ions, various anions, such as carbonate ion (CO_3^{2-}) are important biologically, and some others such as cyanide (CN) are harmful. Some anions, such as nitrate ions, which are formed as a result of rain water interaction with atmospheric forms of nitrogen, are responsible for ground water pollution. In addition, various anthropogenic sources of nitrate are septic tanks, and excessive use of nitrogenous fertilizers (which leach to the ground water), applied in order to improve crop productivity. The harmful effects of nitrate are blue baby syndrome or methemoglobinemia (reduced ability of RBCs to release oxygen to tissues). Hence, preventive measures must be taken so as to avoid this situation. The concentration of all these ions should be maintained in a fine limit, as a slight excess or deficiency produces undesirable, unwanted and toxic effects. In order to minimize the pollution caused by heavy metal ions, various detection methods have been employed, such as atomic absorption spectrometry [10], inductively coupled plasma mass spectrometry [11], capillary electrophoresis [12], X-ray fluorescence spectrometry [13] and microprobes [14] with high sensitivity, but, due to high cost, complicated instruments and the need of trained people to handle them, these are not in much use [15]. Thus, it is necessary to develop highly selective and responsive analytical tools to avoid the damaging effects of pollution due to heavy metals in the very early stage and has long been a focus of research. QDs offer several advantages over traditional chemical fluorophores for ion sensing. Many reports on sensing cations and anions of both biological and ecological importance using quantum dots (QDs) have been published [1]. In this review, we focus on the utilization of CdSe and CdSe based core/shell QDs for sensing various such ions. We first discuss quantum dots and their use as sensors.

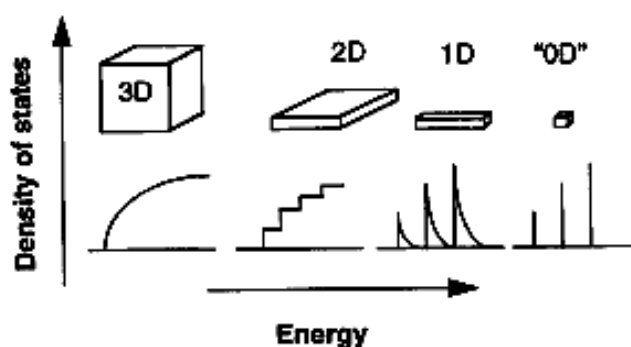


Fig. 1. Illustration of density of states in semiconductors as a function of dimension [19].

2. Quantum dots

Quantum dots are a special class of inorganic semiconductor nanocrystal materials, composed of atoms of periodic groups of II-VI, III-V, or IV-VI materials. They are constrained in three dimensions to a somewhat spherical shape, typically with a diameter of 2 - 8 nm, containing

approximately 200 - 10,000 atoms [16, 17, 18]. Fig. 1 shows that in semiconductors, the density of states is a function of dimension, and since QDs are zero-dimensional semiconductors, their density of states is sharp and discrete [19].

QDs are exciting candidates in the field of nanotechnology due to their unique optical and electronic properties, such as high quantum yield, narrow, tunable and symmetric emission spectra, broad absorption spectra, their ability to span the electromagnetic spectrum from visible to infrared and resistance towards photo-oxidation and photobleaching [20, 21]. They exhibit size tunable fluorescence properties and simultaneous excitation of multiple fluorescence colors due to quantum confinement effects [22-30]. Their long-term photostability makes them attractive in the area of sensing. Sensing by QDs is based on their fluorescence property. Fluorescence is a type of photoluminescence, but can be distinguished from other types of photoluminescence, as the excited electron returns immediately to the ground state. In earlier days and even till now, molecular sensing continues to be dominated by organic dye-based fluorescent sensors. However, QDs, the new class of fluorescent compounds, have proven to be better alternatives to conventional organic dyes and have almost replaced them due to their remarkable photophysical properties [18].

Stuczynski et al. [31] first reported, in 1989, the formation of metal-chalcogen bonds by the reaction of metal alkyls with silyl chalcogenides. The most studied colloidal QDs are Cd-chalcogenide QDs due to the ready availability of precursors and the simplicity of crystallization. These are referred to as II-VI semiconductors due to the positions of Cd and the chalcogenide in the periodic table. Amongst all the Cd-chalcogenide QDs, the CdSe QD is found to be of great interest due to its familiar physical properties and its band-gap energy, which covers almost the whole of the electromagnetic spectrum [32]. It is a direct band gap semiconductor.

As a result of their unique optical and electronic properties, such as broad absorption spectra, very narrow emission spectra, long fluorescence lifetime and high photostability, CdSe nanocrystals are considered to be the ideal candidates for various applications such as in biological imaging, laser media, light emitting diodes, in photovoltaics and, most importantly, in analytical chemistry [33-39]. Among the various applications of CdSe QDs, in this review, we are focusing on the ion sensing abilities of CdSe based QDs and core/shell QDs, which depend on the fluorescence efficiency of the QDs. The fluorescence efficiency of QDs is found to be sensitive to the presence of and also on the nature of adsorbates at the surface of QDs [38].

The remarkable properties shown by QDs are a function of their size and a consequence of the effect called the quantum confinement effect, which arises due to change in density of states [16, 19]. A QD-based chemical sensing system employs fluorescence changes induced by the analyte present at the surface or close to the surface of the QD. Sensing via QDs is based on the interaction of the QD with the analyte of interest, thereby influencing the optical properties, which in turn are quite sensitive to the type of

capping ligand used, indicating that surface phenomenon cannot be neglected. The analyte present close to the QDs leads to dramatic changes in the luminescent properties of these QDs, i.e. results either in fluorescence quenching or enhancement, which promotes them to be applied for analytical sensing. Hence, enhancement or quenching of luminescence of QDs due to analyte-quantum dot interaction may guide researchers to design new, specific nanoparticle-based sensors [39]. In this review, an effort has been made to understand the mechanism employed by CdSe and CdSe based core/shell QDs to act as chemical sensors for various ions of biological and environmental interest.

3. Properties of quantum dots

3.1. Quantum confinement

A significant property which makes QDs applicable to be employed for sensing purposes arises from a property known as quantum confinement, which was first reported by Ekimov and Onushchenko in CuCl nanocrystals [40]. A lot of research has been done in the field of quantum confinement effect in semiconductors and in low dimensional nanostructures [41, 42]. This effect is the widening of the band-gap (i.e. gap between the conduction and valence band) with a reduction in the size of the QD. This effect is analogous to the "particle in a box" model in which the energy gap of the particle increases as the size of the box decreases [18]. It is because of the quantum confinement effect that the QDs of identical material but with dissimilar sizes display various colors (Fig. 2) [18]. QDs exhibit exclusive electronic and optical properties due to this effect. The band gap in a material is the energy required to create an electron and a hole at rest (i.e. with zero kinetic energy) at a distance far enough apart that their coulombic attraction is negligible. If one carrier approaches the other, they may form a bound electron-hole pair, i.e. an exciton, whose energy is a few meV lower than the band-gap. The distance between the electron and hole is known as the exciton Bohr radius [43].

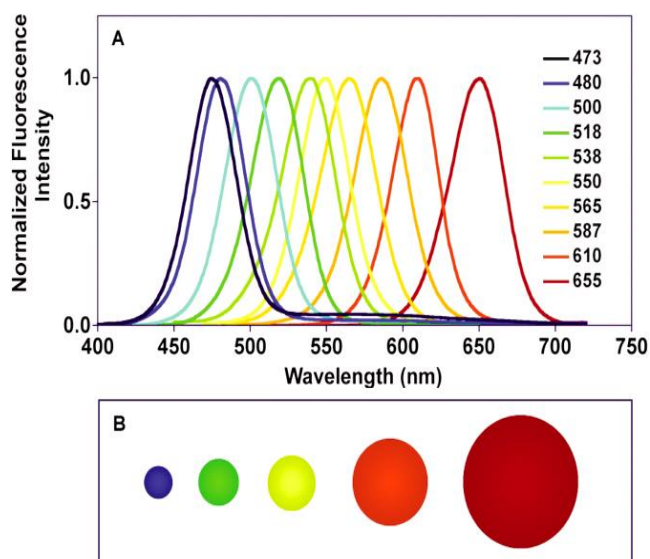


Fig. 2. (A) and (B) Illustration of size-tunable fluorescence spectra of CdSe quantum dots [18].

3.2 Luminescence properties

As already discussed, CdSe QDs are nowadays being widely employed in various applications and have received extensive attention owing to their unusual electronic and optical properties. These properties can be altered by merely manipulating the number of atoms in the QDs while maintaining the same chemical composition. The optical and electronic properties of semiconductor nanoclusters come up from interactions between electrons, holes, and their local environments [44]. QDs undergo photoexcitation on absorption of photons when the excitation energy exceeds their band gap and electrons get promoted from the valence band to the conduction band. The electron in an excited state is a high energy electron. The excited electron and hole form an exciton. The electron and hole may recombine and relax to a lower energy state, ultimately reaching the ground state. The excess energy resulting from recombination and relaxation may be either radiative (emits photon) or nonradiative (emits phonons). The luminescence of QDs is due to radiative relaxation. Measurements of UV-visible spectra reveal a large number of energy states in QDs. A remarkable peak is observed as the first observable peak from the lowest excited energy state. Excitations at shorter wavelengths are also likely due to multiple electronic states present at higher energy levels. The size of CdSe QDs is used to tune the optical gap across a major portion of the visible spectrum [19, 45] (Fig. 2). In case of CdSe QDs, the optical gap can be tuned from deep red (~1.7 eV) to green (~2.4 eV) by reducing the dot diameter from 20 to 2 nm. Thus, tuning their size allows tailoring their optical properties, thereby making QDs hopeful resources for developing various sensing devices [46].

4. Surface modification of quantum dots

QDs, being nano-sized, have very high surface to volume ratio, as a result of which, most of the atoms are present on the surface. These surface atoms are with unsatisfied valencies and act as sites of preferential photodegradation and luminescence quenching, thereby making the surface of QDs highly prone to photobleaching and photooxidation. Therefore, it is highly desirable to modify the surface of these QDs with appropriate ligand molecules in order to make them suitable for interaction with various analytes. These surface ligands alter the sensitivity and selectivity of QDs towards various analytes of interest by altering their fluorescence response, and this response can be further modified by modifying the capping layer. In addition, it has been found that, for the successful development of sensors and for allowing flexibility and functionality of QDs for efficient coupling of these fluorescent probes to various analytes, a control of the surface chemistry of QDs is highly essential [47-52]. However, studies also show that surface modification of QDs may lead to enhancement in their cellular toxicity [53-56].

Alloyed QDs, which offer continuous tuning of quantum confinement by alteration in the size of the QDs or by variation of their chemical composition, have been synthesized. QDs generally do not exhibit aqueous solubility, as they are synthesized in organic solution and are surface-stabilized with hydrophobic organic ligands.

Surface modification with various bifunctional ligands makes them water soluble and enhances their biocompatibility and absorption by cells. Generally, surface modifications involve the conversion of hydrophobic ligands to hydrophilic ones on QD surfaces. This includes ligand exchange (done by exchanging the hydrophobic surfactant molecules with bifunctional molecules, i.e. molecules having a hydrophilic end on one side and a hydrophobic end on the other, the most commonly used bifunctional molecules being cysteine, mercaptosuccinic acid, glutathione and mercaptoacetic acid), silica coatings (done by introducing silica shell covering onto the QDs), adding another ligand layer, and incorporation of QDs into polymeric molecules, or by coating the hydrophobic QD surface with a cross-linked amphiphilic polymer, the hydrophilic component of which provides water solubility and the hydrophobic part interacts with the hydrophobic surface of the QD [57]. Various other coating techniques include electrostatic interaction, micelle encapsulation, and hydroxylation. There are various kinds of interactions by which QDs interact with biomolecules; importantly, hydrophobic and van der Waals interactions, peptide linkages or S-S disulfide bonds, and electrostatic interactions. Various reports based on the sensing capabilities of QDs focus on either organically capped or inorganically capped, i.e. core/shell QDs [36, 58-63].

4.1. Organically capped quantum dots

Organic capping layer allows one to achieve colloidal suspension and the ability to bio-conjugate the QDs. However, to choose the organic ligand that bond with the surface atoms of the QDs is a very delicate subject. The most commonly used organic ligands are phosphenes (e.g., tri-n-octyl phosphene oxide-TOPO) or mercaptans (-SH). The coverage due to these ligands may be sterically hindered due to the size (which is larger than the surface site) and shape of these ligands. Some dangling bonds on the surface are always present when the surface is passivated by organic ligands, since these ligands do not passivate both the cationic as well the anionic sites. Also, QDs passivated with the organic ligands are photounstable due to weak bonding between the surface atoms and capping molecules that leads to the generation of trap states [43, 64-67].

4.2. Inorganically capped QDs: Core/shell QDs

An alternative method employed for passivating the surface of QDs is by the utilization of inorganic layers, mainly a material with a larger band gap. These inorganically capped QDs are called core/shell QDs. Core/shell QDs have improved luminescence quantum yields and acquired properties due to the tailoring of relative band gap positions between the two materials [68-75].

Fig. 3 shows the photoluminescence (PL) spectra of bare CdSe QDs (dashed lines) and CdSe/ZnS (solid lines) QDs. The results of Dabbousi et al. [21] show that the PL quantum yield increases from 5 to 15% for bare CdSe QDs to 30 to 50% for ZnS overcoated CdSe QDs. Also, the quantum yield is higher for smaller dots [21]. Hence, QDs passivated with inorganic material have been found to be more robust than organically passivated dots [76]. Some

examples of core/shell quantum dot structures reported include CdS on CdSe and CdSe on CdS [73], ZnS grown on CdS [75], ZnS on CdSe and the inverse structure [70], CdS/HgS/CdS quantum dot quantum wells [72], ZnSe overcoated CdSe [68] and so on. Fig. 4 illustrates the emission colors of different-sized CdSe/ZnS core/shell QDs excited with a near-UV lamp.

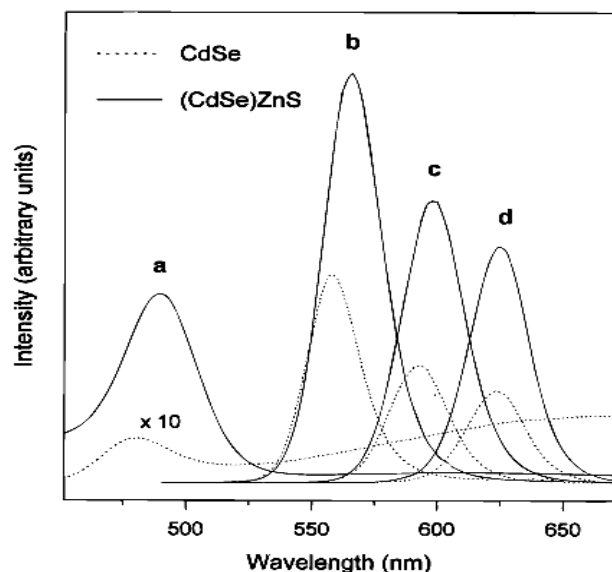


Fig. 3. Photoluminescence spectra for bare CdSe QDs (dashed lines) and CdSe/ZnS core/shell QDs (solid lines) [21].



Fig. 4. Ten distinguishable emission colors of ZnS capped CdSe QDs excited with a near-UV lamp. From left to right (blue to red), the emission maxima are located at 443, 473, 481, 500, 518, 543, 565, 587, 610, and 655 nm [20].

4.3. Comparison with organic fluorophores

Conventionally employed organic fluorophores undergo quite severe problems, both chemically and photophysically. QDs, on the other hand, due to their unique optical and electronic properties, exhibit interesting properties, such as size tunable light emission, broad absorption spectra, narrow emission spectra, simultaneous excitation of multiple fluorescence colors, resistance against photobleaching and hence high photochemical stability which makes them superior to organic dyes and fluorescent proteins. Different excitation wavelengths are required in order to excite each organic dye in a sample of several dyes which is not required in the case of QDs due to their broad absorption spectrum which enables the excitation of a combination of QDs of different emission wavelengths with a single excitation wavelength [19, 21, 77-80].

Fig. 5(A) gives the comparison of the absorption spectrum of the organic dye fluorescein isothiocyanate (FITC) with that of CdSe QDs. FITC shows a narrow absorption band and can only be effectively excited at a wavelength around 470 nm whereas QDs exhibit a broad absorption spectrum that extends from 350 nm to 520 nm. Fig. 5(B) reveals that the emission spectrum of QDs is sharp and symmetric, while that of FITC is broad and has a tail extending to long wavelengths [18].

As can be seen from Fig. 5, QDs possess a broad absorption spectrum which allows the excitation of multiple fluorophores with a single light source. QDs are very much resistant to photobleaching, a common trouble with organic fluorophores [81]. QDs exhibits bright fluorescence due to their large molar extinction coefficients and high quantum yields [82]. QDs also have long fluorescence lifetimes of the order of 20-50 ns, which allow them to be distinguished from background and other fluorophores, thereby exhibiting amplified sensitivity of detection [83].

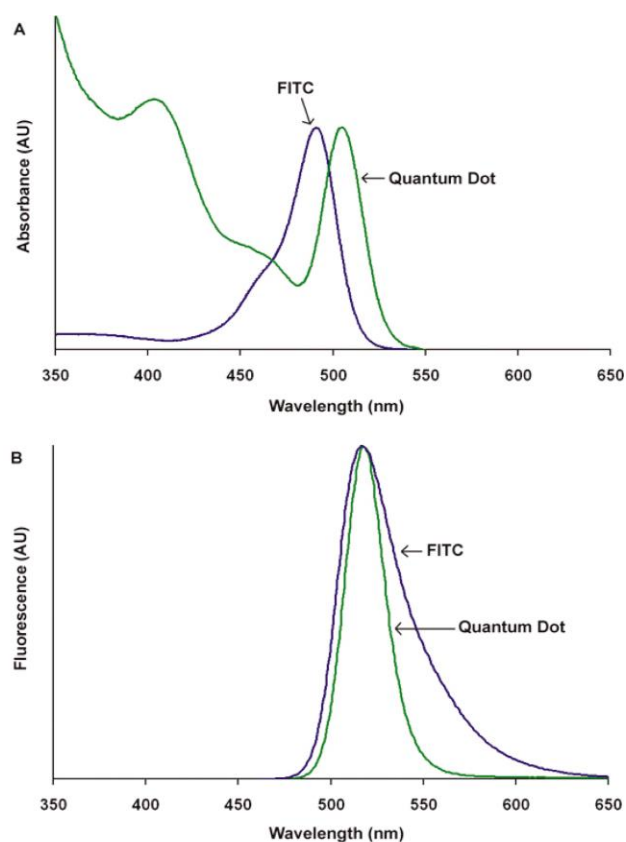


Fig. 5. Comparison of absorption spectra (A) and emission spectra (B) of QDs and fluorescein isothiocyanate organic dye (FITC) [18].

5. Quantum dots as sensors

As has already been discussed, development of robust and sensitive environmental sensors for various ions is in progress and is of main concern currently. Ion sensing can be carried out using QDs via analyte-induced changes in the photoluminescence of QDs [84]. These sensors may be classified into luminescence based sensors, which mainly involve the principle of photoluminescence and chemiluminescence, and absorbance-based sensors which employ changes of the spectral absorbance. The sensing

abilities of surface-modified CdSe QDs and core/shell QDs such as CdSe/ZnS have been intensively studied [85]. For ion detection, fluorescence quenching is the most usual process observed after interaction between quantum dot and organic analytes, usually involving photo-induced electron transfer (PET) and Förster resonance energy transfer (FRET) [86] which are discussed in the next section. The first use of cadmium based QDs was reported in 2002 when CdS quantum dots capped with L-cystein and thioglycerol were employed for the detection of zinc and copper in physiological buffer samples [87].

6. Mechanism involved in sensor design

As discussed, out of the various mechanisms involved in the design of fluorescent sensors, QDs based sensors majorly make use of photoinduced electron transfer (PET) and Förster Resonance Energy Transfer (FRET) mechanisms [86].

6.1. Photoinduced electron transfer (PET)

The mechanism of PET involves the separation and intramolecular charge relocation, such as in photosynthesis. The energy absorbed from sunlight is utilized in promoting an electron to a higher energy level and reduces a chain of electron acceptors with lowered redox potentials, thus producing chemical energy. This PET principle has led researchers to incorporate this mechanism into sensing systems due to its sophistication and modular design. The "switching off" of the PET process by complexation with metal ions leads to the restoration of emission of the fluorophores, such as during cation sensing, the linkage of cation to ionophore prevent the quenching of ionophore leading to increase in quantum yield [88-90]. The idea of the PET mechanism for sensing cations has also been explored for anion sensing [91-93] and sensing of molecules of biological significance like glucose [94, 95]. PET sensors are composed of three distinct and separate components (Fig. 6).

A fluorophore, consisting of aromatic groups or cyclic molecules with π bonds is joined to a receptor via a spacer (Fig. 6). A signaling component of the sensor, the fluorophore extracts information from the analyte via fluorescence. The receptor recognizes the analyte and binds to it through chelation or through some kind of bonding (e.g. hydrogen bonding) by taking part in redox processes with the fluorophore [97]. The use of a spacer is to keep the fluorophore and receptor far apart from each other.

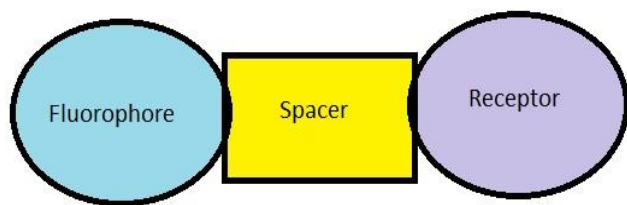


Fig. 6. The "fluorophore-spacer-receptor" format of fluorescent PET sensors.

Fig. 7 explains the molecular orbital energy diagrams of the "OFF" and "ON" states of the sensor. In an "OFF" state

of the sensor, the receptor HOMO lies above that of the fluorophore, while in an "ON" state, there occurs stabilization of the HOMO of an analyte bound receptor and it is found below the fluorophore's HOMO. PET occurs if the oxidation potential of the receptor is smaller in magnitude than that of the fluorophore but, if opposite is the case; there is an "ON" situation [96].

6.2. Förster resonance energy transfer (FRET)

Another important technique frequently employed for sensing analytes using QDs is the Förster Resonance Energy Transfer (FRET) [98-105]. Upon photoexcitation, there occurs generation of electron-hole pairs. Fluorescence light is emitted upon recombination of the electron and hole. This property forms the basis of fluorescence resonance energy transfer (FRET). The FRET process involves the nonradiative transfer of energy from an excited donor fluorophore to a ground-state acceptor fluorophore when these two are in close proximity, typically 1-10 nm, i.e. FRET is the distance dependent nonradiative transfer of electronic energy from a donor to an acceptor molecule. Thus it can be employed very effectively for investigating distances in the range of 1 - 10 nm and can be extremely useful to study molecular interactions in various chemical and biological systems. Hence, by measuring FRET effectiveness, one can determine the distance between two fluorophores [106, 107].

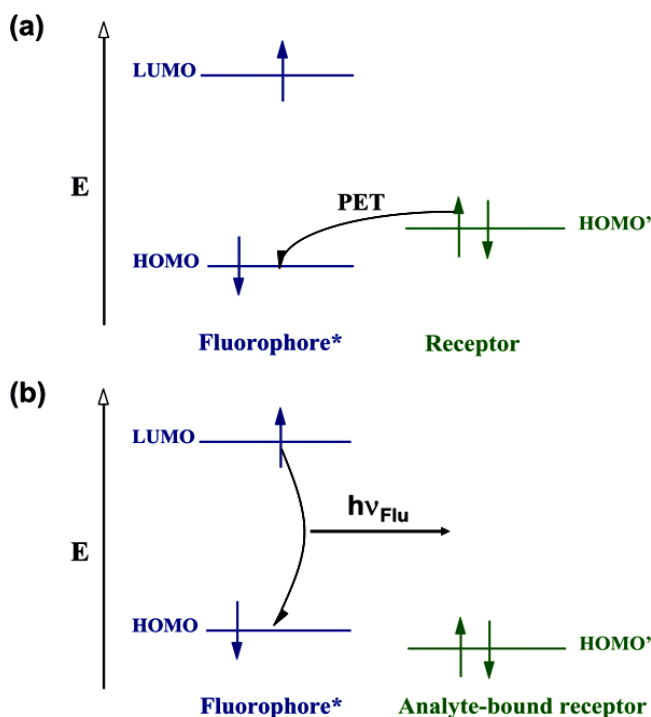


Fig. 7. Molecular orbital energy diagrams which show the relative energetic dispositions of the frontier orbitals of the fluorophore and the receptor in (a) the analyte-free situation and (b) the analyte-bound situation [96-Reproduced by permission of The Royal Society of Chemistry, <http://dx.doi.org/10.1039/b912527m>]

For an effective FRET to occur, the emission spectrum of the donor must overlap the absorption spectrum of the acceptor molecule. The greater the overlap, the higher is the transfer efficiency of electronic energy. FRET takes place via the weak dipole-dipole coupling mechanism

(inversely proportional to the sixth power of the distance between the donor and acceptor and directly proportional to the square of the coupling between them) between the transition moments of donor and acceptor molecules [108-114]. With the process of FRET, there occurs a fall in the fluorescence efficiency of the donor molecule, with a simultaneous increase in the emission intensity of the acceptor molecule [115, 116].

FRET between QDs and various chemical and biomolecules such as QDs and fluorescent proteins [111-116], CdSe/ZnS and rhodamine B for light harvesting [117], QDs and various ions and in pH sensing, and so on has been studied in the literature. Research is still continued to explore the importance of FRET in QDs by investigating their optical properties to determine their possible consequent applications in analytical as well as in life sciences [118]. Due to their broad absorption spectra, QDs are ideal energy acceptors. QDs were investigated as effective FRET donors for the first time by Bawendi et al. [102] who showed that like the organic fluorophores, CdSe QDs could also exhibit nonradiative energy transfer.

In general, the interaction of QDs with various ions leads to a fluorescence quenching that can be ascribed to inner-filter effects, nonradiative recombination pathways and electron transfer processes [119]. In some other cases, fluorescence improvement could also be observed due to passivation of trap states or defects on the surface of the QDs [120].

7. Detection of cations using surface modified CdSe QDs

QDs were first employed as ion probes in 2002 by Chen and Rosenzweig when they made use of L-cystein and thioglycerol capped QDs for detection of zinc and copper [87].

7.1. CdSe: Zinc

Zinc is one of the most important transition metal ions of physiological importance, both extracellular and intracellular, for example, in the synthesis of insulin and serves as a mediator for cell-cell signaling in the central nervous system where the brain tissue contains a high concentration of zinc. Zinc is also a part of two main enzymes carbonic anhydrase, which is vital to the process of conversion of CO₂ into bicarbonate and transformation of bicarbonate to CO₂ and carboxypeptidase for regulation and digestion of proteins. Due to the participation of zinc in various other physiological processes, development of highly sensitive and selective chemical sensors for the Zn²⁺ ion is of great importance at the biological level, i.e. at low concentrations in the presence of other relevant cations and at physiological pH values. Various fluorescent sensors for Zn²⁺ detection based on the linking of a receptor to a fluorophore employing PET or FRET have been reported. Earlier in 2009, Frasco and Chaniotakis [121] first demonstrated that the calixcrown moiety can be conjugated to the QD surface and the resulting structure could be employed as an ion sensor due to its sensitivity towards the presence of low concentrations of metal ions. They carried out their studies on the metal ions copper (0.73 Å) and

sodium (1.02 Å), and ammonium (1.47 Å) which differ in their ionic radii and correlated the fluorescence quenching of QDs with the increase of cation concentration. Later in 2010, Frasco et al. [122] reported a novel hybrid structure based on tetrapyrrolyl substituted porphyrin (5,10,15,20-tetra(4-pyrrolyl)porphyrin [H₂P(pPyr)₄]) functionalized CdSe QDs for the selective sensing of Zn²⁺ ions with a 0.5 μM limit of detection. This conjugated structure upon coordination with zinc ions, shows an increase in the fluorescence efficiency of CdSe QDs which increases with increasing concentrations of zinc ions.

7.2. CdSe: Copper

Copper is an essential element, an important part of electron transport chains (where mainly blue copper proteins like azurin and plastocyanin are involved) in plants and animals. It is vital for the functioning of various enzymes like cytochrome c oxidase and superoxide dismutase. Due to its antibacterial and antimicrobial properties, it is also employed in hospital surfaces and fittings. Various diseases like Alzheimer's disease and Parkinson's disease are linked to copper [123, 124]. In India, cirrhosis of liver is related to cooking acidic food in copper pots [125]. Therefore, detection of Cu²⁺ is of considerable importance. Various spectrophotometric based methods are preferred due to the requirement of reasonably priced instruments which offer reasonable sensitivity when chromogenic reagents such as sodium diethyldithiocarbamate trihydrate, N-ethyl-2-naphthylamine [126], di-2-pyridylketone benzoylhydrazone [127], and thiomichlersketone [128] are employed. Various other methods such as spectrofluorometric methods have also been used for Cu²⁺ determination employing various fluorescent reagents mainly europiumterpyridine-polyaminopolycarboxylate chelate [129] and 5-(3-fluoro-4-chlorophenylazo)-8-aminoquinoline [130] due to their advanced sensitivity.

A novel method for the sensitive determination of Cu(II) ions with a detection limit of 0.2 μg L⁻¹ based on water-soluble luminescent CdSe QDs surface functionalized with 2-mercaptoethane sulphonic acid or with 2-mercaptoacetic acid has been developed by Fernández-Argüelles et al. [131]. They observed that the presence of even ultratrace amounts of copper ions could cause a decrease of the emission luminescence of the modified QDs which could be explained in terms of substitution of surface Cd²⁺ ions by Cu²⁺ ions to form CuSe (with extremely low solubility) on the surface of CdSe QDs. No interference from other cations such as Na⁺, K⁺, Ca²⁺, Mg²⁺, Zn²⁺, Mn²⁺, Co³⁺ and Fe³⁺ even at concentrations upto 300 mg L⁻¹ was observed on the emission signals of the surface modified CdSe QDs [131]. Quintaneg and Santos synthesized CdSe QDs using Horizontal Vapor Phase Crystal (HVPC) Growth Technique in order to analyze Cu²⁺ ion concentration based on the fluorescence quenching mechanism of CdSe QDs [132].

7.3. CdSe: Silver

Liang et al. [133] developed a chemodosimeter for Ag(I) by synthesizing biocompatible, water soluble CdSe QDs

surface modified with mercaptoacetic acid and further absorption of bovine serum albumin (BSA) onto the surface in order to improve their fluorescence intensity and stability in water with detection limit of 7.0×10^{-8} mol L⁻¹ of Ag(I). Ultrasmall particles of Ag₂Se formed at the surface of CdSe QDs by the chemical displacement of surface Cd(II) by Ag(I) and the extremely low solubility of Ag₂Se could quench the luminescence of BSA functionalized CdSe QDs [133]. Later in 2010, Ingole et al. [134] synthesized water soluble, citrate-capped, luminescent CdSe QDs for the selective detection of silver ions in the presence of various ions including physiologically important metal ions such as K⁺, Ca²⁺, Fe³⁺, Zn²⁺, Mg²⁺, Mn²⁺, Cu²⁺, Ag⁺ and toxic metal ions like Pb²⁺ and Cd²⁺. They found the selective luminescence quenching of conjugated QDs predominantly with Ag⁺ ions due to its highest positive redox potential compared to other metal ions under investigation and the limit of detection obtained was between 1.7 and 18 μM for silver ions.

7.4. CdSe: Barium

Barium behaves toxic even at low concentrations since it blocks potassium ion channels which are important for the proper functioning of the nervous system. Therefore, higher doses affect the nervous system causing cardiac irregularities, tremors, weakness, anxiety, dyspnea and paralysis. Mahmoud [135] first reported the detection of barium ions by using water soluble 2-mercaptoethanol capped CdSe QDs with a detection limit of 4.2×10^{-9} mol L⁻¹. He found enhancement in fluorescence emission from CdSe QDs on interaction with barium ions whereas the presence of other metal ions had no significant effect on the PL of QDs [135].

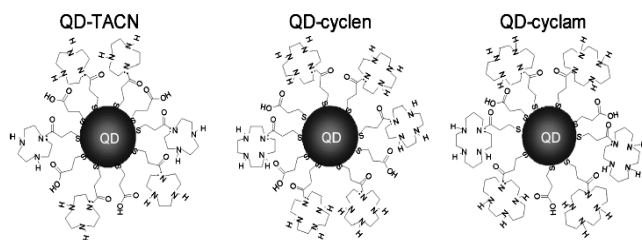


Fig. 8. Structure of QD-TACN, QD-cyclen, QD-cyclam [143].

7.5. CdSe: Mercury

The analysis of Hg (II) ions has been one of the most essential topics because of the significant health hazards it causes even when its concentration is extremely low, of the order of ppm. Deposition of mercury in water bodies can also have an impact on ecosystems and wildlife [136-140]. Chen et al. [141] developed water soluble and biocompatible highly fluorescent L-cysteine CdSe nanosensors for sensing of Hg²⁺ ions with the limit of detection 6.0×10^{-9} mol L⁻¹ based on fluorescence quenching of surface modified-CdSe QDs [141]. Shang et al. [142] have demonstrated the detection of an ion pair by utilizing photoluminescent CdSe QDs surface modified with triethanolamine (TEA-CdSe-QDs) for the detection of Hg²⁺ ions in the presence of I⁻ ions and vice versa for the

first time. The fluorescence of TEA-CdSe-QDs was found to be quenched in presence of both the above ions while no significant effect on fluorescence was observed in the presence of the individual ions. The limit of detection was found to be 1.9×10^{-7} mol L⁻¹ for Hg²⁺ and 2.8×10^{-7} mol L⁻¹ for the I⁻ ion. Formation of a complex between TEA-CdSe-QDs and Hg²⁺ occurs with I⁻ acting as a bridge (QDs-I⁻-Hg²⁺) and fluorescence quenching has been explained in terms of the electron transfer mechanism from QDs to Hg²⁺ ions [142].

8. Detection of cations using surface modified CdSe based core/shell QDs

8.1. CdSe/ZnS: Zinc

The first zinc ion sensors developed using QD nanoparticles in a host-guest and receptor-fluorophore system with a detection limit lower than 2.4 μM were based on the azamacrocyclic derivatization of CdSe/ZnS core/shell QD nanoparticles. Three azamacrocyclic receptors were: TACN (1,4,7-triazacyclononane), cyclen (1,4,7,10-tetraazacyclododecane), and cyclam (1,4,8,11-tetraazacyclotetradecane). Azamacrocyclic adsorbed at the surface of the QD causes fluorescence quenching which could be reversed when the zinc ion enters the azacrown, i.e. an increase in fluorescence intensity was observed on exposure to zinc ions due to the involvement of the lone pair of nitrogen with the zinc ion, thereby disturbing the hole-transfer mechanism and hence switching on the QD emission [143].

Ganguly et al. [144] synthesized CdSe/ZnS QDs surface modified with the multidentate ligand, salen. This hybrid material exhibits selective metal ion sensing towards Fe(II) and Cu(II) by photoluminescence quenching with a limit of detection 30 μM and 25 μM respectively. The selective sensing of ferrous ions could be attributed to the fluorescence energy transfer between the QDs and the surface ferrous-salen complexes while the selective sensing of copper is due to both the fluorescence energy transfer and surface adsorption mechanism. The authors had also investigated the photoluminescence response of QD-Salen towards different biologically relevant metallic cations including Na⁺, K⁺, Cu²⁺, Mn²⁺, Ca²⁺, Co²⁺, Ni²⁺, Fe²⁺, VO²⁺, Zn²⁺ and Cd²⁺ and found that Na⁺, K⁺, Mn²⁺, Ca²⁺, VO²⁺, Zn²⁺ and Cd²⁺ had no significant influence on the fluorescence properties of QDs-Salen, although Co²⁺ and Ni²⁺ also quenched the fluorescence to some extent. This conjugated system could be used for sensing Fe in biological systems since the iron content in physiological fluids is much higher than those of copper, nickel and cobalt.

8.2. CdSe/ZnS: Copper

A variety of research has been done to develop novel hybrids based on CdSe/ZnS core/shell QDs for detection of copper concentration as low as possible. High-quality luminescent CdSe/ZnS QDs, surface modified with bovine serum albumin (BSA) were used as selective copper (II) ion probes with satisfactory results and the detection limit achieved was 10 nM [145]. The authors explained it in terms of the strong binding of Cu²⁺ onto the surface of

CdSe leading to a chemical displacement of Cd^{2+} ions and the formation of CuSe on the surface of the QDs due to the extremely low solubility of CuSe which further quenches the luminescence of BSA capped QDs. Fig. 9 shows that the fluorescence of BSA-QDs was effectively quenched by Cu^{2+} and Fe^{3+} ions in presence of other physiologically vital cations even if their concentrations were 50 times higher than that of Cu^{2+} . The interference of Fe^{3+} with Cu^{2+} ion analysis could be eliminated by adding fluoride ions to form the colorless FeF_6^{3-} complex. The BSA coated QDs can principally be used for the analysis of Cu^{2+} in the presence of a small concentration of Zn^{2+} ions which is of particular importance, since Cu^{2+} and Zn^{2+} generally exhibit analogous reaction to many organic fluorescent indicators [145].

Later in 2007, Jin et al. synthesized water-soluble CdSe/ZnS QDs for the analysis of Cu^{2+} by overcoating the QD surface with thiocalix[4]arene carboxylic acid (TCC) which are highly fluorescent QDs. It was found that the fluorescence of the TCC-QDs was efficiently quenched by Cu^{2+} ions. The presence of other transition metal ions such as Cd^{2+} , Zn^{2+} , Co^{2+} , Fe^{2+} and Fe^{3+} did not cause any interference. These conjugated TCC-coated QDs were highly selective as was determined by the fluorescence response towards transition metal ions such as Fe^{2+} , Fe^{3+} , Co^{2+} , Zn^{2+} , Cd^{2+} and more or less insensitive to other biologically important ions such as Na^+ , K^+ , Mg^{2+} , and Ca^{2+} implying that TCC-coated QDs could be used as a fluorescent Cu^{2+} ion probe for biological samples [146].

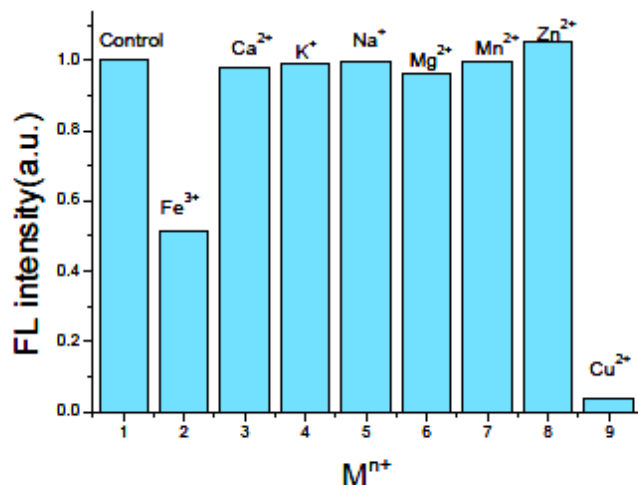


Fig. 9. Effect of biologically relevant ions on the fluorescence of BSA-QDs: concentration of Cu^{2+} : 10^{-6} M; for others: 5×10^{-4} M [145].

In the work presented by Callan and Mulrooney [147], CdSe and CdSe/ZnS QDs were surface functionalized with mercaptosuccinic acid (MSA) rendering them water soluble. MSA plays two important roles: at physiological pH, the negatively charged MSA ensures water solubility and electrostatically attract positively charged substrates close to the QD surface. Thus, this QD conjugate could be employed for sensing positively charged metal ions. It was observed that in a solution with concentration 1×10^{-5} M containing Na^+ , K^+ , Mg^{2+} , Ca^{2+} , Fe^{2+} , Mn^{2+} and Cu^{2+} as their chloride salts in the presence of MSA capped CdSe/ZnS QDs, a photoluminescence quenching was observed in case of Fe^{2+} and Cu^{2+} ions only.

Photoluminescence quenching was explained due to competitive absorption in case of Fe^{2+} ions and due to the formation of CuSe and $\text{Cu}_2\text{S}/\text{CuS}$ at the surface of the MSA capped CdSe and CdSe/ZnS core/shell QDs respectively. Also, greater range of quenching was observed in case of MSA capped CdSe/ZnS core/shell QDs than MSA capped CdSe QDs due to an increased insulation of the CdSe core by the ZnS shell in case of MSA capped CdSe/ZnS core/shell QDs. In another work done by Sutter et al. [1], CdSe/ZnS core/shell QDs Qdot800 (Invitrogen) were synthesized and employed for sensing Cu^{2+} ions as $\text{Cu}^{2+}(\text{H}_2\text{O})_8$ at concentration as low as 1 ppb by fluorescence quenching of QDs, most likely due to resonance energy transfer. In the same year, Sung and Lo (2012) synthesized a fiber-optic sensor for Cu^{2+} detection, where silica shell-encapsulated CdSe/ZnS QDs were overcoated with the polyvinyl chloride (PVA) polymer which exhibits strong quenching of QDs fluorescence in presence of Cu^{2+} ions. They demonstrated that the silica shell plays a key role in fluorescence quenching as it prevents the aggregation of CdSe/ZnS QDs and promotes the adsorption of Cu^{2+} ions on the QD-conjugated nanosensor [148]. Very recently, Zeng et al. [149] have systematically carried out a study in which the effect of different capping ligands on CdSe/ZnS QDs has been discussed in order to demonstrate that the quenching mechanism of QDs upon metal ion binding not only depends on the inherent properties of metal ions but also on the nature of ligands capped on the surface of QDs. The metal ions studied were Cu^{2+} , Pb^{2+} , Hg^{2+} , Fe^{3+} , Co^{2+} , Cr^{3+} , Ni^{2+} , Cd^{2+} , Zn^{2+} , Ba^{2+} , Mn^{2+} , Ca^{2+} , Mg^{2+} and Al^{3+} and the nine ligands chosen were thiolate ligands, namely mercaptoacetic acid (MAA), 3-mercaptopropionic acid (MPA), 11-mercaptoundecanoic acid (MUA), 3-mercaptopropanol (MPO), 2-aminoethanethiol (AET), L-cysteine (Cys), D-penicillamine (DPA), glutathione (GSH) and mercaptosuccinic acid (MSA). They observed a strongest fluorescence quenching by Cu^{2+} ions in no consideration to the capping ligand while Hg^{2+} ions also caused fluorescence quenching along with red shifting of the emission band. They had also found that the ligands with long aliphatic chains could protect the QDs from penetration of metal ions and hence lesser fluorescence quenching should be observed on metal binding when the QD is capped by such ligands [149]. Various papers on the use of CdSe/CdS core/shell QDs for Cu^{2+} ion detection have also been published which have been reviewed below:

8.3. CdSe/CdS : Copper

Lai et al. in 2006 synthesized mercaptoethanol modified CdSe/CdS QDs for the sensitive and selective determination of Cu^{2+} ions in the presence of other biologically important ions [150]. Then, in 2008, Zhang et al. [151] had synthesized L-cysteine coated water soluble CdSe/CdS QDs for the selective determination of Cu^{2+} ions in the presence of other physiologically essential cations such as Ca^{2+} , Mg^{2+} , Zn^{2+} , Al^{3+} , Fe^{3+} , Mn^{2+} and Ni^{2+} etc. with the limit of detection 3.0×10^{-9} mol L^{-1} for Cu^{2+} ions. They observed that fluorescence quenching of the PL of QDs could only be observed with copper ions and was insensitive to the presence of other cations [151].

Promising fluoroionophore candidates sensitive to Cu^{2+} ions have been synthesized by conjugating fluorescent CdSe/CdS core/shell QDs either with oleic acid or with MAO-mPEG in aqueous solutions [152]. Fluorescence quenching was observed when copper ions in both oxidizing and reducing environments i.e. Cu^{2+} and Cu^+ bind the above conjugated nanostructure with limit of detection found to be 16 nM and no interference from other metal ions such as Ag^+ , Al^{3+} , Ba^{2+} , Ca^{2+} , Cd^{2+} , Co^{2+} , Cr^{3+} , Fe^{2+} , Fe^{3+} , Hg^{2+} , K^+ , Mg^{2+} , Mn^{2+} , Na^+ , Ni^{2+} , Pb^{2+} , Sn^{2+} and Zn^{2+} was observed [152].

8.4. CdSe / ZnS: Mercury

Mercury is a well-known dangerous and widespread global pollutant [153] and is considered to be harmful for water and soil due to the long atmospheric residence time of $\text{Hg}(0)$ vapor and its oxidation to the soluble inorganic Hg^{2+} [154]. Sulfur calixarene capped CdSe/ZnS QDs have been reported for the selective and sensitive determination of $\text{Hg}(II)$ using the QD's fluorescence changes. The influence of other metal ions such as Li^+ , Na^+ , K^+ , Mg^{2+} , Ca^{2+} , Cu^{2+} , Zn^{2+} , Mn^{2+} , Co^{2+} , Ni^{2+} was very weak even if present at relatively higher concentration [27].

The use of luminescent and stable L-carnitine capped CdSe/ZnS core/shell QDs, which on interaction with mercury ions lead to quenching of photoluminescence and thus allow a sensitive determination of Hg^{2+} ions via analyte-induced changes in the photoluminescence of nanosensors has been reported [155]. The detection limit was as low as 0.18 μM with no interference of even very high concentrations of other metal ions such as alkali metal ions, alkaline earth metal ions, Ni^{2+} , Zn^{2+} , Fe^{2+} and Ag^+ and anions such as NO_3^- , SO_4^{2-} , CO_3^{2-} and halogen ions. Freeman et al. [156] in 2009 had employed nucleic acid modified CdSe/ZnS core/shell QDs for multiplexed optical detection of both Hg^{2+} and Ag^+ ions. CdSe/ZnS QDs were modified with thymine-rich nucleic acid for the selective analysis of Hg^{2+} and cytosine-rich nucleic acid for the selective analysis of Ag^+ and a luminescence quenching of CdSe/ZnS QDs was observed on interaction with both of these ions [156]. Water-soluble CdSe QDs, surface modified with β -cyclodextrin (β -CD-QDs) have been synthesized in order to discuss the effect of various anions on their photoluminescence and to compare the degree of quenching caused by them [157]. The observed degree of quenching by various anions decreases in the order: monoanion > dianion >> trianion. The fluorescence could be restored by exposing the QDs to sunlight which could further be employed for the detection of various ions such as Ag^+ , Hg^{2+} and Co^{2+} which could quench the restored fluorescence of the β -CD-QDs efficiently.

8.5. CdSe/ZnS: Potassium

Chen et al. (2006) have synthesized 15-crown-5 modified CdSe/ZnS QDs in aqueous solution exhibiting excellent selectivity towards K^+ ion and this recognition is due to the 15-crown-5/ K^+ /15-crown-5 sandwich type of complex formation via the Förster type of energy transfer between two different color QDs with the detection limit of the order of 10^{-6} M. The emission intensities were insensitive to the presence of various physiologically important cations like

Li^+ , Cs^+ , Mg^{2+} and Ca^{2+} . The authors had observed similar energy transfer phenomenon for Ba^{2+} ions as that for the K^+ ions by carrying out Ba^{2+} titration. Due to the almost similar sizes of K^+ (1.52 Å) and Ba^{2+} (1.49 Å) ions, the 15-crown-5/ Ba^{2+} /15-crown-5 sandwich type of association could also be run [158].

8.6. CdSe/ZnS: Cadmium

Cadmium is considered as a widespread health dangerous global pollutant and its level has been increased considerably in many areas due to human activity [159] as a result of mining, smelting, fossil fuel combustion, industrial use as in phosphate fertilizers and waste water sludge [160]. All of these are the cause of large scale environmental contamination by cadmium. Cadmium enters in biological systems through these sources and may lead to renal dysfunction, calcium metabolism disorders and an increased incidence of certain forms of cancer, possibly due to direct inhibition of DNA mismatch repair by cadmium [160-162]. With time, cadmium gets accumulated in tissues and produces severe health hazards. Thus, the sensitive and selective detection of cadmium in primary sources is highly needed. Currently, techniques for cadmium screening are labor intensive and high-priced [160, 163]. Since Cd^{2+} and Zn^{2+} ions occur mutually in nature, most of the chemosensors available are not able to distinguish them. Li and coworkers [164] have developed a sensor which selectively binds to Cd^{2+} in presence of Zn^{2+} by synthesizing L-carnitine (LC) capped CdSe/ZnS core/shell QDs. LC capped QDs are sensitive to cadmium ions (Fig. 10) over other metal ions such as Na^+ , K^+ , Mg^{2+} , Ca^{2+} , Ni^{2+} , Zn^{2+} , Fe^{2+} , Ag^+ and Pb^{2+} with a detection limit of 0.15 μM for Cd^{2+} ions. This could be applied for the determination of cadmium ions both biologically and environmentally.

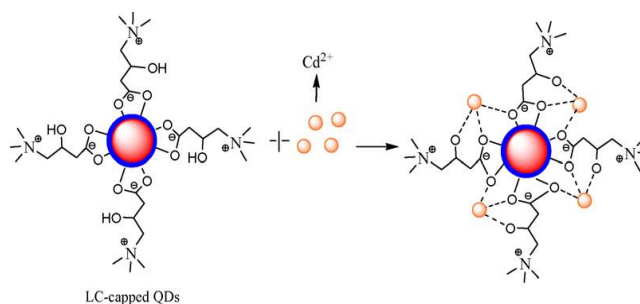


Fig. 10. Schematic illustration of interaction of LC-CdSe/ZnS with Cd^{2+} ions [164].

8.7. CdSe/ZnS: Lead

Although lead is important industrially as it is extensively used in making alloys, batteries, glasses and paints, its compounds are carcinogenic, interfere with the body processes and are considered to be toxic for biological systems as they can harm various body organs and tissues like heart, kidneys, bones and reproductive and nervous systems with symptoms like headache, abdominal pain, memory loss, weakness and pain [165, 166]. Therefore in order to evade heavy metal poisoning by Pb^{2+} ions, it is highly desirable to produce sensors which can selectively analyze Pb^{2+} ions.

Highly luminescent CdZnSe QDs capped with glutathione shells have been developed for the ultrasensitive analysis of Pb^{2+} ions with a 20 nM limit of detection [167]. Fluorescence quenching of the conjugated QD system was observed on interaction with Pb^{2+} ions due to stronger binding between heavy metal ions and the surface glutathione capping. CdSe/ZnS core/shell QD conjugates have been developed for the multiplexed detection of the heavy metal ions, Pb^{2+} and Cu^{2+} with the limit of detection 0.2 nM for Pb^{2+} and 0.5 nM for Cu^{2+} . For this, carboxyl-silanized QDs coupled to DNazymes were employed and the detection was based on FRET. In the absence of metal ions, quenching of QDs fluorescence was observed due to the presence of DNazymes, which act as quenchers, but in the presence of the target metal ion, due to the cleavage of DNazymes from QDs, the emission from QDs was restored [168]. Luan et al. [169] have synthesized mercaptopropionic acid modified CdSe/ZnS QDs for the sensitive detection of Pb^{2+} ions in water. Photoluminescence quenching was observed due to the cation exchange reaction (Zn^{2+} by Pb^{2+}) in water. However, this ion probe has a limitation that if in a sample Ag^+ and Cu^{2+} ions are also present, there is equal probability of replacing Zn^{2+} ions by these ions as that of Pb^{2+} ions and hence a similar quenching phenomenon is observed.

8.8. CdSe/ZnS: Cobalt and nickel

Baranov et al. [170] investigated a different type of optical sensing mechanism by utilizing dissociative luminescence sensors in which they had put in CdSe/ZnS QDs and 1-(2-pyridilazo)-2-naphthol (PAN). Formation of CdSe/ZnS-PAN complexes where PAN binds to the surface Zn^{2+} ions was observed to occur. Due to an efficient spectral overlap between the QDs photoluminescence and the PAN/ Zn^{2+} absorption bands, the QD luminescence is quenched via efficient FRET but in the presence of Co^{2+} and Ni^{2+} ions, reappearance of QD luminescence occurs due to dissociation of the QD/PAN complex and formation of PAN/Co and PAN/Ni complexes [170].

8.9. CdSe/ZnS: pH sensors

Semiconductor based biosensors EIS (electrolyte-insulator-semiconductor) have been employed [171] as pH sensors whose sensitivity depends on the properties of the sensing membrane surface. CdSe/ZnS QDs were deposited on the SiO_2 surface using a layer of chaperonin GroEL protein template and the pH sensitivity of bare SiO_2 were compared with the CdSe/ZnS modified sensing membranes. A more positively charged surface was observed at low pH due to more of H^+ ion concentration and a less positive surface was observed at high pH.

9. Detection of anions using surface modified CdSe QDs

Sensing and recognition of anions is of great importance, as they play a primary role in a wide range of areas such as in medicine, catalysis and various biological processes [172]. A lot of research has been focused on developing colorimetric [173] and fluorescent [174] techniques for

sensing various anions. However, these days major attention has been laid on the development of new fluorescent probes for sensing due to their simplicity and sensitivity. Although the detection technique is at a nascent stage, still QDs can be looked upon as promising candidates for anion sensing [175]. Here also, the same QDs i.e. CdSe and CdSe/ZnS were chosen to have a detailed overview of the work done in the sensing area.

9.1. CdSe: Cyanide

Cyanide finds applications in various industries such as in petrochemicals, polymers like nylon and acrylic plastics (which are also associated with environmental issues) metal extraction, gold mining, metal electroplating, fertilizer factories. These industries are majorly responsible for cyanide poisoning which affects the ability of cells to make use of oxygen. Concentrations of 0.5–3.5 mg per kg of body weight are lethal to humans since it immediately diffuses and binds with target sites very rapidly. Cyanide is also a constituent of tobacco smoke [176-183]. Cyanide containing compounds such as mercury cyanide, copper cyanide, gold cyanide, and silver cyanide release hydrogen cyanide gas which further reacts with acids which are harmful. Cyanide immediately spreads in the body and death can occur within seconds or minutes after a large dose mainly due to permanent neurological disability [184, 185]. Smoke inhalation from structural fires is the main cause of cyanide poisoning in Western countries [186]. Unfortunately no tests have been developed so far which leads to rapid confirmation of cyanide poisoning. Hence, there is a need to develop a novel inexpensive system which is simple to use for the detection of this ion. Jin et al. [187] synthesized novel and highly photoluminescent CdSe QDs surface-modified with *tert*-butyl-*N*-(2-mercaptoethyl)-carbamate (BMC) for the optical determination of cyanide ions and a detection limit of 1.1×10^{-7} M for cyanide ions was obtained. The important thing to be noted is that the effect of other inorganic anions like NO_3^- , Cl^- or SCN^- was negligible even if their concentration was 200 times than that of the CN^- ion concentration. Also, the sensitivity of the BMC-CdSe QDs to CN^- recognition was unchanged even after more than two months of storage [187]. The authors also have synthesized [84] surface-modified CdSe QDs with polar unidentate 2-mercaptoethane sulfonate [188] or mercaptoacetic groups [82] to analyze cyanide ion selectively through fluorescence quenching of the luminescent QD-conjugate in aqueous solution with a detection limit of 1.1×10^{-6} M. The presence of other common ions such as SO_4^{2-} , SO_3^{2-} , NO_3^- , NO_2^- , Cl^- , Br^- and acetate did not cause any interference in cyanide ion detection. Only I^- and SCN^- ions that too at concentrations higher than 2×10^{-4} M produce fluorescence quenching of the QD-conjugate [84]. A combination of TOPO-coated CdSe QDs, 2,2'-bipyridine(bipy) and CuCl_2 has been employed [178] as a cyanide probe. Fluorescence quenching of the QDs is observed as a result of electron transfer between the QD and the complex $[(\text{bipy})\text{CuCl}_2]$ formed as a 1:1 mixture of bipy and CuCl_2 [189]. On addition of cyanide ions, the cyanide reacts with copper ions and forms a stable $[\text{Cu}(\text{CN})_n]^{(n-1)-}$ complex [190] and this reaction is called demetallation of the $[(\text{bipy})\text{CuCl}_2]$ complex which can be used as a tool to detect cyanide ions.

This probe has an advantage that it works at the physiological pH 7.5, in the presence of water and in presence of other anions such as NO_3^- , AcO^- , SO_4^{2-} , F^- , Cl^- , Br^- , I^- , ClO_4^- , HCO_3^- and H_2PO_4^- at pH 7.5 [178].

9.2. CdSe: Nitrite

Nitrite ion detection is also of immense significance both ecologically and for public health fields. A variety of methods based on spectrophotometric [191], chromatographic [192], chemiluminescent [193] and electrochemical techniques [194, 195] have been developed for determination of nitrite ions but many of them are difficult to employ, time consuming and involve tedious sample pretreatment [194]. Liu et al. [196] demonstrated an electrochemiluminescent (ECL) method for the detection of nitrite based on the quenching of ECL emission of thioglycolic acid capped CdSe QDs with a limit of detection in the range from 1 μM to 0.5 mM, where the nitrite ions act as electroactive quenchers. This method is highly selective since the presence of other anions such as NO_3^- and Cl^- ions and cations such as Na^+ , K^+ and NH_4^+ does not cause any interference even at the concentration of 20 mM [196].

9.3. CdSe: Carbonate

Carbonate (CO_3^{2-}), a polyatomic anion, works as an important buffer in our blood and is also important industrially as in detergents, paper liquors, glasses, a chief constituent of limestone and so on.

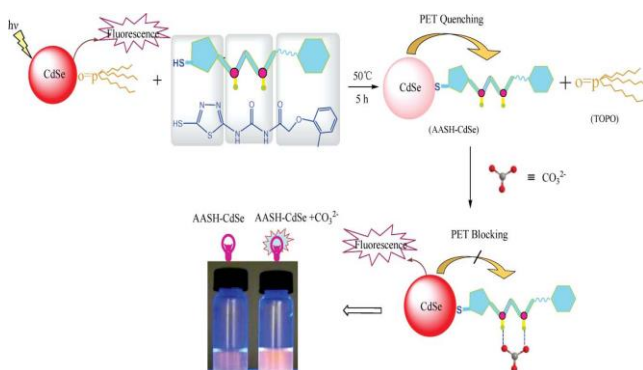


Fig. 11. Synthesis procedures of AASH functionalized CdSe QDs and a possible model for carbonate recognition [197].

A highly selective fluorescence nanosensor for carbonate anion detection has been designed [197] where the CdSe QDs were modified with thio ligands containing urea groups, i.e. N-(5-mercapto-1,3,4-thiadiazol-2-ylcarbamoyl)-2-(*o*-tolylxy) acetamide (AASH-CdSe QDs). The synthesized AASH-CdSe QDs could selectively analyze CO_3^{2-} ion by turning "on" the fluorescence response with a limit of detection 2.3×10^{-8} M. In the absence of CO_3^{2-} ions, recombination of the photogenerated electron is prevented due to transfer of this electron to the low lying π^* energy level on the ligand and hence charge separation occurs and "switches off" the QD emission but in the presence of carbonate anion, an electron transfer mechanism is prevented due to the formation of a complex AASH... CO_3^{2-} (Fig. 11), thereby "switching on" the fluorescence emission. The above conjugated nanosensor

can even analyze CO_3^{2-} anion in presence of anions like F^- , Cl^- , Br^- , I^- , HCO_3^- , CO_3^{2-} , HPO_4^{2-} , H_2PO_4^- , NO_3^- , NO_2^- and HSO_3^- .

10. Detection of anions using surface modified CdSe based core/shell QDs

Callan et al. [198] demonstrated that the surface functionalized CdSe/ZnS quantum dot fluorophore with a receptor 1-(2-mercapto-ethyl)-3-phenyl-thiourea can be adopted as a PET based organic dye sensor with comparable selectivity and sensitivity when an identical receptor was bound to the anthracene fluorophore.

10.1. CdSe/ZnS: Fluoride

Fluoride is of particular interest owing to its role in preventing dental caries and its use as a treatment for osteoporosis. As mentioned above, Callan et al. [198] reported an example of a PET operated quantum dot probe for sensing of anions by selecting 1-(2-mercapto-ethyl)-3-phenyl-thiourea as a receptor bound to CdSe/ZnS QDs. Charge neutral thioureas are useful as receptors for anions when bound to an anthracene fluorophore in a PET format [199]. Addition of Cl^- , F^- and AcO^- caused about 90% of fluorescence quenching due to hydrogen bonding interaction which led to an enhancement in the reduction potential of the receptor thereby increasing the rate of PET from the HOMO of the receptor to the quantum dot [199, 93, 200]. Mulrooney et al. [201] synthesized a sensor for anions using QDs as the signaling unit by modifying the surface of CdSe/ZnS core/shell QDs with 1-(bis(η^5 -cyclopentadienyl)iron)-methyl-3-(5,7-dimercapto-heptyl)-urea (ferrocenyl urea) and demonstrated the effect of the presence of fluoride ions on fluorescence emission of the conjugated structure. They observed that there is no fluorescence emission in the absence of fluoride ions most probably due to the electron transfer mechanism but fluorescence emission was "on" upon binding to fluoride ions due to modulation of the rate of PET between ferrocene units and the QDs.

10.2. CdSe/ZnS: Hydroxide

Gauci et al. [202] investigated the fluorescence quenching of CdSe/ZnS core/shell QDs by an aryl carboxylate moiety by synthesizing surface functionalized CdSe/ZnS core/shell QDs with *p*-mercaptomethyl benzoate to which the addition of hydroxide ions leads to fluorescence quenching as a result of hydrolysis of the ester via a carboxylic acid intermediate to the aryl carboxylate and afterwards photoinduced electron transfer reaction from an electron-rich benzoate moiety to the QD valence band [202].

10.3. CdSe/ZnS: Chloride

Chloride ion sensing is important both biologically and ecologically. Wang et al. [203] demonstrated chloride ion sensing by employing luminescent QDs in order to measure chloride ion concentration in the intracellular range. They had synthesized a QD-conjugate by conjugating a chloride ion receptor, 1-(2-mercapto-ethyl)-3-phenyl-thiourea with the water soluble CdSe/ZnS QDs. It was observed that

binding of chloride ions to the above conjugated QD leads to an electron transfer mechanism which leads to the fluorescence quenching of the QDs. The higher the Cl⁻ ion concentration, higher is the fluorescence quenching of the QD conjugate. They also verified the effectiveness of these nanosensors by employing them to dynamic [Cl⁻]_i measurements in epithelial cells. The above QD-conjugated structure proves to be a sensitive and selective chloride ion nanosensor with properties that can be utilized for drug discovery [204, 205].

Ruedas-Rama et al. [206] analyzed the chloride ion concentration using Cl⁻ ion sensitive QD-lucigenin conjugates where lucigenin serves as a chloride-sensitive indicator dye. A drastic drop off in the photoluminescence lifetime of both the QD and lucigenin was observed on combining these two, but on binding the chloride ion, the photoluminescence lifetime of QDs increased while that of the lucigenin dye decreased and an overall linear response was observed for Cl⁻ ion in the limit of 0.5 to 50 mM concentration. The above conjugate nanosensors can be widely employed for intracellular sensing of Cl⁻ ions.

11. Conclusion

CdSe and CdSe/ZnS core/shell quantum dots have emerged as promising candidates in the area of sensing of ions. This is due to the presence of extraordinary electronic and optical properties possessed by these nanostructures, thereby making them one of the most prolific nanomaterials alternatives to traditional fluorophores in a wide range of applications. This is attributed to the quantum confinement effect which makes them so unique. The tendency of tuning the band gap by varying the size of QDs has allowed scientists and researchers to play with these magical nanoclusters. All the colors of QDs can be excited by a single excitation source which makes it much easier to achieve multiplexed detection than traditional dyes that requires the excitation light source to be tuned into its respective absorption. In this review, we have reported how photoluminescent semiconductor nanocrystals, CdSe QDs and CdSe based core/shell QDs have been employed as selective and sensitive ion detectors by utilizing their optical properties. The mechanisms involved in sensing are mainly PET and FRET. In the majority of the sensing cases, we observe quenching of fluorescence while in some others enhancement is also observed depending on the electron transfer mechanism. We presume that this approach could lead to invention of novel luminescent sensors in the area of sensing various other types of analytes.

12. Future perspectives

Quantum dots, owing to their unique optical and electronic properties have emerged as potential analytical tools for the multiplexed, selective and sensitive determination of various analytes. Although quantum dot expertise is not in much use biologically due to their toxicity, hydrophobicity and difficulty in understanding the fluorescence quenching or enhancement mechanism, once the mechanism is fully understood, they can further be employed to detect ions at still lower concentrations and by carrying out various surface modifications. In future these novel nanosensors will drastically enlarge the scope to use them for studying

various biologically important ions in intracellular fluids. Prediction also exists to build up superior sources and detectors for use in optical gas sensors for analyzing concentrations of various harmful gases in the environment. This will provide helpful information aiming to design fluorophores with great versatility and flexibility.

13. Abbreviations

AASH N-(5-mercapto-1,3,4-thiadiazol-2-ylcarbamoyl)-2-(*o*-tolylxy) acetamide, **β-CD** β-Cyclodextrin, **bipy** 2,2'-bipyridine, **BMC** *tert*-butyl-*N*-(2-mercaptoethyl)-carbamate, **BSA** Bovine serum albumin, **Cys** L-cysteine, **DPA** D-penicillamine, **ECL** Electrochemiluminescent, **EIS** Electrolyte-insulator-semiconductor, **FITC** Fluorescein isothiocyanate, **FRET** Förster Resonance Energy Transfer, **GSH** Glutathione, **LC** L-carnitine, **MAA** Mercaptoacetic acid, **MPA** 3-mercaptopropionic acid, **MPO** 3-mercapto-1-propanol, 2-aminoethanethiol, **MSA** Mercaptosuccinic acid, **MUA** 11-mercaptoundecanoic acid, **MSA** Mercaptosuccinic acid, **PAN** 1-(2-pyridilazo)-2-naphthol, **PL** Photoluminescence, **PET** Photoinduced Electron Transfer, **PVA** Polyvinyl chloride, **QDs** Quantum dots, **TEA** Triethanolamine, **TCC** Thiocalix[4]arene carboxylic acid.

Acknowledgements

Financial assistance from "Delhi University's Scheme to Strengthen Research by Providing Funds to Faculty" is gratefully acknowledged. PM thanks the Council for Scientific and Industrial Research (CSIR), New Delhi, for a Senior Research Fellowship (Grant No. 09/045(0873)/2009 EMR-I) and JS gratefully thanks Hansraj College, University of Delhi for valuable support.

Reference

- Tiwari, A.; Demir, M. M.; (Ed.), *Advanced Sensor and Detection Materials*. WILEY-Scrivener Publishing LLC, USA, 2014. ISBN: [978-1-118-77348-2](#)
- Tiwari, A.; Tiwari, A.; (Ed.), *Bioengineered Nanomaterials*. CRC Press, USA, 2013. ISBN: [978-1-4665-8595-9](#)
- Tiwari, A.; Tiwari, A.; (Ed.), *Nanomaterials in Drug Delivery, Imaging and Tissue Engineering*. WILEY-Scrivener Publishing LLC, USA, 2013. ISBN: [978-1-1182-9032-3](#)
- Tiwari, A.; Ramalingam, M.; Kobayashi, H.; Turner, A. P. F.; (Ed.), *Biomedical Materials and Diagnostic Devices*. WILEY-Scrivener Publishing LLC, USA, 2012. ISBN: [978-11-180301-41](#)
- Tiwari, A.; Turner, A. P. F.; (Ed.), *Biosensors Nanotechnology*. WILEY-Scrivener Publishing LLC, USA, 2014. ISBN: [978-1-118-77351-2](#)
- Rogers, J. T.; Richards, J. G.; Wood, C. M. *Aquat. Toxicol.* **2003**, *64*, 215. DOI: [10.1016/S0166-445X\(03\)00053-5](#)
- Miyake, Y.; Togashi, H.; Tashiro, M.; Yamaguchi, H.; Oda, S.; Kudo, M.; Tanaka, Y.; Kondo, Y.; Sawa, R.; Fujimoto, T.; Machinami, T.; Ono, A. *J. Am. Chem. Soc.* **2006**, *128*, 2172. DOI: [10.1021/ja056354d](#)
- Verma, N.; Singh, M. *BioMetals* **2005**, *18*, 121. DOI: [10.1007/s10534-004-5787-3](#)
- Kanmani, S.; Gandhimathi, R. *App. Water Sci.* **2013**, *3*, 193. DOI: [10.1007/s13201-012-0072-z](#)
- Kunkel, R.; Manahan, S. E. *Anal. Chem.* **1973**, *45*, 1465. DOI: [10.1021/ac60330a024](#)
- Bings, N. H.; Bogaerts, A.; Broekaert, J. A. C. *Anal. Chem.* **2006**, *78*, 3917. DOI: [10.1021/ac060597m](#)
- Tanyanyiwa, J.; Hauser, P. C. *Electrophoresis* **2002**, *23*, 3781.
- Lorber, K. E. *Waste Manage Res.* 1986, *4*, 3. DOI: [10.1177/0734242X8600400102](#)
- Bertsch, P. M.; Hunter, D. B. *Chem. Rev.* **2001**, *101*, 1809. DOI: [10.1021/cr990070s](#)
- Czarnik, A. W. *Chem. Biol.* **1995**, *2*, 423. DOI: [10.1016/1074-5521\(95\)90257-0](#)
- Alivisatos, A. P. *J. Phys. Chem.* **1996**, *100*, 13226. DOI: [10.1021/jp9535506](#)

17. Sutherland, A. J. *Curr. Opin. Solid State Mater. Sci.* **2002**, 6, 365
DOI: [10.1016/S1359-0286\(02\)00081-5](https://doi.org/10.1016/S1359-0286(02)00081-5)
18. Smith, A. M.; Nie, S. *Analyst* **2004**, 129, 672.
DOI: [10.1039/b404498n](https://doi.org/10.1039/b404498n)
19. Alivisatos, A. P. *Science* **1996**, 271, 933.
DOI: [10.1126/science.271.5251.933](https://doi.org/10.1126/science.271.5251.933)
20. Chan, W. C. W.; Maxwell, D. J.; Gao, X.; Bailey, R. E.; Han, M.; Nie, S. *Curr. Opin. Biotechnol.* **2002**, 13, 40.
DOI: [10.1016/s0958-1669\(02\)00282-3](https://doi.org/10.1016/s0958-1669(02)00282-3)
21. Dabbousi, B. O.; Rodriguez-Viejo, J.; Mikulec, F. V.; Heine, J. R.; Mattoussi, H.; Ober, R.; Jensen, K. F.; Bawendi, M. G. *J. Phys. Chem. B* **1997**, 101, 9463.
DOI: [10.1021/jp971091y](https://doi.org/10.1021/jp971091y)
22. Frasco, M. F.; Chaniotakis, N. *Sensors* **2009**, 9, 7266.
DOI: [10.3390/s90907266](https://doi.org/10.3390/s90907266)
23. Smith, A. M.; Shuming, N. *Acc. Chem. Res.* **2010**, 43, 190.
DOI: [10.1021/ar9001069](https://doi.org/10.1021/ar9001069)
24. Nirmal, M.; Brus, L. *Acc. Chem. Res.* **1999**, 32, 407.
DOI: [10.1021/ar9700320](https://doi.org/10.1021/ar9700320)
25. Liu J.; Li H.; Wang W.; Xu H.; Yang X.; Liang, J.; He, Z. *Small* **2006**, 2, 999.
DOI: [10.1002/smll.200500421](https://doi.org/10.1002/smll.200500421)
26. Li, H.; Xiong, W.; Yan, Y.; Liu, J.; Xu, H.; Yang, X. *Mater. Letts.* **2006**, 60, 703.
DOI: [10.1016/j.matlet.2005.09.067](https://doi.org/10.1016/j.matlet.2005.09.067)
27. Li, H.; Zhang, Y.; Wang, X.; Xiong, D.; Bai, Y. *Mater. Letts.* **2007**, 61, 1474.
DOI: [10.1016/j.matlet.2006.07.064](https://doi.org/10.1016/j.matlet.2006.07.064)
28. Liang, J. -G.; Zhang, S. -S.; Ai, X. -P.; Ji, X. -H.; He, Z. -K. *Spectrochimica Acta Part A.* **2005**, 61, 2974.
DOI: [10.1016/j.saa.2004.11.013](https://doi.org/10.1016/j.saa.2004.11.013)
29. Ma, N.; Yang, J.; Stewart, K. M.; Kelley, S. O. *Langmuir* **2007**, 23, 12783.
DOI: [10.1021/la7017727](https://doi.org/10.1021/la7017727)
30. Michalet, X.; Pinaud, F. F.; Bentolila, L. A.; Tsay, J. M.; Doose, S.; Li, J. J.; Sundaresan, G.; Wu, A. M.; Gambhir, S. S.; Weiss, S. *Science* **2005**, 307, 538.
DOI: [10.1126/science.1104274](https://doi.org/10.1126/science.1104274)
31. Stuczynski, S. M.; Brennan, J. G.; Steigerwald, M. L. *Inorg. Chem.* **1989**, 28, 4431. DOI: [10.1021/ic00324a001](https://doi.org/10.1021/ic00324a001)
32. Yoon, J. -H.; Chae, W. -S.; Im, S. -J.; Kim, Y. -R. *Mater. Lett.* **2005**, 59, 1430.
DOI: [10.1016/j.matlet.2004.11.056](https://doi.org/10.1016/j.matlet.2004.11.056)
33. Kamat, P.V. *J. Phys. Chem. Lett.* **2013**, 4, 908.
DOI: [10.1021/jz4000522](https://doi.org/10.1021/jz4000522)
34. Costa-Fernández, J. M.; Pereiro, R.; Sanz-Medel, A. *Trends Anal. Chem.* **2006**, 25, 207.
DOI: [10.1016/j.trac.2005.07.008](https://doi.org/10.1016/j.trac.2005.07.008)
35. Lim, J.; Jun, S.; Jang, E.; Baik, H.; Kim, H.; Cho, J. *Adv. Mater.* **2007**, 19, 1927.
DOI: [10.1002/adma.200602642](https://doi.org/10.1002/adma.200602642)
36. Medintz, I. L.; Uyeda, H. T.; Goldman, E. R.; Mattoussi, H. *Nat. Mater.* **2005**, 4, 435.
DOI: [10.1038/nmat1390](https://doi.org/10.1038/nmat1390)
37. Robel, I.; Subramanian, V.; Kuno, M.; Kamat, P. V. *J. Am. Chem. Soc.* **2006**, 128, 2385.
DOI: [10.1021/ja056494n](https://doi.org/10.1021/ja056494n)
38. Murphy, C. J. *Anal. Chem.* **2002**, 74, 520A.
DOI: [10.1021/ac022124v](https://doi.org/10.1021/ac022124v)
39. Galian, R. E.; de la Guardia, M. *Trends in Analytical Chemistry* **2009**, 28, 279.
DOI: [10.1016/j.trac.2008.12.001](https://doi.org/10.1016/j.trac.2008.12.001)
40. Ekimov, A. I.; Onushchenko, A. A. *Sov. Phys. Semicond.* **1982**, 16, 775.
41. Brus, L. E. *J. Chem. Phys.* **1983**, 79, 5566.
DOI: [10.1063/1.445676](https://doi.org/10.1063/1.445676)
42. Efros, Al. L.; Efros, A. L. *Sov. Phys. Semicond.* **1982**, 16, 772.
43. Bera, D.; Qian, L.; Tseng T. -K.; Holloway, P. H. *Materials*, **2010**, 3, 2260.
DOI: [10.3390/ma3042260](https://doi.org/10.3390/ma3042260)
44. Gulia, S.; Kakkar, R. *Adv. Mater. Lett.* **2013**, 4, 876.
DOI: [10.5185/amlett.2013.3440](https://doi.org/10.5185/amlett.2013.3440)
45. Murray, C. B.; Norris, D. J.; Bawendi, M. G. *J. Am. Chem. Soc.* **1993**, 115, 8706.
DOI: [10.1021/ja00072a025](https://doi.org/10.1021/ja00072a025)
46. Troparevsky, M. C.; Kronik, L.; Chelikowsky, J. R. *J. Chem. Phys.* **2003**, 119, 2284.
DOI: [10.1063/1.1585013](https://doi.org/10.1063/1.1585013)
47. Cai, W.; Shin, D. -W.; Chen, K.; Gheysens, O.; Cao, Q.; Wang, S. X.; Gambhir, S. S.; Chen, X. *Nano Lett.* **2006**, 6, 669.
DOI: [10.1021/nl052405t](https://doi.org/10.1021/nl052405t)
48. Derfus, A. M.; Chen, A. A.; Min, D. -H.; Ruoslahti, E.; Bhatia, S. N. *Bioconjugate Chem.* **2007**, 18, 1391.
DOI: [10.1021/bc060367e](https://doi.org/10.1021/bc060367e)
49. Lee, J.; Govorov, A. O.; Dulka, J.; Kotov, N. A. *Nano Lett.* **2004**, 4, 2323.
DOI: [10.1021/nl048669h](https://doi.org/10.1021/nl048669h)
50. Rozenzhak, S. M.; Kadakia, M. P.; Caserta, T. M.; Westbrook, T. R.; Stone, M. O.; Naik, R. R. *Chem. Commun.* **2005**, 2217.
DOI: [10.1039/b418454h](https://doi.org/10.1039/b418454h)
51. Vu, T. Q.; Maddipati, R.; Blute, T. A.; Nehilla, B. J.; Nusblat, L.; Desai, T. A. *Nano Lett.* **2005**, 5, 603.
DOI: [10.1021/nl047977c](https://doi.org/10.1021/nl047977c)
52. Zhang, Y.; So, M. K.; Rao, J. *Nano Lett.* **2006**, 6, 1988.
DOI: [10.1021/nl0611586](https://doi.org/10.1021/nl0611586)
53. Derfus, A. M.; Chan, W. C. W.; Bhatia, S. N. *Nano Lett.* **2004**, 4, 11.
DOI: [10.1021/nl0347334](https://doi.org/10.1021/nl0347334)
54. Hoshino, A.; Fujioka, K.; Oku, T.; Suga, M.; Sasaki, Y. F.; Ohta, T.; Yasuhara, M.; Suzuki, K.; Yamamoto, K. *Nano Lett.* **2004**, 4, 2163.
DOI: [10.1021/nl048715d](https://doi.org/10.1021/nl048715d)
55. Mancini, M. C.; Kairdolf, B. A.; Smith, A. M.; Nie, S. *J. Am. Chem. Soc.* **2008**, 130, 10836.
DOI: [10.1021/ja8040477](https://doi.org/10.1021/ja8040477)
56. Moussodia, R. -O.; Balan, L.; Merlin, C.; Mustin, C.; Schneider, R. *J. Mater. Chem.* **2010**, 20, 1147.
DOI: [10.1039/b917629b](https://doi.org/10.1039/b917629b)
57. Oh, J. K.; *J. Mater. Chem.* **2010**, 20, 8433.
DOI: [10.1039/c0jm01084g](https://doi.org/10.1039/c0jm01084g)
58. Malik, P.; Gulia, S.; Kakkar, R. *Adv. Mat. Lett.* **2013**, 4, 811.
DOI: [10.5185/amlett.2013.3437](https://doi.org/10.5185/amlett.2013.3437)
59. Dubois, F.; Mahler, B.; Dubertret, B.; Doris, E.; Mioskowski, C. J. *Am. Chem. Soc.* **2007**, 129, 482.
DOI: [10.1021/ja067742y](https://doi.org/10.1021/ja067742y)
60. Alivisatos, P. *Nat. Biotechnol.* **2004**, 22, 47.
DOI: [10.1038/nbt927](https://doi.org/10.1038/nbt927)
61. Schlamp, M. C.; Peng, X.; Alivisatos, A. P. *J. Appl. Phys.* **1997**, 82, 5837.
DOI: [10.1063/1.366452](https://doi.org/10.1063/1.366452)
62. Wang, J.; Han, S.; Ke, D.; Wang, R. *J. Nanomater.* **2012**, 2012, 1.
DOI: [10.1155/2012/129041](https://doi.org/10.1155/2012/129041)
63. Tiwari, A.; Mishra, A. K.; Kobayashi, H.; Turner, A. P. F.; (Ed.), *Intelligent Nanomaterials*. WILEY-Scrivener Publishing LLC, USA, **2012**, pp 16-17.
ISBN: 978-04-709387-99
64. Colvin, V. L.; Goldstein, A. N.; Alivisatos, A. P. *J. Am. Chem. Soc.* **1992**, 114, 5221. DOI: [10.1021/ja00039a038](https://doi.org/10.1021/ja00039a038)
65. Dabbousi, B. O.; Murray, C. B.; Rubner, M. F.; Bawendi, M. G. *Chem. Mater.* **1994**, 6, 216.
DOI: [10.1021/cm00038a020](https://doi.org/10.1021/cm00038a020)
66. Murray, C. B.; Kagan, C. R.; Bawendi, M. G. *Science* **1995**, 270, 1335.
DOI: [10.1126/science.270.5240.1335](https://doi.org/10.1126/science.270.5240.1335)
67. Wang, Q.; Kuo, Y.; Wang, Y.; Shin, G.; Ruengruglikit, C.; Huang, Q. *J. Phys. Chem. B* **2006**, 110, 16860.
DOI: [10.1021/jp062279x](https://doi.org/10.1021/jp062279x)
68. Danek, M.; Jensen, K. F.; Murray, C. B.; Bawendi, M. G. *Chem. Mater.* **1996**, 8, 173.
DOI: [10.1021/cm9503137](https://doi.org/10.1021/cm9503137)
69. Hines, M. A.; Guyot-Sionnest, P. *J. Phys. Chem.* **1996**, 100, 468.
DOI: [10.1021/jp9530562](https://doi.org/10.1021/jp9530562)
70. Kortan, A. R.; Hull, R.; Opila, R. L.; Bawendi, M. G.; Steigerwald, M. L.; Carroll, P. J.; Brus, L. E. *J. Am. Chem. Soc.* **1990**, 112, 1327.
DOI: [10.1021/ja00160a005](https://doi.org/10.1021/ja00160a005)
71. Littau, K. A.; Szajowski, P. J.; Muller, A. J.; Kortan, A. R.; Brus, L. E. *J. Phys. Chem.* **1993**, 97, 1224.
DOI: [10.1021/j100108a019](https://doi.org/10.1021/j100108a019)
72. Mews, A.; Eychmüller, A.; Giersig, M.; Schooss, D.; Weller, H. *J. Phys. Chem.* **1994**, 98, 934.
DOI: [10.1021/j100054a032](https://doi.org/10.1021/j100054a032)
73. Tian, Y.; Newton, T.; Kotov, N. A.; Guldi, D. M.; Fendler, J. H. *J. Chem. Phys.* **1996**, 100, 8927.

- DOI: [10.1021/jp9519651](https://doi.org/10.1021/jp9519651)
74. Wilson, W. L.; Szajowski, P. F.; Brus, L. E. *Science* **1993**, 262, 1242.
DOI: [10.1126/science.262.5137.1242](https://doi.org/10.1126/science.262.5137.1242)
75. Youn, H. -C.; Baral, S.; Fendler, J. H. *J. Phys. Chem.* **1988**, 92, 6320.
DOI: [10.1021/j100333a029](https://doi.org/10.1021/j100333a029)
76. Peter, R.; Protière, M.; Li, L. *Small* **2009**, 5, 154.
DOI: [10.1002/smll.200800841](https://doi.org/10.1002/smll.200800841)
77. Henglein, A. *Chem. Rev.* **1989**, 89, 1861.
DOI: [10.1021/cr00098a010](https://doi.org/10.1021/cr00098a010)
78. Pons, T.; Medintz, I. L.; Wang, X.; English, D. S.; Mattoussi, H. *J. Am. Chem. Soc.* **2006**, 128, 15324.
DOI: [10.1021/ja0657253](https://doi.org/10.1021/ja0657253)
79. Miller, J. N. *Analyst*, **2005**, 130, 265.
DOI: [10.1039/b314346p](https://doi.org/10.1039/b314346p)
80. Resch-Genger, U.; Grabolle, M.; Cavaliere-Jaricot, S.; Nitschke, R.; Nann, T. *Nature Methods* **2008**, 5, 763.
DOI: [10.1038/nmeth.1248](https://doi.org/10.1038/nmeth.1248)
81. Wu, X.; Liu, H.; Liu, J.; Haley, K. N.; Treadway, J. A.; Larson, J. P.; Ge, N.; Peale, F.; Bruchez, M. P. *Nat. Biotechnol.* **2003**, 21, 41.
DOI: [10.1038/nbt764](https://doi.org/10.1038/nbt764)
82. Chan, W. C. W.; Nie, S. *Science* **1998**, 281, 2016.
DOI: [10.1126/science.281.5385.2016](https://doi.org/10.1126/science.281.5385.2016)
83. Bruchez, Jr. M.; Moronne, M.; Gin, P.; Weiss, S.; Alivisatos, A. P. *Science* **1998**, 281, 2013.
DOI: [10.1126/science.281.5385.2013](https://doi.org/10.1126/science.281.5385.2013)
84. Jin, W. J.; Fernández-Argüelles, M. T.; Costa-Fernández, J. M.; Pereiro, R.; Sanz-Medel, A. *Chem. Commun.* **2005**, 883.
DOI: [10.1039/b414858d](https://doi.org/10.1039/b414858d)
85. Valledor, M.; Campo, J. C.; Ferrero, F. J.; Fernandez-Arguelles, M. T.; Sanz-Medel, A. *Instrumentation and Measurement, Technology Conference - IMTC 2007, Warsaw, Poland, May 1-3, 2007*, 1. ISSN: 1091-5281
DOI: [10.1109/IMTC.2007.379412](https://doi.org/10.1109/IMTC.2007.379412)
86. Callan, J. F.; De Silva, A. P.; Mulrooney, R. C.; Mc Caughan, B. *J. Inclusion Phenom. Macrocycl. Chem.* **2007**, 58, 257.
DOI: [10.1007/s10847-006-9152-8](https://doi.org/10.1007/s10847-006-9152-8)
87. Chen, Y.; Rosenzweig, Z. *Anal. Chem.* **2002**, 74, 5132.
DOI: [10.1021/ac0258251](https://doi.org/10.1021/ac0258251)
88. de Silva, A. P.; Gunaratne, H. Q. N.; Gunnlaugsson, T.; Huxley, A. J. M.; McCoy, C. P.; Rademacher, J. T.; Rice, T. E. *Chem. Rev.* **1997**, 97, 1515.
DOI: [10.1021/cr960386p](https://doi.org/10.1021/cr960386p)
89. Chatterjee, A.; Suzuki, T. M.; Takahashi, Y.; Tanaka, D. A. P. *Chem. Eur. J.* **2003**, 9, 3920.
DOI: [10.1002/chem.200204613](https://doi.org/10.1002/chem.200204613)
90. Fahmi, C. J.; Yang, L.; VanDerveer, D. G. *J. Am. Chem. Soc.* **2003**, 125, 3799.
DOI: [10.1021/ja028266o](https://doi.org/10.1021/ja028266o)
91. Gunnlaugsson, T.; Davis, A. P.; Glynn, M. *Chem. Commun.* **2001**, 2556.
DOI: [10.1039/b107608f](https://doi.org/10.1039/b107608f)
92. Gunnlaugsson, T.; Davis, A. P.; O'Brien, J. E.; Glynn, M. *Org. Lett.* **2002**, 4, 2449.
DOI: [10.1021/ol026004l](https://doi.org/10.1021/ol026004l)
93. Gunnlaugsson, T.; Davis, A. P.; O'Brien, J. E.; Glynn, M. *Org. Biomol. Chem.* **2005**, 3, 48.
DOI: [10.1039/B409018G](https://doi.org/10.1039/B409018G)
94. Arimori, S.; Bell, M. L.; Oh, C. S.; Frimat, K. A.; James, T. D. *J. Chem. Soc., Perkin Trans.* **2002**, 1, 803-808.
DOI: [10.1039/b108998f](https://doi.org/10.1039/b108998f)
95. Cooper, C. R.; James, T. D. *J. Chem. Soc. Perkin Trans.* **2000**, 1, 963. DOI: [10.1039/a909145i](https://doi.org/10.1039/a909145i)
96. de Silva, A. P.; Moody, T. S.; Wright, G. D. *Analyst* **2009**, 134, 2385.
DOI: [10.1039/b912527m](https://doi.org/10.1039/b912527m)
97. de Silva, A. P.; Fox, D. B.; Huxley, A. J. M.; Moody, T. S. *Coord. Chem. Rev.* **2000**, 205, 41.
DOI: [10.1016/S0010-8545\(00\)00238-1](https://doi.org/10.1016/S0010-8545(00)00238-1)
98. Anni, M.; Manna, L.; Cingolani, R.; Valerini, D.; Creti, A.; Lomascolo, M. *Appl. Phys. Lett.* **2004**, 85, 4169.
DOI: [10.1063/1.1814795](https://doi.org/10.1063/1.1814795)
99. Clapp, A. R.; Medintz, I. L.; Mauro, J. M.; Fisher, B. R.; Bawendi, M. G.; Mattoussi, H. *J. Am. Chem. Soc.* **2004**, 126, 301.
DOI: [10.1021/ja037088b](https://doi.org/10.1021/ja037088b)
100. Clapp, A. R.; Medintz, I. L.; Fisher, B. R.; Anderson, G. P.; Mattoussi, H. *J. Am. Chem. Soc.* **2005**, 127, 1242.
DOI: [10.1021/ja045676z](https://doi.org/10.1021/ja045676z)
101. Goldman, E. R.; Medintz, I. L.; Whitley, J. L.; Hayhurst, A.; Clapp, A. R.; Uyeda, H. T.; Deschamps, J. R.; Lassman, M. E.; Mattoussi, H. *J. Am. Chem. Soc.* **2005**, 127, 6744.
DOI: [10.1021/ja043677l](https://doi.org/10.1021/ja043677l)
102. Kagan, C. R.; Murray, C. B.; Nirmal, M.; Bawendi, M. G. *Phys. Rev. Lett.* **1996**, 76, 1517.
DOI: [10.1103/PhysRevLett.76.1517](https://doi.org/10.1103/PhysRevLett.76.1517)
103. Mamedova, N. N.; Kotov, N. A.; Rogach, A. L.; Studer, J. *Nano Letters* **2001**, 1, 281.
DOI: [10.1021/nl015519n](https://doi.org/10.1021/nl015519n)
104. Medintz, I. L.; Clapp, A. R.; Mattoussi, H.; Goldman, E. R.; Fisher, B. R.; Mauro, J. M. *Nat. Mater.* **2003**, 2, 630.
DOI: [10.1038/nmat961](https://doi.org/10.1038/nmat961)
105. Willard, D. M.; Carillo, L. L.; Jung, J.; & Orden, A. V. *Nano Lett.* **2001**, 1, 469.
DOI: [10.1021/nl015565n](https://doi.org/10.1021/nl015565n)
106. Förster, T. *Discuss. Faraday Soc.* **1959**, 27, 7.
DOI: [10.1039/DF9592700007](https://doi.org/10.1039/DF9592700007)
107. Zheng, J. Spectroscopy-Based Quantitative Fluorescence Resonance Energy Transfer Analysis. In Stockand, J. D.; Shapiro, M. S.; (Eds.) *Methods in Molecular Biology, Ion Channels: Methods and Protocols*, Totowa, New Jersey: Humana Press. **2006**, 337, 65. ISBN: 978-1-59745-095-9.
108. Sapsford, K. E.; Berti L.; Medintz, I. L. *Angew. Chem. Int. Ed.*, **2006**, 45, 4562.
DOI: [10.1002/anie.200503873](https://doi.org/10.1002/anie.200503873)
109. Morello, G.; Anni, M.; Cozzoli, P. D.; Manna, L.; Cingolani, R.; Giorgi, M. D. *J. Phys. Chem. C* **2007**, 111, 10541.
DOI: [10.1021/jp072783h](https://doi.org/10.1021/jp072783h)
110. Mutlugün, E.; Nizamoglu, S.; Demir, H. V. *Appl. Phys. Lett.* **2009**, 95, 033106.
DOI: [10.1063/1.3182798](https://doi.org/10.1063/1.3182798)
111. Zhou, M.; Ghosh, I. *Biopolymers (PeptideScience)* **2006**, 88, 325.
DOI: [10.1002/bip.20655](https://doi.org/10.1002/bip.20655)
112. Forster, T. *Annalen der Physik* **1948**, 437, 55.
DOI: [10.1002/andp.19484370105](https://doi.org/10.1002/andp.19484370105)
113. Clegg, R. M. "Fluorescence Resonance Energy Transfer," In: Wang, X. F. & Herman, B. Eds., *Fluorescence Imaging Spectroscopy and Microscopy*, 1996, John Wiley, New York, pp. 179-252.
ISBN: 978-0-471-01527-7
114. Lackowicz, J. R. *Principles of Fluorescence Spectroscopy*, **2007**, 3rd Edition, Springer Science and Business Media, LLC, New York. ISBN: 13: 978-0-387-46312-7
115. Somers, R. C.; Bawendi, M. G.; Nocera, D. G. *Chem. Soc. Rev.* **2007**, 36, 579.
DOI: [10.1039/b517613c](https://doi.org/10.1039/b517613c)
116. Rogach, A. L.; Klar, T. A.; Lupton, J. M.; Meijerink, A.; Feldmann, J. *J. Mater. Chem.* **2009**, 19, 1208.
DOI: [10.1039/b812884g](https://doi.org/10.1039/b812884g)
117. Smith, A. M.; Duan, H.; Mohs, A. M.; Nie, S. *Adv. Drug Deliv. Rev.* **2008**, 60, 1226.
DOI: [10.1016/j.addr.2008.03.015](https://doi.org/10.1016/j.addr.2008.03.015)
118. Shivkumar, M. A.; Inamdar, L. S.; Rabinal, M. H. K.; Mulimani, B. G.; Rao, G. M. A.; Inamdar, S. R. *Open Journal of Physical Chemistry* **2013**, 3, 40.
DOI: [10.4236/ojpc.2013.31006](https://doi.org/10.4236/ojpc.2013.31006)
119. Wang, X.; Ruedas-Rama, M. J.; Hall, E. A. H. *Anal. Lett.* **2007**, 40, 1497.
DOI: [10.1080/00032710701381044](https://doi.org/10.1080/00032710701381044)
120. Moore, D. E.; Patel, K. *Langmuir* **2001**, 17, 2541.
DOI: [10.1021/la001416t](https://doi.org/10.1021/la001416t)
121. Frasco, M. F.; Chaniotakis, N. A. *Semiconductor International Conference CAS 2009*, 12-14 Oct. **2009**, 1, 77.
DOI: [10.1109/SMICND.2009.5336603](https://doi.org/10.1109/SMICND.2009.5336603)
122. Frasco, M. F.; Vamvakaki, V.; Chaniotakis, N. *J. Nanopart. Res.* **2010**, 12, 1449.
DOI: [10.1007/s11051-009-9714-y](https://doi.org/10.1007/s11051-009-9714-y)
123. Sarell, C. J.; Wilkinson, S. R.; Viles, J. H. *J. Biol. Chem.* **2010**, 285, 41533.
DOI: [10.1074/jbc.M110.171355](https://doi.org/10.1074/jbc.M110.171355)
124. Dudzik, C. G.; Walter, E. D.; Millhauser, G. L. *Biochemistry* **2011**, 50, 1771. DOI: [10.1021/bi101912q](https://doi.org/10.1021/bi101912q)
125. Tanner, M. S. *Am. J. Clin. Nutr.* **1998**, 67, 1074S.
126. Mori, I.; Fujimoto, T.; Fujita, Y.; Matsuo, T. *Talanta* **1995**, 42, 77.
DOI: [10.1016/0039-9140\(94\)00219-1](https://doi.org/10.1016/0039-9140(94)00219-1)

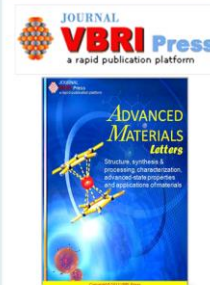
127. Pinto, J. J.; Moreno, C.; García-Vargas, M. *Anal. Bioanal. Chem.* **2002**, 373, 844.
DOI: [10.1007/s00216-002-1403-y](https://doi.org/10.1007/s00216-002-1403-y)
128. Fu, D.; Yuan, D. *Spectrochim. Acta A* **2007**, 66, 434.
DOI: [10.1016/j.saa.2006.03.018](https://doi.org/10.1016/j.saa.2006.03.018)
129. Kessler, M. A. *Anal. Chim. Acta.* **1998**, 364, 125.
DOI: [10.1016/S0003-2670\(98\)00152-4](https://doi.org/10.1016/S0003-2670(98)00152-4)
130. Cao, Q. -E.; Wang, K.; Hu, Z.; Xu, Q. *Talanta* **1998**, 47, 921.
DOI: [10.1016/S0039-9140\(98\)00161-1](https://doi.org/10.1016/S0039-9140(98)00161-1)
131. Fernández-Argüelles, M. T.; Jin, W. J.; Costa-Fernández, J. M.; Pereiro, R.; Sanz-Medel, A. *Anal. Chim. Acta.* **2005**, 549, 20.
DOI: [10.1016/j.aca.2005.06.013](https://doi.org/10.1016/j.aca.2005.06.013)
132. Quitaneg, A. C.; Santos, G. N. C. *International Journal of Scientific & Engineering Research*, **2011** (December), 2.
ISSN: [2229-5518](https://doi.org/10.2229-5518)
133. Liang, J. -G.; Ai, X. -P.; He, Z. -K.; Pang, D. -W. *Analyst* **2004**, 129, 619.
DOI: [10.1039/b317044f](https://doi.org/10.1039/b317044f)
134. Ingole, P. P.; Abhyankar, R. M.; Prasad, B. L. V.; Haram, S. K. *Mat. Sci. Eng. B* **2010**, 168, 60.
DOI: [10.1016/j.mseb.2009.10.033](https://doi.org/10.1016/j.mseb.2009.10.033)
135. Mahmoud, W. E. *Sensors and Actuators B* **2012**, 164, 76.
DOI: [10.1016/j.snb.2012.01.073](https://doi.org/10.1016/j.snb.2012.01.073)
136. U.S. EPA 2005. *Regulatory Impact Analysis of the Final Clean Air Mercury Rule: Basic Information*. Washington, DC: U.S. Environmental Protection Agency.
http://www.epa.gov/ttnecas1/regdata/RIAs/mercury_ria_final.pdf
137. Šandor, M.; Geistmann, F. & Schuster, M. *Anal. Chim. Acta* **1999**, 388, 19.
DOI: [10.1016/S0003-2670\(99\)00096-3](https://doi.org/10.1016/S0003-2670(99)00096-3)
138. Lista, A. G.; Palomeque, M. E.; Band, B. S. F. *Talanta* **1999**, 50, 881.
DOI: [10.1016/S0039-9140\(99\)00181-2](https://doi.org/10.1016/S0039-9140(99)00181-2)
139. Juskowiak, B. *Anal. Chim. Acta* **1996**, 320, 115.
DOI: [10.1016/0003-2670\(95\)00511-0](https://doi.org/10.1016/0003-2670(95)00511-0)
140. Hosseini, M. S.; Hashemi-Moghaddam, H. *Anal. Sci.* **2004**, 20, 1449.
DOI: [10.2116/analsci.20.1449](https://doi.org/10.2116/analsci.20.1449)
141. Chen, J.; Gao, Y. C.; Xu, Z. B.; Wu, G. H.; Chen, Y. C.; Zhu, C. Q. *Anal. Chim. Acta* **2006**, 577, 77.
DOI: [10.1016/j.aca.2006.06.039](https://doi.org/10.1016/j.aca.2006.06.039)
142. Shang, Z. B.; Wang, Y.; Jin, W. J. *Talanta* **2009**, 78, 364.
DOI: [10.1016/j.talanta.2008.11.025](https://doi.org/10.1016/j.talanta.2008.11.025)
143. Ruedas-Rama, M. J.; Hall, E. A. H. *Anal. Chem.* **2008**, 80, 8260.
DOI: [10.1021/ac801396y](https://doi.org/10.1021/ac801396y)
144. Ganguly, R.; Wang, S.; Huang, D. *Nanosci. Nanotechnol. Lett.* **2010**, 2, 208.
DOI: [10.1166/nml.2010.1060](https://doi.org/10.1166/nml.2010.1060)
145. Xie, H. -Y.; Liang, J. -G.; Zhang, Z. -L.; Liu, Y.; He, Z. -K.; Pang, D. -W. *Spectrochim. Acta. A* **2004**, 60, 2527.
DOI: [10.1016/j.saa.2003.12.039](https://doi.org/10.1016/j.saa.2003.12.039)
146. Jin, T.; Fujii, F.; Yamada, E.; Nodasaka, Y.; Kinjo, M. *Comb. Chem. High T. Scr.* **2007**, 10, 473.
DOI: [10.2174/138620707781996466](https://doi.org/10.2174/138620707781996466)
147. Callan, J. F.; Mulrooney, R. C. *Phys. Status Solidi C* **2009**, 6, 920.
DOI: [10.1002/pssc.200880571](https://doi.org/10.1002/pssc.200880571)
148. Sung, T. -W.; Lo, Y. -L. *Sensor Actuat. B-Chem.* **2012**, 165, 119.
DOI: [10.1016/j.snb.2012.02.028](https://doi.org/10.1016/j.snb.2012.02.028)
149. Zeng, T.; Hu, Y.; Wang, N.; Xia, C.; Li, S.; Zu, Y.; Liu, L.; Yao, Z.; Zhao, Y.; Wu, H. -C. *Phys. Chem. Chem. Phys.* **2013**, 15, 18710.
DOI: [10.1039/c3cp52666f](https://doi.org/10.1039/c3cp52666f)
150. Lai, Y.; Yu, Y.; Zhong, P.; Wu, J.; Long Z.; Liang, C. *Anal. Lett.* **2006**, 39, 1201.
DOI: [10.1080/00032710600622290](https://doi.org/10.1080/00032710600622290)
151. Zhang, Y. -h.; Zhang, H. -s.; Guo, X. -f.; Wang, H. *Microchem. J.* **2008**, 89, 142.
DOI: [10.1016/j.microc.2008.01.008](https://doi.org/10.1016/j.microc.2008.01.008)
152. Cao, Z.; Gu, Z.; Zeng, J. -L.; Liu, J. -H.; Deng, Q.; Fan, J. -B.; Xiang, J. -N. *Anal. Sci. The Japan Society for Analytical Chemistry* **2011**, 27, 643.
DOI: [10.2116/analsci.27.643](https://doi.org/10.2116/analsci.27.643)
153. Driscoll, C. T.; Mason, R. P.; Chan, H. M.; Jacob, D. J.; Pirrone, N. *Environ. Sci. Technol.* **2013**, 47, 4967.
DOI: [10.1021/es305071v](https://doi.org/10.1021/es305071v)
154. Boeing, D. W. *Chemosphere* **2000**, 40, 1335.
DOI: [10.1016/S0045-6535\(99\)00283-0](https://doi.org/10.1016/S0045-6535(99)00283-0)
155. Li, H.; Zhang, Y.; Wang, X.; Gao, Z. *Microchim. Acta* **2008**, 160, 119.
DOI: [10.1007/s00604-007-0816-x](https://doi.org/10.1007/s00604-007-0816-x)
156. Freeman, R.; Finder, T.; Willner, I. *Angew. Chem. Int. Ed.* **2009**, 48, 7818.
DOI: [10.1002/anie.200902395](https://doi.org/10.1002/anie.200902395)
157. Shang, Z. B.; Hu, S.; Wang, Y.; Jin, W. J. *Luminescence* **2011**, 26, 585.
DOI: [10.1002/bio.1274](https://doi.org/10.1002/bio.1274)
158. Chen, C. -Y.; Cheng, C. -T.; Lai, C. -W.; Wu, P. -W.; Wu, K. -C.; Chou, P. -T.; Chou, Y. -H.; Chiu, H. -T. *Chem. Commun.* **2006**, 263.
DOI: [10.1039/b512677k](https://doi.org/10.1039/b512677k)
159. Chaney, R. L.; Ryan, J. A.; Li, Y. -M.; Brown, S. L. *Developments in Plant and Soil Sciences, Cadmium in Soils and Plants*. Chapter 9 - Soil cadmium as a threat to human health. In **1999**, McLaughlin, M. J. & Singh, B. R. (Eds.) Boston: Kluwer. Academic Publishers.
ISBN: [0-7923-5843-0](https://doi.org/10.1007/978-1-4020-0518-0)
160. Dobson, S. Institute of Terrestrial Ecology, United Kingdom, Cadmium – Environmental Aspects, World Health Organization (Geneva), **1992**, Environmental Health Criteria 135.
<http://www.inchem.org/documents/ehc/ehc/ehc135.htm>
161. Friberg, L.; Elinger, C. G.; Kjellström, T. Karolinska Institute, Sweden, Cadmium, World Health Organization (Geneva). **1992**, International Programme on Chemical Safety, Environmental Health Criteria 134.
<http://www.inchem.org/documents/ehc/ehc/ehc134.htm>
162. 162. McMurray, C. T.; Tainer, J. A. *Nat. Genet.* **2003**, 34, 239.
DOI: [10.1038/ng0703-239](https://doi.org/10.1038/ng0703-239)
163. Garrido, M. L.; Muñoz-Olivas, R.; Cámara, C. *J. Anal. At. Spectrom.* **1998**, 13, 1145.
DOI: [10.1039/A803526A](https://doi.org/10.1039/A803526A)
164. 164. Li, H.; Zhang, Y.; Wang, X. *Sensors and Actuators B* **2007**, 127, 593.
DOI: [10.1016/j.snb.2007.05.013](https://doi.org/10.1016/j.snb.2007.05.013)
165. 165. Pearce, J. M. *European neurology* **2007**, 57, 118.
DOI: [10.1159/000098100](https://doi.org/10.1159/000098100)
166. 166. Landrigan, P. J.; Todd, A. C. *West. J. Med.* **1994**, 161, 153.
PMCID: [1022528](https://doi.org/10.22528)
167. Ali, E. M.; Zheng, Y.; Yu, H. -h.; Ying, J. Y. *Anal. Chem.* **2007**, 79, 9452.
DOI: [10.1021/ac071074x](https://doi.org/10.1021/ac071074x)
168. Wu, C. -S.; Oo, M. K. K.; Fan, X. *ACS Nano* **2010**, 4, 5897.
DOI: [10.1021/nn1021988](https://doi.org/10.1021/nn1021988)
169. Luan, W.; Yang, H.; Wan, Z.; Yuan, B.; Yu, X.; Tu, S. -t. *J. Nanopart. Res.* **2012**, 14, 762.
DOI: [10.1007/s11051-012-0762-3](https://doi.org/10.1007/s11051-012-0762-3)
170. Baranov, A. V.; Orlova, A. O.; Maslov, V. G.; Toporova, Y. A.; Ushakova, E. V.; Fedorov, A. V.; Artemyev, M. V.; Perova, T. S.; Berwick, K. J. *Appl. Phys.* **2010**, 108, 074306.
DOI: [10.1063/1.3490218](https://doi.org/10.1063/1.3490218)
171. Kumar, P.; Prakash, A.; Maikap, S. *The Electrochemical Society* **2012**, Abstract #1634, 221st ECS Meeting.
http://ma.ecsdl.org/content/MA2012-01/45/1634_full.pdf
172. Gale, P.A.; Garcia-Garrido, S.E. *J. Chem. Soc. Rev.* **2008**, 37, 151.
DOI: [10.1039/b715825d](https://doi.org/10.1039/b715825d)
173. Yeo, H. M.; Ryu, B. J.; Nam, K. C. *Org. Lett.*, **2008**, 10, 2931.
DOI: [10.1021/ol801153d](https://doi.org/10.1021/ol801153d)
174. Hennrich, G.; Sonnenschein, H.; Resch-Genger, U. *Tetrahedron Lett.* **2001**, 42, 2805.
DOI: [10.1016/S0040-4039\(01\)00324-0](https://doi.org/10.1016/S0040-4039(01)00324-0)
175. Zhang, X.; Xiao, Y.; Qian, X. *Angew. Chem., Int. Ed.* **2008**, 47, 8025.
DOI: [10.1002/anie.200803246](https://doi.org/10.1002/anie.200803246)
176. Steinmaus, C.; Miller, M. D.; Howd, R. *Environ Health Perspect* **2007**, 115, 1333.
DOI: [10.1289/ehp.10300](https://doi.org/10.1289/ehp.10300)
177. Brauer, V. F. H.; Below, H.; Kramer, A.; Führer, D.; Paschke, R. *Eur. J. Endocrinol.* **2006**, 154, 229.
DOI: [10.1530/eje.1.02076](https://doi.org/10.1530/eje.1.02076)
178. Touceda-Varela, A.; Stevenson, E. I.; Galve-Gasi6n, J. A.; Dryden, D. T. F.; Mareque-Rivas, J. C. *Chem. Commun.* **2008**, 1998.
DOI: [10.1039/b716194h](https://doi.org/10.1039/b716194h)
179. Anzenbacher, Jr. P.; Tyson, D. S.; Jursk6v6, K.; Castellano, F. N. *J. Am. Chem. Soc.* **2002**, 124, 6232.
DOI: [10.1021/ja0259180](https://doi.org/10.1021/ja0259180)
180. Badugu, R.; Lakowicz, J. R.; Geddes, C. D. *J. Am. Chem. Soc.* **2005**, 127, 3635.

- DOI: [10.1021/ja044421j](https://doi.org/10.1021/ja044421j)
181. Ros-Lis, J. V.; Martínez-Máñez, R.; Soto, J. *Chem. Commun.* **2005**, 5260.
DOI: [10.1039/b510710e](https://doi.org/10.1039/b510710e)
182. Timofeyenko, Y. G.; Rosentreter, J. J.; Mayo, S. *Anal. Chem.* **2007**, 79, 251.
DOI: [10.1021/ac060890m](https://doi.org/10.1021/ac060890m)
183. Kim, Y. -H.; Hong, J. -I. *Chem. Commun.* **2002**, 512.
DOI: [10.1039/b109596j](https://doi.org/10.1039/b109596j)
184. Borowitz, J. L.; Rathinavelu, A.; Kanthasamy, A.; Wilsbacher, J.; Isom, G. E. *Toxicol. Appl. Pharmacol.* **1994**, 129, 80.
DOI: [10.1006/taap.1994.1230](https://doi.org/10.1006/taap.1994.1230)
185. Rachinger, J.; Fellner, F. A.; Stieglbauer, K.; Trenkler, J. *AJNR Am. J. Neuroradiol.* **2002**, 23, 1398.
186. Borron, S. W. *J. Emerg. Nurs.* **2006**, 32, S11.
DOI: [10.1016/j.jen.2006.05.011](https://doi.org/10.1016/j.jen.2006.05.011)
187. Jin, W. J.; Costa-Fernández, J. M.; Pereiro, R.; Sanz-Medel, A. *Anal. Chim. Acta* **2004**, 522, 1.
DOI: [10.1016/j.aca.2004.06.057](https://doi.org/10.1016/j.aca.2004.06.057)
188. Miyake, M.; Matsumoto, H.; Nishizawa, M.; Sakata, T.; Mori, H.; Kuwabata, S.; Yoneyama, H. *Langmuir* **1997**, 13, 742.
DOI: [10.1021/la960702v](https://doi.org/10.1021/la960702v)
189. Hernández-Molina, M.; González-Platas, J.; Ruiz-Pérez, C.; Lloret, F.; Julve, M. *Inorg. Chim. Acta* **1999**, 284, 258.
DOI: [10.1016/S0020-1693\(98\)00300-4](https://doi.org/10.1016/S0020-1693(98)00300-4)
190. Kurnia, K.; Giles, D. E.; May, P. M.; Singh, P.; Hefter, G. T. *Talanta*, **1996**, 43, 2045.
DOI: [10.1016/S0039-9140\(96\)01875-9](https://doi.org/10.1016/S0039-9140(96)01875-9)
191. Aydın, A.; Ercan, Ö.; Taşcioğlu, S. *Talanta* **2005**, 66, 1181-1186.
DOI: [10.1016/j.talanta.2005.01.024](https://doi.org/10.1016/j.talanta.2005.01.024)
192. Ferreira, I.M.P.L.V.O.; Silva, S. *Talanta* **2008**, 74, 1598.
DOI: [10.1016/j.talanta.2007.10.004](https://doi.org/10.1016/j.talanta.2007.10.004)
193. Mikuška, P.; Večeřa, Z. *Anal. Chim. Acta* **2003**, 495, 225.
DOI: [10.1016/j.aca.2003.08.013](https://doi.org/10.1016/j.aca.2003.08.013)
194. Thenmozhi, K.; Narayanan, S. S. *Electroanalysis* **2007**, 19, 2362.
DOI: [10.1002/elan.200703995](https://doi.org/10.1002/elan.200703995)
195. Kamyabi, M. A.; Aghajanloo, F. *J. Electroanal. Chem.* **2008**, 614, 157.
DOI: [10.1016/j.jelechem.2007.11.026](https://doi.org/10.1016/j.jelechem.2007.11.026)
196. Liu, X.; Guo, L.; Cheng, L.; Ju, H. *Talanta* **2009**, 78, 691.
DOI: [10.1016/j.talanta.2008.12.035](https://doi.org/10.1016/j.talanta.2008.12.035)
197. Han, C.; Cui, Z.; Zou, Z.; Sabahaiti.; Tian, D.; Li, H. *Photochem. Photobiol. Sci.*, **2010**, 9, 1269.
DOI: [10.1039/c0pp00119h](https://doi.org/10.1039/c0pp00119h)
198. Callan, J. F.; Mulrooney, R. C.; Kamila, S.; McCaughan, B. *J. Fluoresc.* **2008**, 18, 527.
DOI: [10.1007/s10895-007-0295-9](https://doi.org/10.1007/s10895-007-0295-9)
199. Gunnlaugsson, T.; Davis, A. P.; Hussey, G. M.; Tierney, J.; Glynn, M. *Org. Biomol. Chem.* **2004**, 2, 1856.
DOI: [10.1039/b404706k](https://doi.org/10.1039/b404706k)
200. Martínez-Máñez, R.; Sancenón, F. *Chem. Rev.* **2003**, 103, 4419.
DOI: [10.1021/cr010421e](https://doi.org/10.1021/cr010421e)
201. Mulrooney, R. C.; Singh, N.; Kaur, N.; Callan, J. F. *Chem. Commun.* **2009**, 686.
DOI: [10.1039/b817569a](https://doi.org/10.1039/b817569a)
202. Gauci, L. A.; Kelland, L. G.; Magri, D. C. *J. Fluoresc.* **2013**, 23, 793.
DOI: [10.1007/s10895-013-1212-z](https://doi.org/10.1007/s10895-013-1212-z)
203. Wang, Y.; Mao, H.; Wong, L. B. *Nanotechnology* **2010**, 21, 055101.
DOI: [10.1088/0957-4484/21/5/055101](https://doi.org/10.1088/0957-4484/21/5/055101)
204. Verkman, A. S.; Galletta, L. J. V. *Nat. Rev. Drug Discov.* **2009**, 8, 153.
DOI: [10.1038/nrd2780](https://doi.org/10.1038/nrd2780)
205. Dunlop, J.; Bowlby, M.; Peri, R.; Vasilyev, D. Arias, R. *Nat. Rev. Drug Discov.* **2008**, 7, 358.
DOI: [10.1038/nrd2552](https://doi.org/10.1038/nrd2552)
206. Ruedas-Rama, M. J.; Orte, A.; Hall, E. A. H.; Alvarez-Pez, J. M.; Talavera, E. M. *Analyst* **2012**, 137, 1500.
DOI: [10.1039/c2an15851e](https://doi.org/10.1039/c2an15851e)

Advanced Materials Letters

Publish your article in this journal

ADVANCED MATERIALS Letters is an international journal published quarterly. The journal is intended to provide top-quality peer-reviewed research papers in the fascinating field of materials science particularly in the area of structure, synthesis and processing, characterization, advanced-state properties, and applications of materials. All articles are indexed on various databases including DOI and are available for download for free. The manuscript management system is completely electronic and has fast and fair peer-review process. The journal includes review articles, research articles, notes, letter to editor and short communications.



A DFT Study of Interaction of $(\text{CdSe})_3$ Quantum Dots with Nucleobases

Pragati Malik and Rita Kakkar*

Computational Chemistry Laboratory, Department of Chemistry, University of Delhi, Delhi-110 007, India

Submitted on (DD-Month-YYYY format)

1 Dr. Pragati Malik: Computational Chemistry Laboratory, Department of Chemistry, University of Delhi, Delhi-110 007, INDIA

2 Prof. Rita Kakkar: Department of Chemistry, University of Delhi, Delhi-110 007, INDIA

Corresponding Author Name: Prof. Rita Kakkar

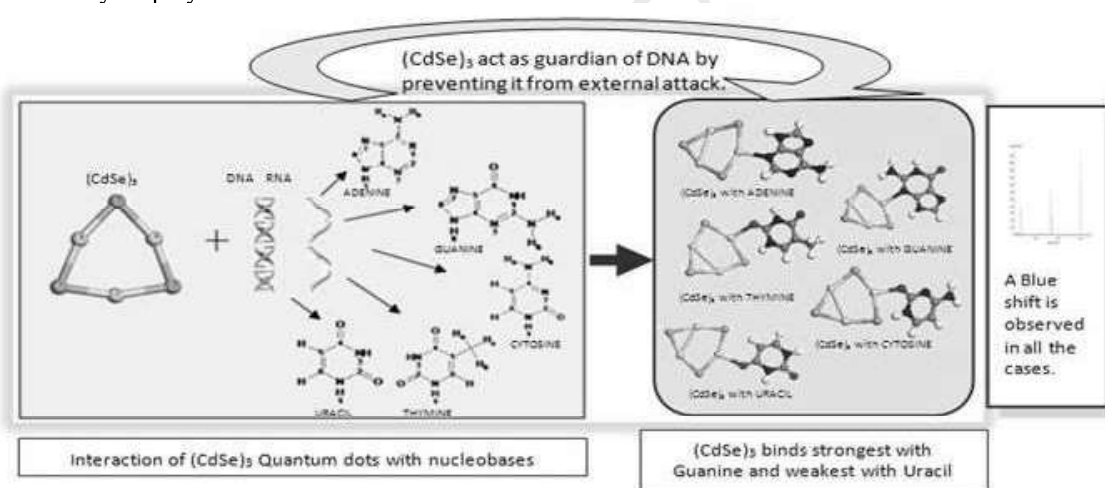
Address: Department of Chemistry, University of Delhi, Delhi-110 007, INDIA

Tel: +911127666313

Email: rkakkar@chemistry.du.ac.in

ABSTRACT

Deoxyribonucleic acid (DNA) and ribonucleic acid (RNA) play important roles in the storage of genetic information and protein biosynthesis. Nucleobases, which are nitrogenous bases, are the functional units of these nucleic acids. It is very important to detect changes in the sequence of DNA/RNA, as any mutations in them may cause harm to the organism. Our aim is to verify the use of $(\text{CdSe})_3$ Quantum Dots (QDs), owing to their distinctive optical and electronic properties, for sensing changes in DNA/RNA. Hence, in this work, we have focused on studying the interaction between $(\text{CdSe})_3$ QDs and the five nucleobases (adenine, guanine, cytosine, thymine and uracil) at various probable sites by means of density functional calculations. Several structural, electronic and optical properties, and charge transfer on interaction between the two, have been discussed. The present band gap and charge transfer calculations indicate that binding of $(\text{CdSe})_3$ to guanine is strongest, and is weakest with uracil. The vibrational spectral analysis indicates that the intensities of the peaks due to $(\text{CdSe})_3$ enhance on interacting with the nucleobase, and a blue shift is observed in all the interactions. The presence of both the frontier orbitals (HOMO and LUMO) on the QD indicates that $(\text{CdSe})_3$ acts as a guardian of DNA and prevents it from damage. Hence, our studies directs that CdSe QDs can be successfully employed as sensors for these nucleobases.



Introduction

Nucleobases are nitrogen-containing biological compounds found in DNA and RNA. The helical structure of DNA and RNA is due to the ability of the nucleobases present in them to exist in the form of base-pairs through hydrogen bonds and stacking upon one another. Important nucleobases are adenine (A), guanine (G), cytosine (C), thymine (T) and uracil (U), out of which A, G, C are found in both DNA and RNA, T is found in DNA only, while U is found only in RNA. In the normal helical structure of DNA, bases form pairs sandwiched between the two strands, A with T and C with G

Effects of increasing number of rings on the ion sensing ability of CdSe quantum dots: a theoretical study

Pragati Malik · Rita Kakkar

Received: 25 December 2017 / Accepted: 6 April 2018 / Published online: 22 April 2018
© Springer Science+Business Media B.V., part of Springer Nature 2018

Abstract A computational study on the structural and electronic properties of a special class of artificial atoms, known as quantum dots, has been carried out. These are semiconductors with unique optical and electronic properties and have been widely used in various applications, such as bio-sensing, bio-imaging, and so on. We have considered quantum dots belonging to II–VI types of semiconductors, due to their wide band gap, possession of large exciton binding energies and unique optical and electronic properties. We have studied their applications as chemical ion sensors by beginning with the study of the ion sensing ability of $(\text{CdSe})_n$ ($n = 3, 6, 9$ which are in the size range of $\sim 0.24, 0.49, 0.74$ nm, respectively) quantum dots for cations of the zinc triad, namely Zn^{2+} , Cd^{2+} , Hg^{2+} , and various anions of biological and environmental importance, and studied the effect of increasing number of rings on their ion sensing ability. The various structural, electronic, and optical properties, their interaction energies, and charge transfer on interaction with metal ions and anions have been calculated and reported. Our studies indicate that the CdSe quantum dots can be employed as sensors for both divalent cations and anions, but they can sense cations better than anions.

Keywords Metal ions · Quantum dots · Sensing · Binding energy · Interaction energy · HOMO · LUMO · Nanoelectronics applications

P. Malik · R. Kakkar (✉)
Computational Chemistry Laboratory, Department of Chemistry,
University of Delhi, Delhi 110 007, India
e-mail: rkakkar@chemistry.du.ac.in

Introduction

Development of a potential analytical multiplexed, sensitive technique, which could detect heavy metal ions both quantitatively and qualitatively is a strong current scientific main concern, and is highly desirable in order to avoid fatal environmental pollution as soon as possible. Therefore, there is a strong need to develop nanoscale assemblies capable of sensing and monitoring changes induced with changes in concentrations of the target species. Metal ion sensing, done via analyte-induced changes in the photoluminescence of quantum dots, is nowadays a very active research area, and the development of nanomaterial optical sensors has proved to be an important development in the area of continuous, real-time monitoring of various analytes (Shi et al. 2004). Depending on the origin of the optical signals, these sensors may be classified into luminescence-based and absorbance-based sensors. Luminescence-based sensors are based on detection by photoluminescence and chemiluminescence, while absorbance-based sensors employ detection via changes in the spectral absorbance (García-Campaña and Baeyens 2001).

Significance of metal ions

Metal ions are important, both biologically and ecologically. Metal ions that are absolutely indispensable due to their role in various processes are known as essential metal ions and no other metal ion can replace their function, whereas those whose presence or absence does not affect the functioning of the

biological system are known as nonessential metal ions. Metal ions required in very small amount, but essential, are called trace metal ions. Some other metal ions, the presence of which produces toxic effects, are called toxic metal ions. Therefore, the concentration of all these metal ions should be maintained in a fine limit, as a slight excess or deficiency produces undesirable, unwanted, and toxic effects. Some of the heavy metals, such as copper (Brewer 2010; Wu et al. 2009), iron (Brewer 2010; Bruins et al. 2000), and zinc (Todd et al. 1995), are biologically essential and are required by organisms in a certain essential amount, but can lead to toxicity at higher concentrations. On the other hand, some other heavy metals such as lead (Rogers et al. 2003) and mercury (Miyake et al. 2006) are not biologically essential and are harmful to organisms even at very low concentrations because they lead to excessive free-radical proliferation (Hussein et al. 2005). To minimize the pollution by heavy metals, one way is to develop analytical tools for heavy metal detection and prevent the damaging effects of pollution in the very early stage. Most of the techniques which are conventionally employed for heavy metal analysis include atomic absorption spectrometry (Kunkel and Manahan 1973), inductively coupled plasma mass spectrometry (Bings et al. 2006), capillary electrophoresis (Tanyanyiwa and Hauser 2002), X-ray fluorescence spectrometry (Lorber 1986), and microprobes (Bertsch and Hunter 2001). They detect metal ions with high sensitivity, but the disadvantages of most of these techniques, i.e., they are costly, they involve delicate instruments and skilled human resources, and sample pretreatment, makes it difficult to use them on a regular basis for monitoring the concentrations of metal ions (Czarnik 1995). On the other hand, quantum dots (QDs) offer a new method for quantitative determination of heavy metals (Gao et al. 2005; Michalet et al. 2005; Smith et al. 2004). Recently, many reports have been published for sensing cations of both biological and ecological importance, such as silver, copper, calcium, zinc, cadmium and mercury, and anions such as CO_3^{2-} , F^- , and I^- using CdSe, CdSe/ZnS, and CdSe/CdS core/shell quantum dots (Adegoke and Nyokong 2014; Chen et al. 2008; Dong et al. 2006; Frasco et al. 2010; Gattás-Asfura and Leblanc 2003; Han et al. 2010; Li et al. 2007, 2014; Liang et al. 2004; Ruedas-Rama et al. 2007; Shang et al. 2009; Touceda-

Varela et al. 2008; Xi et al. 2016; Zhang et al. 2014). In the present paper, an effort has been made to explore how a wide band gap semiconductor, CdSe, behaves when it interacts with various metal ions and some anions. For this, we are focusing on the use of uncapped $(\text{CdSe})_n$, where $n = 3, 6,$ and 9 , (which are in the size range of $\sim 0.24, 0.49, 0.74$ nm, respectively) quantum dots cluster for the sensing of these ions.

Mechanism involved in sensor design

The use of cadmium-based quantum dots for analyzing metal ions was first reported in 2002, for the analysis of zinc and copper ions by employing L-cystein- and thioglycerol-capped CdS quantum dots in physiological buffer samples (Chen and Rosenzweig 2002). The use of CdSe quantum dots in ion sensing has also been explored by various researchers. The conventional sensing mechanism is based on the fact that exposure to metal ions either increases or decreases the electron density on CdSe quantum dots. Here, we have considered the interaction of metal ions of the zinc triad, i.e., Zn^{2+} , Cd^{2+} and Hg^{2+} , and various anions with $(\text{CdSe})_n$ clusters, where $n = 3, 6,$ and 9 , in order to observe the structural and electronic changes in both, and to study the effect of increasing the ring size on their interaction.

Computational details

First-principles density-functional (DF) calculations (Hohenberg and Kohn 1964) were performed using DMol³ (Delley 1990, 2000) in the Materials Studio 5.5 package from Accelrys Inc. Numerical basis sets of double zeta quality plus polarization functions (DNP), which is the numerical equivalent of the Gaussian basis, 6-31G**, but is much more accurate, were used in the calculations. The cores were treated using DFT semilocal pseudo-potentials (DSPP), specifically designed for DFT calculations (Delley 2002). The GGA-PBE functional (Perdew et al. 1996) was employed in the calculations. The geometries of various structures were fully optimized, without restrictions, using delocalized internal coordinates (Andzelm et al. 2001; Baker et al. 1996). The reported partial atomic charges were obtained by Hirshfeld partitioning (Hirshfeld 1977). Optical spectra were computed using the TD-DFT method (Delley 2010).

Results and discussion

(CdSe)_n clusters

We constructed stoichiometric (CdSe)_n quantum dot clusters (where $n = 3, 6, 9$). The ground-state geometries of the constructed molecules were fully optimized with respect to the energy.

Structural and electronic properties

All the (CdSe)_n quantum dots considered here have D_{3h} symmetry. Before exploring the effect of increasing number of rings on the stability of the (CdSe)_n clusters, we calculated the properties of the molecular form of CdSe, the bond length of which optimizes to 2.497 Å, which is smaller than the sum of the ionic radii (2.93 Å for Cd²⁺ + Se²⁻), indicating the covalent character of the bond. Table 1 shows the optimized structures of (CdSe)_n quantum dots.

The contour plots showing the HOMOs and LUMOs are shown in Table 2. In all the (CdSe)_n cases, the HOMO is mainly centered on the chalcogenide atom and involves participation of pure *p* orbitals of the chalcogenide and pure *d* orbitals of the metal. The LUMO, which lies mainly on the metal atom, consists of *sp*-hybridized orbitals formed by the metal orbitals. Also, it seems that the *d* orbitals of the chalcogenide also play a crucial role in the LUMOs, as the plots are concentrated around the anionic atoms as well.

The binding energy data, given in Table 3, indicates that the stability of the (CdSe)_n clusters increases with increase in the value of n , or with an increase in the number of rings, since the binding energy per CdSe unit are $-3.34, -3.78,$ and -3.90 eV, respectively, for $n = 3, 6,$ and 9 , compared to -1.33 eV for a single CdSe unit.

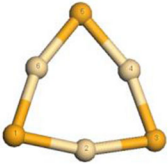
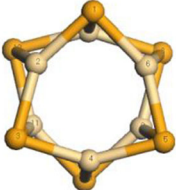
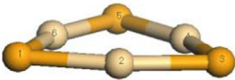
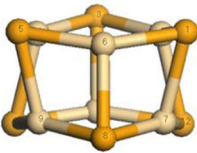
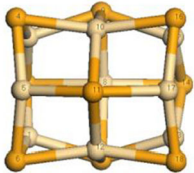
As expected, the conductivity increases with increase in the number of rings, as seen from a decrease in the HOMO-LUMO gap with increase in n . This is also reflected in the computed λ_{max} values, which show a bathochromic shift with increasing number of rings (Table 3 and Fig. 1).

Having studied the properties of the various (CdSe)_n clusters, we investigated the properties of the bare cations with which they are to interact. The elements of the zinc triad have the electronic configurations $d^{10}s^2$. On ionization, the *s* electrons are lost, leaving the *d* orbitals as the highest occupied and the *s* orbitals as the lowest unoccupied levels. In the following sections, we have discussed the changes induced in the properties of these ions, the trend of stabilization, and the structural and electronic changes induced in the nanoclusters on interaction with the above-mentioned ions.

Interaction of (CdSe)_n quantum dots with cations

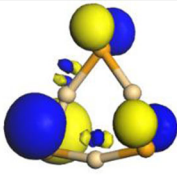
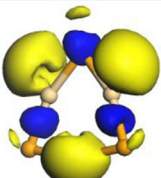
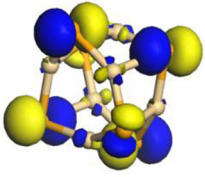
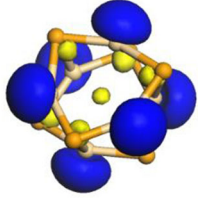
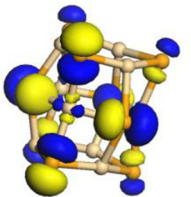
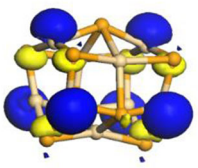
Various initial positions for the interacting ions with respect to the QDs were considered, and in each case, it was found that it positions itself on the peripheral ring on geometry optimization. Therefore, the ions were placed

Table 1 Optimized structures* of (CdSe)_n quantum dots

Position	(CdSe) ₃	(CdSe) ₆	(CdSe) ₉
Top View			
Side View			

*Lighter-colored spheres represent Cd

Table 2 HOMO-LUMO plots of $(\text{CdSe})_n$ quantum dots

Label	HOMO	LUMO
$(\text{CdSe})_3$		
$(\text{CdSe})_6$		
$(\text{CdSe})_9$		

at the center of the ring in case of the $(\text{CdSe})_3$ nanocluster and at the center of the peripheral ring in case of nanoclusters in which more than one ring is involved, i.e., for $(\text{CdSe})_6$ and $(\text{CdSe})_9$ nanoclusters, so that it binds with the maximum number of atoms of the ring.

Structural and electronic properties

On geometry optimization, it was found that all ions interact to different extents with the $(\text{CdSe})_n$ clusters (Table 4) and result in structural changes in the quantum dot, along with actual bond formation.

The HOMO-LUMO isosurfaces obtained for the interaction of cations with $(\text{CdSe})_n$ quantum dots are shown in Table 5. The interaction leads to changes in

the orbital density of the frontier molecular orbitals. The HOMO mainly involves the p orbitals of Se, d orbitals of Cd atom of the ring, and the d orbital of the interacting ion, while the LUMO consists of the p and sp hybrid orbital of Se, d and/or hybrid orbital of Cd atoms, and the pure and/or hybrid orbital of the introduced ion.

The binding energy data (Table 6) indicates that, while $(\text{CdSe})_6$ and $(\text{CdSe})_9$ clusters gain stabilization, the $(\text{CdSe})_3$ cluster gets destabilized by interaction with the metal ions, and becomes unstable towards dissociation.

Before interaction, the CdSe quantum dot is electrically neutral and the cation is di-positively charged. The interaction causes transfer of charge between them. The charge analysis (Table 7) shows that in all the cases of $(\text{CdSe})_n\text{-M}^{2+}$, electrons are transferred from the

Table 3 Calculated data for bandgaps (eV), binding energies (eV), and λ_{max} (nm) for $(\text{CdSe})_n$ clusters

$(\text{CdSe})_n$	Binding energy	HOMO	LUMO	HOMO-LUMO gap	λ_{max}
$(\text{CdSe})_3$	-10.033	-5.303	-2.821	2.482	408
$(\text{CdSe})_6$	-22.706	-5.391	-3.051	2.340	479
$(\text{CdSe})_9$	-35.117	-5.196	-3.096	2.100	582

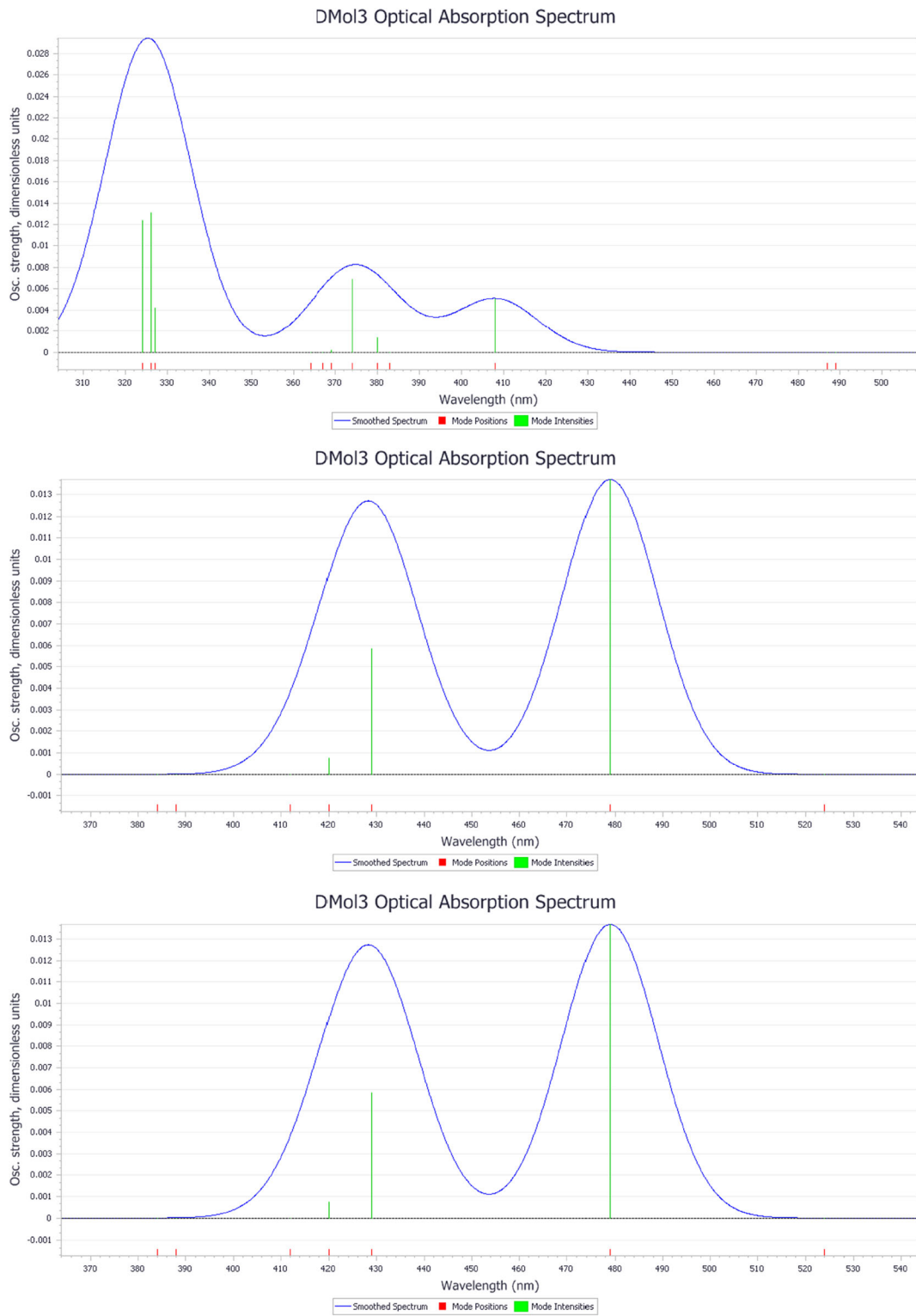
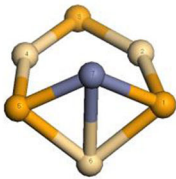
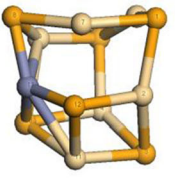
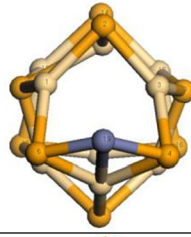
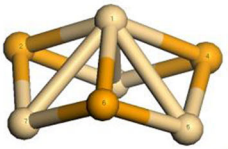
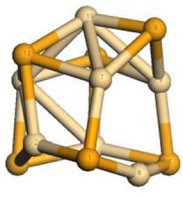
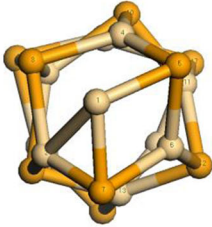
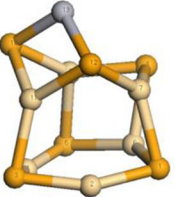


Fig. 1 Simulated optical spectra of (CdSe)₃, (CdSe)₆, and (CdSe)₉

Table 4 Optimized structures of $(\text{CdSe})_n$ clusters interacting with various metal ions of the zinc triad

Metal Ion	$(\text{CdSe})_3$	$(\text{CdSe})_6$	$(\text{CdSe})_9$
Zn^{2+}			
Cd^{2+}			
Hg^{2+}			

nanocluster to the ion, leading to reduction in the positive charge on the metal atom.

The band gap data of bare $(\text{CdSe})_n$ quantum dots indicates that the quantum dots with lower stoichiometry have wider band gaps than those with higher stoichiometry (Table 3), as also seen from the computed λ_{max} values, which increases from 408 to 479 nm and 582 nm with increasing size. Interaction of these $(\text{CdSe})_n$ quantum dots with the three metal ions in general reduces the band gap, exceptions being $(\text{CdSe})_3\text{-Hg}^{2+}$ and $(\text{CdSe})_9\text{-Zn}^{2+}$ (Table 6). Because of the interaction with these positively charged ions, both the HOMO and LUMO are lowered in energy.

Interaction energies

The interaction energy is defined as

$$E_{\text{interaction}} = [E_{\text{total}}(\text{CdSe QD}) + E_{\text{total}}(\text{ion})] - [E_{\text{total}}(\text{CdSe QD-ion})],$$

where E_{total} is the total energy of the system. Positive values for $E_{\text{interaction}}$ imply an exothermic interaction process (Kakkar et al. 2004).

The calculated interaction energies (Table 8) are rather large and show that, for a particular cation, the interaction energy increases with increase in the number of rings, while for a particular $(\text{CdSe})_n$ quantum dot, the interaction energy follows the trend $\text{Hg}^{2+} \approx \text{Zn}^{2+} > \text{Cd}^{2+}$. The positive values indicate that the $(\text{CdSe})_n\text{-M}^{2+}$ interaction is exothermic, and is most highly favored for the $\text{Hg}^{2+}\text{-(CdSe)}_9$ system.

The interaction energies may not provide the entire picture, as part of the released energy may have been utilized to distort the QD on interaction with the cation. We therefore computed the distortion energies of the QD by computing single-point energies of the QD at the optimized geometry of the interacting system after stripping off the cation, and subtracting the energy of the optimized pristine QD. This distortion energy needs to be added to the interaction energies in Table 8 above to get the total interaction energies. There is no trend in the induced distortion energy by a particular cation. The net interaction energies are smallest for Cd^{2+} , and Zn^{2+} appears to have the largest interaction, with Hg^{2+} a close second. In fact, the large Hg^{2+} ion appears to distort the

Table 5 HOMO-LUMO plots for $(\text{CdSe})_n\text{-M}^{2+}$ interaction

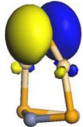
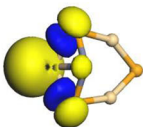
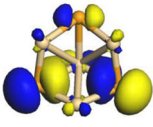
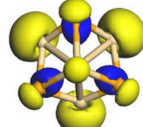
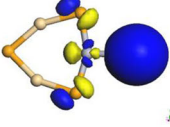
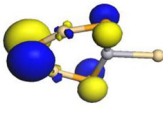
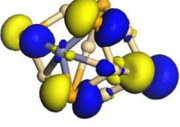
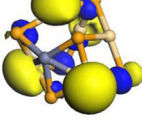
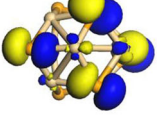
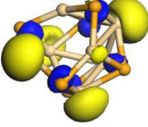
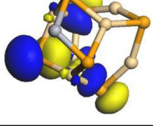
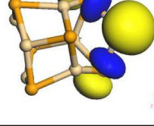
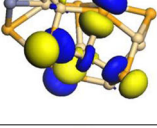
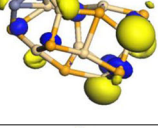
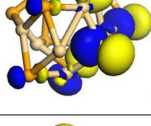
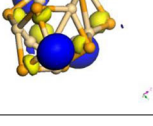
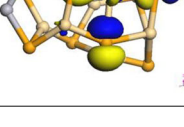
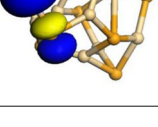
Label	HOMO	LUMO
$(\text{CdSe})_3\text{-Zn}^{2+}$		
$(\text{CdSe})_3\text{-Cd}^{2+}$		
$(\text{CdSe})_3\text{-Hg}^{2+}$		
$(\text{CdSe})_6\text{-Zn}^{2+}$		
$(\text{CdSe})_6\text{-Cd}^{2+}$		
$(\text{CdSe})_6\text{-Hg}^{2+}$		
$(\text{CdSe})_9\text{-Zn}^{2+}$		
$(\text{CdSe})_9\text{-Cd}^{2+}$		
$(\text{CdSe})_9\text{-Hg}^{2+}$		

Table 6 Band gap and binding energy (eV) data, as well as λ_{\max} values (nm) for interaction of $(\text{CdSe})_n$ with various cations

$(\text{CdSe})_n$	Metal ion	Binding energy	HOMO	LUMO	Band gap	λ_{\max}
$(\text{CdSe})_3$	Zn^{2+}	6.707	-12.869	-12.455	0.414	2541
	Cd^{2+}	6.755	-13.882	-11.713	2.169	538
	Hg^{2+}	8.573	-13.344	-10.820	2.524	898
$(\text{CdSe})_6$	Zn^{2+}	-8.384	-12.480	-10.332	2.148	551
	Cd^{2+}	-7.786	-12.443	-10.129	2.314	519
	Hg^{2+}	-7.007	-12.159	-10.670	1.489	823
$(\text{CdSe})_9$	Zn^{2+}	-21.760	-11.304	-9.065	2.239	541
	Cd^{2+}	-21.089	-11.236	-9.165	2.071	583
	Hg^{2+}	-20.795	-11.273	-9.820	1.453	851

smallest ring most and have the highest interaction with this ring.

$(\text{CdSe})_n$ quantum dots as anion sensors

After studying the structural and electronic changes introduced on interaction of $(\text{CdSe})_n$ quantum dots with transition metal cations, we now explored the changes produced in the nanocluster on interaction with some anions. We chose the CN^- , F^- , NO_2^- , and CO_3^{2-} anions for studying the $(\text{CdSe})_n$ -anion interaction.

Structural and electronic properties

All anions interact differently with the $(\text{CdSe})_n$ clusters and the results of geometry optimization are given in Table 9.

The HOMO-LUMO isosurfaces obtained for interaction of anions with the CdSe quantum dots (Table 10) show that the HOMOs are centered mainly on the Se atoms and consist of the p orbital of Se, the d orbitals of Cd and the s and p orbitals of the anion, while the LUMOs, which are mainly centered on the metal atoms,

Table 7 Charge transfer to the metal ion on the basis of Hirshfeld charges

Charge transfer	Zn^{2+}	Cd^{2+}	Hg^{2+}
$(\text{CdSe})_3$	1.552	1.447	1.736
$(\text{CdSe})_6$	1.763	1.601	1.603
$(\text{CdSe})_9$	1.653	1.574	1.632

involve the p and d orbitals of Se, the pure and/or hybrid orbitals of Cd, and the s and p orbitals of the anion. The interaction of the anion leads to a change in the orbital density of the frontier orbital plots.

The interaction causes transfer of charge from the anion to the quantum dot, causing a reduction in the negative charge on the anion, and the $(\text{CdSe})_n$ quantum dot acquires a negative charge, unlike the $(\text{CdSe})_n\text{-M}^{2+}$ case, where the charge transfer occurs in the reverse direction, i.e., from the $(\text{CdSe})_n$ quantum dot.

There appears to be no particular trend in charge transfer. Amongst the univalent anions, the charge transfer is largest for F^- (Table 11). However, the charge transfer is much smaller than that observed in the case of the cations (Table 7). We also observed that the bond orders are also smaller in this case, signifying that the quantum dots are better electron donors than electron acceptors.

The interaction of anions does not reveal any particular trend in the band gaps (Table 12).

Interaction energies

As in the case of cations, here also, for a particular anion, the interaction energy increases with increase in the number of rings (Table 13). The interaction energy data indicates that the $(\text{CdSe})_n$ -anion interaction is also exothermic, but, compared to the cations (Table 8), the interaction energies are much smaller in magnitude. This is in accord with expectations based on the smaller charge transfers and bond orders in this case. The only anion which shows comparable interaction energy is carbonate.

Table 8 Interaction energies* (eV) of the $(\text{CdSe})_n$ quantum dots with various cations

Ion	$(\text{CdSe})_3\text{-M}^{2+}$			$(\text{CdSe})_6\text{-M}^{2+}$			$(\text{CdSe})_9\text{-M}^{2+}$		
	IE	DE	Total	IE	DE	Total	IE	DE	Total
Zn^{2+}	11.559	1.469	13.028	13.978	2.060	16.038	14.942	1.804	16.746
Cd^{2+}	9.566	2.053	11.619	11.435	1.671	13.106	12.326	2.075	14.401
Hg^{2+}	11.032	3.408	14.440	13.940	1.918	15.858	15.317	1.220	16.537

*IE, interaction energy; DE, distortion energy

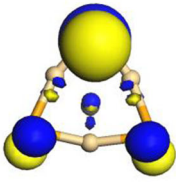
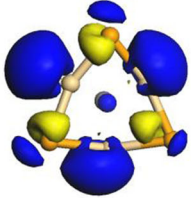
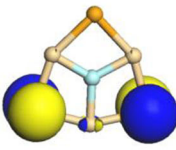
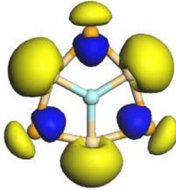
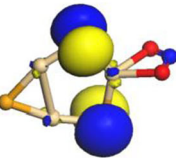
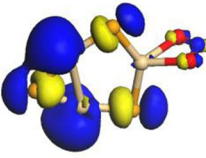
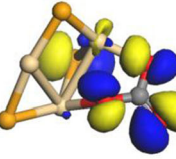
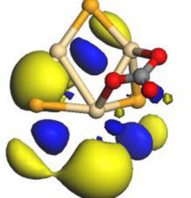
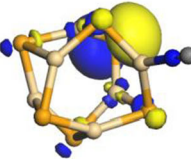
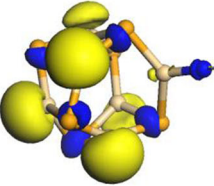
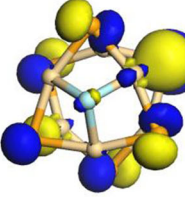
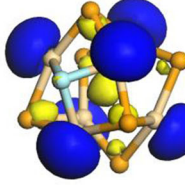
A glance at Table 9 reveals that considerable distortion of the QD occurs on interaction with the anions, particularly nitrite and carbonate, in which both interact with the Cd atoms through their oxygens. Thus, the computed interaction energies may be deceptively small, and in reality may be larger, since

part of the interaction energy may go into distorting the QD. In line with expectations, the QD suffers the largest distortion on interaction with the carbonate anion. On including the distortion energy, the interaction energy for carbonate becomes comparable to that for the cations. Moreover, we have not included

Table 9 Interaction of $(\text{CdSe})_n$ with various anions

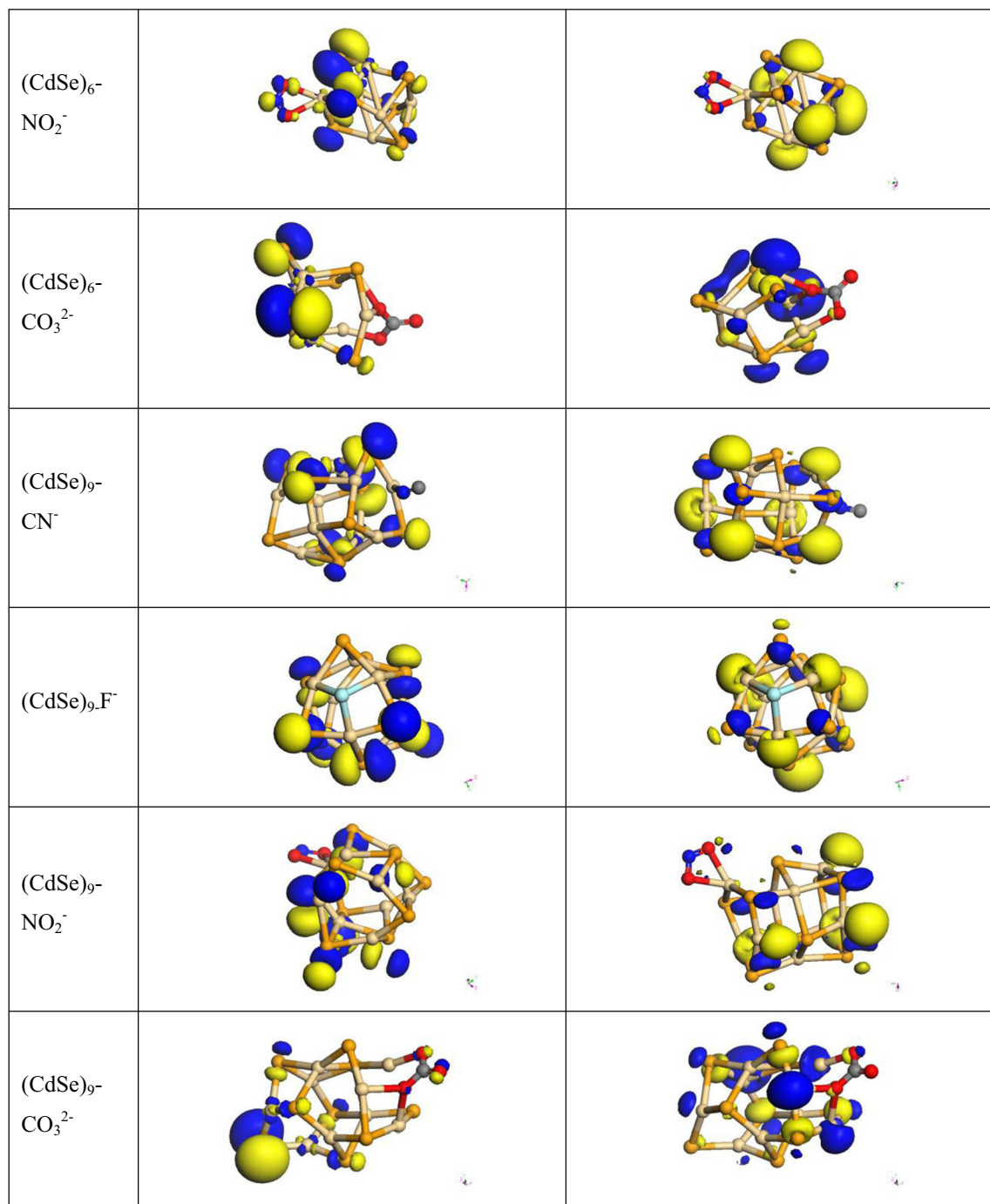
Anion	$(\text{CdSe})_3$	$(\text{CdSe})_6$	$(\text{CdSe})_9$
CN^-			
F^-			
NO_2^-			
CO_3^{2-}			

Table 10 HOMO and LUMO plots of the $(\text{CdSe})_n$ -Anion systems

Label	HOMO	LUMO
$(\text{CdSe})_3$ - CN^-		
$(\text{CdSe})_3$ - F^-		
$(\text{CdSe})_3$ - NO_2^-		
$(\text{CdSe})_3$ - CO_3^{2-}		
$(\text{CdSe})_6$ - CN^-		
$(\text{CdSe})_6$ - F^-		

the distortion energy of carbonate, which is also expected to be large as it loses nearly one electron to the QD. In the following section, we consider

interaction with zinc carbonate, since these two ions produce the larger interaction energy with the largest QD under study.



Interaction with both anion and cation

It would be interesting to explore the interaction energies when the QD interacts with both a cation and an anion, which would give a more realistic

picture. Also, the distortion produced by one ion would influence the adsorption of the other. We considered Zn²⁺ and CO₃²⁻ as the cation and anion, respectively, and the largest cluster (CdSe)₉ as the QD (Fig. 2).

Table 11 Transfer of charge from anion to the QD based on Hirshfeld charges

Charge transfer	CN ⁻	F ⁻	NO ₂ ⁻	CO ₃ ²⁻
(CdSe) ₃	0.426	0.698	0.491	0.922
(CdSe) ₆	0.451	0.595	0.513	1.067
(CdSe) ₉	0.425	0.602	0.519	1.075

Due to the presence of the anion, the charge transfer to Zn²⁺ increases to 1.719 from 1.653 (Table 7). The interaction energy increases to a phenomenal 33.643 eV. The distortion energies of the QD and the anion are, respectively, 0.826 and 0.423 eV, so that the total interaction energy is 34.892 eV, which is larger than the sum of the individual total interaction energies of Zn²⁺ (16.746 eV) and carbonate (10.013 eV) by 8.133 eV. We may thus conclude that the presence of the anion makes the cation binding even stronger, since the anion enhances the electron donor properties of the quantum dots. This is important, since a designed sensor to sense these metal ions will also have anions as counterions.

A strong conclusion is that these QDs are more effective electron donors than electron acceptors, since charge transfer by the (CdSe)₉ QD to Zn²⁺, for example, is 1.653 (Table 7), but that by CO₃²⁻ is only 1.076 (Table 11). This property could be due to the polarizability of Se ions in the clusters. To explore whether this property is unique to Se ions, we made a comparison of

the interaction of zinc and carbonate ions (both of which exhibit the largest charge transfer) with (CdE)₉ clusters, where E = S, Se, and Te.

Comparison with (CdE)₉, E = S, Se, Te

In order to probe the role of Se ions, we replaced the chalcogenide by S and Te, respectively, and explored the quantum of charge transfer to Zn²⁺ and charge transfer from CO₃²⁻, respectively. Table 14 compares the three quantum dots.

In each case, the interaction is stronger with the cation than with the anion, confirming that this property is not unique to the CdSe clusters. Examination of Table 14 reveals a steady decrease in the bandgap of the quantum dot as the size of the chalcogenide is increased. The amount of charge transfer to Zn²⁺ also increases. However, no such trend is observed in the remaining parameters, i.e., interaction energies and charge transfer from carbonate. The difference in the cation and anion interaction energies is ~3 eV for (CdS)₉, ~7 eV for (CdSe)₉, and ~5 eV for (CdTe)₉. The smaller than expected interaction energy with Zn²⁺ for the Te analogue is due to its smaller electronegativity (~2.1 on the Pauling scale) compared to S and Se, whose electronegativity is ~2.6, which imparts a metallic character to it (Chivers and Laitinen 2015), so that it interacts less strongly than expected with metal ions and more strongly with anions.

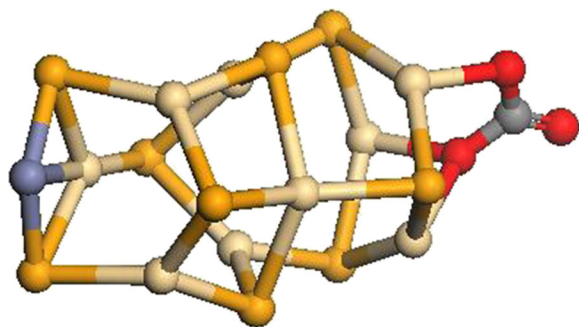
Table 12 Band gap and binding energy data (eV) for interaction of (CdSe)_n with various anions

(CdSe) _n	Anion	Binding energy	HOMO	LUMO	Band gap
(CdSe) ₃	CN ⁻	-23.583	-1.469	0.971	2.440
	F ⁻	-14.947	-0.996	0.596	1.592
	NO ₂ ⁻	-26.227	-1.617	1.024	2.641
	CO ₃ ²⁻	-34.836	2.631	4.625	1.994
(CdSe) ₆	CN ⁻	-36.812	-1.836	-0.080	1.756
	F ⁻	-29.124	-1.814	0.408	2.222
	NO ₂ ⁻	-38.969	-2.189	0.603	2.792
	CO ₃ ²⁻	-48.329	1.265	3.333	2.068
(CdSe) ₉	CN ⁻	-48.925	-2.355	-0.290	2.065
	F ⁻	-41.988	-2.178	-0.067	2.111
	NO ₂ ⁻	-51.498	-2.458	-0.285	2.173
	CO ₃ ²⁻	-61.708	0.507	2.548	2.041

Table 13 Interaction energies* (eV) for (CdSe)_n-anion systems

Anion	(CdSe) ₃			(CdSe) ₆			(CdSe) ₉		
	IE	DE	Total	IE	DE	Total	IE	DE	Total
CN ⁻	2.103	0.293	2.396	2.660	0.776	3.436	2.361	0.447	2.808
F ⁻	2.006	0.729	2.735	3.510	0.539	4.049	3.963	0.468	4.431
NO ₂ ⁻	2.764	0.279	3.043	2.834	0.356	3.190	2.951	0.525	3.476
CO ₃ ²⁻	6.262	0.934	7.196	7.083	2.165	9.248	8.050	1.963	10.013

*IE, interaction energy; DE, distortion energy

**Fig. 2** Interaction of Zn²⁺ + CO₃²⁻ with the (CdSe)₉ quantum dot

Conclusions

In this work, we have considered the interaction of some anions and cations with (CdSe)_n ($n = 3, 6, 9$) nanoclusters. This has been done with an aim to study the effect of increasing number of rings on the sensing of ions and to check whether it is possible to sense these ions using CdSe quantum dots, even when their concentrations are very low. Interaction of the cations with the Se of the quantum dots results in favorable interaction, with the formation of strong covalent bonds. In some cases, covalent interaction with the Cd atoms of the cluster is also seen. These interactions are accompanied by large charge transfers from the quantum dot to the metal ion, reducing

the band gaps of the quantum dots. The interaction energies are quite high.

In contrast, the interaction with anions is not so favorable. Weaker bonds are formed and lesser amount of charge transfer takes place, showing that the quantum dot is a reluctant electron acceptor. However, each of the quantum dots exhibits similar behavior with a particular anion. Thus, the cyanide ion interacts through its nitrogen with a cadmium atom, the fluoride ion interacts simultaneously with three cadmiums, both oxygens of the nitrite ion interact simultaneously with the same cadmium atom, and one of the carbonate oxygens interacts with two, or even three, cadmium atoms, one of which is also weakly bonded to another of the carbonate oxygens. The third oxygen gets more firmly bonded to the carbon atom, forming a C=O double bond. This is the only case where significant charge transfer takes place.

We may therefore conclude that the CdSe quantum dot can “sense” divalent cations and anions, particularly the former, since it is a better electron donor than an electron acceptor. This property is shown to be common to all the cadmium chalcogenides, including sulfides, selenides, and tellurides. Because of the metallic property of tellurium, it reacts less effectively than expected with metal ions and more with the anions, leaving the selenides with the most effective metal ion sensing properties.

Table 14 Comparison of the three QDs (CdE)₉, E = S, Se, and Te

QD	Binding energy (eV)	Bandgap (eV)	Charge transfer to Zn ²⁺	Interaction energy with Zn ²⁺ (eV)	Charge transfer from CO ₃ ²⁻	Interaction energy with CO ₃ ²⁻ (eV)
(CdS) ₉	-38.973	2.353	1.228	11.553	1.083	8.557
(CdSe) ₉	-35.117	2.100	1.653	14.942	1.075	8.050
(CdTe) ₉	-32.422	1.676	1.871	13.591	1.110	8.246

Author contribution Both the authors contributed equally. Both the authors read and approved the final manuscript. Funding information This study was funded by the Council for Scientific and Industrial Research (CSIR), New Delhi, for a Senior Research Fellowship (Grant no. 09/045(0873)/2009 EMR-I) and also received a financial support from “Delhi University’s system to strengthen faculty by providing funds.”

Compliance with ethical standards

Conflict of interest The authors declare that they have no conflict of interest.

References

- Adegoke O, Nyokong T (2014) Conjugation of mono-substituted phthalocyanine derivatives to CdSe@ZnS quantum dots and their applications as fluorescent-based sensors. *Synth Met* 188:35–45 <https://doi.org/10.1016/j.synthmet.2013.11.016>
- Andzelm J, King-Smith RD, Fitzgerald G (2001) Geometry optimization of solids using delocalized internal coordinates. *Chem Phys Lett* 335:321–326 [https://doi.org/10.1016/S0009-2614\(01\)00030-6](https://doi.org/10.1016/S0009-2614(01)00030-6)
- Baker J, Kessi A, Delley B (1996) The generation and use of delocalized internal coordinates in geometry optimization. *J Chem Phys* 105:192–212. <https://doi.org/10.1063/1.471864>
- Bertsch PM, Hunter DB (2001) Applications of synchrotron-based X-ray microprobes. *Chem Rev* 101:1809–1842. <https://doi.org/10.1021/cr990070s>
- Bings NH, Bogaerts A, Broekaert JAC (2006) Atomic Spectroscopy. *Anal Chem* 78:3917–3946. <https://doi.org/10.1021/ac060597m>
- Brewer GJ (2010) Risks of copper and Iron toxicity during aging in humans. *Chem Res Toxicol* 23:319–326. <https://doi.org/10.1021/tx900338d>
- Bruins MR, Kapil S, Oehme FW (2000) Microbial resistance to metals in the environment. *Ecotoxicol Environ Safety* 45: 198–207. <https://doi.org/10.1006/eesa.1999.1860>
- Chen Y, Rosenzweig Z (2002) Luminescent CdS quantum dots as selective ion probes. *Anal Chem* 74:5132–5138. <https://doi.org/10.1021/ac0258251>
- Chen J, Zheng AF, Gao Y, He C, Wu G, Chen Y, Kai X, Zhu C (2008) Functionalized CdS quantum dots-based luminescence probe for detection of heavy and transition metal ions in aqueous solution. *Spectrochim. Acta A* 69:1044–1052. <https://doi.org/10.1016/j.saa.2007.06.021>
- Chivers T, Laitinen RS (2015) Tellurium: a maverick among the chalcogens. *Chem Soc Rev* 44:1725–1739. <https://doi.org/10.1039/c4cs00434a>
- Czarnik AW (1995) Desperately seeking sensors. *Chem Biol* 2: 423–428. [https://doi.org/10.1016/1074-5521\(95\)90257-0](https://doi.org/10.1016/1074-5521(95)90257-0)
- Delley B (1990) An all-electron numerical method for solving the local density functional for polyatomic molecules. *J Chem Phys* 92:508–517 <https://doi.org/10.1063/1.458452>
- Delley B (2000) From molecules to solids with the DMol³ approach. *J Chem Phys* 113:7756–7764 <https://doi.org/10.1063/1.1316015>
- Delley B (2002) Hardness conserving semilocal pseudopotentials. *Phys Rev B* 66:155125/1–155125/9 <https://journals.aps.org/prb/pdf/10.1103/PhysRevB.66.155125>
- Delley B (2010) Time-dependent density functional theory with DMol³. *J Phys Condens Matter* 22:384208/1–384208/6. <https://doi.org/10.1088/0953-8984/22/38/384208>
- Dong C, Qian H, Fang N, Ren J (2006) Study of fluorescence quenching and dialysis process of CdTe quantum dots, using ensemble techniques and fluorescence correlation spectroscopy. *J Phys Chem B* 110:11069–11075. <https://doi.org/10.1021/jp060279r>
- Frasco MF, Vamvakaki V, Chaniotakis N (2010) Porphyrin decorated CdSe quantum dots for direct fluorescent sensing of metal ions. *J Nanopart Res* 12:1449–1458. <https://doi.org/10.1007/s11051-009-9714-y>
- Gao X, Yang L, Patros JA, Marshall FF, Simons JW, Nie S (2005) In vivo molecular and cellular imaging with quantum dots. *Curr Opin Biotechnol* 16:63–72. <https://doi.org/10.1016/j.copbio.2004.11.003>
- García-Campaña AM, Baeyens WRG (eds) (2001) Chemiluminescence in Analytical Chemistry. Marcel Dekker, CRC Press, New York, p 568
- Gattás-Asfura KM, Leblanc RM (2003) Peptide-coated CdS quantum dots for the optical detection of copper(II) and silver(I). *Chem Commun*:2684–2685. <https://doi.org/10.1039/B308991F>
- Han C, Cui Z, Zou Z, Sabahaiti TD, Li H (2010) Urea-type ligand-modified CdSe quantum dots as a fluorescence “turn-on” sensor for CO₃²⁻ anions. *Photochem Photobiol Sci* 9:1269–1273. <https://doi.org/10.1039/C0PP00119H>
- Hirshfeld FL (1977) Bonded-atom fragments for describing molecular charge densities. *Theor Claim Acta (Berl)* 44:129–138. <https://doi.org/10.1007/BF00549096>
- Hohenberg P, Kohn W (1964) Inhomogeneous electron gas. *Phys Rev B* 136:B864–B871 <https://doi.org/10.1103/PhysRev.136.B864>
- Hussein H, Farag S, Kandil K, Moawad H (2005) Tolerance and uptake of heavy metals by *Pseudomonads*. *Process Biochem* 40:955–961. <https://doi.org/10.1016/j.procbio.2004.04.001>
- Kakkar R, Kapoor PN, Klabunde KJ (2004) Theoretical study of the adsorption of formaldehyde on magnesium oxide nanosurfaces: size effects and the role of low-coordinated and defect sites. *J Phys Chem B* 108:18140–18148 <https://doi.org/10.1021/jp0470546>
- Kunkel R, Manahan SE (1973) Atomic absorption analysis of strong heavy metal chelating agents in water and waste water. *Anal Chem* 45:1465–1468. <https://doi.org/10.1021/ac60330a024>
- Li H, Zhang Y, Wang X (2007) L-carnitine capped quantum dots as luminescent probes for cadmium ions. *Sensors Actuators B Chem* 127:593–597. <https://doi.org/10.1016/j.snb.2007.05.013>
- Li L, Chen Y, Tian G, Akpe V, Xu H, Gan L-M, Skrtic S, Luo Y, Brismar H, Fu Y (2014) Reversible modification of CdSe–CdS/ZnS quantum dot fluorescence by surrounding Ca²⁺ ions. *J Phys Chem C* 118:10424–10433. <https://doi.org/10.1021/jp500853h>

- Liang J-G, Ai X-P, He Z-K, Pang D-W (2004) Functionalized CdSe quantum dots as selective silver ion chemodosimeter. *Analyst* 129:619–622. <https://doi.org/10.1039/B317044F>
- Lorber KE (1986) Monitoring of heavy metals by energy dispersive X-ray fluorescence spectrometry. *Waste Manag Res* 4:3–13. <https://doi.org/10.1177/0734242X8600400102>
- Michalet X, Pinaud FF, Bentolila LA, Tsay JM, Doose S, Li JJ, Sunderesan G, Wu AM, Gambhir SS, Weiss S (2005) Quantum dots for live cells, in vivo imaging, and diagnostics. *Science* 307:538–544. <https://doi.org/10.1126/science.1104274>
- Miyake Y, Togashi H, Tashiro M, Yamaguchi H, Oda S, Kudo M, Tanaka Y, Kondo Y, Sawa R, Fujimoto T, Machinami T, Ono A (2006) Mercury^{II}-mediated formation of thymine-Hg^{II}-Thymine Base pairs in DNA duplexes. *J Am Chem Soc* 128:2172–2173. <https://doi.org/10.1021/ja056354d>
- Perdew JP, Burke K, Ernzerhof M (1996) Generalized gradient approximation made simple. *Phys Rev Lett* 77: 3865–3868, Erratum: *Phys. Rev. Lett.* 77: 1396 (1997). <https://doi.org/10.1103/PhysRevLett.77.3865>
- Rogers JT, Richards JG, Wood CM (2003) Ionoregulatory disruption as the acute toxic mechanism for lead in the rainbow trout. (*Oncorhynchus mykiss*). *Aquat. Toxicology* 64:215–234. [https://doi.org/10.1016/S0166-445X\(03\)00053-5](https://doi.org/10.1016/S0166-445X(03)00053-5)
- Ruedas-Rama MJ, Wang X, Hall EAH (2007) A multi-ion particle sensor. *Chem Commun*:1544–1546. <https://doi.org/10.1039/B618514B>
- Shang ZB, Wang Y, Jin WJ (2009) Triethanolamine-capped CdSe quantum dots as fluorescent sensors for reciprocal recognition of mercury (II) and iodide in aqueous solution. *Talanta* 78:364–369. <https://doi.org/10.1016/j.talanta.2008.11.025>
- Shi J, Zhu Y, Zhang X, Baeyens WRG, García-Campaña AM (2004) Recent developments in nanomaterial optical sensors. *Trends Anal Chem* 23:351–360. [https://doi.org/10.1016/S0165-9936\(04\)00519-9](https://doi.org/10.1016/S0165-9936(04)00519-9)
- Smith AM, Gao X, Nie S (2004) Quantum dot nanocrystals for in vivo molecular and cellular imaging. *Photochem Photobiol* 80:377–385. <https://doi.org/10.1111/j.1751-1097.2004.tb00102.x>
- Tanyanyiwa J, Hauser PC (2002) High-voltage contactless conductivity detection of metal ions in capillary electrophoresis. *Electrophoresis* 23:3781–3786. [https://doi.org/10.1002/1522-2683\(200211\)23:21<3781::AID-ELPS3781>3.0.CO;2-L](https://doi.org/10.1002/1522-2683(200211)23:21<3781::AID-ELPS3781>3.0.CO;2-L)
- Todd MD, Lee MJ, Williams JL, Nalezny JM, Gee P, Benjamin MB, Farr SB (1995) The CAT-Tox (L) assay: a sensitive and specific measure of stress-induced transcription in transformed human liver cells. *Fundam Appl Toxicol* 28:118–128. <https://doi.org/10.1006/faat.1995.1153>
- Touceda-Varela A, Stevenson EI, Galve-Gasi3n JA, Dryden DTF, Mareque-Rivas JC (2008) Selective turn-on fluorescence detection of cyanide in water using hydrophobic CdSe quantum dots. *Chem Commun*:1998–2000. <https://doi.org/10.1039/B716194H>
- Wu C-S, Cupps JM, Fan X (2009) Compact quantum dot probes for rapid and sensitive DNA detection using highly efficient fluorescence resonant energy transfer. *Nanotechnology* 20: 305502/1–305502/7. <https://doi.org/10.1088/0957-4484/20/30/305502>
- Xi L-L, Ma H-B, Tao G-H (2016) Thiourea functionalized CdSe/CdS quantum dots as a fluorescent sensor for mercury ion detection. *Chin Chem Lett* 27:1531–1536. <https://doi.org/10.1016/j.ccl.2016.03.002>
- Zhang K, Guo J, Nie J, Du B, Xu D (2014) Ultrasensitive and selective detection of Cu²⁺ in aqueous solution with fluorescence enhanced CdSe quantum dots. *Sensors Actuators B Chem* 190:279–287. <https://doi.org/10.1016/j.snb.2013.08.093>

Terms and Conditions

Springer Nature journal content, brought to you courtesy of Springer Nature Customer Service Center GmbH (“Springer Nature”). Springer Nature supports a reasonable amount of sharing of research papers by authors, subscribers and authorised users (“Users”), for small-scale personal, non-commercial use provided that all copyright, trade and service marks and other proprietary notices are maintained. By accessing, sharing, receiving or otherwise using the Springer Nature journal content you agree to these terms of use (“Terms”). For these purposes, Springer Nature considers academic use (by researchers and students) to be non-commercial.

These Terms are supplementary and will apply in addition to any applicable website terms and conditions, a relevant site licence or a personal subscription. These Terms will prevail over any conflict or ambiguity with regards to the relevant terms, a site licence or a personal subscription (to the extent of the conflict or ambiguity only). For Creative Commons-licensed articles, the terms of the Creative Commons license used will apply.

We collect and use personal data to provide access to the Springer Nature journal content. We may also use these personal data internally within ResearchGate and Springer Nature and as agreed share it, in an anonymised way, for purposes of tracking, analysis and reporting. We will not otherwise disclose your personal data outside the ResearchGate or the Springer Nature group of companies unless we have your permission as detailed in the Privacy Policy.

While Users may use the Springer Nature journal content for small scale, personal non-commercial use, it is important to note that Users may not:

1. use such content for the purpose of providing other users with access on a regular or large scale basis or as a means to circumvent access control;
2. use such content where to do so would be considered a criminal or statutory offence in any jurisdiction, or gives rise to civil liability, or is otherwise unlawful;
3. falsely or misleadingly imply or suggest endorsement, approval, sponsorship, or association unless explicitly agreed to by Springer Nature in writing;
4. use bots or other automated methods to access the content or redirect messages
5. override any security feature or exclusionary protocol; or
6. share the content in order to create substitute for Springer Nature products or services or a systematic database of Springer Nature journal content.

In line with the restriction against commercial use, Springer Nature does not permit the creation of a product or service that creates revenue, royalties, rent or income from our content or its inclusion as part of a paid for service or for other commercial gain. Springer Nature journal content cannot be used for inter-library loans and librarians may not upload Springer Nature journal content on a large scale into their, or any other, institutional repository.

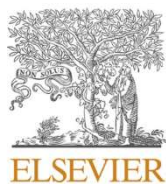
These terms of use are reviewed regularly and may be amended at any time. Springer Nature is not obligated to publish any information or content on this website and may remove it or features or functionality at our sole discretion, at any time with or without notice. Springer Nature may revoke this licence to you at any time and remove access to any copies of the Springer Nature journal content which have been saved.

To the fullest extent permitted by law, Springer Nature makes no warranties, representations or guarantees to Users, either express or implied with respect to the Springer nature journal content and all parties disclaim and waive any implied warranties or warranties imposed by law, including merchantability or fitness for any particular purpose.

Please note that these rights do not automatically extend to content, data or other material published by Springer Nature that may be licensed from third parties.

If you would like to use or distribute our Springer Nature journal content to a wider audience or on a regular basis or in any other manner not expressly permitted by these Terms, please contact Springer Nature at

onlineservice@springernature.com



Contents lists available at ScienceDirect

Journal of Molecular Graphics and Modelling

journal homepage: www.elsevier.com/locate/jmglm

II-VI core/shell quantum dots and doping with transition metal ions as a means of tuning the magnetoelectronic properties of CdS/ZnS core/shell QDs: A DFT study

Pragati Malik, Rakhi Thareja, Jyoti Singh, Rita Kakkar*

Computational Chemistry Laboratory, Department of Chemistry, University of Delhi, Delhi, 110 007, India

ARTICLE INFO

Keywords:

Quantum dots
Core/shell
Structural
Electronic
Magnetic
Fermi energy
Hirshfeld charges
Transition metal ions
Doping

ABSTRACT

This paper examines the alterations in the properties of II-VI Quantum Dots (QDs) when these are coated with a shell made of another material of the same family and investigates the structural, electronic and magnetic properties of doped CdS/ZnS core/shell QDs. The core/shell QDs have been constructed by building the shell over the bare core QD and it is found that this construction of a shell over the bare QD can bring about dramatic changes in its optical properties. On changing the shell by varying either the cation or the anion, substantial variations are brought about in the band gap and electrophilicity. The trend of Fermi energies is more negative for core/shell QDs than for the QDs without a shell, and the value is almost the same for core/shell QDs with the same core. Swapping of the core and the shell materials brings greater stability in the case of shells of the wider band gap materials. Binding energy data demonstrates that the CdS/ZnS, CdSe/ZnSe, CdSe/CdS core/shell systems are more stable than ZnS/CdS, ZnSe/CdSe, CdS/CdSe core/shell systems, respectively. An augmentation in the properties is found on doping the QD with transition metal ions. The binding energies are found to be functions of the kind of dopant as well as the spin multiplicity and account for the stability of one spin state over the other at a specific site of the QD. The most fascinating property that plays a decisive role in the extant work is the introduction of magnetism in core/shell QDs as a result of the entry of unpaired electrons within the CdS/ZnS QDs on doping with transition metal ions. The deviation of the observed magnetic moments from the expected values increases as the dopant is varied from Mn^{2+} to Fe^{2+} to Co^{2+} to Ni^{2+} to Cu^{2+} . Hirshfeld charge analysis shows that the doped ion accepts negative charge from the sulfide ions in the core, with the smallest charge transfer seen in the case of Hg^{2+} ions. As we move from Mn^{2+} to Hg^{2+} , the trend followed for the Hirshfeld charges indicates that the overall charge on the core is lower and that on the shell is higher for all the doped cases in comparison to the undoped CdS/ZnS core/shell QD. The band gap values reveal that the Fe^{2+} doped CdS/ZnS core/shell structures have the smallest band gaps. Hence, we expect that this paper will help researchers to develop a strategy to produce QDs of the anticipated properties for various applications, and transition metal ions can be successfully employed for modification of various magnetoelectronic properties of the host semiconductor for future applications in nanotechnology.

1. Introduction

Recent advances in the synthesis of highly monodisperse nanocrystallites have paved the way for numerous spectroscopic studies assigning the quantum dot (QD) electronic states and mapping out their evolution as a function of size. QDs, due to their reduced dimensions, have very high surface to volume ratios, with roughly 80% of the atoms residing on the surface. Hence, their optical and structural properties are

significantly affected by the atoms present on the surface. The presence of atoms on the surface with unsaturated valencies, called surface defects, leads to the generation of surface trap-states acting as non-radiative recombination sites, which degrade the fluorescence quantum yield of the QDs [1]. On passivating the QD surface with organic ligands, these trap states get reduced, but still the complete passivation of surface defects does not occur. In order to passivate the surface in a more complete manner, a secondary layer of semiconductor may be

Abbreviations: QDs, Quantum dots; NCs, Nanocrystals; DOS, Density of states; PDOS, Partial density of states; DSPP, DFT–semilocal pseudopotentials.

* Corresponding author.

E-mail address: rkakkar@chemistry.du.ac.in (R. Kakkar).

<https://doi.org/10.1016/j.jmglm.2021.108099>

Received 5 August 2021; Received in revised form 14 November 2021; Accepted 27 November 2021

Available online 2 December 2021

1093-3263/© 2021 Elsevier Inc. All rights reserved.

epitaxially grown over the surface surrounding the core semiconductor. This secondary layer is called the shell, and the resulting structure is called a core/shell QD or simply a core/shell structure. The quantum yield has been shown to increase up to ten times, with increased resistance toward photo-oxidation on overgrowing shells around the semiconductor material [2].

1.1. Types of core/shell QDs

The material for an overgrowing shell layer depends upon the properties we require from the resultant structure. Based on this, we have three types of core/shell systems, type I core/shell, reverse type I core/shell and type II core/shell systems (Fig. 1). These all differ in the alignment of the valence and conduction bands between the core and shell. Type I core/shell systems are the most common, where the shell is composed of the higher band gap semiconductor material, confining the exciton (an electron-hole pair) to the core. These types of systems are employed when high quantum yield is desired, e.g. CdSe/ZnS. In reverse type-I systems, a shell of a narrower band gap semiconductor is grown on the higher band gap core. Here, the charge carriers are partially delocalized from the core to the shell. Such types of systems are required when red shifting of the fluorescence spectrum is required, e.g. CdS/CdSe and ZnSe/CdSe. In type-II core/shell systems, the lowest energy states for the electrons and holes are in different semiconductors, setting an energy gradient at the interfaces tending to spatially separate electrons and holes, e.g. ZnTe/CdSe and CdTe/CdSe. These types of systems are majorly employed in photovoltaic technologies [3].

It has been observed that nanocrystallites passivated with higher band gap semiconductor materials exhibit improved photoluminescence quantum yields [4,5]. The choice of the shell material highly depends upon both the alignment of its valence and conduction bands relative to those of the core material. It is also necessary to match the band alignment and lattice parameters between the core and shell, since new defects are formed at the interface if the lattice mismatch between core and shell is too great, which reduces the fluorescence quantum yield [1].

Core/shell type composite QDs exhibit novel properties, making them attractive from both an experimental and practical point of view [5–12]. Overcoating nanocrystallites with higher band gap inorganic materials has been shown to improve the photoluminescence quantum yields by passivating the surface nonradiative recombination sites. Some examples of core/shell QD structures reported earlier include CdS on CdSe and CdSe on CdS [10], ZnS grown on CdS [12], ZnS on CdSe, and the inverse structure [7], CdS/HgS/CdS QD quantum wells [9], ZnSe overcoated CdSe [6], and SiO₂ on Si [8,11]. (CdSe)ZnS nanocrystallites at room temperature show upto 50% fluorescence quantum yield [5]. Various core/shell structures have been studied computationally also; high-quality CdSe/CdS core/shell QDs have been studied to understand the effects of oxygen on the photoluminescence of QDs at both the single dot and ensemble (on substrate and in solution) levels [13]. In another study [14], the third-order optical nonlinearity in CdSe and CdSe–CdS core-shell QDs with particle sizes in the range 4.4–5.2 nm has been investigated by the z-scan technique and the quantum confinement effect has been discussed extensively. CdTe@HgTe Core@Shell nanostructures have been produced [15] by a partial Hg²⁺ → Cd²⁺ cation exchange reaction in colloidal CdTe nanocrystals of ~4–6 nm size. A study of CdSe/CdS core-shell NCs using density functional theory was carried out [16] to understand the dependence of the properties of these

NCs on core types and interfaces between the core and the shell, as well as on the core/shell ratio. TDDFT studies have been performed [17] to describe the effects of morphology on the optical response of QDs. The microstructural and optical properties of CdSe/CdS/ZnS core-shell-shell QDs have been determined [18]. Type-I CdSe/ZnS core/shell QDs have been found to effectively sensitize single crystal TiO₂ electrodes and are maintained to work in a regenerative mode in an aerated iodide electrolyte for more than 20 h. On the other hand, core CdSe QDs degrade promptly in the same electrolyte probably due to the formation of CdI₂ [19].

In order to further enhance the properties of these core/shell QDs, transition-metal ion doped semiconductor nanocrystals (NCs) have attracted much attention in the past two decades due to their promising applications in light-emitting devices [20,21], biological imaging [22, 23], and spin-based electronics [24]. The structural and electronic properties are tremendously affected on introduction of an inorganic shell outside the QD which may act as the core. The results of some studies [25] suggest that the complete coverage of the CdS core with the wider energy band gap ZnS enhances the photoluminescence of the CdS core. Hence, in the present work, we have coated the toxic core of CdS with a shell of the less toxic ZnS in order to enhance its optical, electronic and magnetic properties further. The experimental findings [26] suggest that uniform shell coverage is obtained only for a graded CdS/ZnS core/shell material and is found to be critical for achieving near 100% quantum yield.

In line with this, we have developed a theoretical model of core/shell QDs, which comprises a core and an inorganic shell formed from the chalcogenides of the zinc triad. The idea is to form a stable model to make it interact with other molecules of scientific interest in order to sense them. Core/shell structures of QDs are the latest trend in the manifestation of reduced dimensionality.

Several experimental groups are enthusiastically pursuing the synthesis of magnetic semiconducting nanoparticles and the production of magnetically doped II-VI semiconductors. Doping of impurities into semiconductor nanocrystals in a controlled manner is essential for producing and enhancing optical and magnetic functionalities. This has opened new gates for scientists to explore how these dopants can influence semiconductor nanocrystals. Transition metal ions are unique dopants, because doping with these ions has the effect of injecting localized luminescence centers and electronic spins into semiconductors. As a result, semiconductor nanocrystals doped with transition metal ions are the key materials for future optronic and spintronic devices [27]. Incorporation of dopants into semiconductor nanocrystals has been used to tailor the optical, electronic, and magnetic properties of nanocrystals [28–35]. Much effort has been poured into realizing doping II-VI semiconductor QDs with impurities, especially to obtain dilute magnetic semiconductors (DMS). Undoped nanocrystals are highly fluorescent, the fluorescence depending upon the size. The lasers based on this emission are inefficient. Several approaches can improve this situation [36], and one way is to incorporate dopants that can provide carriers. Dopants in nanocrystals lead to phenomena which are not found in bulk semiconductors, as the electronic states in nanocrystals or QDs are confined to a small volume and in all the three dimensions. Historically, a major motivation for the exploration of transition metal doped semiconductors has been the use of luminescence activators such as Mn²⁺ or Cu²⁺ for sensitized photoluminescence and electroluminescence applications [24,37–39].

It is clearly revealed from the earlier studies that doping with transition metals with half and more than half filled *d*-orbitals is of great significance in causing an alteration in their own properties as well as in the properties of the host moiety. Mn doping has been extensively investigated, such as Mn doped CdS/ZnS in order to reveal the surface effects and position-dependent properties of the doped core/shell QDs [40,41], tunable magnetic exchange interactions in Mn²⁺ doped inverted core-shell ZnSe/CdSe nanocrystals [42], enhanced photoluminescence from Mn²⁺-doped CdS nanocrystals capped with ZnS

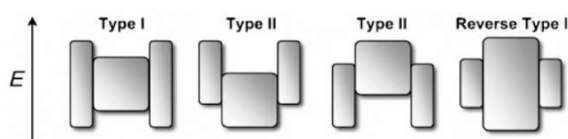


Fig. 1. Energy-level alignment in three different types of core/shell systems [1].

(CdS:Mn/ZnS core/shell) [43], photoluminescence dynamics dependent on the Mn^{2+} ion concentration in Mn^{2+} -doped CdS/ZnS core/shell nanocrystals [27], Mn-doped CdS core/shell nanocrystals [44], an application of Mn^{2+} -doped ZnS core/shell QDs in detection of silver ions [45], synthesis of non-toxic, less expensive Mn:ZnSe/ZnS core/shell and Mn:ZnSeS shell-alloyed doped nanocrystals [46], Mn^{2+} doping in MnS/ZnS core/shell QDs [47], and a green synthetic approach of low-toxic Mn:ZnSe/ZnS core/shell luminescent nanocrystals to label antibodies for its potential application in the detection of human immunoglobulin G (IgG) [48]. Recently, it has been found that the thermal stability of the Mn-doped QD emissions significantly depends on the shell thickness and the host band gap [49]. Bui & Nguyen [50] have proved that Mn-doped ZnSe/ZnS core/shell QDs could be successfully applied in the detection of *Escherichia coli* and methicillin-resistant *Staphylococcus aureus* and this has inordinate potential for use in the food industry to avoid occurrences of food-borne infections. Doping with other transition metals has also been done, such as Fe doping in ZnS core/shell (ZnS:Fe/ZnS) nanocrystals [51]. Fe^{3+} doped QDs have been investigated [52] to study the effect of doping on the magnetic and optical properties, and Co doping in ZnO/ZnOcore/shell colloidal QDs [53]. Cu doping has also been extensively done such as in $Zn_{1-x}Cd_xS$ QDs and their core/shell structure [54], ZnS core/shell nanocrystals [55], and inverted ZnSe/CdSe core/shell nanocrystals [56], and highly photostable CdSe/CdS:Al core/shell QDs [57].

The dopants chosen for the present work include transition metal atoms from manganese to zinc, along with mercury. The aim is to extend our study to explore and investigate the deviations/amplification in the properties of core/shell nanocrystals on doping the CdS/ZnS core/shell QDs at the atom centered position of the QDs. One of the candidate methods for fabricating nanocrystals doped with impurity ions is that of constructing a core/shell structure, i.e. core semiconductor nanocrystals doped with impurities are coated with a non-doped semiconductor shell layer [43,58–60].

Another reason for choosing doping in the core of the QD is that a nonmagnetic coating is used routinely for magnetic core stabilization and surface functionalization for biomedical applications [61]. Also, an antiferromagnetic coating over a ferromagnetic core led to exchange bias and improvements in the thermal stability of the core [62]. Compared with these two different types of core/shell systems, a bimagnetic core/shell one, where both the core and shell are strongly magnetic (ferro- or ferri-magnetic) is less studied, yet more interesting due to its potential in electromagnetic and permanent magnetic applications [63,64]. In such a system, the intimate contact between the core and shell leads to effective exchange coupling and therefore cooperative magnetic switching, facilitating the fabrication of nanostructured magnetic materials with tunable properties. Thus, an interesting magnetic nanoparticle system is that of core/shell structured nanoparticles in which the magnetic core is coated with a layer of a nonmagnetic, antiferromagnetic, or ferro/ferrimagnetic shell. Recently, it has been demonstrated that the eco-friendly copper doped InP/ZnSe core/shell QD (InP/ZnSe:Cu) is a substitute to traditional Cd/Pb-based QDs in light-emitting technologies [65]. Composition-tunable Cu-doped ZnInS/ZnS nanocrystals were synthesized [66], which show that a change in the Zn/In ratio tunes the percentage assimilation of Cu in nanocrystals.

In the present work, firstly, the cores of cadmium chalcogenides were constructed with the shells comprising the respective chalcogenides of the zinc triad. This work includes the following core/shell structures: CdS/ZnS, CdS/HgS, CdSe/ZnSe, CdSe/HgSe, CdTe/ZnTe and CdTe/HgTe. All these core/shell structures have been compared with similar sized bare uncapped non-stoichiometric QDs comprising the core without any shell. Then, we chose a few core/shell systems and interchanged their core and shell materials in order to examine the effect of interchanging the core and shell materials on the properties of these systems. In the subsequent section, the CdS/ZnS core/shell QD, which has a core of CdS and a ZnS shell and is a well-known wide band gap

semiconductor, with a diameter of 15 Å and a binding energy -77.69 eV, has been specifically chosen as the most stable non-stoichiometric core/shell QD amongst all the core/shell nanocrystals considered for doping with transition metal ions. We have restricted our study to doping of only the atom at the center of the atom-centered core/shell QDs. Detailed comparison with the undoped analogous CdS/ZnS QDs has been done in order to have an in-depth knowledge of the effect of doping with these single transition metal ions on the structural, electronic and magnetic properties.

1.2. Computational details

First-principles density functional (DF) calculations [67] were performed by means of the DMol³ code [68–74], obtained from Accelrys Inc. in the Materials Studio 4.4 package. High quality numerical functions on an atom-centered grid were used as the atomic basis in these calculations. The basis set used was DNP, which is of double zeta quality plus polarization functions, and is the numerical equivalent of the Gaussian basis, 6-31G** [74].

All the structures were optimized using DFT–semilocal pseudopotentials (DSPP) [72] to define the cores, using the GGA-PBE (generalized gradient approximation-Perdew Burke Ernzerhof) functional [75]. Hirshfeld’s method was used to carry out charge partitioning [76] and the covalent bond orders were calculated using Mayer’s procedure [77].

2. Results and discussion

2.1. DFT study of various core/shell QDs

In traditional type QDs, a low band gap core material is coated with a second semiconductor with a wider band gap than the core material [78, 79]. It has been shown that coating a core semiconductor with a larger band gap material of the same kind improves the properties of nanocrystals [80,81]. As mentioned earlier, we have selected a core of the cadmium chalcogenides, with the shells comprising the respective chalcogenides of the zinc triad. These structures were compared with similar sized bare uncapped non-stoichiometric QDs. These clusters, being non-stoichiometric in nature, were centered on a central cadmium atom. All the clusters were constructed based on the wurtzite crystal structure as the basis structure and typical structures (of CdS and CdS/ZnS core/shell QDs), showing the numbering of atoms, are depicted in Fig. 2. The complete range of structures used is given in Fig. S1 of the Supporting Information (SI). These structures show that the surfaces have unsatisfied valencies, because of which they can interact or, rather, get capped further to enhance their properties. The metal atoms on the exterior are di-coordinated, whereas the interior ones are tetra-coordinated. The exterior chalcogenide atoms are tri-coordinated, and the interior ones are tetra-coordinated in this case.

The surface reconstruction has a critical effect on the optical and electronic properties of these QDs. The surface structure of the QDs is, however, not very well understood, and only limited experimental and theoretical evidence is available. Thus, an effort has been made in this work to explain the unrevealed properties of the non-stoichiometric II-VI core/shell QDs. All the clusters shown in Figs. 2 and S1 have been fully optimized, and then investigated to study the effect of introducing the shell outside the core of the basic QDs, while keeping the overall size of the QD constant. The change in the chemical constituent also causes a significant shift in the structural and electronic properties of these QDs. All these properties are discussed in detail in the sections that follow.

2.2. CdS, CdSe and CdTe QDs (without any shell)

The QDs considered in the present section provide an interesting understanding about the wide range of tunable band gaps available for altering the properties of many electronic devices. The QDs considered here represent the uncapped, non-interacting colloidal nanoclusters of

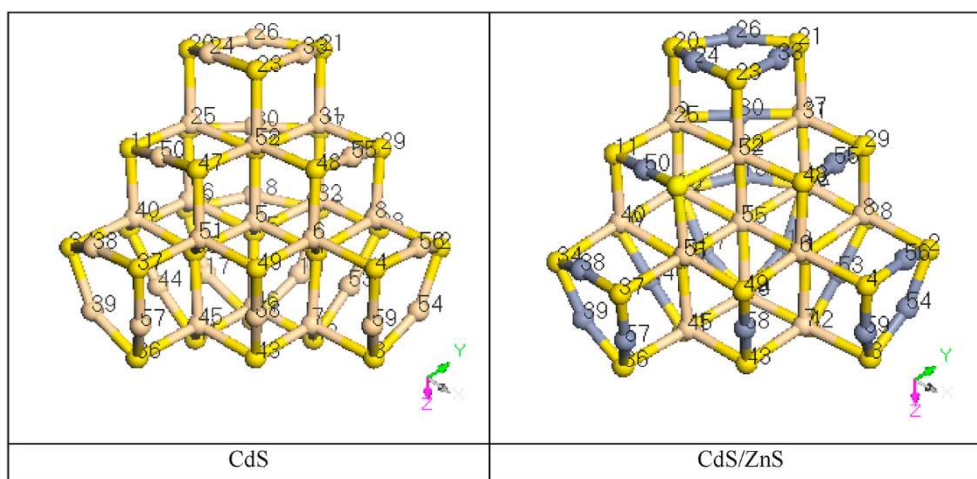


Fig. 2. Optimized structures of bare CdS and CdS/ZnS core/shell QDs. Bluish Gray- Zinc, Off-white- Cadmium, Yellow- Sulfur. (For interpretation of the references to colour in this figure legend, the reader is referred to the Web version of this article.)

diameter 15 Å. They are spherical in shape, atom-centered and non-stoichiometric. Because of the difference in the number of metal atoms and chalcogenide atoms, these clusters are charged. We assigned a charge of +6 to these QDs, as the metal ions in the QD outnumber the chalcogenide atoms. The positively charged QDs are found to have longer lifetimes, quick captures and brilliant radiation frequency, which makes them far more superior to neutral QDs. These can therefore be used in applications for spintronics [82–84]. The optimized models were then used for further studies and to study the enhancement in the properties after the introduction of an inorganic shell, while keeping the size of the spherical core/shell QD constant.

Three different kinds of bonding patterns are observed in the atom-centered, optimized bare and core/shell QDs. These are described as follows:

- Bonding between a di-coordinated metal atom and a tri-coordinated chalcogenide atom (on the surface corresponding to the shell). Two types of bonds are observed, which we have labeled type A bonds (e.g. M38-E34, see Fig. 2) and type B bonds (e.g. M58-E49). Here M represents the metal and E the chalcogenide ion.
- Bonding between a tetra-coordinated metal atom and a tri-coordinated chalcogenide atom (interior). Here again two kinds of bonding patterns can be observed (Type A, e.g. M40-E10 and Type B, e.g. M40-E34).
- Bonding between a tetra-coordinated metal atom and a tetra-coordinated chalcogenide atom (interior). These bonds correspond to the core of the heterostructure, and are also of two types, labeled Type A, in which the metal atom of the core forms a bond with the chalcogenide of the core (e.g. M40-E35), and Type B, in which the central atom bonds with the chalcogenide of the core (e.g. M5-E1).

The bond lengths corresponding to the above types of bonding patterns are given in Table 1. The atom-centered bond length corresponding to the bonding pattern (c) represents the four equal bond lengths which the central tetra-coordinated cadmium atom forms with the four tetra-coordinated chalcogenide atoms comprising the core.

Table 1 shows that the optimized bond lengths in case of the CdS, CdSe and CdTe QDs are smaller than the sums of the respective ionic radii of their M^{2+} and A^{2-} ions (2.51 Å, 2.93 Å and 3.30 Å, respectively), which clearly indicates the covalent character of the bonds of the nanoparticles of the semiconductors. However, the external field produced by the larger number of surrounding ions increases the ionic

Table 1

Optimized bond lengths (Å) in bare and core/shell QDs.

QD	Bonding type					
	(a)		(b)		(c)	
	A-type	B-type	A-type	B-type	A-type	Atom-centered
CdS	2.450	2.369	2.751	2.590	2.737	2.683
CdS/ZnS	2.216	2.164	2.775	2.584	2.671	2.641
CdS/HgS	2.453	2.380	2.596	2.779	2.731	2.678
CdSe	2.547	2.502	2.849	2.702	2.819	2.790
CdSe/ZnSe	2.350	2.308	2.877	2.698	2.802	2.744
CdSe/HgSe	2.580	2.509	2.873	2.713	2.823	2.788
CdTe	2.764	2.702	2.906	3.055	3.011	2.964
CdTe/ZnTe	2.556	2.518	3.080	2.902	2.953	2.922
CdTe/HgTe	2.769	2.708	2.914	3.070	2.992	2.957
CdS/ZnS	2.216	2.164	2.775	2.584	2.671	2.641
ZnS/CdS	2.452	2.361	2.509	2.373	2.546	2.472
CdSe/ZnSe	2.350	2.308	2.877	2.698	2.802	2.744
ZnSe/CdSe	2.575	2.484	2.620	2.508	2.636	2.563
CdS/CdSe	2.573	2.498	2.857	2.711	2.701	2.691
CdSe/CdS	2.453	2.376	2.583	2.741	2.841	2.764

character of the M-A bonds in the interior of the QDs, which results in the resemblance of the corresponding bond lengths (for (b) and (c)) closer to the ionic limit, while the terminal bonds in each of the cases (a) are found to be closer to the molecular bond lengths (2.329 Å, 2.497 Å and 2.731 Å for CdS, CdSe and CdTe, respectively), as these have unsaturated valencies.

The same conclusions can be drawn from the computed Mayer covalent bond orders (Table 2), which show that the covalent bonding is stronger in bonding pattern (a) compared to the other two.

The HOMO-LUMO plots (Figs. 3 and S2) clearly show the participation of the *p* orbitals of the chalcogenides, along with a small contribution of the *d* orbitals of the cadmium atoms in the HOMO of CdS, but the LUMOs comprise only the chalcogenide orbitals.

The Fermi energy is the highest energy level that an electron (a fermion) can occupy at the absolute zero of temperature. It is a crucially important concept for understanding the thermal and electrical properties of semiconductors. In the present case, as expected, the Fermi energy increases with increase in the number of electrons in a system (Table 3).

The effect of quantum confinement is manifested in the higher magnitudes of the HOMO-LUMO gaps for CdSe and CdTe QDs, but the computed HOMO-LUMO gap is smaller than the experimental band gap for CdS. The reason is seen from the HOMO-LUMO plots (Fig. 3), which reveal a mixing of the metal *d* orbitals only in the case of CdS, resulting

Table 2

Calculated Mayer bond orders for the atom pairs in various bare and core/shell QDs.

Bond	Bonding type					
	(a)		(b)		(c)	
	A-type	B-type	A-type	B-type	A-type	Atom centered
CdS	0.883	0.932	0.637	0.329	0.500	0.529
CdS/ZnS	0.937	0.949	0.648	0.450	0.526	0.536
CdS/HgS	0.865	0.931	0.200	0.460	0.497	0.534
CdSe	0.821	0.870	0.600	0.477	0.503	0.528
CdSe/ZnSe	0.859	0.868	0.624	0.454	0.499	0.542
CdSe/HgSe	0.835	0.903	0.588	0.448	0.501	0.530
CdTe	0.826	0.859	0.625	0.493	0.517	0.565
CdTe/ZnTe	0.844	0.867	0.635	0.468	0.539	0.573
CdTe/HgTe	0.813	0.865	0.616	0.477	0.533	0.565
CdS/ZnS	0.937	0.949	0.648	0.450	0.526	0.536
ZnS/CdS	0.880	0.962	0.668	0.548	0.549	0.573
CdSe/ZnSe	0.859	0.868	0.624	0.454	0.499	0.542
ZnSe/CdSe	0.820	0.901	0.580	0.502	0.514	0.546
CdS/CdSe	0.826	0.874	0.603	0.477	0.504	0.519
CdSe/CdS	0.876	0.921	0.636	0.482	0.485	0.537

Table 3

Band gap (eV) variation for the CdS, CdSe and CdTe hexa-cationically charged QDs.

QD	HOMO	LUMO	Band gap (eV)		Fermi energy (eV)
			LUMO-HOMO	Expt.	
			CdS	-17.91	
CdSe	-17.03	-14.92	2.11	1.73 ^a	-0.590
CdTe	-15.92	-13.83	2.09	1.49 ^b	-0.551
CdS	-17.91	-15.59	2.32	-	-0.619
CdS/ZnS	-18.58	-15.89	2.69	-	-0.636
CdS/HgS	-18.31	-16.00	2.31	-	-0.635
CdSe	-17.03	-14.92	2.11	-	-0.590
CdSe/ZnSe	-17.61	-15.07	2.54	-	-0.603
CdSe/HgSe	-17.25	-15.20	2.04	-	-0.601
CdTe	-15.92	-13.83	2.10	-	-0.551
CdTe/ZnTe	-16.37	-13.93	2.44	-	-0.562
CdTe/HgTe	-16.04	-14.07	1.97	-	-0.559

^a Ref. [85].

^b Ref. [86].

in an underestimated value of the band gap when compared with experiment.

As the size of the anion in the QD increases, the quantum confinement effect is observed, and the band gap decreases. Before we move on to construct core/shell QDs, we may state that our elementary studies clearly indicate that the density functional packages can be easily used to study and interpret the structural and electronic properties of QDs. This is of great help and serves as an effective tool for verifying the experimental observations and making predictions.

2.3. Core/shell QDs with CdS as the core

In the previous section, we had discussed CdS QDs (without any shell) of diameter 15 Å and now in the present section, while keeping the size constant, the outermost shell/layer is replaced by the sulfide of zinc and then by the sulfide of mercury. This way, we can compare the effect of changing the size of the cation/metal atom in the outermost shell and take note of the properties of the core/shell QD thus formed. All the observations regarding this are put in the next subsections.

2.4. CdS/ZnS core/shell QDs

The covering of the cadmium sulfide QD with a zinc sulfide shell causes a modification in the properties of the QD. The surface bond lengths are reduced and the bond angles also change, causing the bond

to move inward toward the core. The optimized structures have been shown in Figs. 2 and S1. The stabilization of the HOMO is greater in comparison to the LUMO, resulting in a wider band gap in comparison to the CdS QD (Table 3). The HOMO involves participation from both the *p* and *s* orbitals of the sulfide ions on the surface, whereas the LUMO involves only the *s* orbitals of the surface sulfide ions. The metal ions do not participate in either the HOMO or the LUMO (Figs. 3 and S2).

2.5. CdS/HgS core/shell QDs

The shell cover of the cadmium sulfide QD by mercury sulfide brings about a slight increase in the surface bond lengths, and the bond angles slightly widen up to open the structure to a little extent.

The stabilization of the LUMO is greater in comparison to that of the HOMO, resulting in a slightly smaller band gap in comparison to the CdS QD (Table 3). The HOMO involves participation from the *p* orbitals of the sulfide ions and the *d* orbitals of some mercury ions on the surface, whereas the LUMO involves the *s* orbitals of sulfur atoms and the *d* orbitals of most of the surface mercury atoms; cadmium atoms are not involved in either the HOMO or LUMO (Figs. 3 and S2).

The trend of Fermi energy for core/shell systems, when compared with the QDs without any shell, shows that the Fermi level goes down on introduction of an inorganic shell, but for both the CdS/ZnS and CdS/HgS core shell QDs, i.e. core/shell QDs with the same core, the Fermi energy is approximately the same. Thus, we conclude that there is very little/no effect of changing shells on the Fermi energy of core/shell QDs with the same core.

2.6. Core/shell QDs with CdSe as the core

We have already discussed the CdSe QD of diameter 15 Å and in the present section, while keeping the overall size constant, the outermost shell/layer is replaced by the selenide of zinc and then by the selenide of mercury. Here also, we have compared the effect of changing the surface cadmium atoms with the relatively smaller sized zinc atoms and the larger sized mercury atoms.

2.7. CdSe/ZnSe core/shell QDs

Cadmium selenide QDs with a zinc selenide shell have reduced surface bond lengths, and changes in bond angles that cause the bond to move inward toward the core. The optimized structures are shown in Fig. 2 (S1). The HOMO is stabilized more than the LUMO, resulting in a wider band gap in comparison to the CdSe QD (Table 3). The HOMO involves participation from the *p* orbitals of the selenide atoms on the surface as well as the *d* orbitals of some of the surface zinc atoms and cadmium atoms in the interior, whereas the LUMO involves only the *s* orbitals of the surface sulfide ions (Fig. S2). A change that is to be noted is the active participation of the *d* orbitals from the cadmium and zinc atoms in comparison to the CdS/ZnS core/shell QDs, which results in a complete alteration of the properties of the QD. The HOMO is stabilized by the participation of the anion.

2.8. CdSe/HgSe core/shell QDs

In this case, too, the surface bond lengths increase slightly, and the bond angles slightly widen up to open the structure to a small extent (Fig. S1). The stabilization of the LUMO in comparison to the HOMO results in a smaller band gap in comparison to the CdSe QD without the shell (Table 3). The HOMO involves participation from the *p* orbitals of the selenide atoms and the *d* orbitals of some mercury atoms on the surface as well as a couple of cadmium atoms (Fig. S2). The orbitals from one half of the structure participate more than the other half. The LUMO involves the *s* orbitals of the selenium atoms and the *d_{z²}* orbital of the mercury atoms of the shell. Cadmium atoms do not participate in the LUMO. Here also, the Fermi energy shows the same trend as that in the

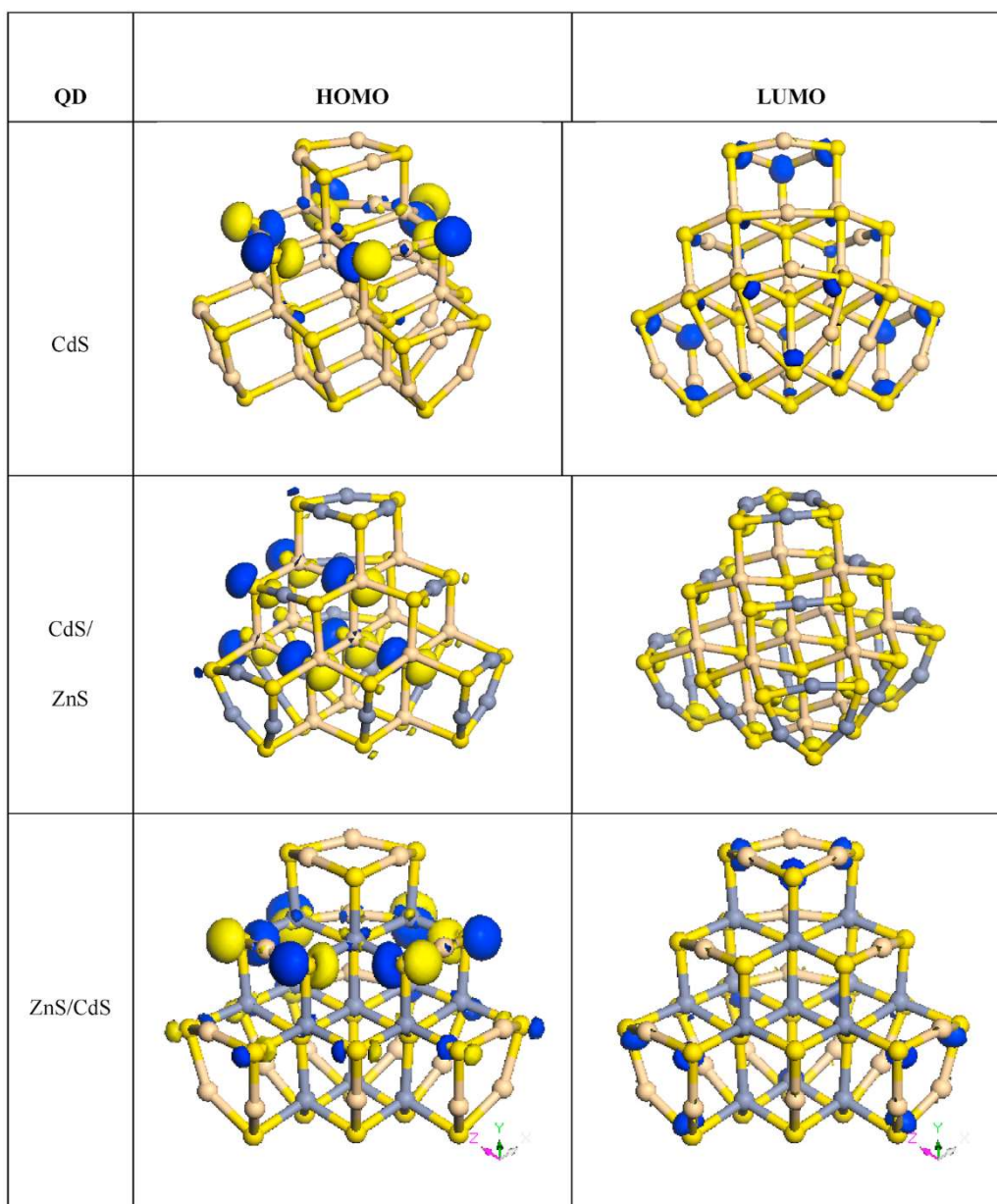


Fig. 3. HOMO-LUMO plots for bare CdS hexa-cationically charged QDs, CdS/ZnS and ZnS/CdS core/shell QDs. Bluish Gray- Zinc, Off-white- Cadmium, Yellow- Sulfur. (For interpretation of the references to colour in this figure legend, the reader is referred to the Web version of this article.)

case of CdS QDs without any shell and core/shell QDs having CdS as the core, i.e. it is more negative for CdSe based core/shell QDs than for the bare CdSe QDs without any shell. Also, the CdSe/ZnSe and CdSe/HgSe core/shell QDs have nearly the same values for the Fermi energy.

2.9. Core/shell QDs with CdTe as the core

After checking the noticeable changes in the properties of CdS and CdSe on bringing about surface modification, it becomes obvious that the CdTe QD would also show changes in its structural and electronic properties. Hence, in the next subsections, the effects of the inorganic shell of the telluride of zinc and mercury on CdTe as the core are discussed briefly. These changes can then be utilized for further studies to make these core/shell QDs interact with other biological and inorganic molecules of interest for a wide range of applications.

2.10. CdTe/ZnTe core/shell QDs

The optimized structures of these QDs are shown in Fig. S1. There is a significant band gap widening in this case owing to the shifts in the values of the HOMO and LUMO energies of the cadmium telluride QD (Table 3). The HOMO in this case involves participation from the *p* orbitals of a few telluride atoms and only a small contribution from the metal atoms, while the LUMO comprises only the *s* orbitals of the zinc atoms which form the inorganic shell outside. This *sp* interaction results in widening of the band gap by about 16%. The reactive centers in this case are fewer in comparison to the QDs discussed in the previous sections, due to lesser participation in the valence and conduction bands by the surface atoms. There is effectively no participation from the atoms in the interior of the QD (Fig. S2).

2.11. CdTe/HgTe core/shell QDs

As in the previous cases, the surface bond lengths increase a little,

and the bond angles widen up slightly to open the structure (Fig. S1). The HOMO involves participation from the p orbitals of tellurium and the d orbitals of only a few Cd and Hg atoms, while the LUMO involves participation from the d_{z^2} orbitals of Hg and the s orbitals of the surface tellurium atoms (Fig. S2). As in the previous cases, the band gap value for the CdTe/HgTe QD decreases in comparison to the CdTe QDs without any shell by about 6%, which implies improved conducting properties of the CdTe QD when covered with a shell of the corresponding chalcogenide of the bigger sized mercury atoms (Table 3). The trend of Fermi energy is the same as discussed in the previous sections. It is more negative for core/shell QDs than for the QDs without any shell, and the value is almost the same for the core/shell QDs with the same core.

We now investigate the effect of interchanging the core and shell materials in order to understand if this has any effect on the properties of the QDs.

3. Effect of interchange of core and shell materials

Here, we have constructed spherical, atom-centered and non-stoichiometric, passivated colloidal nanoclusters of diameter 15 Å having charge +6. These structures were fully optimized (Figs. 2 and S1) in order to study the differences in the structural and electronic properties produced on interchanging the core and shell materials.

The following three cases have been considered:

- (i) CdS/CdSe and CdSe/CdS
- (ii) CdS/ZnS and ZnS/CdS
- (iii) CdSe/ZnSe and ZnSe/CdSe

Here also, as we saw earlier, three different kinds of bonding patterns are observed, i.e. (a) bonding between a di-coordinated metal atom and a tri-coordinated chalcogenide atom, (b) bonding between a tetra-coordinated metal atom and a tri-coordinated chalcogenide atom, and (c) bonding between a tetra-coordinated metal atom and a tetra-coordinated chalcogenide atom. All these bonding patterns are characterized by different bond lengths (Table 1). On comparing the bond length data for CdS/ZnS and ZnS/CdS, we observe that the surface bonds (a) between the di-coordinated metal and the tri-coordinated chalcogenide lengthen in the latter because of the presence of the larger sized Cd atoms on the surface, while the inner bond lengths (b) and (c) exhibit the opposite trend. A similar trend is observed in the case of the CdSe/ZnSe and ZnSe/CdSe systems. Between CdSe/CdS and CdS/CdSe, it is CdS/CdSe which shows longer surface bond lengths and smaller inner bond lengths due to the larger sized Se^{2-} anion on the surface and smaller sized S^{2-} anion in the core, respectively.

The Mayer bond orders of the different types of bonding patterns in core/shell QDs are given in Table 2. It is again found that the bonds on the surface (a) are more covalent than those in the interior (b) and (c). The HOMO-LUMO isosurfaces (Figs. 3 and S2) show the participation of the p orbitals of the chalcogenides, along with slight participation of the d orbitals of cadmium and zinc atoms in the HOMO, and that of the s orbitals of the chalcogenide in the LUMO. From the binding energy data (Table 4), we conclude that the CdS/ZnS core/shell system is more stable than the ZnS/CdS system. Similarly, the CdSe/ZnSe core/shell system is more stable than the ZnSe/CdSe system, and the CdSe/CdS

Table 4
Binding energies (eV) and band gaps (eV) for the core/shell systems.

QD	HOMO	LUMO	Band gap	Binding energy
CdS/ZnS	-18.58	-15.89	2.69	-77.69
ZnS/CdS	-18.33	-16.08	2.25	-73.10
CdSe/ZnSe	-17.61	-15.07	2.54	-65.65
ZnSe/CdSe	-17.38	-15.38	2.00	-62.14
CdS/CdSe	-17.07	-14.96	2.11	-57.79
CdSe/CdS	-17.73	-15.56	2.17	-64.82

core/shell system is more stable than CdS/CdSe. Thus, QDs with the heavier metal and the lighter chalcogenide in the shell are more stable.

The band gaps for each of the semiconductor systems considered above, i.e. bare ZnS, ZnSe, CdS, and CdSe are 2.87, 2.66, 2.32, and 2.11 eV, respectively. From the data in Table 4, we can also draw a general conclusion that the core/shell system with the wider band gap shell material is more stable than the one with a narrower band gap shell material, and our results are consistent with the already reported results on various core/shell systems [87].

A key feature causing surface reconstruction is the charge redistribution, which is highly responsible for the enhancement of the electronic properties of the QD. The Hirshfeld charges are presented in Table 5. Construction of a ZnS or an HgS shell outside the CdS core causes an increase in the positive charge of the core while that of the shell reduces. Here at this point, we may note that the increase of the positive charge marks an increase in the electrophilicity, while a decrease marks an enhancement in the nucleophilicity of that part of the QD. In this case, the shell reduces the positive charge on the surface and hence its electrophilicity.

In the case of coating of CdSe, too, covering of the QD by either ZnSe or HgSe reduces its electrophilicity. The behavior of the core/shell in terms of the charges is similar when the shell is covered by the larger sized mercury selenide or the smaller sized zinc selenide, which clearly indicates that the electrophilicity on the surface reduces whether it is coated by a shell of a smaller sized or larger sized cationic selenide. A similar trend of charge redistribution is observed in the case of cadmium telluride on surface modification, i.e. the QD becomes less electrophilic on either modification. In all cases, the variations are smaller on coating with a shell containing the bigger sized mercury atoms when compared with the shell containing the smaller sized zinc atoms.

Comparison of the positive charges on the shells of CdS/ZnS and ZnS/CdS core/shell QDs indicates that the latter are more electrophilic. Thus, a QD with a shell of the high molecular weight chalcogenide of the zinc triad is more electrophilic than one with the lighter one. The same conclusion is reached on comparing CdSe/ZnSe and ZnSe/CdSe core/shell QDs, as well as the CdS/CdSe and CdSe/CdS core-shell QDs (Table 5).

4. Doping of CdS/ZnS core/shell quantum dots with transition metal ions

We have considered seven transition metal dipositive ions, i.e. Mn^{2+} , Fe^{2+} , Co^{2+} , Ni^{2+} , Cu^{2+} , Zn^{2+} and Hg^{2+} in order to maintain the overall charge on the core/shell system and to study their role in enhancing the structural and electronic properties of the CdS/ZnS core/shell QDs for its

Table 5
Hirshfeld charges on the cations and anions of core and shell.

QD	Core			Shell		
	Cation	Anion	Net charge	Cations	Anions	Net charge
CdS	3.520	-1.472	2.048	7.866	-4.013	3.853
CdSe	2.949	-1.306	1.642	6.924	-2.664	4.260
CdTe	2.112	-1.064	1.048	5.617	-0.763	4.853
CdS/ZnS	3.865	-1.362	2.503	6.633	-3.234	3.399
CdS/HgS	3.524	-1.430	2.093	6.406	-2.596	3.810
CdSe/ZnSe	3.249	-1.270	1.979	5.647	-1.736	3.911
CdSe/ HgSe	3.018	-1.269	1.748	5.512	-1.357	4.155
CdTe/ ZnTe	2.307	-0.977	1.330	4.541	0.003	4.544
CdTe/ HgTe	2.173	-0.989	1.184	4.262	0.457	4.719
ZnS/CdS	2.491	-1.228	1.263	8.137	-3.497	4.640
ZnSe/CdSe	2.038	-1.055	0.983	7.139	-2.220	4.919
CdS/CdSe	3.016	-1.400	1.617	6.941	-2.654	4.286
CdSe/CdS	3.457	-1.346	2.111	7.826	-4.036	3.791

use in various fields such as spintronics, in integrated novel magneto-electronic devices such as spin-LEDs, mid IR lasing, etc. Zn^{2+} and Hg^{2+} , being d^{10} ions, belong to a closed shell system; therefore, they have singlet ground states. Cu^{2+} is a d^9 ion with a doublet ground state. The situation is complicated in the case of Mn^{2+} , Fe^{2+} , Co^{2+} and Ni^{2+} , all of which may exist in high as well as low spin states. Ni^{2+} exists in the singlet and triplet spin states, Mn^{2+} in doublet, quartet and sextet spin states, Co^{2+} in doublet and quartet spin states, and Fe^{2+} in singlet, triplet and quintet spin states. Therefore, we have considered all the various spin multiplicities possible with respect to each transition metal ion in order to explore the effect of spin for deciding the most stable spin state in each of the cases. In addition, the structural and electronic properties of doped CdS/ZnS QDs have been compared in order to gain an insight into the changes caused due to doping with different transition metal ions. The important properties calculated in the previous section for non-stoichiometric atom-centered undoped CdS/ZnS core/shell QDs have also been noted.

As already stated, we have chosen the atom-centered site (center of the CdS core) for doping the core/shell QDs, i.e. the atom-centered position where the cadmium atom resides (Fig. 2). In each of the doped cases, it has been replaced with the desired transition metal ion of interest. Moreover, II-VI semiconductors can crystallize in either the cubic zinc blende or the hexagonal wurtzite phase, in both of which each atom is tetrahedrally coordinated. It is because of this reason that we have specifically considered the four-fold coordination sites over the other sites available for doping (Fig. 2).

The properties of the doped structures (with doping at the atom-centered site) are discussed in detail in the following sections. The stabilities and the enhancement in their properties are discussed for all the doped cases with all the spin multiplicities possible.

5. Doping at the atom centered position in the CdS/ZnS core/shell QD

5.1. Spin multiplicities

We first determined the most stable spin state of the transition metal ions used for doping. The most stable spin state in case of the Mn^{2+} doped CdS/ZnS core/shell QD is the sextet spin state, which is 1.36 eV lower in energy than the doublet spin state, and 1.32 eV lower than the quartet spin state (Table 6). This observation is easily attributable to the additional stability achieved by Mn^{2+} because of the presence of half-filled d -orbitals in the sextet case. The size of manganese is not significant for it to attain a spin-paired configuration in the presence of the low field of the surrounding selenium and cadmium atoms. The CdS/ZnS core/shell QD doped with the d^6 ion, Fe^{2+} , is most stable in the low-spin singlet state. On the other hand, Co^{2+} (d^7) doped CdS/ZnS core/shell QDs prefer the quartet state over the doublet. This indicates that the electrostatic environment created by the expanded d orbitals of the Co^{2+} ion and the field created by the surrounding selenium and cadmium atoms is not sufficiently strong to pair up the spin and hence the spin-paired configuration is not attained. Moreover, as the size and mass of the transition metal atom increases, the tendency to form spin paired compounds increases, since Δ_0 increases. Therefore, the Ni^{2+} ground state spin is singlet with no unpaired electrons.

Table 6
Calculated binding energies (eV) of transition metal ion doped CdS/ZnS core/shell QDs.

Spin	Mn^{2+}	Fe^{2+}	Co^{2+}	Ni^{2+}	Cu^{2+}	Zn^{2+}	Hg^{2+}
Singlet	–	–80.36	–	–81.64	–	–78.15	–76.78
Doublet	–77.43	–	–81.89	–	–78.72	–	–
Triplet	–	–79.95	–	–81.61	–	–	–
Quartet	–77.47	–	–82.80	–	–	–	–
Quintet	–	–80.35	–	–	–	–	–
Sextet	–78.79	–	–	–	–	–	–

One important fact that can be noted from Table 6 is that the binding energies for different spin multiplicities of the same ion do not show much variation in most of the cases.

5.2. Structural properties

Fig. S3 shows the geometry optimized structures obtained on doping a CdS/ZnS core/shell QD at the atom-centered site with different transition metal ions for the most stable spin state for each ion. One notices that there is no change in the coordination at the doped site for all the transition metal ions considered. Hence, the comparison of doped and undoped structures indicates that doping does not result in a reorganization of the bonds. The structure looks identical in shape to the undoped one (Fig. S1), since no dissociation or new bond formation occurs.

The bond lengths around the center, however, do vary, depending upon the type of dopant chosen. Table 7 gives the optimized bond lengths around the doped site, as well as the other bonds. There is a gradual decrease in the bond lengths from Mn^{2+} to Cu^{2+} doping, commensurate with the slight decrease in atomic sizes.

Generally, it is observed that if a low coordinated site of the metal atom is chosen for doping, then the alterations in the covalency properties may be characterized by an effect analogous to the nephelauxetic effect, wherein the d electron cloud expands into the region of the ligand field, thereby increasing the covalency to some extent. Then the dissociation and formation of the metal-metal bonds may be attributed to the delocalization of the d electrons within the moiety of the QD, which increases the covalent character of the metals involved in a particular nanostructure. In this case, since the site chosen for doping is the most stable atom-centered position with maximum coordination number, i.e. four, this may be summed up as the reason for no significant structural transformation of doping.

However, there are marked changes in the electronic properties of these QDs, which may be of great interest to scientists for further research. Table 8 lists the Mayer bond orders between the doped atom and its neighbors, and between the other undoped sites and their neighbors, in the CdS/ZnS core/shell QD.

The values clearly indicate that there is strengthening of the core in case of doping with Mn^{2+} , Fe^{2+} , Co^{2+} and Ni^{2+} , as the M – S bond orders in these cases are higher than the Cd–S bond they replace. For the remaining three ions, Cu^{2+} , Zn^{2+} and Hg^{2+} , the bond order decreases,

Table 7
Bond length data for undoped and doped CdS/ZnS core/shell QDs.

Central atom	Bonding pattern					
	(a)		(b)		(c)	
	A-type	B-type	A-type	B-type	A-type	Atom-centered
Cd	2.216	2.164	2.584	2.775	2.671	2.641
Mn	2.219	2.169	2.581	2.788	2.691	2.481
Fe	2.229	2.166	2.582	2.788	2.689	2.413
Co	2.218	2.168	2.589	2.789	2.688	2.394
Ni	2.219	2.164	2.579	2.792	2.686	2.360
Cu	2.214	2.164	2.580	2.793	2.675	2.395
Zn	2.214	2.165	2.579	2.790	2.681	2.438
Hg	2.220	2.169	2.582	2.795	2.683	2.670

Table 8

Calculated Mayer bond orders for atom-pairs in undoped and transition metal ion doped CdS/ZnS core/shell QDs.

Central atom	Mayer Bond Orders					
	(a)		(b)		(c)	
	A-type	B-type	A-type	B-type	A-type	Atom-centered
Cd	0.936	0.949	0.647	0.449	0.526	0.535
Mn	0.937	0.905	0.668	0.455	0.557	0.619
Fe	0.940	0.911	0.667	0.452	0.551	0.661
Co	0.941	0.932	0.657	0.445	0.539	0.675
Ni	0.944	0.941	0.654	0.437	0.529	0.623
Cu	0.943	0.941	0.651	0.435	0.538	0.508
Zn	0.547	0.508	0.466	0.324	0.380	0.314
Hg	0.935	0.932	0.655	0.446	0.529	0.529

and is least for Zn²⁺, which is also the core shell material. Because of its complete *d* shell, Zn has a tendency to form ionic bonds. The bond orders corresponding to the other bonds are also least for the zinc doped case.

5.3. Magnetic properties

The free valence index indicates whether free electrons are available for bonding on a particular atom. It is zero for closed-shell systems. For open-shell systems, it is a measure of reactivity. Most of the transition metals exhibit magnetism due to the presence of unpaired electrons in their valence *d* orbitals. For transition metals, the magnetic moment is calculated using the relation $\mu = \sqrt{n(n+2)}$ BM, where *n* is the number of unpaired electrons and the unit is the Bohr Magnetron. Zn²⁺ and Hg²⁺, both being closed shell systems, induce no magnetic property, as they have no unpaired electrons.

Table 9 gives the Mayer free valence and the magnetic moments for various doped CdS/ZnS core/shell QDs. All the values for the Mayer free valence as well as the magnetic moments are underestimated. This may be attributed to the core/shell interactions, as a result of which there is a significant deviation from the expected values. Another reason for the lowered values may be the *sp-d* hybridization between the localized 3*d* electrons of the transition metal atoms placed at the atom center and the delocalized *s* and *p* valence states of the CdS core of the QDs. The deviations of the magnetic moment values calculated using the Mayer free valence and the values expected from the number of unpaired electrons vary from 15% for Mn²⁺ to 30% for Fe²⁺ to about 83% for Cu²⁺. This observation definitely confirms that the valence electrons of the dopant interact very strongly with the entire QD moiety, as a result of which magnetic moments lower than the expected values are observed for them.

5.4. Electronic properties

The undoped CdS/ZnS core/shell QD, which is a closed shell system (958 electrons), has its Fermi level at -0.636 eV. Metal doping raises the energy of the Fermi level in all the cases, except for Zn²⁺ and Hg²⁺, where it becomes more negative. The Fermi energy for even electronic doped atomic systems, i.e. for the CdS/ZnS QDs doped with Fe²⁺, Ni²⁺,

Table 9

Calculated Mayer free valence and magnetic moments (BM) for transition metal ion doped CdS/ZnS core/shell QDs.

Transition metal ion	Calculated		Expected	
	Mayer free valence	Magnetic moment	No. of unpaired electrons	Magnetic moment
Mn ²⁺	4.12	5.02	5	5.92
Fe ²⁺	2.59	3.45	4	4.90
Co ²⁺	2.01	2.83	3	3.87
Ni ²⁺	0.63	1.29	2	2.82
Cu ²⁺	0.04	0.30	1	1.73

Zn²⁺ and Hg²⁺ are comparable, i.e. the Fermi energy lies around ~ -0.64 eV.

The CdS/ZnS QDs doped with Mn²⁺, Co²⁺, and Cu²⁺ are odd electron systems, possessing 961, 963 and 965 electrons, respectively. For these, the Fermi energy lies around -0.46 eV (spin up) and ~ -0.63 eV (spin down). This observation clearly shows the noteworthy role of valence electrons of the dopant in manipulating the Fermi energy values. The data for the Fermi energy with increasing number of electrons in the *d* orbitals is given in Table 10.

The highest Fermi energy is for Ni²⁺, whose outermost electronic configuration is commonly written as 3*d*⁸ formed after two electrons are lost from the 3*d*⁸4*s*² neutral state of Ni. The Fermi energies observed in the present case do not follow the expected trend, as there should be an increase in the Fermi energy with increase in the number of electrons in the same valence shell as one moves from Mn²⁺ to Zn²⁺, but on the contrary the trend observed is random.

As mentioned in the previous section, the formation of a shell outside the QD leads to a significant charge redistribution which is also the case here. The charge redistribution is just not due to the surface reconstruction, but also due to the change caused inside the core of the CdS/ZnS core/shell QD by doping it exactly at its central atom position. A detailed analysis of the Hirshfeld charges is discussed here owing to the significant changes in the electronic properties that the dopant causes by interacting with the two layered QDs.

The charges on the various atoms in the doped CdS/ZnS core/shell QDs display the featured distribution of electronic density within and outside the core of the cluster. Table 11 gives the Hirshfeld charge on the transition metal ions in comparison to the Cd²⁺ ion that they replace. We can infer that there occurs a transfer of charge from the sulfide ions of the core to the transition metal ions placed at the atom-centered position, thereby decreasing the positive charge in the order Hg²⁺ > Zn²⁺ > Cu²⁺ > Mn²⁺ > Ni²⁺ > Co²⁺ > Fe²⁺, i.e. the charge transfer is largest for Fe²⁺ and least for Hg²⁺, but is still larger than the observed charge transfer in the undoped system.

Doping therefore causes charge transfer from other parts of the system to the doped atom, particularly for the transition metal ions from Mn²⁺ to Cu²⁺, and this is reflected in a decrease of the negative charge on the sulfide ions in the core (Table 11). However, the total positive charge on the cations of the core is also smaller than that for the undoped system for all the doped cases, indicating that the cations of the core too are involved in the charge transfer to the doped position.

Similarly, we compare the overall charges on the cations and anions of the ZnS shell and try to probe the effect of doping the core on it. We see that there is very little charge redistribution that occurs in the shell. The largest increase in the cationic charge of about 0.6% on the shell is observed for doping with Fe²⁺ (in comparison to the normal overall charge on the zinc atoms of the shell of CdS/ZnS core/shell QDs), and there is no regular trend observed as the atomic number of the transition metal atom increases.

A better understanding can be obtained if we sum up and calculate the overall charge on the core and shell for each of the doped core/shell QDs considered (Table 11). The positive charge of +6 is distributed in the core and shell approximately in the ratio 2.5:3.5, and there is very

Table 10

Fermi energy (eV) data for transition metal ion doped CdS/ZnS core/shell QDs.

Transition metal	Fermi energy	
	Spin up	Spin down
Mn ²⁺	-0.464	-0.632
Fe ²⁺	-0.634	-0.634
Co ²⁺	-0.460	-0.632
Ni ²⁺	-0.642	-0.642
Cu ²⁺	-0.459	-0.633
Zn ²⁺	-0.638	-0.638
Hg ²⁺	-0.639	-0.639

Table 11
Hirshfeld charges on the cations and anions of undoped and doped CdS/ZnS core/shell QDs.

Central metal	Hirshfeld charge	Core			Shell		
		Cations	Anions	Total	Cations	Anions	Total
Cd	0.277	3.865	-1.362	2.503	6.633	-3.234	3.399
Mn	0.088	3.611	-1.206	2.405	6.649	-3.154	3.495
Fe	0.022	3.531	-1.150	2.381	6.674	-3.154	3.520
Co	0.023	3.557	-1.140	2.417	6.644	-3.158	3.486
Ni	0.030	3.514	-1.109	2.405	6.656	-3.161	3.495
Cu	0.137	3.670	-1.263	2.407	6.640	-3.145	3.495
Zn	0.201	3.746	-1.303	2.443	6.625	-3.167	3.458
Hg	0.212	3.800	-1.320	2.480	6.646	-3.226	3.420

little variation on doping with the various metal ions, although there is a slight decrease in the positive charge in the core and a corresponding increase in the positive charge in the shell. In the core, the decrease is mainly due to a decrease in the negative charge on the sulfides, which donate electron density to the doped ion.

The charge redistribution may be attributed to the shift in the energies of the valence and conduction bands of the core/shell QDs in each of the cases (Fig. 4). A large variation in the band gap is observed with doping, significant among these being the cases of doping with Fe²⁺ and Ni²⁺.

The conducting properties are tremendously enhanced on doping the CdS/ZnS core/shell QDs, the most conducting QD being the one doped with Fe²⁺ and the least conducting being the one doped with Zn²⁺ (Table 12). There is no fixed trend followed for the values of the band gap on going from manganese to zinc, as shown in Fig. 4. In fact, the values fluctuate as we move from one doped case to the other with every unit increase in the atomic number of the dopant. On moving down the group from Zn²⁺ to Hg²⁺, the band gap is again reduced slightly (by about 8%).

The variation of the band gap can be further understood by looking at the contour plots exhibiting orbital participation for the valence and the conduction band in each of the cases (Fig. S4). The contour plots clearly justify the values obtained for the band gap in each of the cases. The Mn²⁺ doped CdS/ZnS QD shows participation of the *p* orbitals of some core as well as shell sulfide atoms. There is a small participation also of the *s* orbitals on the shell, but the latter majorly contributes to the conduction band/LUMO. Therefore, the band gap is lowered, but not significantly, in comparison to the other transition metal ion doped QDs.

The most conducting is the iron doped CdS/ZnS QD (Fig. S4). This is attributed to the participation of the *d* orbitals of Fe, which actively contribute toward both the valence as well as the conduction band. Besides, the *p* orbitals of the core as well as the shell sulfide atoms are also involved in the HOMO, but the LUMO comprises only the *d* orbitals

Table 12
Calculated electronic properties (eV) of transition metal ion doped CdS/ZnS core/shell QDs.

Central atom	HOMO	LUMO	Band Gap
Cd	-18.58	-15.89	2.69
Mn	-18.07	-16.02	2.05
Fe	-16.92	-15.99	0.93
Co	-18.14	-16.22	1.92
Ni	-18.06	-17.06	0.99
Cu	-18.03	-15.89	2.14
Zn	-18.63	-15.91	2.72
Hg	-18.52	-16.03	2.49

of Fe, which makes the core highly reactive and readily available for accepting electrons from any interacting molecule.

The cobalt doped CdS/ZnS core/shell structure also exhibits a conducting band gap. The plots are similar to the previous case, as here also the *d* orbitals of cobalt actively participate both in the HOMO and LUMO, but are wider than in the previous case. The reason may be the additional involvement of the *p* orbitals of mainly the core and a couple of the shell sulfide atoms in the HOMO, and only those of the core participate in the LUMO as well.

Further, another doped core/shell QD with enhanced conductivity is the one doped with Ni²⁺ with greater participation coming from the shell *p* orbitals of the sulfide atoms in the HOMO. However, greater participation of the *p* orbitals of the core sulfide atoms, along with the *d* orbital of nickel is still noted. The LUMO involves participation from a handful of the inner core *p* orbitals of the sulfide atoms, as well the *d* orbital of nickel. Due to common participation coming from both the contours, the nickel doped QDs are found to be the second best conducting amongst all the doped cases considered (Fig. S2).

As we move from nickel doped to copper doped CdS/ZnS core/shell QDs, there is significant widening of the band gap (by about 116% in comparison to Ni²⁺), owing to no commonality in the HOMO and LUMO plots, as the *d*_{z² orbitals of copper, along with the *p* orbital of the core sulfide atoms, contribute majorly toward the HOMO, and the *s* orbitals of the shell zinc atoms as well as shell sulfide atoms mark the formation of the LUMO, making the shell highly reactive and electron deficient. Following similar lines as the previous case, we may account for the widest band gap amongst all the cases investigated in the present section for zinc doped CdS/ZnS QDs. The HOMO involves participation of the inner *p* orbitals of the core sulfide atoms and the *d* orbital of the atom-centered zinc atom used for doping the central atom. The LUMO, however, involves participation of the *s* orbitals of only the shell sulfide atoms.}

The mercury doped CdS/ZnS core/shell QD falls in a different category, as the doped atom belongs to a different period in the periodic table. Here the *d* orbital of mercury, along with the *p* orbitals of the inner core, as well as the shell sulfide atoms, form the HOMO, but the LUMO is marked by the participation of the *s* orbitals of mercury along with the *s* orbital of the sulfide atoms throughout the core/shell of the CdS/ZnS QDs.

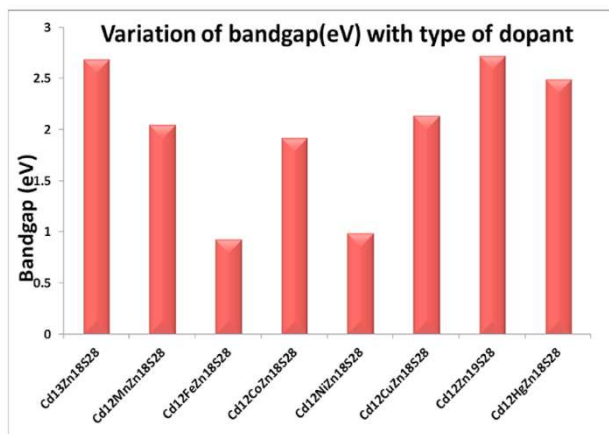


Fig. 4. Variation of the band gap of CdS/ZnS core/shell QD on doping with various transition metal ions.

Fig. 5 shows the variation of the HOMO and LUMO energies of the transition metal ion doped CdS/ZnS core/shell QDs, which clearly indicates that the greater stabilization of the HOMO in case of Zn^{2+} doping accounts for the widening of the band gap.

These contour plots help in the justification of the band gap values, revealing the reason for the increase or decrease in the energy levels corresponding to either the HOMO or LUMO in each case. We now clearly understand the reasons for the most conducting and the least conducting core/shell QDs from amongst the cases considered.

The density of states (DOS) is basically the number of different states at a particular energy level that the electrons are allowed to occupy, i.e. the number of electron states per unit volume per unit energy. The partial density of states (PDOS) tells us the relative contribution of a particular atom/orbital to the total density of states and is essential for determining the carrier concentrations and energy distributions of carriers within quantum dots. Various bulk properties like specific heat, paramagnetic susceptibility, conductivity, etc. depend on this function [88].

In systems with smaller HOMO-LUMO energy gaps and hence weaker electronic confinement, the electron is more delocalized and the lowest obtainable transition energy is lowered inside the QDs. It is reported that doping of a semiconductor increases the concentration of charge carriers and lifts the Fermi level, which in turn affects the conductivity [89]. As in the present case, it is Ni^{2+} with the lower HOMO-LUMO gap, which has the largest shift in the Fermi level. With a larger HOMO-LUMO energy gap, the higher energy barrier strengthens the quantum confinement and results in more discrete transition energies.

Fig. 6 gives the partial density of states (PDOS) plot for the undoped CdS/ZnS core/shell QD. The *s* orbitals span mainly the regions -4.36 Ha (-119 eV) to -4.81 Ha (-131 eV) and -0.31 Ha (-8.43 eV) to 0.22 Ha (6.00 eV), *p* orbitals span mainly between -5.40 Ha (-147 eV) and -5.55 Ha (-151 eV), -2.90 Ha (-78.9 eV) and -3.10 Ha (-84.4 eV) and -0.50 Ha (-13.6 eV) to 0.20 Ha (5.44 eV), while the *d* orbitals show only one peak between -0.50 Ha (-13.61 eV) and 0.20 Ha (5.43 eV).

The PDOS plots of doped CdS/ZnS core/shell QDs with transition metal ions (Fig. S5) are very much similar to those of the pure CdS/ZnS core/shell QDs (Fig. 6), except in the case of Fe^{2+} , Co^{2+} and Ni^{2+} , where one extra low energy band is also observed at around -7.5 Ha (-204 eV).

6. Conclusions

In this paper, we have thoroughly investigated the modifications in properties brought about by coating a II-VI QD with another material of the same family. Thus, we have considered shells in which the cation is varied, or the anion is varied, and, in each case, significant variations in the bonding characteristics are brought about, depending on the shell material. Interchanging the material of the core with that of the shell

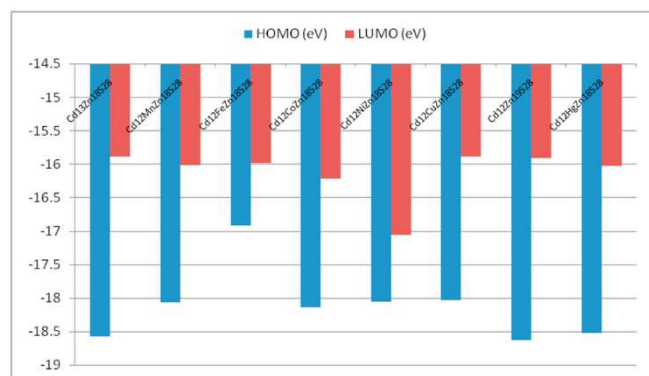


Fig. 5. Variation of HOMO and LUMO energy levels of CdS/ZnS core/shell QD on doping with the transition metal ions.

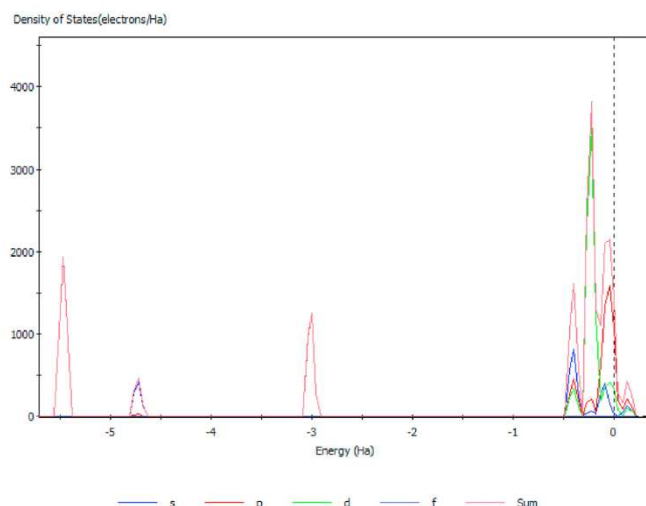


Fig. 6. Partial density of states (PDOS) plot for the undoped CdS/ZnS core/shell QDs.

also brings about profound changes in the properties, significant among them being the band gap and electrophilicity. Exploration of the HOMOs and LUMOs has indicated a mixing of orbitals of the metal and the chalcogenide as the possible reason for modification of the band gap. In cases of interchange of the core and shell materials, it is found that shells of the wider band gap material provide greater stability to the resulting structures. Most importantly, such variations in electronic properties resulting from variation in the core/shell material imply that it is possible to fine tune the desired properties by appropriate surface modification.

We have also investigated the structural, electronic and magnetic properties of doped CdS/ZnS core/shell QDs. Doping with the seven transition metal ions considered causes enhancement in the properties in some or the other way. The binding energies, as expected, vary with the kind of dopant as well as the spin multiplicity. The reasons for one spin state being more stable than the other at a particular site of the QD structure are clearly understood.

An interesting property that plays a crucial role in the present work is the introduction of magnetism in core/shell QDs on introduction of transition metal impurities, which introduce unpaired electrons within the CdS/ZnS QDs. However, the calculated values for the magnetic moments are smaller than the expected values based on the number of unpaired electrons. An increase in the deviation is observed as the dopant is changed from Mn^{2+} to Fe^{2+} to Co^{2+} to Ni^{2+} to Cu^{2+} .

Doping affects the Fermi energy levels. Hirshfeld charge analysis shows that the doped ion accepts negative charge from the sulfide ions in the core, with the minimum charge transfer being seen in the case of Hg^{2+} ions. As we move from Mn^{2+} to Hg^{2+} , the trend followed for the Hirshfeld charges indicates that the overall charge on the core is lower and that on the shell is higher for all the doped cases compared with the undoped CdS/ZnS core/shell QD.

The band gap values reveal that the Fe^{2+} doped CdS/ZnS core/shell structures could be promising candidates for electronic applications due to their lowest band gap values. The properties considered in the previous sections throw a guiding light for carrying out effective doping of one of the most widely studied core/shell QDs, CdS/ZnS, with a transition metal ion ranging from divalent manganese to zinc. Changing the dopant causes drastic changes in the electronic properties of the CdS/ZnS QDs.

It is hoped that the conclusions from this work will help design QDs of the desired properties for various applications and our studies clearly show that transition metal ions can be used as means for tuning the magnetoelectronic properties of the host semiconductor for future applications in nanotechnology.

Declaration of competing interest

The authors declare that they have no known competing financial interests or personal relationships that could have appeared to influence the work reported in this paper.

Acknowledgements

We thank the Council of Scientific and Industrial Research (CSIR), New Delhi, India, for providing Senior Research Fellowships to PM, RT and JS. Also, monetary support from “Delhi University’s system to build up Research by providing resources to Faculty” is gratefully acknowledged.

Appendix A. Supplementary data

Supplementary data to this article can be found online at <https://doi.org/10.1016/j.jmngm.2021.108099>.

References

- [1] P. Reiss, M. Protière, L. Li, *Small* 5 (2009) 154–168.
- [2] M. Grabolle, J. Ziegler, A. Merkulov, T. Nann, U. Resch-Genger, *Ann. N. Y. Acad. Sci.* 1130 (2008) 235–241.
- [3] S.A. Ivanov, A. Piryatinski, J. Nanda, S. Tretiak, K.R. Zavadil, W.O. Wallace, D. Werder, V.I. Klimov, *J. Am. Chem. Soc.* 129 (2007) 11708–11719.
- [4] B.O. Dabbousi, J. Rodriguez-Viejo, F.V. Mikulec, J.R. Heine, H. Mattoussi, R. Ober, K.F. Jensen, M.G. Bawendi, *J. Phys. Chem.* B101 (1997) 9463–9475.
- [5] M.A. Hines, P. Guyot-Sionnest, *J. Phys. Chem.* 100 (1996) 468–471.
- [6] M. Danek, K.F. Jensen, C.B. Murray, M.G. Bawendi, *Chem. Mater.* 8 (1996) 173–180.
- [7] A.R. Kortan, R. Hull, R.L. Opila, M.G. Bawendi, M.L. Steigerwald, P.J. Carroll, L. E. Brus, *J. Am. Chem. Soc.* 112 (1990) 1327–1332.
- [8] K.A. Littau, P.J. Szajowski, A.J. Muller, A.R. Kortan, L.E. Brus, *J. Phys. Chem.* 97 (1993) 1224–1230.
- [9] A. Mews, A. Eychmüller, M. Giersig, D. Schooss, H. Weller, *J. Phys. Chem.* 98 (1994) 934–941.
- [10] Y. Tian, T. Newton, N.A. Kotov, D.M. Guldi, J. Fendler, *J. Chem. Phys.* 100 (1996) 8927–8939.
- [11] W.L. Wilson, P.F. Szajowski, L.E. Brus, *Science* 262 (1993) 1242–1244.
- [12] H.-C. Youn, S. Baral, J.H. Fendler, *J. Phys. Chem.* 92 (1988) 6320–6327.
- [13] Z. Hu, L. Liu, H. Qin, J. Zhou, X. Peng, *J. Am. Chem. Soc.* 142 (2020) 4254–4264.
- [14] S. Mathew, A.D. Saran, B.S. Bhardwaj, S.A. Joseph, P. Radhakrishnan, V.P. N. Nampoori, C.P.G. Vallabhan, J.R. Bellare, *J. Appl. Phys.* 111 (2012), 074312.
- [15] I. Rosina, B. Martín-García, D. Spirito, Z. Dang, G. Gariano, S. Marras, Mirko Prato, R. Krahnle, L.D. Trizio, L. Manna, *Chem. Mater.* 32 (2020) 2978–2985.
- [16] V. Kocovski, J. Ruz, O. Eriksson, *Sci. Rep.* 5 (2015) 10865.
- [17] S.V. Kilina, P.K. Tamukong, D.S. Kilin, *Acc. Chem. Res.* 49 (2016) 2127–2135.
- [18] D.U. Lee, D.H. Kim, D.H. Choi, S.W. Kim, H.S. Lee, K.-H. Yoo, T.W. Kim, *J. Opt. Soc. Am.* 24 (2016) A350.
- [19] J.B. Sambur, B.A. Parkinson, *J. Am. Chem. Soc.* 132 (2010) 2130.
- [20] V. Wood, J.E. Halpert, M.J. Panzer, M.G. Bawendi, B. Vladimir, *Nano Lett.* 9 (2009).
- [21] H. Yang, P.H. Holloway, B.B. Ratna, *J. Appl. Phys.* 93 (2003) 586–592.
- [22] R. Thakar, Y. Chen, P.T. Snee, *Nano Lett.* 7 (2007) 3429–3432.
- [23] J. Zhuang, X. Zhang, G. Wang, D. Li, W. Yang, T. Li, *J. Mater. Chem.* 13 (2003) 1853–1857.
- [24] R. Beaulac, P.I. Archer, S.T. Ochsenbein, D.R. Gamelin, *Adv. Funct. Mater.* 18 (2008) 3873–3891.
- [25] P. Verma, A.C. Pandey, *J. Biomaterials Nanobiotechnol.* 2 (2011) 409–413.
- [26] J. McBride, J. Treadway, L.C. Feldman, S.J. Pennycook, S.J. Rosenthal, *Nano Lett.* 6 (2006) 1496–1501.
- [27] A. Ishizumi, E. Jojima, A. Yamamoto, Y. Kanemitsu, *J. Phys. Soc. Jpn.* 77 (2008), 053705. /1-053705/4.
- [28] J.D. Bryan, D.R. Gamelin, *Prog. Inorg. Chem.* 54 (2005) 47–126.
- [29] S.C. Erwin, L. Zu, M.I. Haftel, A.L. Efros, T.A. Kennedy, D.J. Norris, *Nature* 436 (2005) 91–94.
- [30] K.M. Hanif, R.W. Meulenberg, G.F. Strouse, *J. Am. Chem. Soc.* 124 (2002) 11495–11502.
- [31] F.V. Mikulec, M.G. Bawendi, *J. Am. Chem. Soc.* 122 (2000) 12142–12150.
- [32] D.J. Norris, A.L. Efros, S.C. Erwin, *Science* 319 (2008) 1776–1779.
- [33] M. Shim, C. Wang, D.J. Norris, P. Guyot-Sionnest, *MRS Bull.* (2001) 1005–1008.
- [34] C.A. Stowell, R.J. Wiaczek, A.E. Saunders, B.A. Korgel, *Nano Lett.* 3 (2003) 1441–1447.
- [35] D.V. Talapin, C.B. Murray, *Science* 310 (2005) 86–89.
- [36] V.I. Klimov, S.A. Ivanov, J. Nanda, M. Achermann, I. Bezel, J.A. McGuire, A. Piryatinski, *Nature* 447 (2007) 441–446.
- [37] G. Blasse, B.C. Grabmaier, *Luminescent Materials*, Springer-Verlag Telos, Berlin, Germany, 1994.
- [38] Y.A. Ono, *Annu. Rev. Mater. Sci.* 27 (1997) 283–303.
- [39] C. Ronda, *Luminescence: from Theory to Applications*, Wiley-VCH, Verlag GmbH & Co. KGaA, Weinheim, Germany, 2008.
- [40] Y. Yang, O. Chen, A. Angerhofer, Y.C. Cao, *J. Am. Chem. Soc.* 130 (2008) 15650–15661.
- [41] Y. Yang, O. Chen, A. Angerhofer, Y.C. Cao, *Chem. Eur J.* 15 (2009) 3186–3197.
- [42] D.A. Bussian, S.A. Crooker, M. Yin, M. Brynda, A.L. Efros, V.I. Klimov, *Nature* 8 (2009) 35–40.
- [43] H. Yang, P.H. Holloway, *Appl. Phys. Lett.* 82 (2003) 1965–1967.
- [44] A. Ishizumi, Y. Kanemitsu, *Adv. Mater.* 18 (2006) 1083–1085.
- [45] B.-H. Zang, L. Qi, F.-Y. Wu, *Microchim. Acta* 170 (2010) 147–153.
- [46] R. Zeng, T. Zhang, G. Dai, B. Zou, *J. Phys. Chem. C* 115 (2011) 3005–3010.
- [47] J. Zheng, X. Yuan, M. Ikezawa, P. Jing, X. Liu, Z. Zheng, X. Kong, J. Zhao, Y. Masumoto, *J. Phys. Chem. C* 113 (2009) 16969–16974.
- [48] D. Zhu, X. Jiang, C. Zhao, X. Sun, J. Zhang, J.-J. Zhu, *Chem. Commun.* 46 (2010) 5226–5228.
- [49] X. Yuan, J. Zheng, R. Zeng, P. Jing, W. Ji, J. Zhao, W. Yang, H. Li, *Nanoscale* 6 (2014) 300–307.
- [50] T.-D. Bui, Q.-L. Nguyen, T.-B. Luong, V.T. Le, V.-D. Doan, *Advances in Materials Science and Engineering Hindawi Advances in Materials Science and Engineering* 2020, Article ID 9718706, 10 pages.
- [51] L. Li, Y. Gu, R. Xie, J. Zhu, *Appl. Mech. Mater.* 148–149 (2012) 900–903.
- [52] S.B. Singh, M.V. Limaye, S.K. Date, S. Gokhale, S.K. Kulkarni, *Phys. Rev. B* 80 (2009) 235421. /1-235421/8.
- [53] P. Lommens, K. Lambert, F. Loncke, D.D. Muynck, T. Balkan, F. Vanhaecke, H. Vrielinck, F. Callens, Z. Hens, *ChemPhysChem* 9 (2008) 484–491.
- [54] J.-U. Kim, Y.K. Kim, H. Yang, *J. Colloid Interface Sci.* 341 (2010) 59–63.
- [55] C. Corrado, M. Hawker, G. Livingston, S. Medling, F. Bridges, J.Z. Zhang, *Nanoscale* 2 (2010) 1213–1221.
- [56] R. Viswanatha, S. Brovelli, A. Pandey, S.A. Crooker, V.I. Klimov, *Nano Lett.* 11 (2011) 4753–4758.
- [57] Z. Li, W. Yao, L. Kong, Y. Zhao, L. Li, *J. Am. Chem. Soc.* 137 (39) (2015) 12430–12433.
- [58] V. Radovanovic, D.R. Gamelin, *J. Am. Chem. Soc.* 123 (2001) 12207–12214.
- [59] H. Yang, P.H. Holloway, G. Cunningham, K.S. Schanze, *J. Chem. Phys.* 121 (2004) 10233–10240.
- [60] Y. Yang, O. Chen, A. Angerhofer, Y.C. Cao, *J. Am. Chem. Soc.* 128 (2006) 12428–12429.
- [61] C.C. Berry, A.S.G. Curtis, *J. Phys. D Appl. Phys.* 36 (2003) R198–R206.
- [62] V. Skumryev, S. Stoyanov, Y. Zhang, G. Hadjipanayis, D. Givord, J. Nogués, *Nature* 423 (2003) 850–853.
- [63] E.E. Carpenter, S. Calvin, R.M. Stroud, V.G. Harris, *Chem. Mater.* 15 (2003) 3245–3246.
- [64] H. Zeng, J. Li, J.P. Liu, Z.L. Wang, S. Sun, *Nature* 420 (2002) 395–398.
- [65] H. Zhao, X. Li, M. Cai, C. Liu, Y. You, R. Wang, A.I. Channa, F. Lin, D. Huo, G. Xu, X. Tong, Z.M. Wang, *Advanced energy materials*. <https://doi.org/10.1002/aenm.202101230>, 2021.
- [66] M. Kaur, A. Sharma, M. Olutas, O. Erdem, A. Kumar, M. Sharma, H.V. Demir, *Nanoscale Res. Lett.* 13 (2018) 182.
- [67] P. Hohenberg, W. Kohn, *Phys. Rev. B* 136 (1964) B864.
- [68] B. Delley, *J. Chem. Phys.* 92 (1990) 508.
- [69] B. Delley, *J. Chem. Phys.* 94 (1991) 7245.
- [70] B. Delley, *J. Comput. Chem.* 17 (1996) 1152.
- [71] B. Delley, *J. Chem. Phys.* 113 (2000) 7756.
- [72] B. Delley, *Phys. Rev. B* 66 (2002) 155125. /1.
- [73] N. Matsuzawa, J. Seto, D.A. Dixon, *J. Phys. Chem. A* 101 (1997) 9391.
- [74] P. Batra, R. Gaba, U. Issar, R. Kalkar, *J. Theor. Chem.* (2013) 14, 2013.
- [75] J.P. Perdew, K. Burke, M. Ernzerhof, *Phys. Rev. Lett.* 77 (1996) 3865.
- [76] F.L. Hirshfeld, *Isr. J. Chem.* 16 (1977) 198.
- [77] I. Mayer, *Int. J. Quant. Chem.* 29 (1986) 477.
- [78] V. Chandrasekaran, M. Tessier, D. Dupont, P. Geiregat, Z. Hens, E. Brainin, et al., *Nano Lett.* 17 (2017) 6104.
- [79] A. Brodu, M.V. Ballottin, J. Buhot, E.J. van Harten, D. Dupont, A. La Porta, et al., *ACS Photonics* 5 (2018) 3353–3362.
- [80] N. Shambetova, Y. Chen, H. Xu, L. Li, J. Solandt, Y. Zhou, et al., *J. Phys. Chem. C* 120 (2016) 3519–3529.
- [81] C. Tshangana, T. Nyokong, *Spectrochim. Acta Part A Mol Biomol Spectrosc* 151 (2015) 397–404.
- [82] K. Gundogdu, K.C. Hall, T.F. Boggess, Oleg Shchekin, D.G. Deppe, *Appl. Phys. Lett.* 84 (2003) 2793.
- [83] Q. Liu, H. Li, Q. Xia, Y. Liu, K. Xiao, *Int. J. Nanomed.* 10 (2015) 7073–7088.
- [84] I.P. Moura, P.E.C. Filho, M.B. Seabra, G. Pereira, G.A.L. Pereira, A. Fontes, B. S. Santos, *J. Lumin.* 201 (2018) 284–289.
- [85] B.G. Streetman, S. Banerjee, in: *Solid State Electronic Devices*, fifth ed., Prentice Hall, New Jersey, 2000, ISBN 0-13-025538-6, p. 524.
- [86] O. Madelung, *Semiconductors - Basic Data*, 2nd rev, Springer-Verlag, 1996, ISBN 3-540-60883-4.
- [87] B.O. Dabbousi, J. Rodriguez-Viejo, F.V. Mikulec, J.R. Heine, H. Mattoussi, R. Ober, K.F. Jensen, M.G. Bawendi, *J. Phys. Chem. B* 101 (1997) 9463–9475.
- [88] M. Sachs, *Solid State Theory*, pp1vols. 59–160, McGraw-Hill Book Company, New York, 1963, pp. 238–242.
- [89] V.I. Arkhipov, P. Heremans, E.V. Emelianova, H. Bäessler, *Physical Review B* 71: 045214/1-7, 2005.



Size-dependent structural and electronic properties of stoichiometric II–VI quantum dots and gas sensing ability of CdSe quantum dots: a DFT study

Jyoti Singh · Rakhi Thareja · Pragati Malik · Rita Kakkar

Received: 13 September 2021 / Accepted: 10 January 2022
© The Author(s), under exclusive licence to Springer Nature B.V. 2022

Abstract The structural, electronic, and quantum confinement effects observed in II–VI quantum dots have been described using density functional theory. Various properties like binding energy, Fermi energy, charge distribution, and band gap of various clusters have been determined as a function of cluster size in order to find out the most stable of all the clusters considered. The binding energies are found to be a function of the cluster size but converge to a maximum. Cadmium is observed to possess a larger tendency to form clusters with higher coordination numbers compared to zinc and mercury. In mercury sulfide (HgS_n), the clusters with $n=6$ and 13 get dissociated into two graphene-like parallel layers. The adsorptions of single gas molecules on the $(\text{CdSe})_{13}$ quantum dots are exothermic, indicating that most of the gas molecules adsorb spontaneously on the CdSe quantum dots. Among the various gases, O_2 and NO_2 are the gas molecules that get most strongly chemisorbed. The CdSe quantum dot acts as an electron donor when it interacts with the oxidizing gases, O_2 , CO , NO_2 , and SO_2 gases. The vibrational analysis of the combined systems indicates that the intensities

of the peaks due to CdSe reduce after adsorption. Extra peaks appear at higher frequencies due to the adsorbed gas molecules. The present work shows insights into the gas sensing properties of the quantum dots under study.

Keywords Quantum dots · Stoichiometric · Band gap · Binding energy · DFT calculations · Structural properties · Electronic properties · HOMO · LUMO

Abbreviations

QDs	Quantum dots
NCs	Nanocrystals
HOMO	Highest occupied molecular orbital
LUMO	Lowest unoccupied molecular orbital

Introduction

The developments in semiconductor technology over the past few years have proved to be a new route to the world of nanotechnology and electronics. The importance of semiconductors arises from the assembly of the atoms that build up the semiconductor crystals. A semiconductor has its electrical properties between those of a conductor and an insulator. An important feature of semiconductors is the energy gap between the valence band and the conduction band (Patterson and Bailey 2007).

Bulk semiconductor materials have continuous valence and conduction energy states, and some

Supplementary Information The online version contains supplementary material available at <https://doi.org/10.1007/s11051-022-05406-6>.

J. Singh · R. Thareja · P. Malik · R. Kakkar (✉)
Computational Chemistry Laboratory, Department
of Chemistry, University of Delhi, Delhi 110007, India
e-mail: rkakkar@chemistry.du.ac.in

minimum amount of energy (E_g) is required to promote an electron from the valence band to the conduction band. When energy higher than E_g is provided, the electron leaves a hole in the valence band. A bound state of an electron–hole pair in their lowest energy state is termed an exciton, and the distance between them is the exciton Bohr radius (r_B) (Smith and Nie 2010). When the radius of the nanocrystal (r) becomes smaller or equal to the exciton Bohr radius, i.e., $r \leq r_B$, the motion of the electrons and holes is spatially confined to the dimension of the quantum dot (QD). In this regime, depending on the size of the nanocrystal (NC), the QD exhibits size-dependent absorption and emission with discrete electronic transitions (Yoffe 1993, 2001). This effect is called the quantum confinement effect. The optical properties of semiconductors can be controlled by band gap variation, and this makes them suitable candidates for application in photonics. Hence, the size-dependent optoelectronic properties are a consequence of the quantum confinement effect (Katz et al. 2002).

Cheatnoy et al. (Cheatnoy et al. 1986) explained the control of nanocrystal size and the physical picture of finite size effects on solvent phase synthesized II–VI quantum dots. Using II–VI quantum dots as the prototype, a number of interactions have been studied on finite size effects (Behboudnia and Sen 2001; Burnin and Belbruno 2002; Calandra et al. 2003; Hu et al. 2001; Kho et al. 2000; Li et al. 2001; Nanda and Sarma 2001; Nanda et al. 2000; Weller 1996). II–VI quantum dots, such as ZnS (Huang et al. 2007; Matxain et al. 2000, 2001), ZnSe (Xu et al. 2009), CdS (Wang et al. 2007), CdSe (Andersen et al. 2002), CdTe (Wang et al. 2008), HgTe (Wang et al. 2004), and so on, are particularly interesting and have been the focus of many experimental and theoretical investigations in recent years. Studies have been done for stoichiometric and non-stoichiometric II–VI compounds, viz. Zn_mS_n (Pal et al. 2005), Zn_nSe_n clusters (Xu et al. 2009), Cd_mSe_n clusters (Sarkar and Springborg 2003), and Cd_nSe_n clusters (Troparevsky et al. 2003; Xu et al. 2010). Malik and Kakkar (Malik and Kakkar 2018) explored the sensing ability of CdSe quantum dots for sensing metal ions and anions using density functional methods. In a study (Han et al. 2021) on II–VI quantum dots, both the electronic and excitonic properties of blue-emitting colloidal quantum dots were investigated for both quantum confinement and surface ligand effects.

As is already known, quantum confinement leads to an increase in the band gap as the size of the quantum dot is decreased. Since this is observed as an increase in the energy of the lowest exciton peak as the radius of the quantum dot is decreased (Norris et al. 1996; Rodrigues et al. 1995), research in this area has focused almost exclusively on understanding the energy spectrum of an exciton as a function of quantum dot radius (Yoffe 1993; Leung and Whaley 1999; Wang and Zunger 1996) in order to predict the optical properties of CdSe quantum dots of an arbitrary size. However, in principle, quantum confinement should affect every electronic state within the quantum dot, but not equally (Andersen et al. 2002). The most extensively studied systems are group II–VI semiconductor QDs, mainly ZnS, ZnSe, ZnO, CdSe, and CdS, whose band gaps can be tailored by varying the composition and size. Most common QDs are made of CdE (E = S, Se, Te) which are toxic. Current environmental guidelines limit the practice of toxic metals and therefore QDs comprising nontoxic metals such as Zn are of great importance.

Quantum dots have wide applications. One of their applications is as gas sensors for the detection of the main air pollutants even when their concentration is very low. Nowadays, detection of gas molecules pertinent to chemical and biochemical processes is of utmost importance in industrial, environmental, and medical monitoring (Özgür et al. 2005; Schmidt-Mende and MacManus-Driscoll 2007; Yamazoe 1991). The adsorption of gases on the surface of a semiconductor leads to changes in the equilibrium carrier concentration near the surface where the adsorption occurs. For example, when adsorption of a reduction gas, i.e., donor gas, takes place on an n -type adsorbent, the electrons from the adsorbed atoms or molecules transfer to the semiconductor, thus increasing the concentration of the free carriers and thus the conductivity of a sample. When an oxidizing, or acceptor, gas adsorbs on the surface of an n -type semiconductor, the number of carriers and the conductivity decreases. The values of these changes give information about the presence of different gases in the environment and enable their concentrations to be defined.

Quantum dots have been widely explored as gas sensors, like the wide-gap semiconductors, CdSe/ZnO nanocomposites can be used for NO gas detection (Chizhov et al. 2014), ZnSe@CdS

core/shell structures as NO₂ sensors (Chizhov et al. 2019), and ZnO QDs as CO₂ gas sensors (Bhakat et al. 2021). NO₂ gas sensors based on ZnO, SnO₃, and In₂O₃ sensitized with CdSe quantum dots (Chizhov et al. 2016) can be used as gas detectors (Weitzel and Monteith 1974).

In the present work, we present the results of our theoretical calculations on the structural and electronic properties of (ME)_n quantum dots as a function of size, where $n=3, 6, 10,$ and 13 . Group II–VI semiconductors may adopt several crystal structures, of which zinc blende (sphalerite) is one of the most common and is dominant under ambient conditions for several binary compounds like ZnSe, ZnTe, CdS, HgS, HgSe, and HgTe. Its hexagonal analogue is wurtzite, which derives its name from the zinc iron sulfide mineral (Zn,Fe)S. Under ambient conditions, the binary compounds that adopt this structure include ZnS, CdS, and CdSe. Given their structural similarities, it is to be expected that there would be little difference in the unit cell and energies of the two structural polymorphs. Even for those semiconductors for which wurtzite is not the most stable structure, their nanocrystals would still adopt this structure. For example, of the three crystalline forms known for CdSe, the wurtzite form is the most stable. The sphalerite (cubic) structure is unstable and readily converts to the stable wurtzite form on moderate heating. The third form, i.e., the rock salt (cubic) structure, is only observed at high pressure. Hence, the wurtzite (hexagonal) structure was chosen for our studies.

The quantum dots chosen are the group 12 chalcogenides with wide tunable band gaps. We have optimized the structures, where the initial structures of the quantum dots are the stoichiometric moiety of the wurtzite crystal structure, having stacked or fused hexagonal rings. We have primarily focused on the Mulliken population analysis, electronic energy levels, band gaps, Fermi energies, and stabilities as a function of size for all types of II–VI quantum dots with a view to understanding their conductivities as a function of size as well as the nature of the anion and cation. Furthermore, an effort has been made to explore how a wide band gap semiconductor, CdSe quantum dot, will behave when it interacts with various gas molecules. This study will help in understanding the sensing abilities of CdSe quantum dots for the chosen gas molecules.

Computational details

The DMol³ code (Delley 1990, 1991, 1996, 2000, 2002), available from Accelrys Inc. in the Materials Studio 4.4 package, was used to perform first-principles density functional (DF) computations (Hohenberg and Kohn 1964). We used double zeta quality plus polarization function (DNP) numerical basis sets, which are comparable to the Gaussian basis, 6-31G**, in our calculations. Using delocalized internal coordinates, the geometries of the various nanoclusters were fully optimized without limitations. We utilized the GGA-PBE (Perdew et al. 1996) functional for the calculations because the findings of our previous work (Kakkar et al. 2006) suggested that it is the most trustworthy for replicating the experimental geometries. For geometry optimization, the Hellmann–Feynman force threshold on each atom was preserved at $0.004 E_h^{-1}$, while the energy threshold was set at $2 \times 10^{-5} E_h$ and 1×10^{-5} was chosen as the SCF tolerance. DFT–semilocal pseudopotentials (DSPP) were used to optimize all of the structures (Delley 2002).

Results and discussion

As mentioned earlier, we selected neutral hexagonally stacked clusters of group 12 chalcogenides with the common formula (ME)_n where $n=3, 6, 10,$ and 13 and $M=Zn, Cd,$ and $Hg, E=S, Se,$ and Te . These clusters, being stoichiometric in nature, were centered on the M–E bond. A bottom-up approach was used for construction of these clusters on the basis of the wurtzite crystal structure. Considering one of the metal chalcogenides (ZnS)_n, the basic bonding pattern in the un-optimized structures is shown in Fig. S1 (Supporting Information, SI). This was further applied to the other metal chalcogenides, and the (ME)_n were constructed and optimized (Fig. S2, SI). These structures reveal that the surfaces have unsatisfied valencies, allowing them to interact with other moieties or, more importantly, to be easily capped to improve their properties. The (ME)₃ trimer is believed to be the building block for the growth of these clusters. The metal and chalcogenide atoms are di-coordinated in the case of (ME)₃ and tri-coordinated in (ME)₆. In the case of (ME)₁₀ and (ME)₁₃, both the metal and chalcogenide atoms are tri-coordinated,

except in those places where the hexagonal structures are fused, where the atoms are tetra-coordinated instead.

The general trend is that the coordination number for the metal and chalcogenide atoms increases as the cluster grows. The surface reconstruction has a critical effect on the optical and electronic properties of these quantum dots. However, the surface structure of the quantum dots is not very well understood, and only limited experimental and theoretical evidence is available. As a result, an attempt has been made in this paper to explain the features of stoichiometric II–VI quantum dots that are yet to be discovered. All the clusters were fully optimized and then investigated to study the effect of increase in cluster size and change of chemical composition on their structural and electronic properties. These properties are discussed in detail in the following sections.

Structural properties

Before exploring the properties of the quantum dots, we calculated those of the corresponding molecular forms ME of the chalcogenides of the zinc triad, and these are given in Table 1. The M–E bond lengths are found to be smaller than the sum of the ionic radii of M^{2+} and E^{2-} , indicating covalent character of the bonds. When we look at the bond lengths for a given metal atom, we can see that they approach the ionic radii as we progress from the sulfide to the selenide to the telluride. Therefore, we can say that the covalent character decreases with increase in the atomic number of the chalcogenide atom.

(ME)₃

(ME)₃, a trimer, can be considered as the first real building unit of the wurtzite crystal structure. In contrast to the bulk, where six-membered rings appear only in the chair conformation in cubic zinc blende or in the chair as well as in the boat conformation in wurtzite, the isolated ring is planar (Deglmann et al. 2002). In our studies also, all the nine nanoclusters with D_{3h} ($-6m2$) symmetry are planar, as confirmed by their dihedral angles. Both the metal (M) and chalcogenide (E) atoms in these structures are twofold coordinated (Fig. S2), and the hexagonal ring structure optimizes to a distorted hexagonal structure. The optimized average M–E bond lengths are greater than

those of the molecular forms, except for CdTe and the mercury chalcogenides (Table 1). It is also clear that the bond lengths are smaller than the sum of the ionic radii, indicating covalent character of the bonds in these hexagonal rings, as also seen in the molecular forms. Table 2 gives the variation of the bond angles of the (ME)₃ structures. It is apparent that the bond angle about the metal atom is obtuse and increases as we move from S to Se to Te, whereas that about the chalcogenide decreases due to the greater repulsion between the negatively charged chalcogenide atoms for the smaller, more electronegative sulfur than for Te.

The metal atoms have a strong tendency to show higher coordination in their structures. In the case of (CdS)₃, the cadmium increases its coordination number to four. An additional bond is formed between the cadmium atoms (Fig. S2). The structure adopts a shape similar to an equilateral triangle, formed between the three cadmium atoms, with a Cd–Cd bond length of 3.192 Å. No increase in the coordination number for the metal atom is observed in any other case. A study of similar quantum dots of ZnSe and ZnTe using the DFT/B3LYP/LANL2DZ method had yielded 2.431 Å and 2.618 Å as the respective ZnSe and ZnTe bond lengths (Xu et al. 2009). Our findings (Table 1) are comparable, prompting us to continue with the computations for the other clusters so that we can compare them based on their size and stoichiometry.

(ME)₆

(ME)₆ is the smallest wurtzite cage cluster. This geometry is obtained by the anti-parallel stacking of two (ME)₃ hexagonal rings, resulting in closed polyhedral cages composed of four-membered and six-membered rings (Fig. S2). The initial un-optimized structure of these quantum dots had three-fold coordination for both the metal and chalcogenides atoms (Fig. S1). When these structures were allowed to relax, a change in the coordination of the metal and chalcogenide atoms was observed. All the quantum dots rearrange their atoms to approach D_{3d} ($-3m$) symmetry, except CdSe and CdTe, which have C_i (-1) symmetry.

For the zinc chalcogenides, no change in coordination for zinc is observed. In the case of cadmium chalcogenides, all the metal atoms change their coordination numbers to five for CdS, some increase it

Table 1 Calculated bond lengths (Å) of (ME)_n

Bond length	(ME) _n	ZnS	ZnSe	ZnTe	CdS	CdSe	CdTe	HgS	HgSe	HgTe
M-E (calculated)	Molecular form of	2.097	2.258	2.578	2.238	2.506	2.830	2.484	2.777	3.063
M ²⁺ + E ²⁻	nanocluster (ME)	2.58	2.72	2.95	2.79	2.93	3.16	2.86	3.00	3.23
M-E	(ME) ₃	2.190 (2.228 ^a)	2.328 (2.431 ^b)	2.533	2.410	2.544 (2.597 ^c , 2.569 ^d)	2.733 (2.22 ^e)	2.426	2.555	2.745
M-E	(ME) ₁₃	2.337	2.468	2.666	2.564	2.687	2.868	2.535	2.696	2.900
M-M		2.780	-	-	3.185	3.241	-	-	-	-
M-E	(ME) ₁₀	2.322	2.446	2.648	2.553	2.673	2.866	2.528	2.661	2.853
M-M		2.759	-	-	3.199	3.209	-	-	-	-
Facial bond length	(ME) ₆	2.290	2.431	2.642	2.497	2.626	2.822	2.453	2.592	2.798
Interfacial bond length		2.470	2.579	2.755	2.754	2.857	2.887	3.224	3.218	2.262

^a(Chuchev and Bel Bruno 2005)

^b(Xu et al. 2009)

^c(Chung et al. 2009)

^d(Xu et al. 2010)

^e(Wang et al. 2009)

Table 2 Calculated bond angles ($^{\circ}$) in $(ME)_3$

Bond angle	ZnS	ZnSe	ZnTe	CdS	CdSe	CdTe	HgS	HgSe	HgTe
M-E-M	80.4	77.5	74.9	82.9	81.3	77.8	81.5	79.7	77.6
E-M-E	159.6	162.5	165.1	157.1	159.7	162.2	158.5	160.5	162.4

to four in CdSe, and no increase in coordination is observed for CdTe. For the mercury chalcogenides, all the metal atoms, as well as the chalcogenide atoms, decrease their coordination numbers to two. Thus, we can say that the $(HgE)_6$ ($E = S, Se, Te$) exist as two hexagonal rings of $(HgE)_3$ stacked one on top of the other without direct covalent bonding (Fig. S2). The structure reveals in each of the cases that the interlayer bond lengths, i.e., those between the two hexagonal rings, are greater than the facial bond lengths, i.e., those of the hexagonal ring structures on the faces. The previously reported values using DFT/B3LYP/LANL2DZ (Xu et al. 2009) for similar QDs of ZnSe and ZnTe for the facial bond lengths are 2.538 Å and 2.731 Å and the reported interlayer bond lengths equal 2.676 Å and 2.863 Å, respectively. On similar lines, the reported values for the CdSe quantum dots with the same stoichiometry are 2.699 Å for the facial bond length and 2.867 Å for the interlayer distance (Chung et al. 2009). Our calculated results (Table 1) closely resemble these values.

$(ME)_{10}$

The initial structures used for the geometry optimization consist of only threefold coordination sites for both the metal and the chalcogenide atoms. Geometry optimization leads to a change in the coordination numbers of both the metal and chalcogenide atoms in these quantum dots too. All the quantum dots are found to have C_{2h} ($2/m$) symmetry.

In the case of $(ZnS)_{10}$, the coordination of the metal atom increases to four for atom numbers 1, 9, 15, and 19 (Fig. S2). The coordination of the metal atoms in the selenide and telluride of the same metal remains the same as that of the initial structure. For cadmium chalcogenides, there is a change in the coordination number of some of the cadmium atoms. Atom numbers 3, 9, 15, and 19 increase their covalency to five and four, respectively, for $(CdS)_{10}$ and $(CdSe)_{10}$. In CdS, the metal atoms are tetra-coordinated, except Cd5 and Cd11, both being tri-coordinated. In the mercury chalcogenides, a decrease in

the coordination numbers for some of the metal (atom numbers 1, 15, 9, 19) and chalcogenide (atom numbers 2, 14, 8, 20) atoms from three to two is observed. The optimized structures clearly reveal that, as the size of the metal atom increases from zinc, cadmium to mercury, the two adjacent faces which are stacked together try to move away from each other but are still held together by a few bonds between them. For example, in the case of all the mercury chalcogenides, the two layers are held together by only four bonds each (Table 1).

$(ME)_{13}$

This structure can be described as a stacked structure of two layers of three fused hexagonal rings. All $(ME)_{13}$ belong to the C_{3v} ($3m$) symmetry point group, except CdTe which has C_1 (1) symmetry. In all of these, the chalcogenide atoms are three-fold coordinated, except those present at the fused site, which are four-fold coordinated. An increase in the covalency of the metal atoms is noted for zinc and cadmium in ZnS, CdS, and CdSe due to the formation of M-M bonds, leading to an increase in their coordination number to five in each of these cases. For the rest of the QDs, no such increase in coordination is observed. The QDs of mercury chalcogenides open up on optimization. This is greatest in the case of HgS, followed by HgSe and HgTe, as the number of interlayer bonds present in the optimized structures follows the reverse order. $(HgS)_{13}$ upon optimization yields two layers, each of which contains 13 atoms. The stoichiometric QD $(HgS)_{13}$ thus has two non-stoichiometric layers of Hg_7S_6 and Hg_6S_7 stacked one on top of the other without covalent bonding (Fig. S2) between the two layers. These graphitic-like structures are believed to be the precursors to the wurtzite structure (Freeman et al. 2006).

$(HgSe)_{13}$ and $(HgTe)_{13}$ still have the two faces connected to each other by interlayer bonds. Here also, in all cases, the interlayer bond lengths are larger than the facial bond lengths, but the difference in their lengths is smaller in comparison to the other QDs of

lower stoichiometry that exist with fused hexagonal rings. The average bond length for each of the QDs is given in Table 1.

Electronic properties

Binding energies

Table 3 gives the calculated electronic properties of the systems under study. The binding energy reported in the table is the energy required to separate a molecule into its constituent atoms at infinite separation and is hence a measure of the stability of the QD. It is clear that the binding energy decreases to less negative values as the size of the cation or anion increases. To bring the calculations to a level platform, the binding energy per formula unit was calculated and was found to increase with the size of the cluster, reaching a constant value at cluster size of 10 to 13 formula units (Fig. 1). This constant value is the highest in magnitude for $(\text{ZnS})_{13}$ (-5.21 eV), followed by $(\text{ZnSe})_{10}$ (-4.58 eV), and is least for $(\text{HgTe})_{13}$ (-2.54 eV).

Quantum confinement effects: Fermi energies and band gaps

Fermi energy (E_F) is a crucially important concept for understanding the electronic properties of insulators, metals, and semiconductors. It is defined as the highest energy which is occupied by an electron of the material at temperature 0 K and determines the conductivity of the material. The contour plots showing the valence (highest occupied molecular orbital, HOMO) and conduction (lowest unoccupied molecular orbital, LUMO) bands, along with their respective energies, are given in Fig. S3.

For ZnS, the HOMO energies are ~ -5.5 eV, whereas the LUMO energies are ~ -2.5 eV, giving band gaps of ~ 3 eV for the various-sized clusters. The Fermi level (~ -2.80 eV) lies closer to the conduction band, making this material a good conductor. The situation is similar for the other zinc chalcogenides, though there is a slight increase in the conductivity with the size of the anion.

For cadmium sulfide, the position of the valence band does not change much (~ -5.5 eV), but the conduction band moves a little up (~ -2.3 eV). As a result, the band gap increases to ~ 3.3 eV, and the

distance between the conduction level increases somewhat, making CdS a poorer conductor than ZnS. The situation changes somewhat for CdSe, where the largest cluster under study has its valence and conduction bands at -5.2 and -2.8 eV, respectively, and the Fermi energy is -3.2 eV, making CdSe a good conductor because of its small band gap and proximity of the Fermi level to the conduction band. By the same token, CdTe is slightly more conducting than the other two cadmium compounds.

The trend continues with the mercury compounds, with the valence band not moving much, but the conduction band is moving lower to -3.8 eV, leading to a small energy gap of 1.6 eV and a Fermi energy (-4.2 eV) which is close to the bottom of the conduction band, confirming that these are *n*-type semiconductors. Both the valence and conduction bands move higher as the size of the anion is increased, and the band gap decreases a little.

The variation of Fermi energies with the QD is pictorially represented in Fig. 2. The magnitude of the Fermi energy is highest for all the sulfides, with HgS having the maximum value. Though the zinc compounds do not follow a steady trend, the other compounds (except CdTe) show an increase in the magnitude of the Fermi energy with the size of the quantum dot, decrease in magnitude on increasing the size of the anion, and an opposite trend on increasing the cation size.

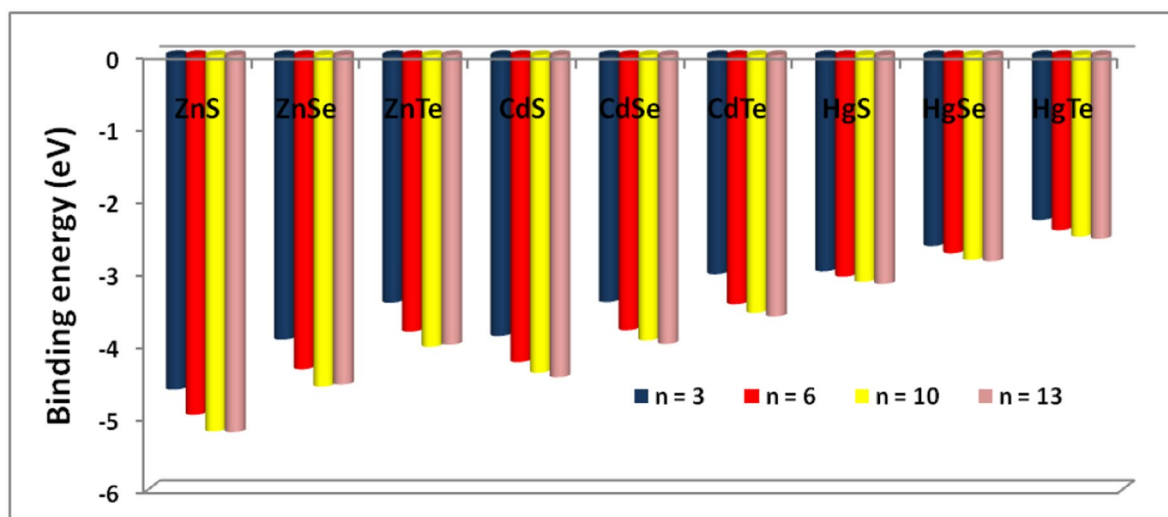
The variation of the band gap with the size and composition of the quantum dot is depicted in Fig. 3. The expected quantum confinement effect is observed for almost all the cadmium and mercury chalcogenides, where the QDs with lower stoichiometry have wider band gaps than those with the higher stoichiometry. Cadmium telluride and the zinc chalcogenides (Fig. 3) are exceptions to the expected trend. We had found a similar situation in the case of MgO nanoclusters (Kakkar et al. 2004). Generally, the HOMO is composed of the anion orbitals and the LUMO of the cation orbitals. In that case, the quantum confinement effects would be purely size-dependent. In the present case, the HOMO is majorly composed of the anion orbitals as expected, but the anion orbitals also take part in the LUMO (Fig. S3). This means that the LUMO energies are also dependent on anion repulsion due to the overlap of their orbitals, and thus, they depend on the shape of the QD as well. The anomalies are found only in those cases where the cation is much

Table 3 Calculated properties of $(ME)_n$ ($n=3, 6, 10, 13$)

$(ME)_n$	Binding energy (eV)	Binding energy per formula unit (eV)	Fermi energy (eV)	HOMO energy (eV)	LUMO energy (eV)	Band gap (eV)	Mulliken charge on the metal
	ZnS						0.266
3	-13.86	-4.62	-2.61	-5.44	-2.21	3.23	0.212
6	-29.81	-4.97	-3.05	-5.48	-2.65	2.84	0.295
10	-51.96	-5.20	-2.99	-5.53	-2.58	2.94	0.195
13	-67.74	-5.21	-2.80	-5.65	-2.39	3.26 (1.73 ^a , 3.83 ^b)	0.272
	ZnSe						0.310
3	-11.78	-3.93	-2.50	-5.08	-2.10	2.98	0.363
6	-26.05	-4.34	-2.93	-5.18	-2.53	2.65	0.401
10	-45.84	-4.58	-2.93	-5.12	-2.53	2.59	0.403
13	-59.21	-4.56	-2.72	-5.33	-2.28	3.05 (3.53 ^c)	0.392
	ZnTe						0.180
3	-10.25	-3.42	-2.56	-4.73	-2.15	2.58	0.241
6	-22.91	-3.82	-2.95	-4.86	-2.52	2.34	0.281
10	-40.28	-4.03	-3.00	-4.84	-2.58	2.26	0.288
13	-51.99	-4.00	-2.80	-4.98	-2.27	2.71	0.255
	CdS						0.340
3	-11.63	-3.88	-2.79	-5.16	-2.39	2.77	0.382
6	-25.41	-4.24	-3.13	-5.26	-2.73	2.53	0.465
10	-43.87	-4.39	-3.23	-5.32	-2.82	2.50	0.468
13	-57.83	-4.45	-3.34	-5.41	-2.93	2.48 (2.32 ^d)	0.471
	CdSe						0.343
3	-10.23	-3.41	-2.75	-4.85	-2.35	2.50	0.451
6	-22.81	-3.80	-2.99	-5.01	-2.58	2.43	0.499
10	-39.42	-3.94	-3.07	-5.07	-2.66	2.41	0.489
13	-51.92	-3.99	-3.21	-5.16	-2.80	2.36 (2.57 ^e)	0.491
	CdTe						0.203
3	-9.10	-3.03	-2.60	-4.55	-2.18	2.37	0.316
6	-20.64	-3.44	-2.90	-4.73	-2.43	2.30	0.371
10	-35.60	-3.56	-2.89	-4.74	-2.41	2.33	0.291
13	-46.89	-3.61	-3.03	-4.86	-2.58	2.28 (2.38 ^f , 1.606 ^g , 0.195 ^h)	0.359
	HgS						0.184
3	-8.98	-2.99	-3.30	-5.36	-2.90	2.46	0.255
6	-18.37	-3.06	-3.56	-5.29	-3.13	2.16	0.287
10	-31.32	-3.13	-3.95	-5.38	-3.53	1.85	0.291
13	-41.02	-3.16	-4.18	-5.36	-3.77	1.59 (1.4 ⁱ)	0.293
	HgSe						0.129
3	-7.92	-2.64	-3.21	-5.03	-2.81	2.22	0.322
6	-16.47	-2.75	-3.51	-4.94	-3.05	1.89	0.346
10	-28.26	-2.83	-3.76	-4.90	-3.34	1.56	0.335
13	-37.02	-2.85	-3.99	-4.98	-3.59	1.39 (1.5 ^j)	0.330
	HgTe						0.060
3	-6.84	-2.28	-3.02	-4.61	-2.56	2.05	0.187
6	-14.52	-2.42	-3.34	-4.52	-2.87	1.65	0.212
10	-25.18	-2.52	-3.45	-4.52	-2.93	1.59	0.201

Table 3 (continued)

(ME) _n	Binding energy (eV)	Binding energy per formula unit (eV)	Fermi energy (eV)	HOMO energy (eV)	LUMO energy (eV)	Band gap (eV)	Mulliken charge on the metal
13	-33.08	-2.54	-3.67	-4.66	-3.23	1.43 (1.3 ^g)	0.196

^a(Pal et al. 2009)^b(Salavati-Niasari et al. 2009)^c(Nikesh and Mahamuni 2001)^d(Wijayantha et al. 2004)^e(Chung et al. 2009)^f(Wang et al. 2009)^g(Woggon and Gaponenko 1995)^h(Bhattachary and Kshirsagar 2007)ⁱ(Patel et al. 2007)^j(Liu et al. 2004)**Fig. 1** Variation of binding energy (eV) plot for II–VI nanoclusters as a function of cluster size

smaller than the anion. It is observed (Table 2) that the angle about the metal is almost linear to maximize the distance between two anion atoms and hence minimize their mutual repulsion. For smaller cations, the distance between the two chalcogenide ions flanking it is less, and hence, the band width not only depends on the size, but also on the shape of the cluster.

In the case of (ME)₃, the HOMO is mainly centered on the chalcogenide atom and the LUMO on the metal atom, but the situation changes for the larger clusters (Fig. S3). For these, the HOMO comprises the pure *p* orbitals of the chalcogenide and pure

d orbitals of the metal, with very little mixing. The LUMO consists of *sp* hybrid orbitals formed by the hybridization of the metal orbitals. Also, it seems that the *d* orbitals of the chalcogenides also play a crucial role in the LUMOs, as the plots are concentrated around the anionic atoms as well. Hence, the HOMO energies do not vary much with the type of chalcogenide and its size. However, the mixing of cation and anion orbitals accounts for the variation of the LUMO energies and hence the band gap.

It must be emphasized that though DFT is known for underestimating band gaps, the calculated values

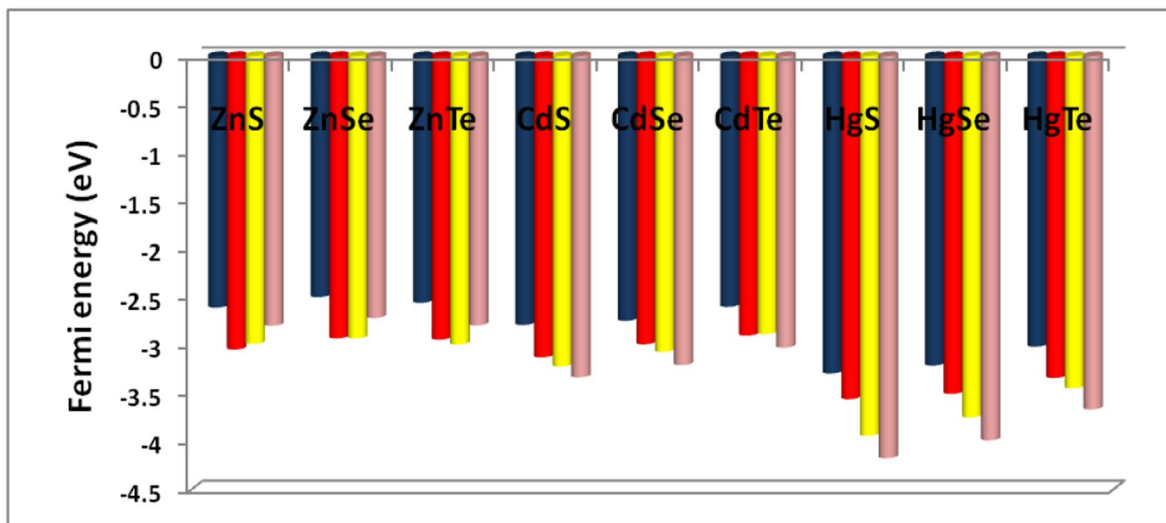


Fig. 2 Variation of Fermi energy (eV) plot for II–VI nanoclusters as a function of the cluster size

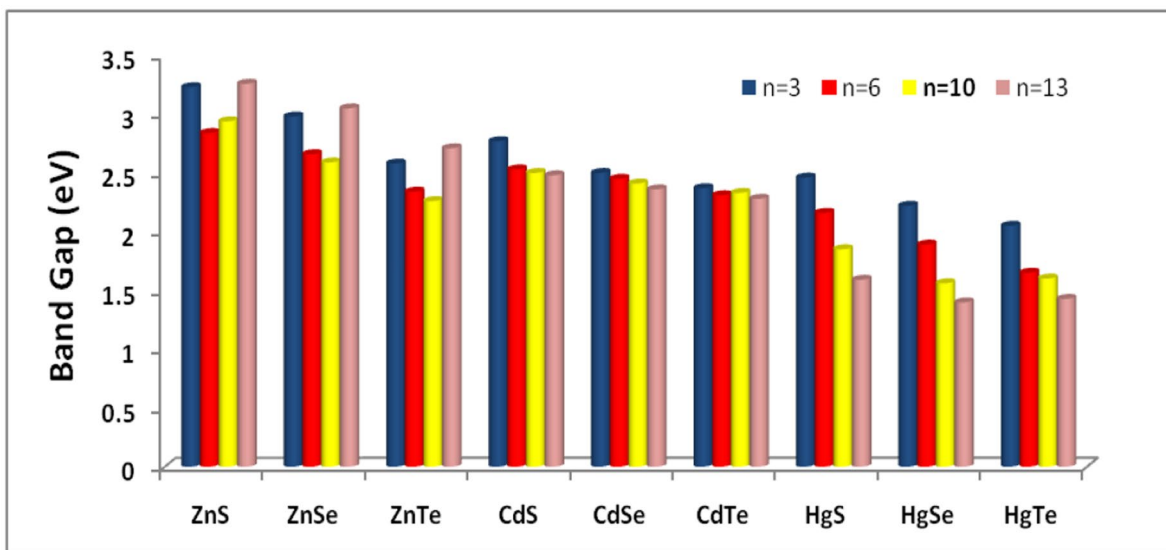


Fig. 3 Variation of the band gap (eV) for II–VI nanoclusters as a function of cluster size

(Table 3) are in fair agreement with those reported in the literature (Chung et al. 2009; Wang et al. 2009; Freeman et al. 2006; Pal et al. 2009; Salavati-Niasari et al. 2009; Nikesh and Mahamuni 2001; Wijayantha et al. 2004; Woggon and Gaponenko 1995; Bhattachary and Kshirsagar 2007; Patel et al. 2007). Moreover, the calculated HOMO and LUMO energies imply that the ionization energies (IE) are in the

range 4.5 to 5.7 eV and the electron affinities (EA) are 2.1 to 3.8 eV according to Koopmans' theorem. Typical semiconductors of interest in inorganic or organic electronics have IEs and EAs in the range of 4.5–6.5 eV and 2–4 eV, respectively, which agree with these values.

The conclusion of these studies is that (i) all of the studied compounds are good semiconductors, having

small band gaps and Fermi energies that lie close to the bottom of the conduction bands, (ii) the conductivity of the semiconductor QD increases as the size of the cation or anion is increased, and (iii) it also increases as the size of the QD itself increases. The Hg compounds display these trends in almost copy-book style, the Fermi energy going up from -3.3 eV to -3.0 eV, and the band gap decreasing from 2.5 to 2.1 eV on changing the anion from S to Te for the smallest sized QD. Similarly, for HgS, for example, the Fermi energy is gradually lowered from -3.3 to -4.2 eV as the size of the QD increases, and there is a concomitant decrease in the band gap from 2.5 to 1.6 eV. The trend is repeated for the other mercury chalcogenides, showing that the conductivity increases on increasing the size of the anion and the QD.

Charge distribution

The calculated Mulliken charges are given in Table 3, where the Mulliken charge on the metal ion in the molecular form is also given against each compound. Because of the 1:1 stoichiometry, the charge on the chalcogenide is equal, but opposite, to the metal charge. The computed charges on the metal ion in the molecular form indicate large transfer of charge from the anion and a considerable covalent character. The charge separation is largest for the selenides.

Though the Mulliken charges are not considered reliable, as they are dependent on the size of the basis set, here we are only interested in the trends and these are correctly reflected by these charges. Moreover, we are working with a fairly large basis set. Because of decreasing electronegativity of the chalcogenide, the charges are expected to decrease from the sulfides to the tellurides, but, surprisingly, the metal charge first increases from the sulfides to the selenides and then again decreases for the tellurides. This may be due to the anisotropic behavior of the charge distribution in these small QDs which is attributed to the decrease in covalent character with size. This drift in the trend from the bulk structures is similar to the molecular forms of the zinc triad which also possess an anisotropic charge distribution. It may be concluded that the selenides have the most ionic character.

After having studied various stoichiometric QDs and their relative conductivities, we explored their properties as gas sensors. The typical sensing process is based on the fact that charge transfer between the QD and the adsorbed gas molecules either enhances or decreases the electrical conductivity of the QD. For this study, the $(\text{CdSe})_{13}$ QD was chosen as a model system to study the gas sensing ability of group II–VI QDs toward various small gas molecules. We chose this QD as it has intermediate properties among the chosen QDs for analysis.

CdSe quantum dots as sensors for detection of various gas molecules

We have considered the adsorption of small gas molecules, i.e., H_2 , N_2 , O_2 , CO , H_2O , CO_2 , NO_2 , SO_2 , and HCHO on CdSe quantum dots in order to explore the structural and electronic changes in both the adsorbent and adsorbate molecules on their interaction. Detection of these gas molecules is important for monitoring the environmental, medical, or industrial conditions. O_2 , H_2 , and CO molecules are typical components present in the feedstock for fuel cells. CO_2 , CO , NO_2 , and SO_2 are common gaseous pollutants comprising the main determinants of automotive emission. CO and CO_2 are also harmful pollutants which are produced in combustion processes. CO_2 is also one of the greatest contributors to the greenhouse effect. Understanding the adsorption behavior of these molecules is therefore of both practical and fundamental interest.

In general, the adsorption behavior can be classified as physisorption, chemisorption, and molecular chemisorption. Molecular chemisorption is an intermediate adsorption between physisorption and chemisorption, as characterized by a small amount of charge transfer between the adsorbate and adsorbent and by moderate adsorption energy and distance, with some bond length change at the adsorption site.

The various gas molecules considered for adsorption were geometry optimized with respect to the energy, and the results obtained are given in Table S1, SI. These gas molecules were then made to interact with the CdSe QD.

CdSe quantum dot as an adsorbent

Experimental findings have suggested that the ligands coordinate exclusively with Cd^{2+} ions during the growth process of CdSe QDs (Liu et al. 2004; Soloviev et al. 2000; Manna et al. 2000). Therefore, the gas molecules were placed in the close vicinity of a peripheral cadmium atom, i.e., Cd17 only (Fig. 4). Two different modes were chosen—one in which the gas molecule was placed parallel to the surface, thereby allowing all the atoms of the gas molecule to interact uniformly with the cadmium atom (mode A), and the second in which the molecule was placed perpendicular to the surface, above the cadmium atom, and therefore, the cadmium atom forms a close contact with only one atom of the gas molecule, as in mode B (Fig. 4).

On the basis of the adsorption energies (calculated as the difference in the binding energies of the products and reactants), it was found that for H_2 , mode A is preferred by 0.65 eV. On the other hand, mode B is the preferred mode for N_2 and H_2O . The adsorption of O_2 and CO on the CdSe quantum dots shows that both the modes give the same optimized structure. The side and top views and the binding energy of each product are given in Fig. S4 (SI).

Structural properties

Fig. S4 reveals that the adsorption of gas molecules causes changes in the structure of the QD, but no actual bond is formed between the gas molecule and the CdSe QD in most of the cases. The two exceptions

are O_2 and NO_2 , which directly interact with the CdSe QD by forming a chemical bond with the peripheral cadmium atom. These are both open-shell molecules. The bond length of the O_2 molecule is increased by 0.1 Å as a result of this interaction. The length of the bond formed between Cd and O is 2.390 Å. The NO_2 molecule is involved in bond formation with the CdSe QD through its oxygen atom, the Cd–O bond length being 2.426 Å. This interaction leads to an increase in the N–O bond length of NO_2 from 1.209 to 1.256 Å.

The rest of the gas molecules interact without direct bond formation with the CdSe QD moiety. The CO molecule lies at a distance of 2.700 Å from the CdSe QD with no change in its own bond length. The interaction of CO_2 with the QD causes an increase in the length of one of the C–O bonds by 0.001 Å, and the other C–O bond length is decreased by 0.002 Å, showing that this is basically a case of physisorption. In the case of SO_2 , the interaction causes an increase in the bond length of the S–O bond by 0.025 Å. The structural changes reveal that the adsorption of some gas molecules causes significant changes in the properties of the CdSe QD as well (Table 4), as can be observed from the increase in the average Cd–Se bond length from 2.687 Å (Table 1).

Adsorption and deformation energies

The adsorption energy is defined as $E_{\text{adsorption}} = [E_{\text{binding}}(\text{CdSe quantum dot} + \text{gas molecule})] - [E_{\text{binding}}(\text{CdSe quantum dot}) + E_{\text{binding}}(\text{gas molecule})]$, where E_{binding} is the binding energy of the respective system. A negative (positive) value for $E_{\text{adsorption}}$ implies

Fig. 4 Initial structure used for adsorption of gas molecules

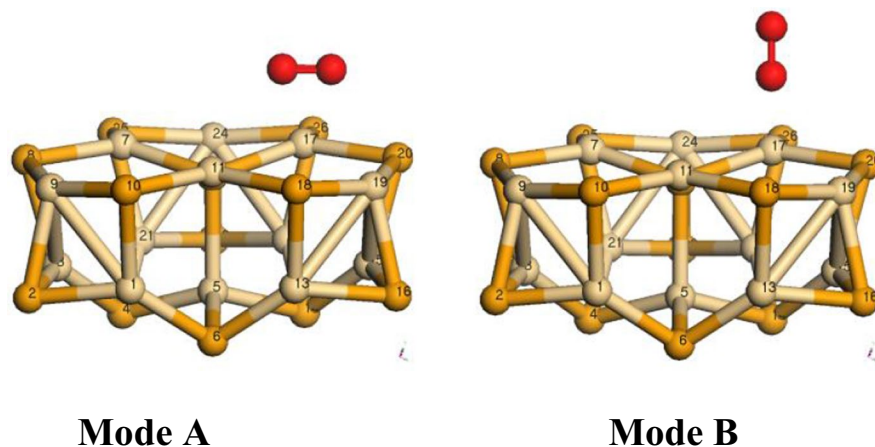


Table 4 Properties of the gas-QD adsorbed systems

Property	QD	QD with adsorbed gas								
		H ₂	N ₂	O ₂	CO	H ₂ O	CO ₂	NO ₂	SO ₂	HCHO
Cd-Se (Å)	2.687	2.740	2.740	2.686	2.726	2.730	2.740	2.697	2.718	2.730
Adsorption energy (eV)	-	-0.28	0.08	-0.80	-0.04	-0.56	-0.00	-0.42	0.00	-0.15
Deformation energy (QD) (eV)	-	0.03	0.03	0.50	0.02	0.01	0.03	0.63	0.02	0.00
Deformation energy (Gas) (eV)	-	0.00	0.00	0.20	0.00	0.00	0.00	0.56	0.02	0.00
Charge on QD	-	-0.004	-0.004	0.381	0.028	-0.060	0.000	0.415	0.098	0.026
Fermi energy (eV)	-3.21	-3.19	-3.19	-4.30	-3.24	-3.11	-3.18	-5.05	-4.71	-3.46
HOMO energy (eV)	-5.16	-5.16	-5.15	-4.53	-5.16	-5.11	-5.15	-5.26	-5.16	-5.08
LUMO energy (eV)	-2.80	-2.78	-2.77	-2.78	-2.77	-2.70	-2.77	-2.85	-4.46	-3.05
Band gap (eV)	2.36	2.38	2.39	1.75	2.39	2.41	2.38	2.41	0.70	2.03

an exothermic (endothermic) adsorption process. The adsorption energies are also listed in Table 4, which reveals that the strongest exothermic adsorption is observed in the case of O₂, while H₂O, NO₂ and H₂ also show exothermic adsorptions. Only in the case of N₂ is the adsorption endothermic. Both SO₂ and CO₂ show negligible interaction, as is also indicated by the negligible change in their bond lengths, as discussed earlier.

The small adsorption energy in some cases could be due to part of the energy released during adsorption being taken up to distort the two molecules. Table 4 also lists the deformation energies for the CdSe QD and the gas molecules in each of the cases considered. These were calculated as the difference in the single-point energies of each component at the optimized geometry of the combined system and the optimized geometry of each isolated system. The data clearly reveal that only the chemisorbed O₂ and NO₂ molecules exhibit significant deformation. When these deformation energies are added to the adsorption energies, the adsorption becomes even more significant for NO₂ and O₂.

Electronic properties

Mulliken population analysis gives the overall charge transfer from the CdSe QD to the gas molecule and vice versa. Before interaction, both of the species, i.e., CdSe QD and the gas molecule, were electrically neutral. The interaction causes transfer of charge amongst them. Table 4 also lists the net charge on the QD after interaction with the gas molecule. Positive values indicate transfer of charge from the QD to the gas molecule and vice versa. The charge transfer

from the QD is found to be the largest for dioxygen and nitrogen dioxide, both of which are chemisorbed on the CdSe QD. For CO, SO₂, and HCHO, there is moderate charge transfer from the CdSe QD. In the rest of the cases, the CdSe acts as a moderate charge acceptor. However, except for water (0.060 *e*), the charge transfer to the QD is negligible.

As noted above for the pure QD, the HOMO mainly comprises the chalcogenide atom, i.e., the selenium *p*-orbitals, whereas the LUMO mainly comprises the cadmium *sp* hybrid orbital and selenium *d* orbitals (Fig. S3). The HOMO and LUMO isosurfaces obtained after interaction with the gas molecules, along with their respective energies, are given in Fig. S5. In most of the cases, there is no change in the orbital energies and band gaps on adsorption. The exceptions are SO₂, O₂, and HCHO, where the band gap decreases drastically to 0.70, 1.75, and 2.03 eV, respectively. In contrast, there is only a slight increase in the band gap to 2.41 eV for H₂O adsorption.

The decrease in the band gap in the case of O₂ is understandable because it is also the molecule with the highest adsorption energy (Table 4). The band gap has shrunk due to the raising of the HOMO level, which now includes the O₂ molecule's π* orbitals (Fig. S5), which have received electrons from the CdSe QD (Table 4). The LUMO is unchanged with respect to the QD and remains concentrated on the CdSe QD. We may rationalize this behavior. The closeness of the Fermi level to the bottom of the conduction band (Table 4) indicates that we may classify CdSe as an intrinsic *n*-type semiconductor. Such *n*-type materials have higher Fermi levels than *p*-type ones because of the lower number of free electrons.

The chemisorption of oxygen on such a semiconductor occurs with the capture of the conduction electron, as indicated by the charge transfer from the QD to the gas molecule, leading to the formation of adsorbed O_2^- . The combined system now resembles a *p*-type semiconductor. NO_2 is also an oxidizing gas, forming NO_2^- as the adsorbed species, and behaves similar to O_2 .

In the case of HCHO, the decrease in the band gap is due to lowering of the LUMO energy, which now comprises the $C=O \pi^*$ orbitals, as found for adsorption on MgO nanoparticles (Kakkar et al. 2004). This is consistent with the negligible charge transfer in this case (Table 4). For SO_2 , too, the situation is similar to HCHO. H_2O also exhibits high adsorption energy (Table 4). Both the HOMO and LUMO are raised, the latter to a larger extent, leading to a slight increase in the band gap, though the H_2O molecule does not appear to participate in either of the two (Fig. S3). The Fermi energy is raised, and the conductivity is decreased. The H_2 molecule, a reducing gas, shows strong exothermic adsorption.

The results of this section indicate that the CdSe QD can be explored as a possible sensor for O_2 and NO_2 , which get strongly chemisorbed and accept charge from it.

Vibrational analysis

The vibrational spectra calculated for the CdSe-gas molecule adducts are shown in Fig. S6(a-i). We compared the spectra of the bare CdSe with the combined system of the CdSe QD and the gas molecule. The spectra have been magnified and overlapped over those obtained for the pristine CdSe QDs to show the shift in the vibrational peaks. In all cases, the intensity of the peaks for the CdSe QDs decreases due to interaction with the gas molecules, while there is negligible shift in the peaks. The most intense and extra peaks are mainly due to the vibrational modes of the gas molecules associated with the CdSe QD. Table S2 shows that, in all cases except N_2 , there is a decrease in the wavenumber of the peaks associated with the vibrations of the various gas molecules on interaction with the CdSe QD. The largest decrease is in the case of the chemisorbed oxygen molecule. Oxygen, which is infrared inactive in the gas phase, shows a strong absorption peak on interaction with the CdSe QD. Though CO_2 is physisorbed, a slight

asymmetry is introduced, and the doubly degenerate bending mode splits into two peaks.

Conclusions

We have studied the structural, electronic, and quantum confinement effects observed in II–VI QDs using density functional theory. As expected, the binding energies increase strongly with cluster size but converge to a constant value per formula unit. The Fermi energy follows no specific trend. There is greater charge separation in the case of the selenides of all the metals in comparison to the sulfides and tellurides. The conductivity increases from the sulfides to the selenides to the tellurides for all the QDs of a particular stoichiometry. We have also observed an elongation in the M-E bond length in these QDs with increasing size. This can be attributed to the differences in the coordination of various atoms in a particular QD. For instance, we have found that cadmium has a larger tendency to form clusters with higher coordination numbers when compared to zinc and mercury. From the structural detail, it can be inferred that the interlayer bond distance is always greater than the facial bond lengths in all the QDs. The final optimized structures in all the cases except $(ME)_3$ comprise nonplanar distorted hexagonal faces fused with each other. In mercury sulfides with a stoichiometry of 6 and 13, the magic number plays a role in the sense that the original structures comprising 12 atoms $(HgS)_6$ and 26 atoms $(HgS)_{13}$ get dissociated into two parallel layers, each of which comprises half the number of atoms of the original structure, i.e., the former forms two layers of $(HgS)_3$ and the latter forms one each Hg_6S_7 and Hg_7S_6 . Hence, we conclude that our theoretical results can be useful in identifying the structural and electronic properties of II–VI QDs in order to check out their applications as bare molecules and also when linked with other molecules of chemical significance.

Further, we have considered the adsorption of only single gas molecules on a $(CdSe)_{13}$ QD in order to detect these gas molecules even when they are present in very low concentration. From the information obtained from the binding energy, the most stable approach for the incoming gas molecule varies from one molecule to another. For H_2 , O_2 , and NO_2 , the parallel mode is preferred; for CO , SO_2 , and HCHO,

the perpendicular mode; and for the rest, both parallel and perpendicular modes yield the same structures. Our results clearly show that most of the gas molecules can be adsorbed spontaneously on the CdSe QDs, since the adsorptions are exothermic. O₂ and NO₂ are the two gas molecules which get strongly chemisorbed. One remarkable change that is observed is the relationship between the band gap and charge transfer properties. The CdSe QD acts as an electron donor when it interacts with oxidizing gases like O₂, CO, NO₂, and SO₂. The vibrational analysis of the combined systems, when compared with that of the bare CdSe QD, shows that the intensities of the peaks due to CdSe reduce, while there is a negligible shift in the peaks. The appearance of the extra peaks at higher frequencies is only due to the gas molecules.

We believe that after accomplishing this theoretical work, we can easily embark into experimental studies to prove that CdSe quantum dots can be effective sensors for gas molecules. The combined study should lead to a better understanding of these novel systems. This should pave the way for using CdSe and similar QDs as sensors for volatile organic compounds (VOCs) like formaldehyde and atmospheric pollutants like NO_x and SO_x.

Acknowledgements We thank the Council of Scientific and Industrial Research (CSIR), New Delhi, India, for providing Senior Research Fellowships to JS (EU-IV/2008/JUNE/104686), RT (10-2(5)/2007(i)-EU-IV), and PM (20-6/2008(ii) EU-IV).

Compliance with ethical standards

Conflict of Interest The authors declare no competing interests.

References

- Andersen KE, Fong CY, Pickett WE (2002) Quantum confinement in CdSe nanocrystallites. *J Non-Cryst Solids* 299–302:1105–1110. [https://doi.org/10.1016/S0022-3093\(01\)01132-2](https://doi.org/10.1016/S0022-3093(01)01132-2)
- Behboudnia M, Sen P (2001) Systematics in the nanoparticle band gap of ZnS and Zn_{1-x}M_xS (M=Mn, Fe, Ni) for various dopant concentrations. *Phys Rev B* 63:035316/1-035316/5. <https://doi.org/10.1103/PhysRevB.63.035316>
- Bhakat A, Pal A, Siddarmaiah R (2021) Chattopadhyay A (2021) Complexation-based super crystalline assembly of zinc oxide quantum dots for sensitive carbon dioxide gas sensing. *J Phys Chem C* 125(22):12316–12323. <https://doi.org/10.1021/acs.jpcc.1c02104>

- Bhattachary SK, Kshirsagar A (2007) Ab initio calculations of structural and electronic properties of CdTe Clusters. *Phys Rev B* 75:035402/1-035402/10. <https://doi.org/10.1103/PhysRevB.75.035402>
- Burnin A, Belbruno JJ (2002) Zn_nS_m⁺ Cluster production by laser ablation. *Chem Phys Lett* 362:341–348. [https://doi.org/10.1016/S0009-2614\(02\)01105-3](https://doi.org/10.1016/S0009-2614(02)01105-3)
- Calandra P, Longo A, Liveri VT (2003) Synthesis of ultra small ZnS Nanoparticles by solid solid reaction in the confined space of AOT reverse micelles. *J Phys Chem B* 107:25–30. <https://doi.org/10.1021/jp021223+>
- Cheatnoy N, Harris TD, Hull R, Brus LE (1986) Luminescence and photophysics of cadmium sulfide semiconductor clusters: the nature of the emitting electronic state. *J Phys Chem* 90:3393–3399. <https://doi.org/10.1021/j100406a018>
- Chizhov AS, Rummyantseva RB, Vasiliev DG, Filatova KA, Drozdov IV, Krylov AM, Abakumov AM, Gaskov AM (2014) Visible light activated room temperature gas sensors based on nanocrystalline ZnO sensitized with CdSe quantum dots. *Sensors Actuators B Chem* 205:305–312. <https://doi.org/10.1016/j.snb.2014.08.091>
- Chizhov AS, Rummyantseva MN, Vasiliev RB, Filatova DG, Drozdov KA, Krylov IV, Marchevsky AV, Karakulina OM, Abakumov AM, Gaskov AM (2016) Visible light activation of room temperature NO₂ gas sensors based on ZnO, SnO₃ and In₂O₃ sensitized with CdSe quantum dots. *Thin Solid Films* 618(B):253–262. <https://doi.org/10.1016/j.tsf.2016.09.029>
- Chizhov A, Vasiliev R, Rummyantseva M, Krylov I, Drozdov K, Batuk M, Hadermann J, Abakumov A, Gaskov A (2019) Light-activated Sub-ppm NO₂ detection by hybrid ZnO/QD nanomaterials vs. charge localization in core-shell QD. *Front Mater* 6:231/1-231/14. <https://doi.org/10.3389/fmats.2019.00231>
- Chuchev K, Bel Bruno JJ (2005) Small non stoichiometric zinc sulphide clusters. *J Phys Chem A* 109:1504–1509. <https://doi.org/10.1021/jp0404908>
- Chung SY, Lee S, Liu C, Neuhauser D (2009) Structures and electronic spectra of CdSe–Cys complexes: density functional theory study of a simple peptide-coated nanocluster. *J Phys Chem B* 113:292–301. <https://doi.org/10.1021/jp8062299>
- Deglmann P, Ahlrichs R, Tsereteli K (2002) Theoretical studies of ligand free cadmium selenide and related semiconductor clusters. *J Chem Phys* 116:1585–1597. <https://doi.org/10.1063/1.1427718>
- Delley B (1990) An all-electron numerical method for solving the local density functional for polyatomic molecules. *J Chem Phys* 92:508–517. <https://doi.org/10.1063/1.458452>
- Delley B (1991) Analytical energy derivatives in the numerical local-density functional approach. *J Chem Phys* 94:7245–7250. <https://doi.org/10.1063/1.460208>
- Delley B (1996) High order integration schemes on the unit sphere. *J Comp Chem* 17:1152–1155. [https://doi.org/10.1002/\(SICI\)1096-987X\(19960715\)17:9%3c1152::AID-JCC7%3e3.0.CO;2-R](https://doi.org/10.1002/(SICI)1096-987X(19960715)17:9%3c1152::AID-JCC7%3e3.0.CO;2-R)
- Delley B (2000) From molecules to solids with the DMol³ approach. *J Chem Phys* 113:7756–7764. <https://doi.org/10.1063/1.1316015>

- Delley B (2002) Hardness conserving semilocal pseudopotentials. *Phys Rev B* 66:155125/1-155125/9. <https://doi.org/10.1103/PhysRevB.66.155125>
- Freeman CL, Claeysens F, Allan NL, Harding J (2006) Graphitic nanofilms as precursors to wurtzite films: Theory. *Phys Rev Lett* 96(6):066102. <https://doi.org/10.1103/PhysRevLett.96.066102>
- Han P, Min J, Zeng Z, Garoufalis CS, Baskoutas S, Jia Y, Du Z (2021) Excitonic characteristics of blue-emitting quantum dot materials in group II-VI using hybrid time-dependent density functional theory. *Phys Rev B* 104(4):045404/1-045404/4. <https://doi.org/10.1103/PhysRevB.104.045404>
- Hohenberg P, Kohn W (1964) Inhomogeneous electron gas. *Phys Rev B* 136:864–871. <https://doi.org/10.1103/PhysRev.136.B864>
- Hu J, Li Ls, Yang W, Manna L, Wang Lw, Alivisatos AP (2001) Linearly polarised emission from colloidal semiconductor quantum rods. *Science* 292:2060–2063. <https://doi.org/10.1126/science.1060810>
- Huang TT, Tan K, Lin MH (2007) A theoretical exploration of the interaction of adsorptive molecules with the ZnS clusters. *J Mol Struct Theochem* 821:101–105. <https://doi.org/10.1016/j.theochem.2007.06.032>
- Kakkar R, Kapoor PN, Klabunde KJ (2004) Theoretical study of the adsorption of formaldehyde on magnesium oxide nanosurfaces: size effects and the role of low coordinated and defect sites. *J Phys Chem B* 108:18140–18148. <https://doi.org/10.1021/jp0470546>
- Kakkar R, Grover R, Gahlot P (2006) Density functional study of the properties of isomeric amino phenyl hydroxamic acids and their copper (II) complexes. *Polyhedron* 25:759–766. <https://doi.org/10.1016/j.poly.2005.07.036>
- Katz D, Wizansky T, Millo O, Rothenberg E, Mokari T, Banin U (2002) Size dependant tunnelling and optical spectroscopy of CdSe Quantum Rods. *Phys Rev Lett* 89(8):086801/1-086801/4. <https://doi.org/10.1103/PhysRevLett.89.086801>
- Kho R, Nguyen L, Torres-Martínez CL, Mehra RK (2000) Symmetry and electronic structure of the Mn impurity in ZnS nanocrystals. *Biochem Biophys Res Commun* 272:29–35. <https://doi.org/10.1006/bbrc.2000.2712>
- Leung K, Whaley KB (1999) Surface relaxation of CdSe nanocrystals. *J Chem Phys* 110:11012–11022. <https://doi.org/10.1063/1.479037>
- Li Ls, Hu J, Yang W, Alivisatos AP (2001) Band gap variation of size- and shape controlled colloidal CdSe quantum rods. *Nano Lett* 1:349–351. <https://doi.org/10.1021/nl015559r>
- Liu L, Wu Q, Ding Y, Liu H, Zhang B (2004) Synthesis of HgSe quantum dots through templates controlling and gas-liquid transport with emulsion liquid membrane system. *Colloids Surf A Physicochem Eng Aspects* 240:135–139. <https://doi.org/10.1016/j.colsurfa.2004.03.020>
- Malik P, Kakkar R (2018) Effects of increasing number of rings on the ion sensing ability of CdSe quantum dots: a theoretical study. *J Nanopart Res* 20(4):114/1-114/15. <https://doi.org/10.1007/s11051-018-4218-2>
- Manna L, Scher EC, Alivisatos AP (2000) Synthesis of soluble and process able rod, arrow, teardrop and tetrapod shaped CdSe Nanocrystals. *J Am Chem Soc* 122:12700–12706. <https://doi.org/10.1021/ja003055+>
- Matxain JM, Fowler JE, Ugalde J (2000) Small clusters of group-(II–VI) materials: Zn_iX_i, X=Se, Te, i=1–9. *Phys Rev A* 61:053201/1-053201/8. <https://doi.org/10.1103/PhysRevA.64.053201>
- Matxain JM, Fowler JE, Ugalde J (2001) Electronic excitation energies of Zn_iS_i. *Phys Rev A* 64:013201/1-013201/7. <https://doi.org/10.1103/PhysRevA.64.013201>
- Nanda J, Sarma DD (2001) Photoemission spectroscopy of size selected zinc sulfide nanocrystallites. *J Appl Phys* 90:2504–2510 (<http://eprints.iisc.ac.in/id/eprint/7605>)
- Nanda J, Sapra S, Sarma DD, Chandrasekharan N, Hodes G (2000) Size-selected zinc sulfide nanocrystallites: synthesis, structure, and optical studies. *Chem Mater* 12:1018–1024. <https://doi.org/10.1021/cm990583f>
- Nikesh VV, Mahamuni S (2001) Highly photoluminescent ZnSe/ZnS quantum dots. *Semicond Sci Technol* 16(8):687–690. <https://doi.org/10.1088/0268-1242/16/8/309>
- Norris DJ, Efros AL, Rosen M, Bawendi MG (1996) Size dependence of exciton fine structure in CdSe quantum dots. *Phys Rev B* 53:16347–16354. <https://doi.org/10.1103/PhysRevB.53.16347>
- Özgör Ü, Alivov YI, Liu C, Teke A, Reshchikov MA, Doğan S, Avrutin V, Cho S-J, Morkoç H (2005) A comprehensive review of ZnO materials and devices. *Appl Phys Rev* 98:041301/1-041301/103. <https://doi.org/10.1063/1.1992666>
- Pal S, Goswami B, Sarkara P (2005) Size-dependent properties of Zn_mS_n clusters: a density-functional tight-binding study. *J Chem Phys* 123:044311/1-044311/9. <https://doi.org/10.1063/1.1991853>
- Pal S, Sharma R, Goswami B, Sarkar P (2009) Theoretical predictions of ring structures of ZnS quantum dots. *Chem Phys Lett* 467:365–368. <https://doi.org/10.1016/j.cplett.2008.11.070>
- Patel BK, Rath S, Sarangi SN, Sahu SN (2007) HgS nanoparticles: structure and optical properties. *Appl Phys A* 86:447–450. <https://doi.org/10.1007/s00339-006-3812-9>
- Patterson JD, Bailey BC (2007) *Solid State Physics*. Springer, Berlin. <https://doi.org/10.1007/978-3-540-34933-4>
- Perdew JP, Burke K, Ernzerhof M (1996) Generalized gradient approximation made simple. *Phys Rev Lett* 77:3865–3868. <https://doi.org/10.1103/PhysRevLett.77.3865>
- Rodrigues PAM, Tamulaitis G, Yu PY, Ribsud SH (1995) Size selective photoluminescence excitation spectroscopy in CdSe nanocrystals. *Solid State Commun* 94:583–587. [https://doi.org/10.1016/0038-1098\(95\)00135-2](https://doi.org/10.1016/0038-1098(95)00135-2)
- Salavati-Niasari M, Davar F, Mazaheri M (2009) Synthesis and characterization of ZnS nanoclusters via hydrothermal processing from [bis(salicylidene)zinc(II)]. *J Alloys Compd* 470:502–506. <https://doi.org/10.1016/j.jallcom.2008.03.048>
- Sarkar P, Springborg M (2003) Density-functional study of size-dependent properties of Cd_mSe_n clusters. *Phys Rev B* 68:235409/1-235409/7. <https://doi.org/10.1103/PhysRevB.68.235409>
- Schmidt-Mende L, MacManus-Driscoll JL (2007) ZnO nanostructures, defects, and devices *Mater. Today* 10:40–48. [https://doi.org/10.1016/S1369-7021\(07\)70078-0](https://doi.org/10.1016/S1369-7021(07)70078-0)
- Smith AM, Nie S (2010) Semiconductor nanocrystals: structure, properties, and band gap engineering. *Acc Chem Res* 43:190–200. <https://doi.org/10.1021/ar9001069>

- Soloviev VN, Eichhöfer A, Fenske D, Banin U (2000) Molecular limit of a bulk semiconductor: size dependence of the “band gap” in CdSe cluster molecules. *J Am Chem Soc* 122:2673–2674. <https://doi.org/10.1021/ja9940367>
- Troparevsky MC, Kronik L, Chelikowsky JR (2003) Optical properties of CdSe quantum dots. *J Chem Phys* 119(4):2284–2287. <https://doi.org/10.1063/1.1585013>
- Wang Lw, Zunger A (1996) Pseudopotential calculations of nanoscale CdSe quantum dots. *Phys Rev B* 53:9579–9582. <https://doi.org/10.1103/PhysRevB.53.9579>
- Wang XQ, Clark SJ, Abram RA (2004) Ab initio calculations of the structural and electronic properties of Hg_mTe_n clusters. *Phys Rev B* 70:235328/1-235328/6. <https://doi.org/10.1103/PhysRevB.70.235328>
- Wang CL, Zhang H, Zhang J, Li M, Sun H, Yang B (2007) Application of ultrasonic irradiation in aqueous synthesis of highly fluorescent CdTe/CdS core–shell nanocrystals. *J Phys Chem C* 111:2465–24696. <https://doi.org/10.1021/jp066601f>
- Wang C, Zhang H, Zhang J, Lv N, Li M, Sun H, Yang B (2008) Ligand dynamics of aqueous CdTe nanocrystals at room temperature. *J Phys Chem C* 112:6330–6335. <https://doi.org/10.1021/jp7121664>
- Wang J, Ma L, Zhao J, Jackson KA (2009) Structural growth behavior and polarizability of Cd_nTe_n ($n = 1–14$) clusters. *J Chem Phys* 130(21):214307/1-214307/8. <https://doi.org/10.1063/1.3147519>
- Weitzel CE, Monteith LK (1974) Changes in the photoconductivity of sputtered films of cadmium sulphide resulting from sulphur dioxide chemisorption. *Surf Sci* 44:438–448. [https://doi.org/10.1016/0039-6028\(74\)90129-0](https://doi.org/10.1016/0039-6028(74)90129-0)
- Weller H (1996) Self-organized superlattices of nanoparticles. *Angew Chem Int Ed Engl* 35:1079–1081. <https://doi.org/10.1002/anie.199610791>
- Wijayantha KGU, Peter LM, Otley LC (2004) Fabrication of US quantum dots sensitized solar cells via a pressing route. *Sol Energy Mater Sol Cells* 83(4):363–369. <https://doi.org/10.1016/j.solmat.2003.12.011>
- Woggon U, Gaponenko SV (1995) Excitons in quantum dots. *Phys Stat Sol B* 189:285–343. <https://doi.org/10.1002/pssb.2221890202>
- Xu S, Wang C, Cui Y (2009) Theoretical investigation for ZnSe clusters: influence of solvent and ligand on their characteristics. *J Mol Struct Theochem* 916:168–171. <https://doi.org/10.1016/j.theochem.2009.09.031>
- Xu S, Wang C, Cui Y (2010) Theoretical investigation of CdSe clusters: influence of solvent and ligand on nanocrystals. *J Mol Model* 16:469–473. <https://doi.org/10.1007/s00894-009-0564-4>
- Yamazoe N (1991) New approaches in for improving semiconductor gas sensors. *Sensors Actuators B Chem* 5:7–19. [https://doi.org/10.1016/0925-4005\(91\)80213-4](https://doi.org/10.1016/0925-4005(91)80213-4)
- Yoffe AD (1993) Low dimensional systems: quantum size effects and electronic properties of semiconductor microcrystallites (zero-dimensional systems) and some quasi-two-dimensional systems. *Adv Phys* 42:173–262. <https://doi.org/10.1080/00018739300101484>
- Yoffe AD (2001) Semiconductor quantum dots and related systems: electronic, optical, luminescence and related properties of low dimensional systems. *Adv Phys* 50:1–208. <https://doi.org/10.1080/00018730010006608>

Publisher’s note Springer Nature remains neutral with regard to jurisdictional claims in published maps and institutional affiliations.



Fiber and Textile Engineering in Drug Delivery Systems

THE TEXTILE INSTITUTE BOOK SERIES



Edited by
Navneet Sharma and Bhupendra Singh Butola



Fiber and Textile Engineering in
Drug Delivery Systems





Multifaceted approach for nanofiber fabrication

8

Thareja Rakhi¹, Malik Pragati², Bansal Prerna³ and Singh Jyoti⁴

¹Department of Chemistry, St. Stephen's College, University of Delhi, Delhi, New Delhi, India, ²Department of Chemistry, Acharya Narendra Dev College, University of Delhi, Delhi, New Delhi, India, ³Department of Chemistry, Rajdhani College, University of Delhi, Delhi, New Delhi, India, ⁴Department of Chemistry, Hansraj College, University of Delhi, Delhi, New Delhi, India

8.1 Introduction

Nanofibers are looked upon as exciting materials because of their unique properties like large surface area-to-weight ratio, small pore size, low density, and high porosity, which makes them useful in numerous areas. Nanofibers, with diameter ranging from 50 to 100 nm, can be natural or synthetic or hybrid. Applications include areas of environment, renewable energy, biomedical engineering, wound healing, drug delivery, cosmetics, lithium-ion batteries (LIBs), metal ion adsorptions, and many more. Nanofibers can be synthesized with the help of different methods available like template synthesis, electrospinning, melt blowing, self-assembly, drawing, chemical, and physical vapor deposition. These methods are used for designing a variety of nanofibers like discontinuous fibers, continuous fibers, and atypical nanofibers.

Discontinuous fibers are fabricated using the drawing process. Fibers of a particular diameter are synthesized via template synthesis, and phase separation is used only for some specific polymers. However, the electrospinning technique (Kumar et al., 2012; Luo et al., 2012) is the only method through which continuous polymeric nanofibers can be synthesized, as this method allows manipulation to control not only the diameter but also the parameters like porosity, surface area, and basis weight (fiber weight per area). This technique applies high electrostatic voltage on the polymer solution. Application of such high electrostatic voltage helps in the fabrication of nanofiber of desired diameter and length. Hence, both can be varied from a few nanometers to several micrometers. Modified electrospinning methods such as coaxial nanofiber preparation (Kamperman et al., 2010; Lee et al., 2010) or side-by-side nanofiber preparation lead to the synthesis of atypical nanofibers, such as the production of nano-coils or nano-springs structures (Chen et al., 2009a,b). Nanofibers can be clubbed under four categories based on chemical composition. These are inorganic-based nanofibers, organic-based nanofibers, composite nanofibers, and carbon nanofibers. The availability of a large number of techniques allows one to synthesize nanofibers using different fibrous materials ranging from natural polymers, synthetic polymers, nanofibers of metals, metal oxides, ceramics, and

277

Fiber and Textile Engineering in Drug Delivery Systems. DOI: <https://doi.org/10.1016/B978-0-323-96117-2.00012-1>
© 2023 Elsevier Ltd. All rights reserved.

254

Fiber and Textile Engineering in Drug Delivery Systems

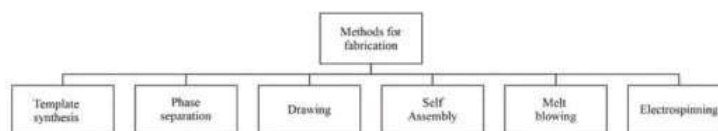


Figure 8.1 Techniques used for fabrication of nanofibers.

more. Some of the widely used techniques adopted for the fabrication of these

